



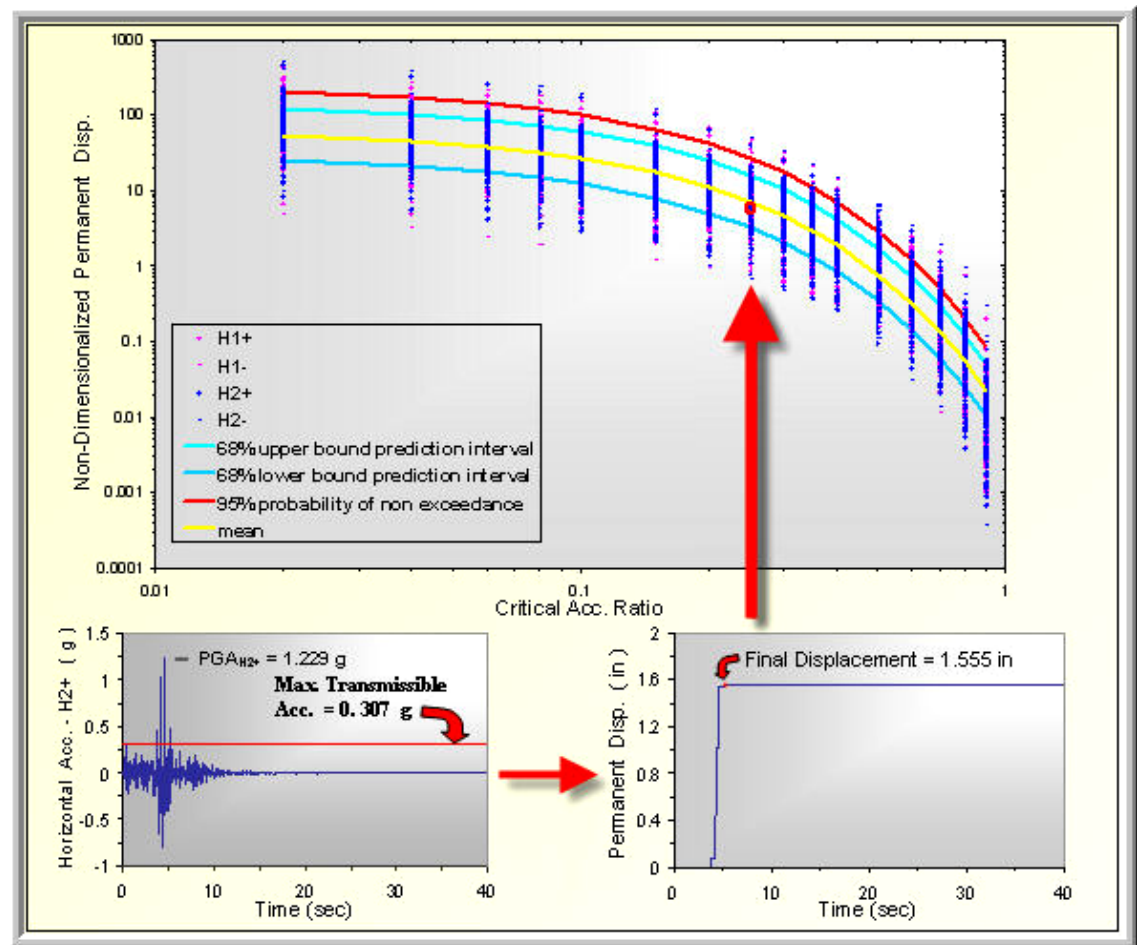
**US Army Corps
of Engineers®**
Engineer Research and
Development Center

Flood and Coastal Storm Damage Reduction Research and Development Program

Permanent Seismically Induced Displacement of Rock-Founded Structures Computed by the Newmark Program

Robert M. Ebeling, Moira T. Fong, Donald E. Yule,
Amos Chase, Sr., and Raju V. Kala

February 2009



Permanent Seismically Induced Displacement of Rock-Founded Structures Computed by the Newmark Program

Robert M. Ebeling and Moira T. Fong

*Information Technology Laboratory
U.S. Army Engineer Research and Development Center
3909 Halls Ferry Road
Vicksburg, MS 39180-6199*

Donald E. Yule, and Raju V. Kala

*Geotechnical and Structures Laboratory
U.S. Army Engineer Research and Development Center
3909 Halls Ferry Road
Vicksburg, MS 39180-6199*

Amos Chase, Sr.

*Science Applications International Corporation
3532 Manor Drive, Suite 4
Vicksburg, MS 39180*

Final report

Approved for public release; distribution is unlimited.

Prepared for Headquarters, U.S. Army Corps of Engineers
Washington, DC 20314-1000

Under Work Unit 142084

Abstract: This research report describes the engineering formulation and corresponding software developed for the translational response of rock-founded structural systems to earthquake ground motions. The PC software Newmark and Newmark_{VM} are developed to perform an analysis of the permanent sliding displacement response for a structural system founded on rock for a user-specified earthquake acceleration time-history via a Complete Time-History Analysis, also known as the Newmark sliding block method of analysis. The PC-based program Newmark performs a permanent sliding block displacement analysis given a baseline-corrected rock site-specific acceleration time-history. Newmark can also conduct regression analyses for sets of rock-founded acceleration time-histories in order to develop up to three user-selected forms of generalized equations of simplified permanent displacement relationships. The rock-founded structural system can be a variety of structural feature types, for example, a concrete gravity dam, a concrete monolith, or a retaining wall.

The conclusions of the regression analyses discussed in this report resulted in simplified permanent displacement relationships that were developed using data generated by Newmark for an extensive database of 122 sets of baseline-corrected rock acceleration time-histories in the range of moment magnitudes of 5 to 7. The resulting simplified permanent displacement relationships allow the engineer to rapidly determine the earthquake-induced permanent displacement for a given rock-founded structural system. This alternative procedure requires only rudimentary design/analysis ground motion characterization and use of a simplified permanent seismic displacement relationship for a sliding block (structural) system model. The resulting simplified permanent displacement relationships discussed in this report are being implemented in other Corps permanent seismically induced displacement software such as C_{Corps}W_{all}Slip and C_{Corps}D_{am}Slip.

DISCLAIMER: The contents of this report are not to be used for advertising, publication, or promotional purposes. Citation of trade names does not constitute an official endorsement or approval of the use of such commercial products. All product names and trademarks cited are the property of their respective owners. The findings of this report are not to be construed as an official Department of the Army position unless so designated by other authorized documents.

DESTROY THIS REPORT WHEN NO LONGER NEEDED. DO NOT RETURN IT TO THE ORIGINATOR.

Contents

Figures and Tables	vi
Preface	ix
Unit Conversion Factors	xi
Notation	xii
1 Introduction to the Translational Response of Structures to Earthquake Ground Motions	1
1.1 Introduction.....	1
1.1.1 Pseudostatic methods with a preselected seismic coefficient.....	3
1.1.2 Stress-deformation methods.....	7
1.1.3 Sliding block methods.....	11
1.2 New rotational analysis model based on a rigid block problem formulation.....	20
1.3 The tendency of a retaining wall to slide or to rotate during earthquake shaking.....	23
1.4 Seismic design criteria for Corps retaining structures.....	24
1.5 Axial load capacity of spillway invert slabs.....	26
1.6 Background and research objective.....	27
1.7 Organization of report.....	29
2 Translational Block Analysis of a Rock Founded Structural Model	31
2.1 Introduction.....	31
2.2 Time-history of permanent structural displacement.....	32
2.2.1 Introduction to a step-by-step solution scheme.....	33
2.2.2 Positive relative accelerations $relA0$ and $relA1$ at times t_i and t_{i+1}	36
2.2.3 Positive relative acceleration $relA0$ at time t_i and negative relative acceleration $relA1$ at t_{i+1}	38
2.2.4 Negative relative accelerations $relA0$ and $relA1$ at times t_i and t_{i+1}	44
2.2.5 Positive relative acceleration $relA0$ at time t_i and negative relative acceleration $relA1$ at t_{i+1}	48
2.2.6 Starting the program Newmark analysis and the initiation of structural translation during a DT time step.....	54
2.2.7 Cessation of structural translation.....	55
3 Regression Analysis	56
3.1 Introduction.....	56
3.2 Three-term regression analysis.....	56
3.3 Two-term regression analysis, linear in natural logarithm transformation.....	64
3.4 Two-term regression analysis, linear in common logarithm transformation.....	70

4	Regression results for ground motions recorded on rock	77
4.1	Introduction	77
4.2	Regression results of earthquakes covering the Moment Magnitude (Mw) range of 6.9 – 8.1 (Magnitude 7).....	89
4.2.1	<i>Three-term regression results</i>	90
4.2.2	<i>Two-term regression results, linear in natural logarithm transformation</i>	94
4.2.3	<i>Two-term regression results, linear in common logarithm transformation</i>	98
4.2.4	<i>Comparison of regression results of all three forms of the simplified non- dimensionalized displacement relationships</i>	102
4.3	Regression results of earthquakes covering the Moment Magnitude (Mw) range of 6.1 – 6.8 (Magnitude 6).....	104
4.3.1	<i>Three-term regression results</i>	104
4.3.2	<i>Two-term regression results, linear in natural logarithm transformation</i>	108
4.3.3	<i>Two-term regression results, linear in common logarithm transformation</i>	112
4.3.4	<i>Comparison of regression results of all three forms of the simplified non- dimensionalized displacement relationships</i>	116
4.4	Regression results of earthquakes covering the Moment Magnitude (Mw) range from 4.9 – 6.1 (Magnitude 5)	118
4.4.1	<i>Three-term regression results</i>	118
4.4.2	<i>Two-term regression results, linear in natural logarithm transformation</i>	122
4.4.3	<i>Two-term regression results, linear in common logarithm transformation</i>	126
4.4.4	<i>Comparison of regression results of all three forms of the simplified non- dimensionalized displacement relationships</i>	130
4.5	Special regression results of Equation Form Two of non-dimensionalized displacement relationships without differentiation of Moment Magnitude	131
4.5.1	<i>Mean relationships</i>	132
4.5.2	<i>Ninety-five percent probability of non-exceedance</i>	134
4.5.3	<i>Sixty-eight percent prediction intervals</i>	135
5	The Visual Modeler for Newmark – Newmark_{VM}	137
5.1	Introduction	137
5.2	The Visual Modeling Environment	137
5.2.1	<i>Significant Tabs relevant to an analysis</i>	138
5.2.2	<i>Multiple Horizontal Time-History Selections (Multiple Analyses only)</i>	139
5.2.3	<i>Earthquake Time-History Horizontal Component 1 and 2 input (Single Analysis or Multiple Analyses)</i>	143
5.2.4	<i>Maximum Transmissible Acceleration input (Single Analysis or Multiple Analyses)</i>	146
5.2.5	<i>The Selection of Time Histories (Multiple Analyses)</i>	147
5.2.6	<i>Analysis results (Single Analysis or Multiple Analyses)</i>	149
5.3	Example 1 – Single Analysis or Sliding Block Analysis	154
5.4	Example 2 – Multiple Analyses with Regression using Equation Form Two.....	156
6	Conclusions and Recommendations	160
6.1	Introduction	160
6.2	Ninety-five percent probability of non-exceedance.....	160
6.2.1	<i>Non-dimensionalized displacements of 23 sets of Moment Magnitude 7 group</i>	160

6.2.2 Non-dimensionalized displacements of 38 sets of Moment Magnitude 6 group	161
6.2.3 Non-dimensionalized displacements of 66 sets of Moment Magnitude 5 group	162
6.2.4 Non-dimensionalized displacements of 122 sets of Moment Magnitude 5 - 7 groups	162
6.3 Mean relationships.....	164
6.3.1 Non-dimensionalized displacements of 23 sets of Moment Magnitude group 7	164
6.3.2 Non-dimensionalized displacements of 38 sets of Moment Magnitude group 6	165
6.3.3 Non-dimensionalized displacements of 66 sets of Moment Magnitude group 5	166
6.3.4 Non-dimensionalized displacements of 122 sets of Moment Magnitude 5 - 7 groups.....	166
6.4 Recommendations	168
References.....	169
Appendix A: Listing and Description of the Newmark ASCII Input Data File (file name: Newmark.in).....	173
Appendix B: Listing of Newmark ASCII Data Output Files	185
Report Documentation Page	

Figures and Tables

Figures

Figure 1.1. Gravity retaining wall and “driving” soil wedge treated as a rigid body. 4

Figure 1.2. Simplified “driving” wedge method of analysis and the Mononobe-Okabe active earth pressure force relationship. 6

Figure 1.3. Elements of the Newmark (rigid) sliding block method of analysis 13

Figure 1.4. Gravity retaining wall and failure wedge treated as a sliding block 16

Figure 1.5. Incremental failure by base sliding 18

Figure 1.6. Idealized permanent, seismically induced displacement due to the rotation about the toe of a rock-founded wall retaining moist backfill, with toe restraint, computed using $C_{corpsWallRotate}$ 19

Figure 1.7. Rock-founded cantilever retaining wall bordering a spillway channel..... 20

Figure 1.8. Permanent, seismically induced displacement due to the rotation about the toe of a rock-founded, partially submerged cantilever retaining wall and with toe restraint, computed using $C_{corpsWallRotate}$ 22

Figure 1.9. Structural wedge with toe resistance retaining a driving soil wedge with a bilinear moist slope analyzed by effective stress analysis with full mobilization of shear resistance within the backfill..... 23

Figure 2.1. Complete equations for relative motions over time increment DT based on linearly varying acceleration..... 34

Figure 2.2. Relative Velocity and displacements at the end of time increment DT based on linearly varying relative acceleration. 37

Figure 2.3. Two possible outcomes for the case of a negative relative acceleration at time t_i and a positive relative acceleration at time t_{i+1} 39

Figure 2.4. Two possible outcomes for the case of negative relative accelerations at times t_i and t_{i+1} 45

Figure 2.5. Two possible outcomes for the case of a positive relative acceleration at time t_i and a negative relative acceleration at time t_{i+1} 49

Figure 4.1. Non-dimensionalized displacements with the mean, 68 percent prediction intervals and 95 percent probability of non-exceedance curves..... 92

Figure 4.2. Non-dimensionalized displacements with the mean, 68 percent prediction intervals and 95 percent probability of non-exceedance curves..... 95

Figure 4.3. Non-dimensionalized displacements with the mean, 68 percent prediction intervals and 95 percent probability of non-exceedance curves..... 99

Figure 4.4. Non-dimensionalized displacements and comparisons of the means of the three regression analysis equations for Magnitude 7 earthquakes. 103

Figure 4.5. Non-dimensionalized displacements with the mean, 68 percent prediction intervals and 95 percent probability of non-exceedance curves..... 105

Figure 4.6. Non-dimensionalized displacements with the mean, 68 percent prediction intervals and 95 percent probability of non-exceedance curves..... 110

Figure 4.7. Non-dimensionalized displacements with the mean, 68 percent prediction intervals and 95 percent probability of non-exceedance curves.....	114
Figure 4.8. Non-dimensionalized displacements and comparisons of the means of the three regression analysis equations for Magnitude 6 earthquakes.	117
Figure 4.9. Non-dimensionalized displacements with the mean, 68 percent prediction intervals and 95 percent probability of non-exceedance curves.....	119
Figure 4.10. Non-dimensionalized displacements with the mean, 68 percent prediction intervals and 95 percent probability of non-exceedance curves.....	124
Figure 4.11. Non-dimensionalized displacements with the mean, 68 percent prediction intervals and 95 percent probability of non-exceedance curves.....	128
Figure 4.12. Non-dimensionalized displacements and comparisons of the means of the three regression analysis equations for Magnitude 5 earthquakes.	131
Figure 4.13. Non-dimensionalized displacements for normalized earthquakes without differentiation of Moment Magnitude (Equation Form Two).	133
Figure 5.1. The Introduction tab features the process of a multiple analysis.	138
Figure 5.2. The Multiple Horizontal Time-History Selections tab ready for user input.	140
Figure 5.3. Selection of horizontal time-history files.....	142
Figure 5.4. Horizontal earthquake time-history ground motion shown in the Earthquake Time-History Horz Comp. 1 tab.....	144
Figure 5.5. Maximum Transmissible Acceleration tab for multiple analyses data entry.	147
Figure 5.6. The Selection of Time Histories tab for data entry used for multiple analyses.	148
Figure 5.7. The Analysis tab used for all analyses.....	150
Figure 5.8. Single and combinations of three equations available for Regression Analyses.	151
Figure 5.9. Illustrative example of Newmark during execution.....	152
Figure 5.10. Resultant output data from multiple analyses.	153
Figure 5.11. Resultant output data from a regression analysis.	153
Figure 5.12. The Analysis tab for Example 1.	154
Figure 5.13. Sliding block time-history results for Example 1.....	155
Figure 5.14. The Analysis tab for Example 2.	157
Figure 5.15. Non-dimensionalized earthquake displacements.	158
Figure 5.16. The mean, 68 percent prediction intervals and 95 percent probability of non-exceedance.....	159
Figure 6.1. 95 percent probability of non-exceedance relationships of non-dimensionalized displacements of four magnitude groups.....	163
Figure 6.2. Mean relationships of non-dimensionalized displacements of all four magnitude groups.	167

Tables

Table 1.1. Approximate magnitudes of movements required to reach minimum active earth pressure conditions (after Clough and Duncan 1991).....	5
Table 3.1. Forms of simplified non-dimensionalized permanent displacement relationships.	56
Table 4.1. Master accelerograph table of magnitude 6.9 – 8.1.....	79

Table 4.2. Master accelerograph table of magnitude 6.1 – 6.8 earthquakes.....	81
Table 4.3. Master accelerograph table of magnitude 4.9 – 6.1 earthquakes.....	84
Table 4.4. Sets of earthquake time-history data classified by moment magnitude ranges.....	89
Table 4.5. Comparison between the Richter and Moment Magnitude Scales.....	89
Table 4.6. Values for the regression equations constants for Moment Magnitude (M_w) range of 6.9 – 8.1 (Magnitude 7).....	90
Table 4.7. Values for the regression equations constants for Moment Magnitude (M_w) range of 6.1 – 6.8 (Magnitude 6).....	104
Table 4.8. Values for the regression equations constants for Moment Magnitude (M_w) range of 4.9 – 6.1 (Magnitude 5).....	118
Table 6.1. 95 percent probability percent of non-exceedance relationships of non- dimensionalized displacements of four magnitude groups.....	164
Table 6.2. Mean relationships of non-dimensionalized displacements of all four magnitude groups.....	168
Table B.1. Output data files used by output buttons in the visual modeler analysis tab.....	185

Preface

This research report describes the engineering formulation and corresponding software developed for the translational response of U.S. Army Corps of Engineers hydraulic structures to earthquake ground motions. The PC software Newmark was developed to perform an analysis of the permanent sliding displacement response for each structural feature (e.g., a rock-founded retaining wall section or a gravity dam section) to a user-specified earthquake acceleration time-history via a complete time-history analysis. PC software Newmark is also used in this R&D effort to perform a statistical analysis of computed permanent displacements for a suite of acceleration time-histories resulting in simplified (seismic) permanent displacement relationships for use in simplified sliding block analysis. This R&D was accomplished and the results summarized in this report for use on rock-founded structural systems. Prior to this publication, the simplified permanent displacement relationships found in the technical literature are for soil-founded structures. Funding to initiate research and software development and engineering study was provided by Headquarters, U.S. Army Corps of Engineers (HQUSACE), as part of the Flood and Coastal Storm Damage Reduction Research and Development Program. The research was performed under the Dam Safety Focus Area, Work Unit 142084 entitled “Simplified Probabilistic Models for Concrete Gravity Dams” for which Dr. Robert M. Ebeling, Computational Science and Engineering (CSED), Information Technology Laboratory (ITL), U.S. Army Engineer Research and Development Center (ERDC), was the Principal Investigator. Additional funding was provided by the Engineering Risk and Reliability Directory of Expertise. Andy Harkness (of Pittsburgh District), Technical Manager of the Engineering Risk and Reliability Directory of Expertise, supervised this R&D effort.

H. Wayne Jones, ITL, was the Dam Safety Focus Area Manager. William R. Curtis, Coastal and Hydraulics Laboratory (CHL), ERDC, was the Flood and Coastal Storm Damage Reduction Research and Development Program Manager, and Dr. Michael Sharp, Geotechnical and Structures Laboratory (GSL), ERDC, was the Water Resources Infrastructure Technical Director.

The resulting engineering methodology and corresponding software is applicable to a variety of structural systems founded on rock. The main focus of this R&D effort was to develop simplified seismic permanent displacement relationships for rock-founded structures for use in a simplified sliding block analysis. Although developed for the evaluation of the permanent displacement of rock-founded structures, PC software Newmark may also be used to compute the permanent displacement of soil-founded structures during earthquake shaking.

This R&D study was conducted by Dr. Robert M. Ebeling and Moira T. Fong, ITL, Donald E. Yule, GSL, Amos Chase, Sr., Science Applications International Corporation, and Raju Kala, GSL. Dr. Ebeling was author of the scope of work for this research. The report was prepared by Dr. Ebeling, Ms. Fong, and Mr. Yule under the supervision of Dr. Robert M. Wallace, Chief, CSED, and Dr. Reed Mosher, Director, ITL.

COL Gary E. Johnston was Commander and Executive Director of ERDC. Dr. James R. Houston was Director.

Unit Conversion Factors

Multiply	By	To Obtain
feet	0.3048	meters
inches	0.0254	meters
pounds (mass)	0.45359237	kilograms

Notation

A	a decimal fraction
$A \bullet g$	the acceleration of the ground
angle β	the direction of the resultant force S of the distributed shear stresses along the interface, as shown in Figure 1.3b
angle θ	the angle inclination of the resultant inertia force ($= 0$ for horizontal accelerations only)
$Area_a$	the positive area under the linear relative acceleration relationship over the time step DT
$Area_v$	the positive area under the positive quadratic relative velocity relationship over the time step DT
$\beta_1, \beta_2, \beta_3, \beta_4, \beta_5$	coefficients
c'	Mohr-Coulomb effective cohesion
COSMOS	Consortium of strong-ground motion observation systems
Δt	a time increment
DSHA	a Deterministic Seismic Hazard Assessment
D, D_1, D_2, D_3	the determinants of a matrix
d_m	permanent displacement (length)
d_s	the standardized maximum displacement
DT, dt	time increments
$DTzeroD$	a time increment
$DTmid$	a time increment

DT_{zeroV}	a time increment
FLAC	a commercially available, two-dimensional, explicit finite difference program, which has been written primarily for geotechnical applications and applied to dynamic analysis of earthen systems
FLUSH	a classic example of a category of software which uses the finite element method and treats the structure and the surrounding retained soil and foundation medium in a single analysis step; used in dynamic soil-structure in interaction analyses
G, g	the acceleration of gravity
GUI	Graphical User Interface
K_{AE}	pseudo-static active earth pressure coefficient
k_c	maximum transmissible acceleration capacity (decimal fraction)
kips	1,000 lbs
k_h and k_v	decimal fraction that, when multiplied times the weight of some body, gives horizontal and vertical pseudo-static inertia force S for use in permanent seismic deformation analyses
$k_m g$	maximum horizontal ground acceleration
k_s	the standardized acceleration expressed as a fraction of $g(0.5)$
$lhsDT$	Left-hand side time increment
ln	the natural log
MCE	Maxim Credible Earthquake
MDE	Maximum Design Earthquake
M_s	surface wave

M_w	moment magnitude scale
N	a decimal fraction of the acceleration imparted to the Figure 1.3a soil sliding mass
N	the total number of non-dimensionalized displacement terms in Figure 3.7
N^*g	the maximum transmissible horizontal acceleration (a constant)
OBE	Operational Basis Earthquake
P	the force that is a resultant of the normal forces shown in Figure 1.3b
PEER	Pacific Earthquake Engineering Research Center
$P \bullet \Delta$	second-order structural deformation effects
ϕ	Mohr-Coulomb angle of internal friction shear strength parameter
ϕ'	Mohr-Coulomb effective angle of internal friction shear strength parameter
PSHA	Probabilistic Seismic Hazard Analysis
P_{resist}	a user-defined force representing the ultimate axial load resistance of a slab
$relA$	relative acceleration
$relA0, relA1$	relative acceleration values at times t_i and t_{i+1} , respectively
$relAmid$	midrange relative acceleration
$relD$	relative displacement
$relD0$	from the value for relative displacement at time t_i
$relD1$	the permanent relative structural displacement at time t_{i+1}

<i>relDmid</i>	midrange relative displacement
<i>relV</i>	relative velocity
<i>relV0</i>	relative velocity at time t_i
<i>relV1</i>	relative velocity at time t_{i+1}
<i>relVmid</i>	midrange relative velocity
<i>rhsDT</i>	right-hand side time increment
<i>S</i>	the resultant force of the distributed shear stresses along the interface, Figure 1.3c
SHAKE	a vertical shear wave propagation program
SOILSTRUCT	an Incremental Construction, Soil-Structure Interaction finite element program
SSI	a soil-structure interaction
S_u	undrained shear strength of soils
$t_i, t_{i+1}, \Delta t$	timesteps
v_m	the maximum ground velocity
v_r	the relative velocity of a wall
v_s	the standardized velocity (29.92 in./sec)
V_s	average shear wave velocity
<i>W</i>	the weight of the sliding mass, as shown in Figure 1.3a

1 Introduction to the Translational Response of Structures to Earthquake Ground Motions

1.1 Introduction

Engineering formulations and software provisions based on sound seismic engineering principles are needed for a wide variety of rock-founded Corps hydraulic structures that translate (i.e., slide) or rotate during earthquake shaking and for massive concrete structures constrained to rocking. The engineering formulation discussed in this report was developed to address the first of these three different modes of structural responses to earthquake shaking.

This research report describes the development of simplified permanent deformation relationships for rock-founded structures subjected to earthquake shaking. The original permanent (translational) deformation procedure of analysis, published by Newmark in 1965, required the use of an earthquake acceleration time-history in order to predict the permanent deformation of a structure (an earthen slope of an embankment in Professor Newmark's examples). This type of analysis is referred to as a "Complete Time-History Permanent (Translational) Displacement Analysis" and is a capability of the PC software developed in support of the R&D discussed in this report. The drawback to a complete time-history permanent deformation analysis is that there are many factors to consider and many stages to the selection of earthquake acceleration time histories for use on a Corps project. Additionally, the time-history selection process requires information that typically is not readily available at the beginning of a Corps project effort. Fortunately, there is an alternative procedure of seismically induced permanent deformation analysis available to District engineers for use on Corps projects. This alternative procedure requires only rudimentary design/analysis ground motion characterization and use of a simplified permanent seismic displacement relationship for a sliding block (structural) system model. This simplified seismic permanent (translational) deformation procedure of analysis was developed for the Corps in 1977 by the WES/ERDC researchers Dr. Franklin and Mr. Chang.

In a subsequent study to that conducted by Newmark (1965), Franklin and Chang (1977) expanded the use of the permanent seismically induced deformation procedure of analysis through the development of “Simplified Sliding Block” relationships. In order to use the Franklin and Chang relationships (which are for computed data presented in figure form), values for peak ground acceleration and peak ground velocity are required. A “Simplified Sliding Block” formulation has the advantage of eliminating the need for the Engineer to directly select an acceleration time-history to characterize earthquake shaking. The Franklin and Chang permanent deformation relationships are a direct product of an evaluation process involving acceleration time histories. Results of their calculations reflect the use of many acceleration time histories. Note that only acceleration time histories recorded during earthquakes occurring through 1977 were included in their study.

Two drawbacks to using the Franklin and Chang (1977) “Simplified Sliding Block” relationships for rock-founded structural systems exist; the focus of the relationships they developed is on soil sites (reflecting the early days when the permanent sliding block displacement based method of analysis was first applied to earthen “structural” systems consisting of slopes and earthen embankments); and since 1977 there have been a number of earthquake events recorded on rock as well as soil sites.

In the subsequent years there have been several studies resulting in seismically induced simplified permanent sliding block relationships, but all of these studies have been dominated by the use of soil site acceleration time-history records (e.g., Makdisi and Seed 1978; Richards and Elms 1979; Whitman and Liao 1985a, 1985b; Ambraseys and Menu 1988; Cai and Bathurst 1996). This research report summarizes the development of seismically induced, simplified sliding block permanent deformation relationships for rock-founded structures and is accomplished by processing data obtained by using a collection of acceleration time histories recorded on different “rock” sites. One hundred and twenty-two sets of horizontal “rock” acceleration time histories recorded during many different earthquake events were carefully selected, base-line corrected and processed (as discussed in Chapter 4) using the PC software Newmark to develop the simplified permanent sliding block displacement relationships summarized in Chapter 6 of this report.

The resulting simplified permanent deformation relationships for rock-founded structures summarized in this report will be implemented within `CorpsWallSlip` (Ebeling et al. 2007) and within `CorpsDamSlip` (in development by Ebeling and Chase) for the seismic Simplified Sliding Block analysis of rock-founded earth retaining structures and rock-founded concrete gravity dams, respectively.

There are three categories of analytical approaches used to perform a seismic stability analysis. They are listed in order of sophistication and complexity:

- Pseudostatic methods with a preselected seismic coefficient.
- Stress-deformation methods.
- Sliding block methods.

Each category will be subsequently discussed so as to put the Newmark sliding block method of analysis in perspective as well as understand some of the input data requirements for the PC software Newmark developed for use in this R&D effort and described in this report. Because sliding block methods are the focus of this report, it will be discussed last. The examples to be discussed will involve either embankment slopes or earth retaining structures.

1.1.1 Pseudostatic methods with a preselected seismic coefficient

Pseudostatic methods with a preselected seismic coefficient in the horizontal and in the vertical direction often require bold assumptions about the manner in which the earthquake shaking is represented and the simplifications made for their use in stability computations. Essentially, it is a force equilibrium method of analysis expressing the safety and stability of an earth retaining structure to dynamic earth forces in terms of the following:

- The factor of safety against sliding along the base of the wall,
- The ability of the wall to resist the earth forces acting to overturn the wall,
- The factor of safety against a bearing capacity failure or crushing of the concrete or rock at the toe in the case of a rock foundation.

An example using 1992 Corps criteria (now outdated) is discussed in Section 6.2 of Chapter 6 in Ebeling and Morrison (1992). Pseudostatic

methods with horizontal and vertical preselected seismic coefficients represent earthquake loading as static forces.

In these types of computations, the earthquake “demand” is represented by a horizontal seismic coefficient, and a vertical seismic coefficient (sometimes specified as zero) acting at mass centers. Values for these coefficients (typical symbols are k_h and k_v), are dimensionless numbers that, when multiplied times the weight of some body, gives a pseudo-static inertia force for use in analysis or design. The horizontal and vertical inertia forces are applied to the mass center of the body, as shown in Figure 1.1. The coefficients k_h and k_v are, in effect, decimal fractions of the acceleration of gravity (g). For some analyses, it is appropriate to use (acceleration) values of $k_h g$ and $k_v g$ smaller than the horizontal and vertical peak accelerations, respectively, anticipated during the design earthquake event. It is important to recognize that this category of method of analysis does not provide quantitative information regarding seismically-induced displacements.

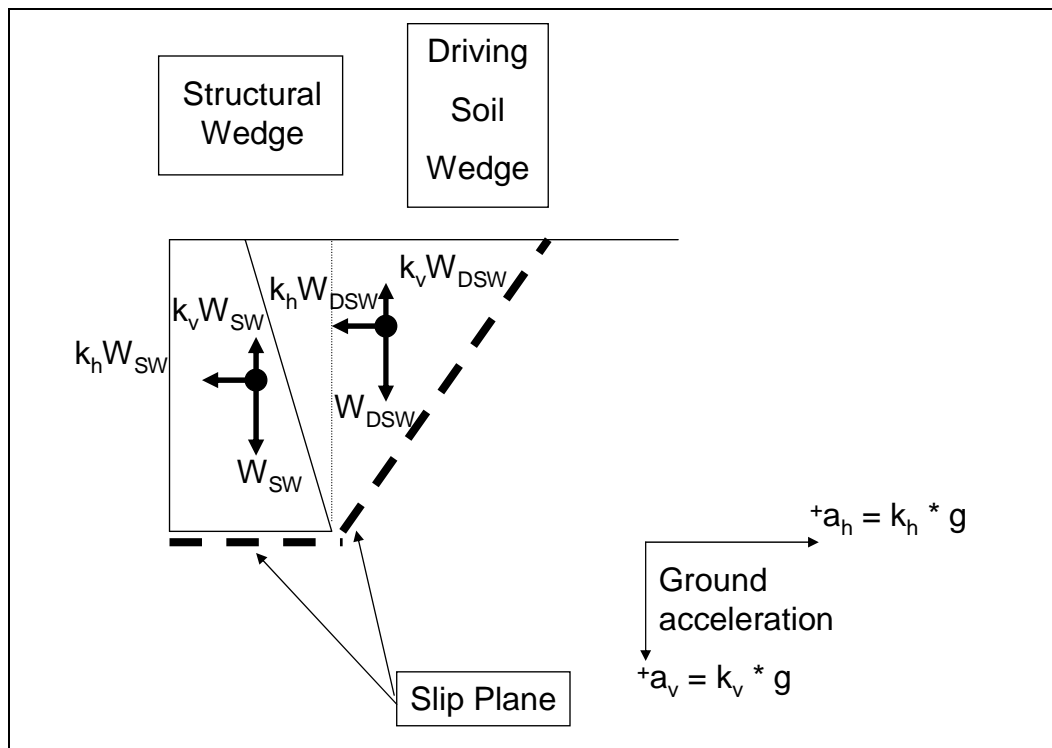


Figure 1.1. Gravity retaining wall and “driving” soil wedge treated as a rigid body.

For retaining walls in which the permanent relative motion of the retaining structure and retained soil (i.e., the backfill) are sufficient to fully mobilize the shear strength in the soil, soil wedge solutions, in which a wedge of soil bounded by the structural wedge and by an assumed failure plane within the retained soil, are considered to move as a rigid body and with the same horizontal acceleration (Figure 1.1). Table 1.1 lists the approximate magnitudes of movements required to reach minimum active earth pressure conditions. Although this Clough and Duncan (1991) guidance is for static loading, after careful evaluation Ebeling and Morrison (1992, in Section 2.2.2) concluded that the Table 1.1 values may also be used as rough guidance for minimum retained soil seismic displacement to fully mobilize a soils shear resistance, resulting in dynamic active earth pressures.

Table 1.1. Approximate magnitudes of movements required to reach minimum active earth pressure conditions (after Clough and Duncan 1991).

Type of Retained Soil	Values of Y/H^1
	Active
Dense Sand	0.001
Medium-Loose Sand	0.002
Loose Sand	0.004
¹ Y = movement of top of wall required to reach minimum active pressure, by tilting or lateral translation; H = Height of wall.	

A commonly-cited expression for the forces the driving soil wedge exerts on the structural wedge was first proposed by Okabe (1924, 1926) and Mononobe and Matsuo (1929). A form of their expression for P_{AE} in use today (see Chapter 4 in Ebeling and Morrison 1992) is given in Figure 1.2. Their formulation is referred to as Mononobe-Okabe with P_{AE} expressed in terms of an active earth pressure coefficient, K_{AE} , with the subscript *A* designating active and the subscript *E* designating earthquake. The Mononobe-Okabe formulation is an extension of Coulomb's theory of static active earth pressures with a horizontal seismic coefficient and a vertical seismic coefficient acting at the center of a Coulomb's "driving" soil wedge mass of a moist retained soil (i.e., with no water table), as shown in this figure. Equation 36 in Chapter 4 of Ebeling and Morrison (1992) gives the Mononobe-Okabe relationship for K_{AE} . The general wedge solution

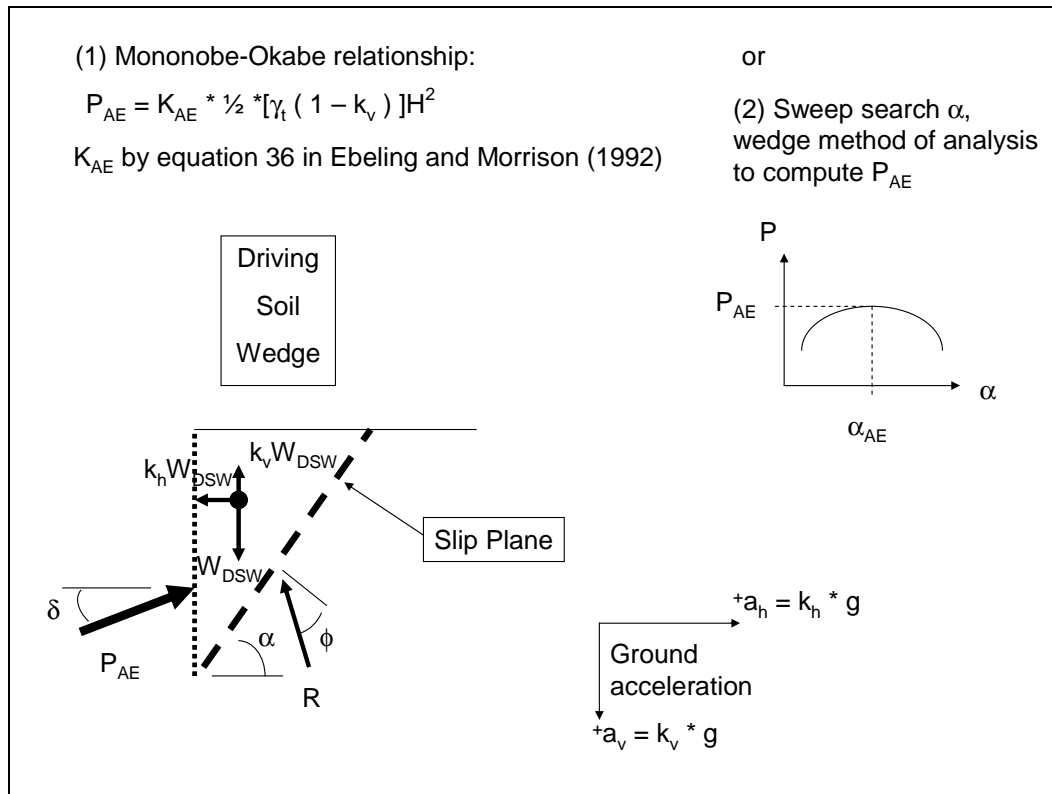


Figure 1.2. Simplified “driving” wedge method of analysis and the Mononobe-Okabe active earth pressure force relationship.

resulting in this same value for P_{AE} as can be calculated by the Mononobe-Okabe relationship is given in Appendix A of Ebeling and Morrison (1992). For retaining wall problems analyzed using the simplified wedge method, EM 1110-2-2100 in Section 5-5, part (3)b provides guidance on assumptions regarding the magnitude of the seismic coefficient k_h that may be used as a fraction of peak ground acceleration. Guidance is also given regarding the magnitude of the seismic coefficient k_v , expressed as a fraction of the value for k_h . Minimum k_h values are cited in Table G-1, Section G-4 of Appendix G, part (a) in EM 1110-2-2100, according to the seismic zone in which the project resides.

Because seismically-induced deformations are not an explicit part of this computational process and given that pseudostatic methods represent earthquake loads by static forces, the results are difficult to interpret. This is because displacement is more closely related to assessment of the seismic performance for a retaining structure than are Factors of Safety in what is fundamentally a dynamic problem where loadings are on the fraction of a second.

1.1.2 Stress-deformation methods

Stress-deformation methods are specialized applications of finite element or finite difference programs for the dynamic analysis of earth retaining structures to seismic loading using numerical techniques to account for the nonlinear engineering properties of soils. The problem being analyzed is often referred to as a soil-structure interaction (SSI) problem. Acceleration time histories are typically used to represent the earthquake ground motions in this type of formulation. The general procedure of stress-deformation dynamic analysis is straightforward and follows the usual engineering approach:

1. Define the problem,
2. Idealize the physical system,
3. Set up the equations of motion for the dynamic problem,
4. Characterize the dynamic engineering properties of the (structure, soil, and/or rock) materials as per the constitutive material model(s) being used,
5. Solve the equations of motion,
6. Evaluate the results.

Steps (1), (2), (4) and (6) are handled by the engineer while steps (3) and (5) are dealt with by the engineering software. A partial listing of computer-based codes for dynamic analysis of soil systems are given in Appendix D of Ebeling and Morrison (1992). Use of this type of advanced engineering software requires specialized knowledge in the fields of geotechnical and structural engineering dynamics as well as in numerical methods. Two computer programs, FLUSH and FLAC, will be discussed briefly to give the reader a sense of what is involved with the application of computationally complex numerical codes in a complete soil-structure interaction dynamic analysis and the numerous input and modeling considerations required.

1.1.2.1 FLUSH

The American Society of Civil Engineers (ASCE) Standard 4-86 (1986) states that SSI denotes the phenomenon of coupling between a structure and its supporting soil or rock medium during earthquake shaking. The resulting dynamic soil pressures are a result of the degree of interactions that occur between the structure and the soil. This response is dependent on the following:

- The characteristics of the ground motion
- The retained and foundation soils (or rock)
- The structure itself.

One method of analysis for SSI is referred to as the Direct method and treats the structure and the surrounding retained soil and foundation medium in a single analysis step. FLUSH is a classic example of this category of software which uses the finite element method in this dynamic analysis (Lysmer et al. 1975).

Two-dimensional (2-D) cross-sections of the retaining structure, and portions of the retained soil and foundation, are typically modeled in the FLUSH analysis. Nonlinear soil behavior is treated through equivalent linearization of the shear stiffness of each soil element, with the effective shear strains that develop during earthquake shaking, for the user specified earthquake acceleration time-history. Material damping is assigned to each soil (and/or rock) element and to each structural element comprising the mesh. Material damping is strain-compatible for each soil, rock and structural material type. FLUSH solves the equation of motion in the frequency domain. The acceleration time-history is introduced through the base nodes of the mesh; fictitious (artificial) boundary conditions that allow for the introduction of vertically propagating shear waves resulting in horizontal motion of the nodes of the mesh during earthquake shaking, and for vertically propagating compression waves that allow for the vertical motion of the nodes. Lateral boundaries are referred to as transmitting boundaries and are imposed on the 2-D mesh to allow for energy absorbing boundary conditions to be specified. Because it is essentially a wave propagation problem being solved, great care is exercised by the seismic engineer to size the mesh so that moderate to high wave frequencies are not artificially excluded in the dynamic numerical analysis. Sizing of the 2-D mesh, as it pertains to the height of the elements and with regard to the maximum shear wave frequency vertically transmitted by the elements, first involves the analysis of representative one-dimensional (1-D) soil columns.

To assess the maximum frequency that may be transmitted by a user-proposed 2-D finite element mesh in a FLUSH analysis, representative imaginary section(s) within the 2-D model problem are first analyzed by the vertical shear wave propagation program SHAKE (Schnabel et al. 1972) and by a 1-D finite element column using FLUSH. Strain-compatible

shear stiffness results from the SHAKE analyses are used to determine the maximum height of the soil elements for the maximum frequency of the vertically propagating shear wave needed to be transmitted in the FLUSH (2-D) analysis. A 1-D soil column is then constructed using finite elements and analyzed using FLUSH to verify that the required vertically propagating shear wave frequencies are being transmitted by the FLUSH mesh. The wavelength associated with the highest frequency transmitted by the mesh is related to the heights of the elements and to the (strain compatible) shear wave velocities via the strain compatible shear stiffness of each of the elements. Recall that FLUSH accounts for nonlinear response of soils during earthquake shaking through adjustments of the soil shear stiffness and material damping parameters as a function of shear strain that develop in each element of the finite element mesh. Note that the results of this assessment are dependent on the characteristics of the acceleration time-history used in the analysis.

FLUSH output obtained via the extraction mode includes time-histories of the dynamic stresses within each element and dynamic displacements at each node in the finite element model. Time-histories of nodal point forces may also be obtained using specialized software. The computed dynamic stresses are then superimposed on the static stresses to attain the total stresses. Static stresses are typically obtained from a SOILSTRUCT finite element analysis (Ebeling et al. 1992).

In a static analysis using SOILSTRUCT, the nonlinear stress-strain behavior of soils are accounted for in an incremental, equivalent linear method of analysis in which the sequential excavation (if any), followed by sequential construction of the structure and incremental placement of retained soil, is made. Examples of this application to Corps structures for static loading(s) are given in Clough and Duncan (1969), Ebeling et al. (1993); Ebeling and Mosher (1996); Ebeling and Wahl (1997); Ebeling et al. (1997b); and Ebeling et al. (1997c). The mesh used in the FLUSH dynamic analysis will be the basis for the mesh used in the SOILSTRUCT static analysis, for the convenience of combining results.

1.1.2.2 FLAC

In 1992, the Corps completed its first research application of FLAC to the seismic analysis of a cantilever retaining wall (Green and Ebeling 2002). FLAC is a commercially available, two-dimensional, explicit finite difference program, which has been written primarily for geotechnical

applications. The basic formulation of FLAC is plane-strain. Dynamic analyses can be performed with FLAC using an optional dynamic calculation module, wherein user-specified acceleration, velocity, or stress time-histories can be input as an exterior boundary condition or as an interior excitation. FLAC allows for energy absorbing boundary conditions to be specified, which limits the numerical reflection of seismic waves at the model perimeter. The nonlinear constitutive models (10 are built-in), in conjunction with the explicit solution scheme, in FLAC give stable solutions to unstable physical processes, such as sliding or overturning of a retaining wall. FLAC solves the full dynamic equations of motion, even for essentially static systems, which enables accurate modeling of unstable processes, e.g., retaining wall failures.

FLAC, like FLUSH, has restrictions associated with the wavelength associated with the highest frequency transmitted within the grid. A procedure similar to that used to design the FLUSH mesh and involving 1-D soil column analyses, via SHAKE, is used to lay out the FLAC grid for the dynamic retaining wall problem analyzed and for the specified acceleration time-history. Section 3.3.4 of Green and Ebeling (2002) discuss the dimensions of the finite difference grid and the maximum frequency that can pass through without numerical distortion.

A disadvantage of FLAC is the long computational times, particularly when modeling stiff materials, which have large physical wave speeds. The size of the time-step depends on the dimension of the elements, the wave speed of the material, and the type of damping specified (i.e., mass proportional or stiffness proportional), where stiffness proportional, to include Rayleigh damping, requires a much smaller time step. The critical time step for numerical stability and accuracy considerations is automatically computed by FLAC, based on these factors listed. For those readers unfamiliar with the concept of critical time-step for numerical stability and accuracy considerations in a seismic time-history engineering analysis procedure, please refer to Ebeling (1992), Part V, or to Ebeling et al. (1997a). The Lagrangian formulation in FLAC updates the grid coordinates each time-step, thus allowing large cumulative deformations to be modeled. This is in contrast to Eulerian formulation in which the material moves and deforms relative to a fixed grid, and is therefore limited to small deformation analyses.

1.1.2.3 FLUSH versus FLAC

The advantages of FLUSH are that it has considerably faster run times than FLAC and has been applied to a number of dynamic SSI problems. FLUSH is now freely downloadable from the Internet. The major disadvantage of FLUSH is that it does not allow for permanent displacement of the wall (although strain softening associated with earthquake-induced soil or rock deformations are accounted for in the analysis). A disadvantage of FLAC is that the earthquake engineering community and the Corps is just now developing modeling procedures for the application of FLAC to dynamic SSI problems, learning how to perform the analyses and interpret the computed results.

1.1.3 Sliding block methods

Sliding block methods of analysis of earth retaining structures can be viewed as a compromise between the simplistic pseudostatic methods, with a preselected seismic coefficient, and the computationally complex finite element or finite-difference based stress-deformation methods of analysis. Sliding block methods of analysis calculate a permanent deformation of a retaining structural system initiated by a user specified design earthquake event.

The numerous variations of rigid sliding block methods of seismic analysis as applied to slopes, earthen dams, retaining wall systems, and foundations have their roots in the methodology outlined in Newmark (1965) and what has come to be known as the Newmark sliding block model.¹ This problem was first studied in detail by Newmark (1965) using the sliding block on a sloping plane analogy. Procedural refinements were contributed by Franklin and Chang (1977); Wong (1982); Whitman and Liao (1985a, 1985b); Ambraseys and Menu (1988); and others. Makdisi and Seed (1978) and Idriss (1985, Figure 47) proposed relationships based on a modification to the Newmark permanent displacement procedure to allow for dynamic response considerations.

¹ An interesting footnote in seismic engineering history is given in Whitman (2000): Dr. Robert Whitman, Professor Emeritus of MIT, in 1953 performed a calculation of the permanent displacement of a slope as a result of earthquake-induced ground motions using a sliding block concept for a consulting job that Professor Donald Taylor (of MIT) had with the U.S. Army Corps of Engineers. Professor Newmark was part of the same consulting panel and sent word back to Dr. Whitman that he found this approach to be interesting, and that if he (Whitman) did not pursue it, he (Newmark) would. Dr. Whitman did not, and Professor Newmark did. Professor Newmark's research culminated in his (now classic) 1965 Geotechnique paper on this topic, the fifth Rankine lecture.

1.1.3.1 Concepts of Newmark's sliding (rigid) block method of analysis

Franklin and Chang (1977) and Hynes-Griffin and Franklin (1984) illustrate key concepts of a Newmark sliding block analysis using a potential sliding mass within an embankment under earthquake loading. The problems' engineering idealization is shown in Figure 1.3. The Figure 1.3a potential sliding mass is in a condition of incipient sliding with full mobilization of the shear resistance for the soil along the slip plane shown in this figure. The corresponding sliding factor of safety is equal to unity. This condition results from the acceleration of the earthen mass into the embankment (i.e., to the left) and away from the cut. W is the weight of the sliding mass. The force N times W in this figure is the inertia force required to reduce the sliding factor of safety to unity. By D'Alembert's principle, the inertia force, N times W , is applied pseudostatically to the soil mass in a direction opposite to acceleration of the mass, N times g , with N being a decimal fraction of the acceleration of gravity g (the universal gravitational constant). The acceleration of the soil mass contained within the slip plane shown in Figure 1.3a is limited to an acceleration value of N times g because the shear stress required for equilibrium along the slip plane can never be less than that of the shear strength of the soil. To state this in another way, the sliding factor of safety can never be less than 1.0. So, if the earthquake induced ground acceleration should increase to a value greater than the value N times g , the Figure 1.3a mass above this slip plane would move downhill relative to the embankment. During this permanent slope displacement, the "sliding" mass would only feel the acceleration value N times g and not the ground acceleration values. The acceleration value of N times g was referred to as the "yield acceleration" in these early publications associated with the seismically induced permanent movement of a slope.

Figure 1.3b shows the force polygon for the "sliding" soil mass. The angle inclination θ of the inertia force may be found as the angle that is most critical; that is, the angle that minimizes N . Franklin and Chang (1977) and Hynes-Griffin and Franklin (1984) state that the angle θ is typically set equal to zero in seismic slope stability analyses. The angle β is the direction of the resultant force S of the distributed shear stresses along the interface and is determined during the course of the slope stability analyses to determine the value of N that results in a sliding factor of safety of 1.0 for the slope's sliding mass. The force P is the resultant of the normal forces.

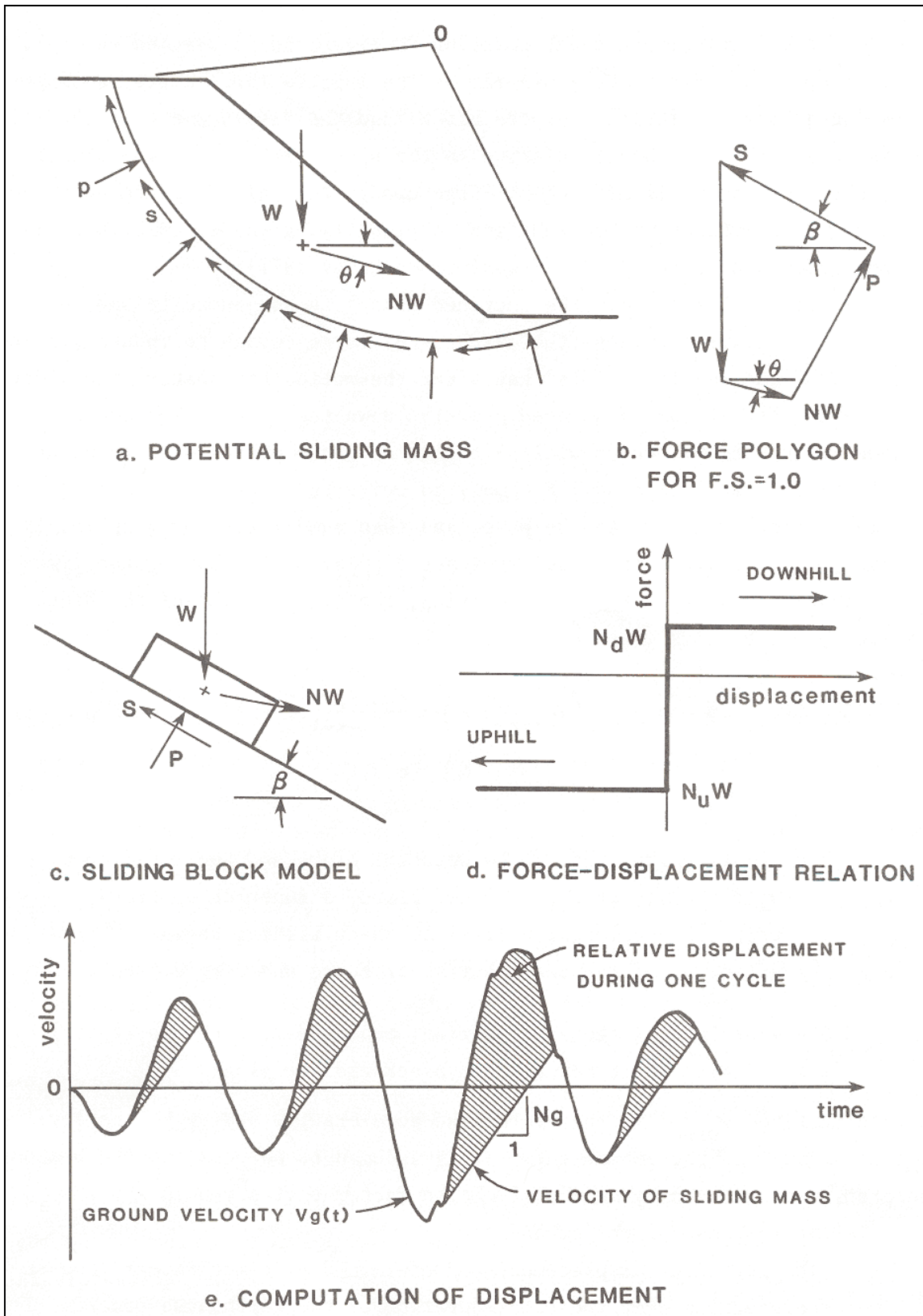


Figure 1.3. Elements of the Newmark (rigid) sliding block method of analysis (from Hynes-Griffin and Franklin 1984).

The Figure 1.3b force polygon for the slope mass being applied to an “idealized” sliding rigid block model on a plane inclined at an angle β to horizontal is illustrated in Figure 1.3c. This idealization is the basis for the designation as the Newmark’s sliding (rigid) block method of analysis, representing the sliding mass of the embankment.

Figure 1.3d is an idealization of the limiting force versus displacement relationships applied to this problem. The resistance to sliding is assumed to be rigid-plastic, as shown in this figure. This resistance to sliding is unsymmetrical because the block can slide downhill more easily than uphill. The usual practice is to assume that uphill sliding never occurs; i.e., a worst-case assumption, and results in the greatest permanent displacement (downhill).

Figure 1.3e shows a time-history plot of the velocity of the embankment during earthquake shaking. Not shown is the corresponding (ground/embankment) acceleration time-history for this particular earthquake event. (Earthquake shaking is usually represented by an acceleration time-history. Because the ground acceleration varies with time, it can be represented by variable fraction A times the constant acceleration of gravity g . Recall that the integral of the acceleration time-history is equal to the Figure 1.3e velocity time-history.) For an embankment that suffers a slope failure caused by seismic ground motions, the total permanent displacement of a sliding mass relative to the base is the sum of the increments of displacement occurring during a number of individual pulses of ground motion. These incremental relative displacements are determined as follows: For each time the acceleration of the embankment, equal to A times g , is greater than the constant N times g , relative displacements (between the slope mass and the embankment) will initiate. There are four of these incremental, permanent displacement pulses occurring in Figure 1.3e. During slope displacements, the sliding mass will move at a slower velocity than will the embankment (designated the ground velocity in this figure). The integral of the difference in velocities between the sliding mass and the embankment velocity is equal to the incremental, relative displacement of the sliding mass. The total permanent downhill displacement is the sum of the four incremental displacement cycles depicted in Figure 1.3e. Note that incremental sliding of the slope terminates when the velocities of the embankment and of the sliding mass converge to the same value.

Summary: The idealized engineering problem depicted in Figure 1.3 describes the essential features of the Newmark sliding (rigid) block method of analysis as first applied to slopes:

- There is a level of earthquake shaking as characterized in terms of a value of acceleration designated N times g (i.e., the yield acceleration), which fully mobilizes the shear resistance along a sliding plane of a potential sliding mass; corresponding to a factor of safety against sliding of 1.0 for that mass.
- For a given embankment (or equivalently, ground) acceleration time-history in which acceleration(s) exceed the value of N times g , incremental permanent displacements will occur.
- The magnitude of the incremental displacements may be numerically quantified using the procedure outlined in Figure 1.3e.
- Total permanent displacement is equal to the sum of the incremental displacement pulses.

Although this procedure has been applied to other types of structures, the essential features of the Newmark (rigid) sliding block method of analysis remain the same.

1.1.3.2 Sliding block method of analysis applied to retaining structures

A variation proposed on the Newmark sliding block method of analysis for earth retaining structures is the displacement controlled approach (Section 6.3 in Ebeling and Morrison 1992). It incorporates retaining wall movements explicitly determined in the stability analysis of earth retaining structures. This methodology is applied as either the displacement-controlled design of (a new) retaining wall, or as an analysis of earthquake induced displacements of an existing retaining wall.

- **The displacement controlled design of retaining wall:** In this approach, the retaining wall geometry is the primary variable. It is, in effect, a procedure for choosing a seismic coefficient based upon explicit choice of an allowable permanent displacement. Having selected the seismic coefficient, the usual stability analysis against sliding is performed, including the use of the Mononobe-Okabe equations (or, alternatively, a sweep search, soil wedge solution). The wall is proportioned to resist the applied earth and inertial force loadings. No safety factor is required to be applied to the required weight of wall evaluated by this approach; the appropriate level of

safety is incorporated into the step used to calculate the horizontal seismic coefficient. This procedure of analysis represents an improved alternative to the conventional equilibrium method of analysis that expresses the stability of a rigid wall (of prescribed geometry and material properties) in terms of a pseudostatic method with a preselected seismic coefficient and preselected factor of safety against sliding along its base, discussed in Section 1.1.1. Section 6.3.1 in Ebeling and Morrison (1992) outlines the computational steps in the (seismic) displacement controlled design of a retaining wall.

- The analysis of earthquake induced displacements of a retaining wall:** The retaining wall geometry and material properties are typically first established for the usual, unusual and extreme load cases with non-seismic loadings. In the subsequent seismic analysis of the retaining wall using the earthquake induced displacement approach, the primary variable is the permanent displacement. The seismic inertia coefficient N^* that reduces the sliding factor of safety for the driving soil wedge and the structural wedge to unity is first determined. Ebeling and Morrison (1992), along with others, have designated the acceleration value N^*g for a retaining wall as its “maximum transmissible acceleration.” Figure 1.4 shows the driving soil wedge and structural wedge treated as a single rigid block in this approach.

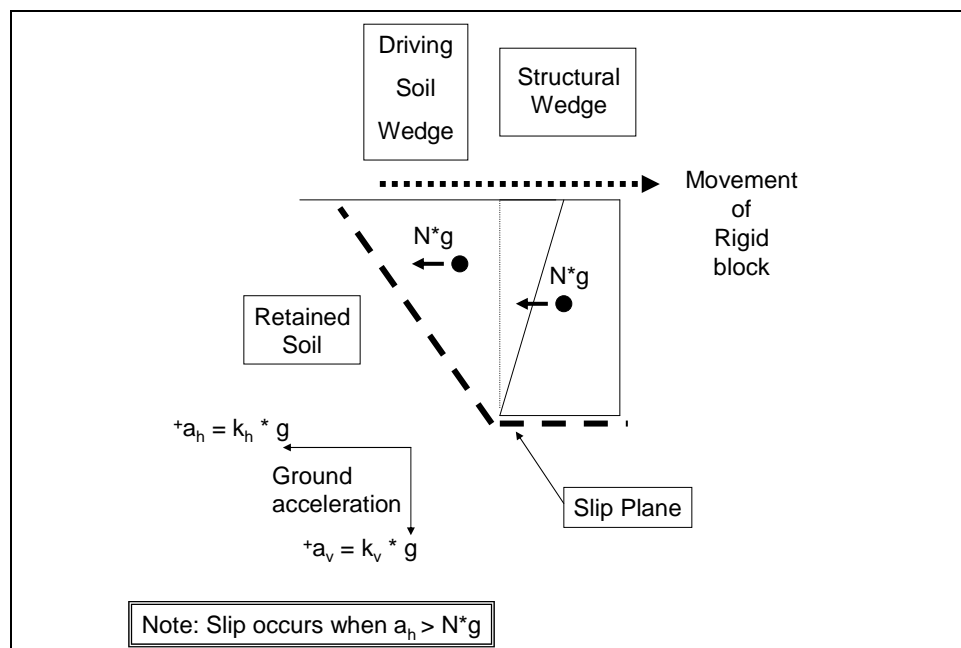


Figure 1.4. Gravity retaining wall and failure wedge treated as a sliding block (after Whitman 1990).

The resulting permanent seismic displacement of the retaining wall is subsequently determined for the earthquake specified by the design engineer. Section 6.3.2 in Ebeling and Morrison (1992) outlines the computational steps in the analysis of earthquake induced displacements of a retaining wall (with specified geometry and material properties).

The analytical procedure that was developed by Richards and Elms (1979) recognizes that for some limiting value of horizontal acceleration, i.e., the maximum transmissible acceleration identified as N^*g in Figure 1.4, the horizontal inertia force acting on a retaining wall with no toe fill will nominally exceed the shear resistance provided by the foundation along the interface between the base of the wall and the foundation.

This implies that although the soil base (i.e., the foundation to the wall) may be accelerating horizontally at values greater than N^*g , the wall will be sliding along the base under the action of the horizontal inertial force that corresponds to the horizontal acceleration N^*g . This results in movement of the soil base relative to the movement of the wall and vice-versa. The relative movement originates at the point in time designated as point *a* in the first time-history shown in Figure 1.5 and continues until the (absolute) velocity of the base is equal to the (absolute) velocity of the wall, designated as time point *b* in the second time-history of this same figure.

The (absolute) velocity of the soil base is equal to the integral over time of the soil acceleration, and the (absolute) velocity of the wall between time points *a* and *b* is equal to the integral of the wall acceleration, which is a constant N^*g . The relative velocity of the wall, v_r , shown in the third time-history is equal to the integral of the difference between the base acceleration and the constant wall acceleration N^*g between time points *a* and *b*, as shown in Figure 1.5. The relative displacement of the wall is the fourth time-history and equal to the integral of the relative velocity of the wall, which occurs between the two points in time labeled *a* and *b* in Figure 1.5. Note that at time point *b*, when the wall is stopping its first increment of relative movement, the acceleration is less than N^*g , as shown in the first time-history. This observation demonstrates that the relative velocity of the wall (shown in the third time-history) controls the cessation of the seismically induced incremental wall movement. Additional incremental relative displacements occur for the wall between the two latter points in time labeled *c* and *d* in Figure 1.5, with the residual relative wall displacements, d_r , equal to the cumulative relative displacements computed during

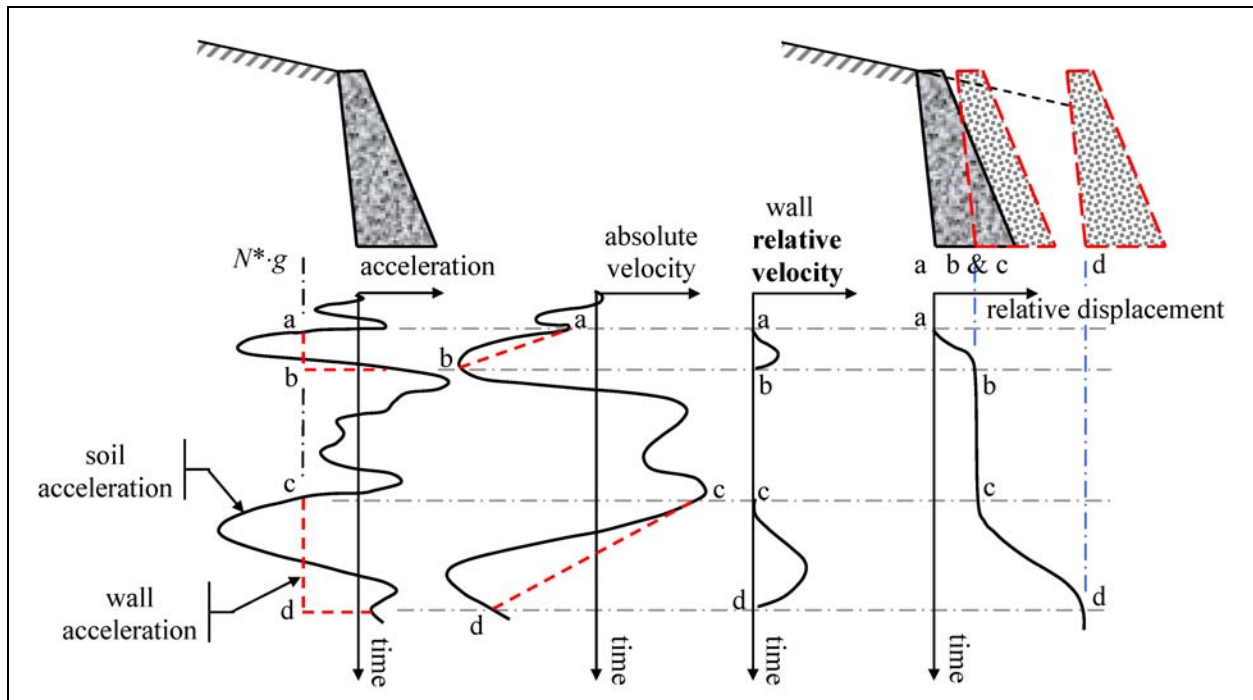


Figure 1.5. Incremental failure by base sliding (adapted from Richards and Elms 1979).

the entire time of earthquake shaking (labeled as point *d* in the fourth time-history). Lastly, although N^*g is referred to as the maximum transmissible acceleration in retaining structure permanent deformation problems, it is equivalent to the yield acceleration that is associated with permanent deformation problems for slopes/embankments. In the permanent deformation research conducted by Cai and Bathurst (1996), the term “critical acceleration” was used. The terms critical acceleration, maximum transmissible acceleration and yield acceleration all describe the same quantity.

Ebeling and Morrison (1992) observe that the approach has been reasonably well validated for the case of walls retaining granular, moist backfills (i.e., no water table). A key item is the selection of suitable shear strength parameters. In an effective stress analysis, the issue of the suitable friction angle is particularly troublesome when the peak friction angle is significantly greater than the residual friction angle. In the displacement controlled approach examples given in Section 6.2 of Ebeling and Morrison (1992), effective stress based shear strength parameters (i.e., effective cohesion c' and effective angle of internal friction ϕ') were used to define the shear strength of the dilative granular backfills, with c' set equal to zero in all cases due to the level of deformations anticipated in a sliding block analysis during seismic shaking. In 1992, Ebeling and Morrison

concluded that using the residual friction angle in a sliding block analysis is conservative, and that this should be the usual practice for displacement based analysis of granular retained soils. For the Ebeling et al. (2007) report discussing $C_{\text{orps}}W_{\text{allSlip}}$, the primary author would broaden the concept to the assignment of effective (or total) shear strength parameters for the retained soil to be consistent with the level of shearing-induced deformations encountered for each design earthquake in a sliding block analysis, and note that active earth pressures are used to define the loading imposed on the structural wedge by the driving soil wedge. (Refer to Table 1.1 for guidance regarding wall movements required to fully mobilize the shear resistance within the retained soil during earthquake shaking.)

$C_{\text{orps}}W_{\text{allSlip}}$ uses a graphical user interface for input of wall geometry, input of material properties, input/verification of earthquake time-history files, and for visualization of results. $C_{\text{orps}}W_{\text{allSlip}}$ has the ability to perform a sliding analysis of a user specified retaining wall section, such as the rock-founded retaining wall shown in Figure 1.6.

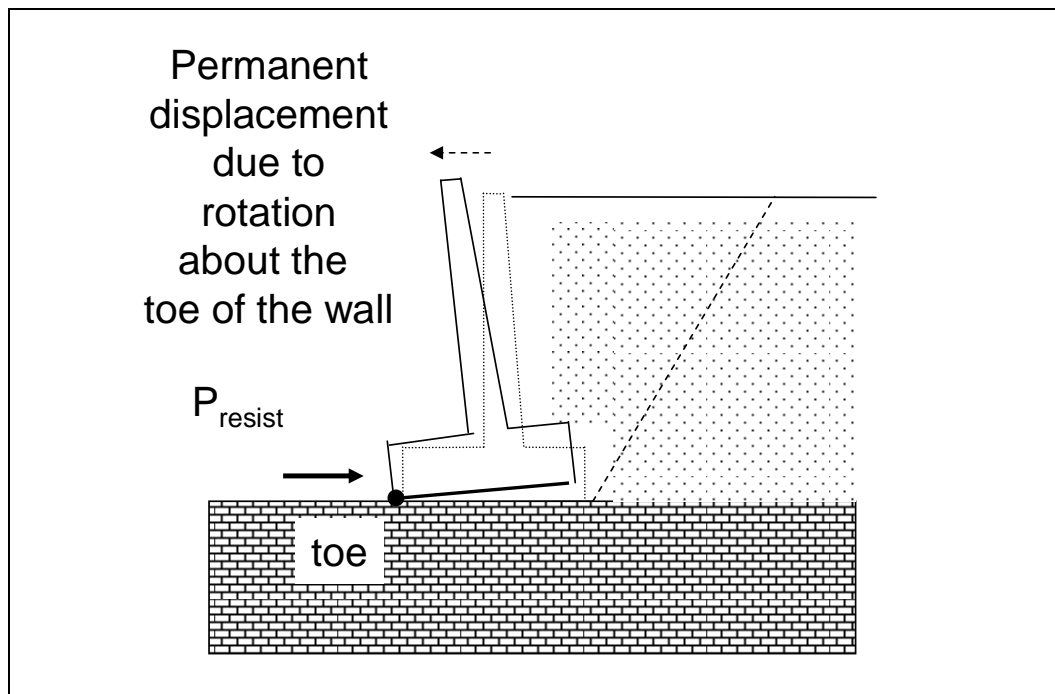


Figure 1.6. Idealized permanent, seismically induced displacement due to the rotation about the toe of a rock-founded wall retaining moist backfill, with toe restraint, computed using $C_{\text{orps}}W_{\text{allRotate}}$.

This retaining wall is an idealization of the Figure 1.7 cantilever retaining wall problem in which the toe of the wall is buttressed by a concrete slab in a spillway channel. The engineer provides the overall wall and retained soil geometry and material properties. This PC-based software will compute for the user the value for the maximum transmissible acceleration of the retaining wall system.

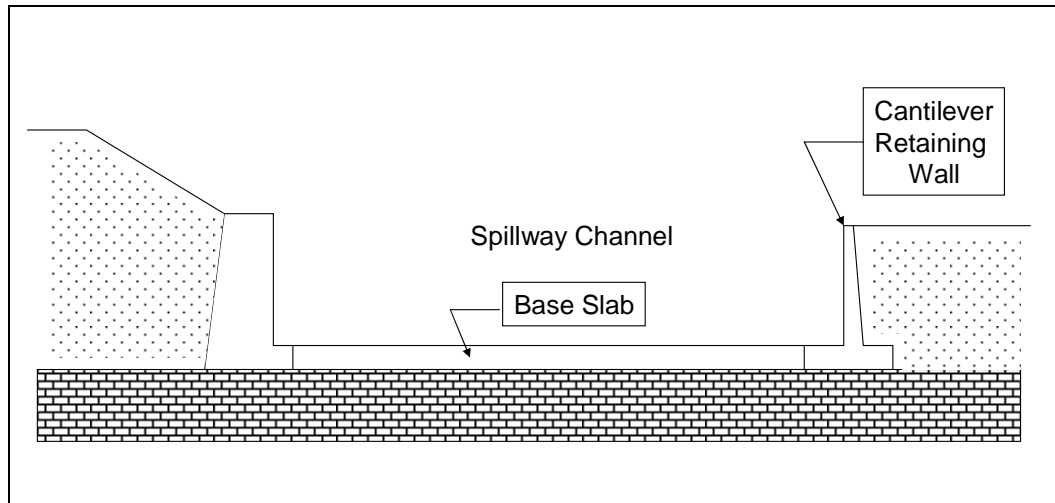


Figure 1.7. Rock-founded cantilever retaining wall bordering a spillway channel.

The PC-based program, Newmark, which is discussed in this report, requires the value for the maximum transmissible acceleration (i.e., the yield acceleration or critical acceleration) as input. For a user specified earth retaining structure, for example, the maximum transmissible acceleration (i.e., the yield acceleration or the critical acceleration) is computed using the hand-calculation procedure outlined in Ebeling and Morrison (1992).

1.2 New rotational analysis model based on a rigid block problem formulation

The permanent displacement of retaining structures is not restricted to walls that slide along their base as a result of inertial forces imparted during earthquake shaking. For some retaining wall system configurations and material properties, permanent displacements may instead result from the rotation of a retaining wall about a point along its wall-to-foundation interface.

The idealized permanent displacement caused by rigid body noncentroidal rotation of a retaining wall about its toe during earthquake shaking and

with toe restraint is shown in Figure 1.6. The buttressing effect of a reinforced concrete slab (Figure 1.7) is represented in this simplified dynamic model by the user-specified force P_{resist} acting on a vertical section extending upward from the toe of the wall as per, for example, Strom and Ebeling (2004).

The Figure 1.7 cantilever retaining wall that is buttressed by an invert spillway slab (which is a reinforced concrete slab), exemplify a category of Corps retaining walls that may be susceptible to earthquake induced rotation. The primary author of this report is of the opinion that the assignment of the point of rotation to the toe of the wall becomes a reasonable simplifying assumption because of the constraint provided by the Figure 1.6 invert spillway slab to lateral translations, combined with the effects of the stiff, competent rock foundation. A key result of a $C_{orps}W_{all}Rotate$ analysis, idealized in Figure 1.6, is the permanent, earthquake-induced displacement of a retaining wall resulting from rotation about the toe of the wall.

Like the Zeng and Steedman (2000) rigid gravity wall formulation, discussed in Ebeling and White (2006), rotation of a rigid block model of the structural retaining wall system in this new formulation is assumed to occur about the toe of the wall (i.e., the rigid block is “pined” to the rigid base at its toe). This new Ebeling and White procedure differs from the Steedman and Zeng formulation by the following:

- Formal consideration of a toe-restraint in the analysis (due to the presence of a reinforced concrete slab against the toe of the wall)
- The ability of the user to assign a vertical acceleration time-history in addition to a horizontal acceleration time-history
- Consideration of a pool of water in front of the wall, a submerged foundation and a partially submerged retained soil (Figure 1.8)
- The implementation of this formulation within corresponding PC software $C_{orps}W_{all}Rotate$ using a graphical user interface for input of geometry, input of material properties, input/verification of earthquake time-history files, and for visualization of results
- A sweep-search wedge formulation within the retained soil is used to determine the value of P_{AE} rather than relying on the Mononobe-Okabe relationship (cited in the Steedman and Zeng 1996 formulation).

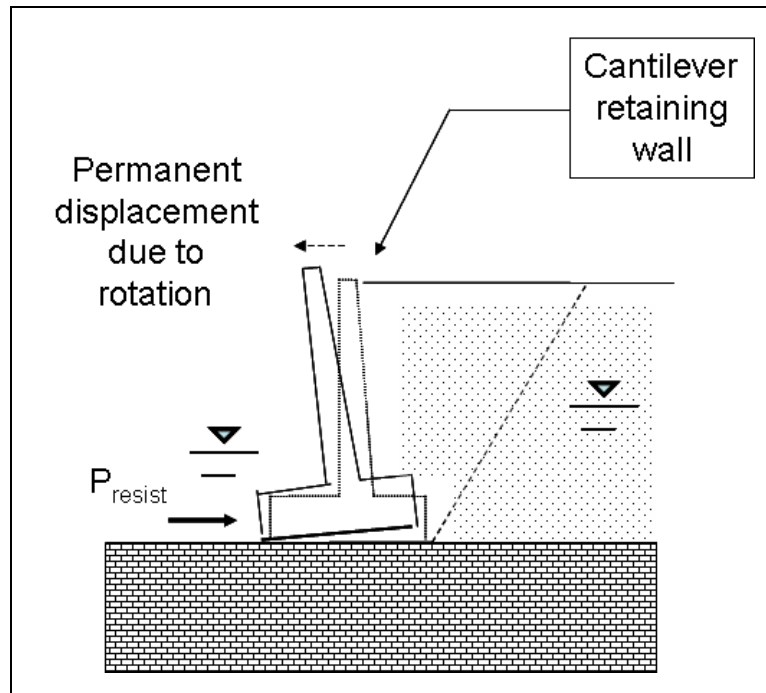


Figure 1.8. Permanent, seismically induced displacement due to the rotation about the toe of a rock-founded, partially submerged cantilever retaining wall and with toe restraint, computed using $C_{orps}W_{all}Rotate$.

Recall that the Mononobe-Okabe relationship is valid for a retained soil with a constant surface slope and whose strength is characterized by the Mohr-Coulomb shear strength parameter ϕ (e.g., refer to Equations 33 through 35 in Ebeling and Morrison 1992).

The advantage of the sweep-search method, as formulated and implemented in $C_{orps}W_{all}Rotate$ and in $C_{orps}W_{all}Slip$, is that it allows for the analysis of bilinear ground surfaces (Figure 1.9) and/or the analysis of “cohesive” (S_u) soils.¹

¹ In the formulation described in this report, a cohesive soil refers to a total stress analysis in which the shear strength of the soil is characterized in terms of its undrained shear strength S_u . Note that minimum wall movements needed to fully mobilize the shear resistance of the soil, on the order of those listed in Table 1.1, will impact the characterization of the retained soil shear strength parameters used in the permanent displacement analysis.

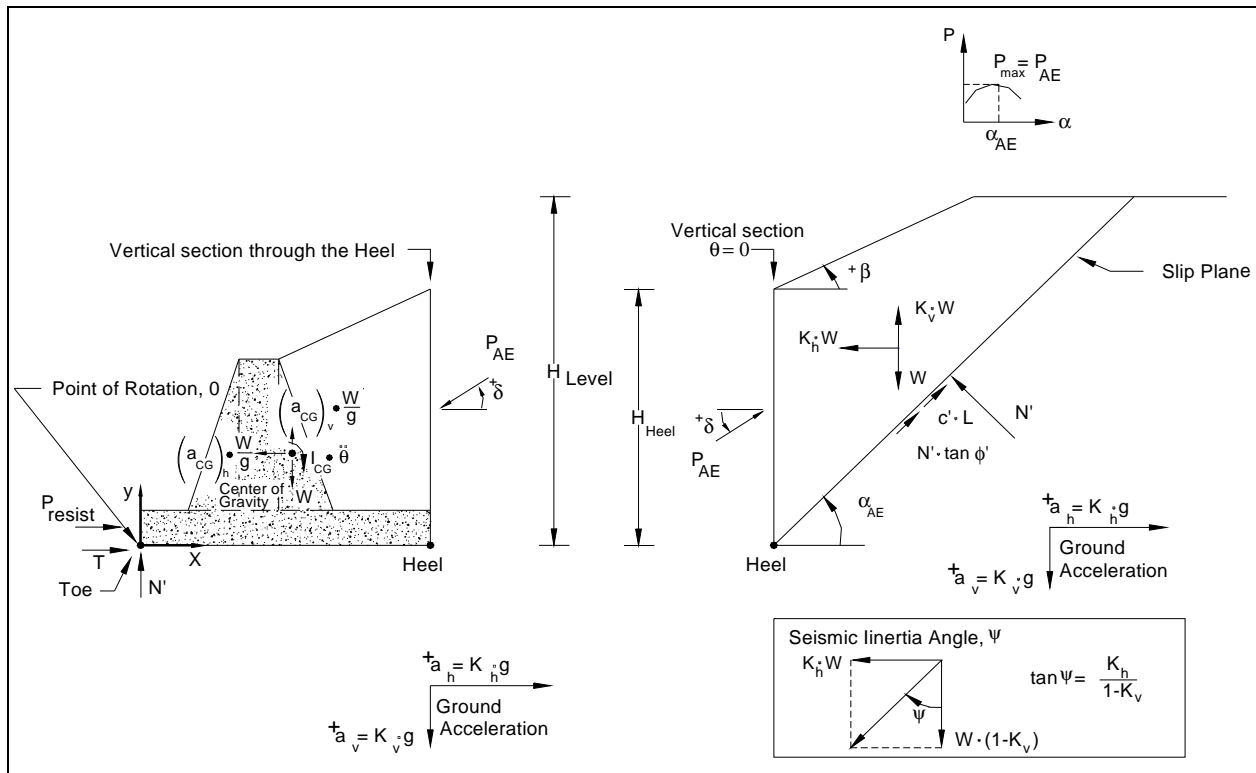


Figure 1.9. Structural wedge with toe resistance retaining a driving soil wedge with a bilinear moist slope (i.e., no water table) analyzed by effective stress analysis with full mobilization of (c', ϕ') shear resistance within the backfill.

1.3 The tendency of a retaining wall to slide or to rotate during earthquake shaking

An important difference between the Newmark sliding block method of analysis for earth retaining structures (i.e., the displacement controlled approach that is discussed in Section 1.1.3) and the rotational analysis of a retaining structure modeled as a rigid block is the acceleration imparted to the rigid block. When a rigid block undergoes permanent sliding displacement during earthquake shaking, the largest magnitude horizontal acceleration felt by the rigid block (and the retaining structure contained within the rigid block) is N^*g , which is less than the peak value for ground acceleration. The maximum transmissible acceleration N^*g (i.e., the yield acceleration or critical acceleration) is not the horizontal ground (or, equivalently, the rigid base) acceleration representing the earthquake. For a rigid block that undergoes rotation during earthquake shaking, the accelerations felt by this rigid block during shaking are those of the ground acceleration time-history. This is because continuous contact between the rigid block undergoing rotation and the ground is maintained at the point of

rotation, i.e., the toe in Figure 1.6, during the entire earthquake shaking process.

Thus for a rigid block that undergoes rotation during earthquake shaking, the horizontal acceleration of (rigid) mass center is a function not only of the horizontal ground acceleration but it is also a function of the angular acceleration and the angular velocity during rotation (see Ebeling and White 2006). This differs from the situation of a rigid block that undergoes permanent sliding displacement during earthquake shaking; the largest magnitude horizontal acceleration felt by this rigid block is N^*g . Recall that N^*g , the maximum transmissible acceleration (i.e., the yield acceleration or critical acceleration) is not the user-defined, horizontal ground (or, equivalently, rigid base) acceleration. Unlike the sliding (rigid) block model, which effectively isolates the sliding block from the shaking base below, the rotating rigid block model continues to transmit horizontal acceleration through the “pin”, located at the toe of the wall, into the wall.

A key step in the evaluation process of the idealized rigid block formulations of Ebeling et al. (2007) and of Ebeling and White (2006) for translation and for rotation is the computation of the maximum transmissible acceleration and the computation of threshold value of acceleration corresponding to lift-off the base of the wall in rotation. Comparison of these values determines if the wall will tend to slide before it will rotate or visa versa. The lower of the two values dictates the kinematic mechanism for the retaining wall system model. Both of these computational steps are incorporated in both $C_{\text{Corps}}W_{\text{allSlip}}$ and $C_{\text{Corps}}W_{\text{allRotate}}$. The PC-based program Newmark, described and used in the R&D of this report, does not perform this check nor does it do rotational permanent deformation analyses. For this type of rotational analysis the reader is referred to $C_{\text{Corps}}W_{\text{allRotate}}$.

1.4 Seismic design criteria for Corps retaining structures

Current Corps engineering methodology is to evaluate retaining walls for Usual, Unusual and Extreme Loadings. Consideration of earthquake loadings is part of the design process for Corps earth retaining structures. Engineer Regulation (ER) 1110-2-1806 (Headquarters, U.S. Army Corps of Engineers (HQUSACE) 1995) provides requirements governing the seismic design and evaluation of structures located at Corps projects. The engineering procedures outlined in this Corps document are applicable to the analysis of existing, or the design of new earth-retaining structures.

The Corps regulation for earthquake loadings, ER 1110-2-1806, specifies two project-specific earthquakes, the Operational Basis Earthquake (OBE) and the Maximum Design Earthquake (MDE).

The OBE is an earthquake that can reasonably be expected to occur within the service life of the project, that is, with a 50-percent probability of exceedance during the service life. (This corresponds to a return period of 144 years for a project with a service life of 100 years.) The associated performance requirement is that the project functions with little or no damage, and without interruption of function. The purpose of the OBE is to protect against economic losses from damage or loss of service, and therefore alternative choices of return period for the OBE may be based on economic considerations. The OBE is determined by a Probabilistic Seismic Hazard Analysis (PSHA). The OBE is classified as an Unusual event. Retaining walls are expected to remain serviceable and operable immediately following an OBE earthquake event, or immediately following any earthquake that can reasonably be expected to occur within the service life of the project.

The MDE is the maximum level of ground motion for which a structure is designed or evaluated. The associated performance requirement is that the project performs without catastrophic failure, such as an uncontrolled release of a reservoir, although severe damage or economic loss may be tolerated. For critical features, the MDE is the same as the Maximum Credible Earthquake (MCE). [Section 5(a) and Table B-1 in ER 1110-2-1806 outlines the assessment of the hazard potential classification of Civil Works projects and is related to the consequences of project failure. Critical features are the engineering structures, natural site conditions, or operating equipment and utilities at high hazard projects whose failure during earthquake could result, in loss of life.] For all other features, the MDE shall be selected as a lesser earthquake than the MCE, which provides economical designs meeting appropriate safety standards. The MDE is the maximum level of ground motion for which a structure is designed or evaluated. Although not formally stated in the ER, recent (limited) application to select, normal Corps (non-critical) structures is to assume the MDE is an earthquake that has a 10 percent chance of being exceeded in a 100-year period (or a 975-year return period). The MDE for normal structures is determined by PSHA. For critical structures, the MDE is the Maximum Credible Earthquake (MCE), which is determined by a deterministic seismic hazard assessment (DSHA). The MCE is defined as the

greatest earthquake that can reasonably be expected to be generated on a specific source, on the basis of seismological and geological evidence. Significant damage resulting from an MDE event can be considered as acceptable provided the damaged structure can be repaired and put back in service without risk to life.

Factors of safety and safety requirements for retaining walls subject to seismic loading conditions are provided in EM 1110-2-2100. This supersedes the stability guidance for retaining walls contained in EM 1110-2-2502 (but not the engineering procedures, which are based on the simplified pseudo-static procedure of analysis).

Factors of safety for sliding and flotation, and the safety provisions related to resultant location and allowable bearing capacity, contained in EM 1110-2-2100 are dependent on:

- Load condition category (usual, unusual, or extreme)
- Site information knowledge (well-defined, ordinary, or limited), and
- Structure importance (normal, or critical)

EM 1110-2-2100 associates each of the three load condition categories to a range in annual probability (or, equivalently, a range in return period). Additional “structure specific” information related to load condition categories and probabilities are contained in Appendix B of EM 1110-2-2100.

1.5 Axial load capacity of spillway invert slabs

Reinforced concrete slabs provide an important contribution to the overall seismic stability of retaining walls. Figure 1.7 shows, for example, an invert spillway buttressing a cantilever retaining wall that borders the spillway channel. Key to the seismic performance of this spillway retaining wall is the stabilizing force that the channel invert slab exerts at the toe of this wall. The magnitude of this stabilizing force will depend on the limit state axial load capacity of this invert slab.

Invert slabs can be founded on earth or rock. Types of construction used by the Corps include an “independent block plan” and a “continuous reinforcing plan”. Invert slabs, when loaded axially, can exhibit either short column or long column behavior, with the later referring to slabs

whose axial capacity is reduced by second-order deformations (i.e., $P \bullet \Delta$ effects).

Slab capacity, in terms of axial load versus moment interaction, is determined based on ultimate strength design principles, which can be applied to both unreinforced (plain concrete) and reinforced concrete invert slab sections. Influences from the subgrade reaction, slab dead load, and axial load eccentricity, when considered in a second-order analysis, suggest the axial load capacity can be based on a short column design with second-order displacements resulting from $P \bullet \Delta$ effects having little if any effect on column axial load capacity, according to the Strom and Ebeling (2004).

The axial load resistance P_{resist} , provided by the Figure 1.7 invert slab, is illustrated in Figure 1.6. Limited investigations, by Strom and Ebeling (2004), based on the Corps minimum thickness for invert slabs constructed on rock and earth, and for both continuous reinforcing plans and independent block plans, indicate the limit state axial load capacity, or ultimate axial load resistance of the slab (P_{resist}) may be on the order of:

- 120 kips per foot width of slab for a 1.0 foot thick invert slab on rock
- 240 kips per foot width of slab for a 2.0 foot thick invert slab on soil

The above values are valid for both anchored and unanchored invert slabs, and for the minimum contraction joint spacings typically found on Corps projects. However, a site-specific evaluation of the limiting axial resisting force resulting from the buttressing effect of the type of slab on the toe of a retaining wall is required. Refer to Strom and Ebeling (2004) for a simplified engineering methodology for the assessment of P_{resist} for all types of slabs buttressing all types of retaining structures, including the Figure 1.7 invert spillway slab.

1.6 Background and research objective

EM 1110-2-2502, Retaining and Flood Walls, gives engineering procedures that are currently being used by District Engineers in their initial assessment of seismic wall performance of existing earth retaining structures and the (preliminary) sizing of new retaining structures. The engineering procedures given in EM 1110-2-2502 for retaining walls make extensive use of the simplified pseudo-static procedure of analysis of earth retaining structures and express wall performance criteria in terms of computed factors of safety against sliding and bearing failure, and base area in

compression. The simplified pseudo-static procedure of analysis makes it difficult to interpret the actual wall performance for Corps projects subjected to “strong” design ground motions because of simplifications made in the procedure of analysis. In a pseudo-static analysis, an oversimplification occurs when the engineer is forced to render the complex, horizontal and vertical earthquake acceleration time-history events to constant values of accelerations and to assume a constant direction for each. These constant values are denoted as the pseudo-static acceleration coefficients in the horizontal and vertical directions (refer to Section 1.1.1 of this report). The engineer is also required to assume a constant direction for each of these components. An acceleration time-history, in actuality, varies both in magnitude and in direction with time.

The simplified pseudo-static procedure does not allow for interpretation of actual wall performance by District Engineers. Intense shaking imparted by the OBE and MCE design events makes the interpretation of the simplified procedure of analysis even more difficult. The more important questions for the wall are whether the wall slides into the spillway basin, or rotates into the spillway basin, or even tips over onto its side during the earthquake event. The simplified pseudo-static procedure of analysis is not capable of answering these questions. The answers depend on the magnitude of the pseudo-static coefficient used in the calculations compared to the magnitude of the peak values for the acceleration pulses as well as the number and duration of these strong shaking acceleration pulses in the design earthquake event time-history. When considering both horizontal and vertical accelerations, the resulting wall response is further complicated by the time-history of phasing between the pulses of horizontal and vertical accelerations. Only the permanent wall sliding displacement/wall rotation method of time-history analysis can answer these questions. Again, wall displacements will influence the seismic earth pressure forces imparted on the wall by the retained soil.

Formal consideration of the permanent seismic wall displacement in the seismic design process for Corps-type retaining structures is given in Ebeling and Morrison (1992). The key aspect of the engineering approach presented in this Corps document is that simplified procedures for computing the seismically induced earth loads on retaining structures are also dependent upon the amount of permanent wall displacement that is expected to occur for each specified design earthquake. The Ebeling and Morrison simplified engineering procedures for Corps retaining structures

are geared toward hand calculations. The engineering formulation and corresponding PC software $C_{\text{Corps}}W_{\text{allSlip}}$ (Ebeling et al. 2007) extend these simplified procedures to walls that slide during earthquake shaking and make possible the use of acceleration time-histories in the Corps design/analysis process when time-histories are made available on Corps projects. $C_{\text{Corps}}W_{\text{allSlip}}$ may be used to predict permanent seismically induced translational displacements of walls retaining backfill, with or without a toe restraint. It is particularly applicable to rock-founded L-walls and T-walls (i.e., cantilever retaining walls) which border spillway channels (Figure 1.7). The PC software Newmark discussed in this report may also be used to perform the same permanent (translational) deformation analysis as $C_{\text{Corps}}W_{\text{allSlip}}$, but does require the additional step of the user computing and providing as input the maximum transmissible acceleration (i.e., the yield acceleration or the critical acceleration).

The software Newmark is also capable of performing regression analyses on multiple horizontal acceleration time histories for up to three pre-set (mathematical) formulations, for the purpose of developing simplified non-dimensional (simplified) permanent displacement relationships for use in a Simplified Sliding Block Analysis of a structural system. The main purpose of developing the software Newmark in this R&D effort is to facilitate the processing of multiple rock acceleration time histories and to perform a statistical analysis of the computed permanent displacements for multiple, user-defined critical accelerations. From these data, simplified permanent displacement relationships are derived, concluding in the selection of recommended relationships. These resulting simplified sliding block relationships based for rock-founded structures are based on data from rock acceleration time histories and will be implemented within $C_{\text{Corps}}W_{\text{allSlip}}$ (Ebeling et al. 2007) for Corps earth retaining structures and within $C_{\text{Corps}}D_{\text{amSlip}}$ (under development by Ebeling and Chase) for Corps rock-founded gravity dams.

1.7 Organization of report

Chapter 2 describes the numerical method implemented in the software Newmark for performing a translational (i.e., sliding) block analysis of a structural system model of e.g., a retaining structure or a rock-founded gravity dam, etc. The formulation used computes the permanent sliding displacement response of a structural system to an earthquake acceleration time-history via a Complete Time-History Analysis.

Chapter 3 describes three formulations used for developing simplified non-dimensional (simplified) permanent displacement relationships for use in a Simplified Sliding Block Analysis of a structural system. The regression analyses result in mean estimates and together with their standard error terms, also determine the 68 percent prediction intervals and 95 percent probability of non-exceedance upper bound estimates to seismically induced permanent (translational) displacement at the end of earthquake shaking.

Chapter 4 discusses the selection process and the characteristics of each of the 122 sets of baseline corrected “rock” acceleration time histories used in the regression analysis and the results of these analyses for the three simplified permanent (translational) displacement relationships introduced in Chapter 3.

Chapter 5 describes key aspects of the visual modeler and visual post-processor Newmark. Specifically, a description of the graphical user interface for input of value(s) of critical acceleration (i.e., the maximum transmissible acceleration or the yield acceleration), input/verification of earthquake time-history files, and for visualization of results is presented to make the user familiar with its operation.

Chapter 6 presents a summary of the recommended simplified permanent (translational) deformation relationships developed during the course of this research, conclusions and recommendations for additional research.

Appendix A is a listing and description of the Newmark ASCII input data file (file name: Newmark.in).

Appendix B is a listing and description of Newmark ASCII Data Output Files.

2 Translational Block Analysis of a Rock Founded Structural Model

2.1 Introduction

This chapter describes an engineering formulation developed for computing the permanent translational response of the Corps rock founded hydraulic structures (e.g., an earth retaining structure, a concrete gravity dam, etc.) to earthquake ground motions. The resulting engineering formulation is implemented within corresponding PC software Newmark using a graphical user interface for input/verification of earthquake time-history files, input of the hydraulic structures critical acceleration (i.e., maximum transmissible acceleration or yield acceleration) and for visualization of results. The PC software Newmark was developed to perform an analysis of the permanent sliding displacement response of a rigid block model of a structural section to a user specified earthquake acceleration time-history via a Complete Time-History Analysis. The Complete Time-History method of analysis is discussed first in this chapter. (Key aspects of the Visual Modeler, the PC-based Graphical User Interface (GUI) to Newmark are described in Chapter 5.) The main purpose of developing the software Newmark in this R&D effort is to facilitate the processing of multiple rock acceleration time histories and perform a statistical analysis (using the procedures discussed in Chapter 3) of the computed permanent displacements for multiple, user-defined critical accelerations. From this data, simplified permanent displacement relationships are derived (discussed in Chapter 4), with recommended relationships summarized in Chapter 6. These resulting simplified sliding block relationships for rock-founded structures will be implemented within $C_{\text{Corps}}W_{\text{allSlip}}$ (Ebeling et al. 2007) for earth retaining structures and within $C_{\text{Corps}}D_{\text{amSlip}}$ (under development by Ebeling and Chase) for Corps rock-founded gravity dams.

The software Newmark may also be used to compute the permanent (translational) displacement of a rigid block model for a single acceleration time-history. Besides an acceleration time-history, a user specified value for the structure's critical acceleration (i.e., maximum transmissible acceleration or yield acceleration) is required. Recall that the value for the critical acceleration (i.e., N^*g ; the maximum transmissible acceleration in Ebeling and Morrison (1992) terminology for retaining walls) is the

horizontal acceleration imparted to the rigid body model, that will nominally exceed the shear resistance provided by the foundation along (or immediately below) the interface between the base of the rigid body and the foundation (refer to Figure 1.4). Earth retaining structures and earthen slope/embankments were discussed in Chapter 1 with regard to (Newmark) permanent displacement based sliding block analysis resulting from earthquake shaking. Hand calculations of the critical acceleration (i.e., the maximum transmissible acceleration or the yield acceleration) for a particular earth retaining structure are described in Ebeling and Morrison (1992). Alternatively, $C_{\text{orps}}W_{\text{allSlip}}$ (Ebeling et al. 2007) may be used to automatically compute the rock-founded earth retaining structure's critical acceleration using the user defined geometry, retained soil and rock foundation properties (as well as the value for the structure's critical acceleration). Several popular slope stability software programs have the capability to compute the critical acceleration for an earthen slope/embankment. The computation of the critical acceleration is done prior to executing Newmark, when evaluating a structure for its permanent displacement to a single user-specified acceleration time-history. (Note that when using the software Newmark in this fashion for a slope/embankment, the acceleration time-history used is likely to an acceleration time-history recorded on a soil site.)

2.2 Time-history of permanent structural displacement

Earthquake shaking of the rock foundation is represented by time histories of acceleration in the translational block formulation implemented in program Newmark for the Complete Time-History Analysis.¹ Since the ground acceleration varies with time, let the horizontal ground acceleration be represented by variable fraction A times the constant acceleration of gravity g in Figure 1.5. Recall that the integral of the acceleration time-history is equal to the velocity time-history and the integral of velocity is displacement (i.e., the permanent structural displacement in this case). For a "rigid block" subjected to an acceleration of value larger than the Figure 1.5 maximum transmissible acceleration, labeled $N*g$ in this figure, the rigid block will displace. When this occurs over several time steps, the total permanent displacement of a sliding block relative to the base (i.e., the rock foundation) is the sum of the increments of displacement occurring during a number of individual

¹ Baseline-corrected, horizontal acceleration time histories are to be used to represent the earthquake ground motions in program Newmark.

pulses of ground motion as shown in Figure 1.5. These incremental relative displacements are determined as follows: For each time the acceleration of the ground, equal to A times g , is greater than the constant N^* times g shown in this figure, relative displacements (between the structure's mass and the rock foundation) will initiate. The integral of the difference in velocities between the sliding rigid block and the rock foundation velocity is equal to the incremental, relative displacement of the sliding structural wedge.

This section describes the numerical method implemented within program Newmark to compute the translational time-history of a rigid block model of a structure during earthquake shaking for the Complete Time-History Analysis. It mirrors the numerical procedure used to compute the translational time-history of a rigid block model of a retaining wall structural wedge, implemented in $C_{\text{orps}}W_{\text{allSlip}}$ and implemented in $C_{\text{orps}}W_{\text{allRotate}}$, which are used in the seismic displacement analysis of retaining walls. Their numerical procedures are discussed in Section 2.4 of Ebeling et al. (2007) and Section 4.4 of Ebeling and White (2006), respectively.

2.2.1 Introduction to a step-by-step solution scheme

Earthquake acceleration time histories are used to represent the earthquake demand in this formulation. They are specified within the rigid base of Figures 1.4 and 1.5. It is the experience of the primary author of this report that the duration of ground acceleration time histories used on Corps projects is on the order of tens of seconds, and up to about one minute of earthquake shaking. The number of time increments (i.e., discrete acceleration point values) contained in the acceleration time-history corresponds to the number of solutions made in the translational structural analysis by program Newmark. The number of time increments is defined by the duration of earthquake shaking and the time increment DT used in digitization of the acceleration time-history. There is no standard time increment DT for the digitization and subsequent processing of acceleration time histories for Corps projects. However, Ebeling et al. (1997a) observe that a DT equal to 0.02, 0.01, or 0.005 seconds is the most common. For example, an earthquake acceleration time-history with 40 seconds of shaking and a time step of 0.02 seconds will contain 2,000 discretized acceleration points. If the acceleration time-history was processed with a DT equal to 0.01 or 0.005 seconds, then the discretized acceleration time histories would contain 4,000, and 8,000 acceleration points, respectively.

A step-by-step solution scheme is followed in order to obtain the structure's permanent translational relative velocity, $relV$, and displacement, $relD$, in the time domain by program Newmark. An overview of the characteristics of this numerical formulation is depicted in Figure 2.1. A key feature of the numerical formulation used is the assumption of a linear variation in relative acceleration $relA$ over time step DT , from time t_i to time t_{i+1} . Values of the user-provided ground acceleration (specified within the rigid base model) are compared against the critical acceleration (i.e., maximum transmissible acceleration or yield acceleration) value at each time step.

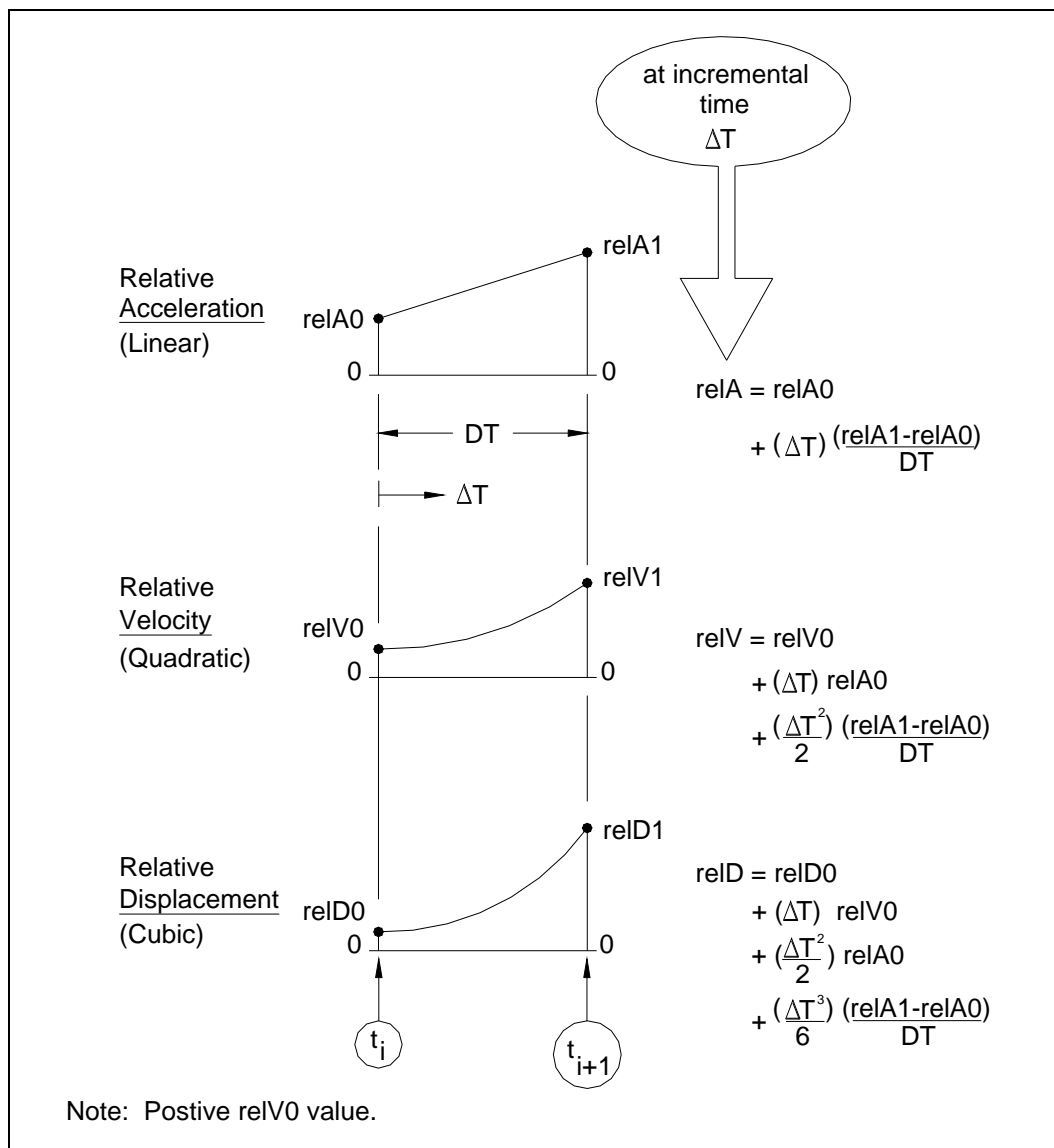


Figure 2.1. Complete equations for relative motions over time increment DT based on linearly varying acceleration.

This idealized figure assumes that the structure is undergoing positive relative acceleration (i.e., the value for acceleration of the ground is greater than the value of critical acceleration, positive relative velocity, and positive (permanent) displacement at time t_i , which continues through time t_{i+1}). The relative acceleration values $relA0$ and $relA1$ are equal to the difference between the horizontal ground acceleration value minus the constant value of critical acceleration at times t_i and t_{i+1} , respectively, and are assumed positive at both time steps. (Other cases will be considered later.) The idealized figure also assumes that the relative acceleration increases in magnitude over this time step DT , as depicted in this figure. The relative velocity is computed by integrating the relative acceleration during each segment of structural translation.

$$relV = \int_0^t relA dt \quad \text{when } relV > 0 \quad (2.1)$$

or

$$relV = 0 \quad \text{when Equation 2.1 gives } relV \text{ less than } 0 \quad (2.2)$$

So, for a linear variation in relative acceleration over time step DT , the relative velocity, $relV$, is a quadratic relationship. Note that program Newmark assumes that the structure cannot slide backwards (i.e., it is impeded by the retained soil for an earth retaining structure or by the pool for a gravity dam, which is expressed by Equation 2.2. Similarly, with the permanent relative displacement of the structure being the integration of the relative velocity, the relative displacement of the structure is a cubic relationship, as listed in Figure 2.1. The permanent relative displacement of the structure is the integration of the relative velocity

$$relD = \int_0^t relV dt \quad (2.3)$$

This series of computations using relative accelerations and Equations 2.1 through 2.3 are repeated for each sequence of structural translations that occurs for the duration of earthquake shaking. The experience of the primary author of this report is that, when the acceleration time histories used as input to program Newmark are based on previously recorded earthquake events (a typical scenario), the permanent displacement occurs

during several, separate pulses occurring throughout the duration of shaking.

In Figure 2.1, the value for relative acceleration $relA$, relative velocity $relV$ and (permanent structural) relative displacement $relD$ at any point in time Δt after t_i and before time t_{i+1} are given by the linear, quadratic and cubic relationships contained on the right-hand side of these three figures (with Δt less than or equal to DT).

Recall that during sliding, the acceleration felt by the structure equals the maximum transmissible acceleration. Thus, the sliding (rigid) block model effectively isolates the sliding block from the shaking (rigid) base below.

2.2.2 Positive relative accelerations $relA0$ and $relA1$ at times t_i and t_{i+1}

Expanding on the details of the computations for the numerical formulation depicted in Figure 2.1, the computation of the relative acceleration, $relA$, relative velocity, $relV$, and relative displacement, $relD$, at time t_{i+1} are made as follows: values for $relA$, $relV$, $relD$, at time t_i are known from the previous computation step in the step-by-step solution scheme. The value for $relA$ at time t_{i+1} (designated $relA1$ in the figure) is computed as the difference between horizontal ground acceleration minus the constant value of critical acceleration. Referring to Figure 2.2, the relative velocity at time t_{i+1} (designated $relV1$) is computed from the value for relative velocity at time t_i (designated $relV0$) plus the positive area under the linear relative acceleration relationship over the time step DT , designated $Area_a$ in this figure. By the trapezoidal rule, $relV1$ at time t_{i+1} is

$$relV1 = relV0 + \frac{DT}{2} \bullet (relA0 + relA1) \quad (2.4)$$

with the values for $relV0$ and $relA0$ now being known values that were computed in the previous solution step. Note that the structure is in motion at time t_i , as reflected by a positive value for relative velocity (designated $relV0$ in Figure 2.2). Similarly, the permanent relative structural displacement at time t_{i+1} (designated $relD1$) is computed from the value for relative displacement at time t_i (designated $relD0$) plus the positive area under the quadratic relative velocity relationship over the time step DT , designated $Area_v$ in this figure. For this linear acceleration method, $relD1$ at time t_{i+1} is

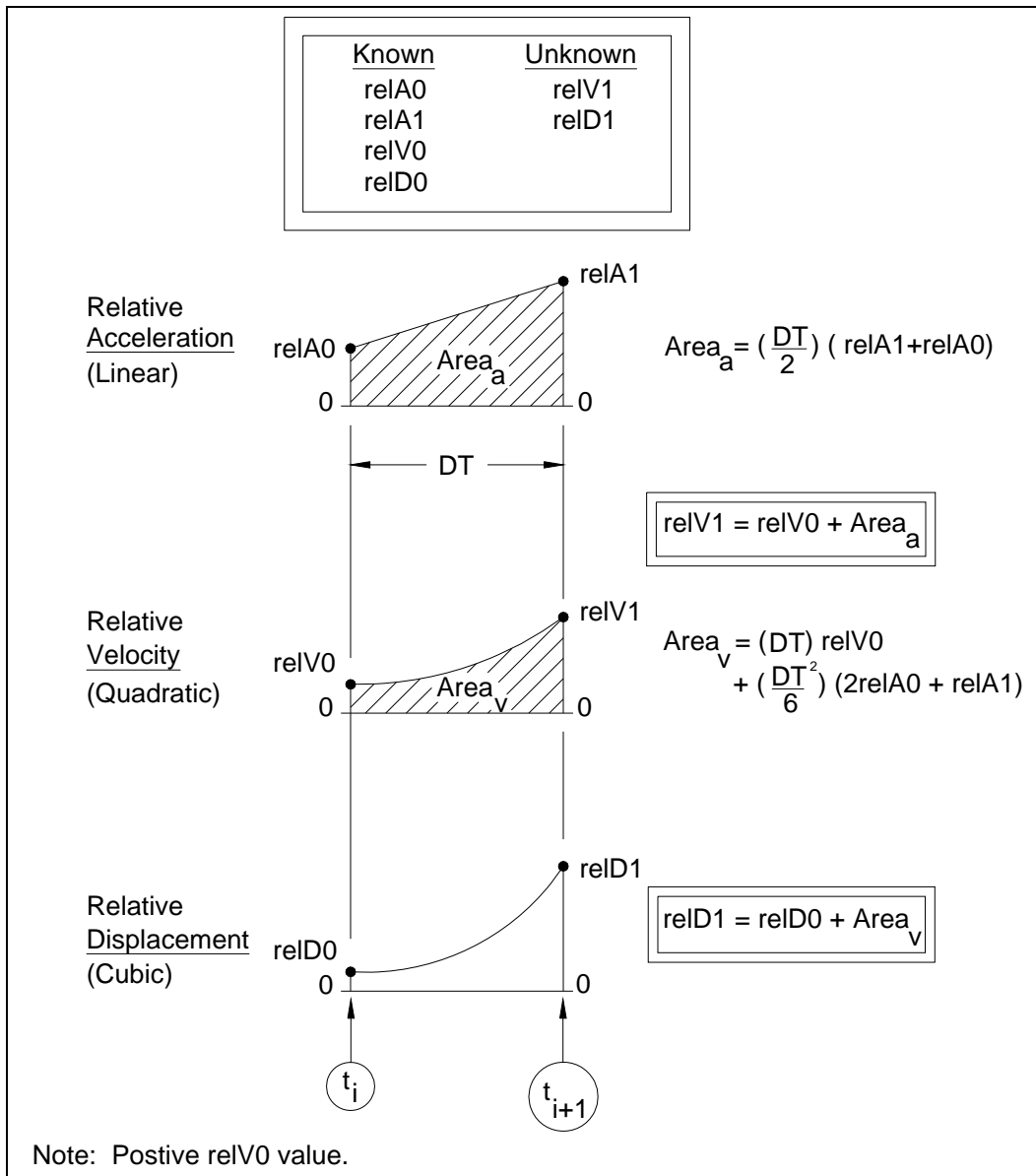


Figure 2.2. Relative Velocity and displacements at the end of time increment DT based on linearly varying relative acceleration.

$$relD1 = relD0 + DT \cdot relV0 + \frac{DT^2}{6} \cdot (2 \cdot relA0 + relA1) \quad (2.5)$$

with the value for $relD0$ being a known value that was computed in the previous solution step. The values for relative velocity $relV$ and (permanent structural) displacement $relD$ at time t_{i+1} are also described in terms of the area relationships contained in Figure 2.2.

In this manor, a step-by-step solution scheme is followed throughout the entire time-history of earthquake shaking in order to obtain the structural

velocity, $reIV$, and relative displacement, $reID$, at each increment in time in the Figure 2.2 case of positive values for $reIA$ at times t_i and t_{i+1} .

In summary, Figure 2.2 outlines a numerical procedure to obtain values for relative velocity and for relative displacement at time t_{i+1} in situations for which values of relative acceleration $reIA$ at times t_i and t_{i+1} are both positive.

However, there are three other situations that can arise during the step-by-step solution:

- The case of a negative value for $reIA$ at time t_i and a positive value for $reIA$ at time t_{i+1}
- The case of structure decelerating over the entire time step DT for which the values of $reIA$ are negative at both times t_i and t_{i+1}
- The case of a positive value for $reIA$ at time t_i and a negative value for $reIA$ at time t_{i+1} .

In all four cases, the assumption of **linear relative acceleration** over time step DT is made and the basic concept of **integrating** positive areas above and/or negative areas below the time-line of relative acceleration $reIA$ to obtain the change in relative velocity $reIV$ and then, in turn, the integration of positive and/or negative areas above and/or below the time-line of $reIV$ to obtain the change in relative displacement $reID$ is used to determine the values for $reIV$ and $reID$, respectively, at time t_{i+1} . These three additional step-by-step solutions will be discussed next. Note the frequent use of the trapezoidal rule for $reIV$ and the linear acceleration method for $reID$ in the solution processes to be described.

2.2.3 Positive relative acceleration $reIA0$ at time t_i and negative relative acceleration $reIA1$ at t_{i+1}

Next, consider a structure in motion (i.e., with a positive value for $reIV$) at time t_i but with the Figure 2.3 case of a negative value for $reIA0$ computed at time step t_i and positive value for $reIA1$ computed at the next time step of t_{i+1} .¹ The first step is to determine the time instant [t_i plus $lhsDT$] at which the relative acceleration $reIA$ is equal to zero, as labeled in the figure. By linear interpolation, this time increment $lhsDT$ is

¹ Note the assumption of a linear variation in relative acceleration over the time step DT in Figure 2.3.

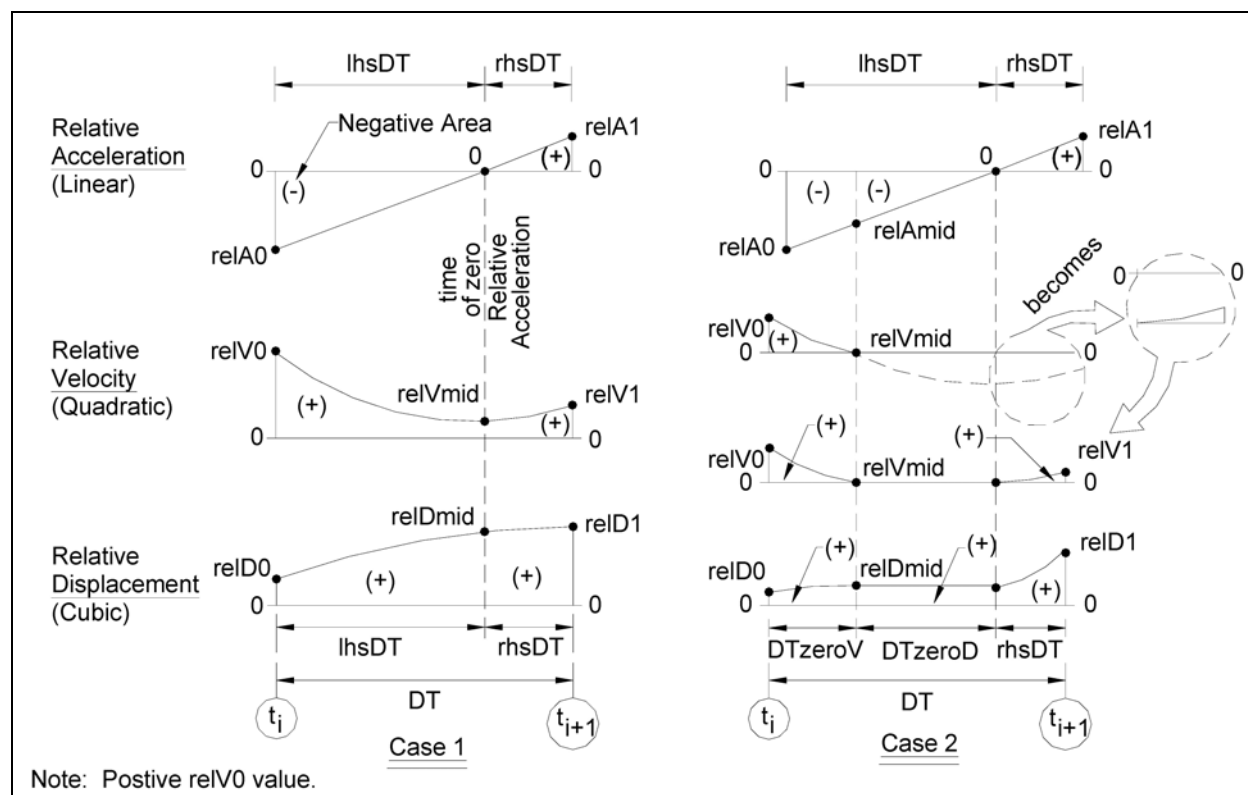


Figure 2.3. Two possible outcomes for the case of a negative relative acceleration at time t_i and a positive relative acceleration at time t_{i+1} .

$$lhsDT = \left| relA0 \cdot \left(\frac{DT}{relA1 - relA0} \right) \right| \quad (2.6)$$

The negative area between the negative portion of the linear acceleration line and the time-line over the Figure 2.3 time increment $lhsDT$ is

$$NegativeArea_{-A+} = \frac{1}{2} \cdot lhsDT \cdot (relA0 + 0) \quad (2.7)$$

Recall that the structure is in motion at time t_i when relative velocity (designated $relV0$ in the figure) is positive. There are two possible outcomes for the Figure 2.3 step-by-step numerical solutions for values of $relV$ and of $relD$ at time t_{i+1} , depending upon the magnitude of $relV0$ relative to the magnitude of $NegativeArea_{-A+}$. These possible scenarios are depicted by two columns of figures in Figure 2.3, labeled as the Case 1 and Case 2 figure groups.

2.2.3.1 Case 1

This case results when the positive value for $relV$ at time t_i is greater than the magnitude of $NegativeArea_{-A+}$ (i.e., the negative area between the negative portion of the linear acceleration line and the time-line over the portion of the Figure 2.3 time increment labeled $lhsDT$). The three left-hand side figures in Figure 2.3 are used to describe the Case 1 step-by-step solution scheme: The top figure describes the relative acceleration $relA$, the middle figure describes the relative velocity $relV$, and the lower figure describes the (permanent) relative structural displacement $relD$.

The top Case 1 figure depicts the case of a (labeled) negative triangular area between the linear relative deceleration $relA$ line and the time-line (i.e., $NegativeArea_{-A+}$ by Equation 2.7), being of less magnitude than the positive value for relative velocity at time t_i (designated $relV_0$). Consequently, the structure will remain in displacement (i.e., sliding) during the entire time step DT . At the increment in time $lhsDT$ after time t_i , a portion of the negative deceleration area reduces the value of relative velocity from the positive value of magnitude $relV_0$ at time t_i to a smaller magnitude value at time $[t_i \text{ plus } lhsDT]$, as shown in this figure. The relative velocity at time $[t_i \text{ plus } lhsDT]$ is

$$relV_{mid} = relV_0 + \frac{1}{2} \bullet lhsDT \bullet (relA_0 + 0) \quad (2.8)$$

The change in relative displacement from time t_i to time $[t_i \text{ plus } lhsDT]$ is equal to the labeled positive area between the quadratic relative velocity curve and the time-line. At time $[t_i \text{ plus } lhsDT]$ the relative structural displacement increases in magnitude from $relD_0$ to $relD_{mid}$.

$$relD_{mid} = relD_0 + lhsDT \bullet relV_0 + \frac{(lhsDT)^2}{6} \bullet (2 \bullet relA_0 + 0) \quad (2.9)$$

The structure continues in motion, with positive relative velocity and with additional permanent deformation after time $[t_i \text{ plus } lhsDT]$ when the relative acceleration of the structure is positive. At time $[t_i \text{ plus } lhsDT]$ the magnitude of structure's relative velocity begins to increase in magnitude as a result of the positive relative acceleration of the structure. The positive (labeled) triangular area between the time-line and the linear acceleration line, shown in the top Case 1 figure, equals the change in relative velocity

and for the structure, consequently, the value for relative velocity at time t_{i+1} (labeled $relV1$ in the Case 1 middle figure) is

$$relV1 = relVmid + \frac{1}{2} \cdot rhsDT \cdot (0 + relA1) \quad (2.10)$$

The change in structural displacement from time [t_i plus $lhsDT$] to time t_{i+1} is equal to the integral of the positive relative velocity of the middle $relV$ -figure. The permanent structural displacement increases in value from $relDmid$ to $relD1$, as depicted in the bottom figure.

$$relD1 = relDmid + rhsDT \cdot relVmid + \frac{(rhsDT)^2}{6} \cdot (2 \cdot 0 + relA1) \quad (2.11)$$

2.2.3.2 Case 2

This case results when the positive value for relative velocity at time t_i is less than the magnitude of $NegativeArea_{-A+}$ (i.e., the negative area between the negative portion of the linear acceleration line and the time-line over the portion of the Figure 2.3 time increment labeled $lhsDT$). The four right-hand side figures in Figure 2.3 are used to describe the Case 2 step-by-step solution scheme. From the top to bottom, one figure describes the relative acceleration, two figures describe the relative velocity, and one figure describes the permanent relative structural displacement.

The top, right-hand side, Case 2 figure depicts the case of a (labeled) negative triangular area between the linear relative deceleration line and the time-line, being of greater magnitude than the positive value for relative velocity at time t_i (designated $relV0$). Consequently, the structure will come to rest before time t_{i+1} is achieved. At an increment in time $DTzeroV$ after time t_i , a portion of the negative deceleration area reduces the value of relative velocity from the positive value of magnitude $relV0$ at time t_i to a value of 0 at time [t_i plus $DTzeroV$], as shown in this figure. At time [t_i plus $DTzeroV$] the relative acceleration is

$$relA_{mid} = DTzeroD \cdot \left(\frac{relA0}{lhsDT} \right) \quad (2.12)$$

where $DTzeroD$ is the time increment shown in Figure 2.3. The Figure 2.3 negative (relative) deceleration area below time increment $DTzeroV$ is

$$AreaTrapezoid_{-A+} = \frac{1}{2} \bullet DTzeroV \bullet (relAO + relAmid) \quad (2.13)$$

The Figure 2.3 negative relative deceleration area below time increment $DTzeroD$ is

$$AreaTriangle_{-A+} = \frac{1}{2} \bullet DTzeroD \bullet (relAmid + 0) \quad (2.14)$$

Thus, the total Figure 2.3 negative relative deceleration area below time increment $lhsDT$ is

$$NegativeArea_{-A+} = AreaTrapezoid_{-A+} + AreaTriangle_{-A+} \quad (2.15)$$

The relative velocity at time $[t_i$ plus $DTzeroV]$ is

$$relVmid = relV0 + AreaTrapezoid_{-A+} \quad (2.16)$$

With a value for $relVmid$ equal to zero, Equation 2.16 becomes

$$0 = relV0 + AreaTrapezoid_{-A+} \quad (2.17)$$

Expanding by adding the term $AreaTriangle_{-A+}$ to both sides, Equation 2.17 becomes

$$AreaTriangle_{-A+} = relV0 + AreaTrapezoid_{-A+} + AreaTriangle_{-A+} \quad (2.18)$$

Which by introducing Equation 2.15, becomes

$$AreaTriangle_{-A+} = relV0 + NegativeArea_{-A+} \quad (2.19)$$

Introducing Equations 2.14 and 2.12 and solving for $DTzeroD$, Equation 2.19 becomes

$$DTzeroD = \sqrt{2 \bullet \left(\frac{lhsDT}{relAO} \right) \bullet (relV0 + NegativeArea_{-A+})} \quad (2.20)$$

Recognizing the time increment $lhsDT$ is equivalent to

$$lhsDT = DTzeroV + DTzeroD \quad (2.21)$$

and by introducing Equations 2.21 and 2.13 into Equation 2.20 and solving for $DTzeroV$,

$$DTzeroV = lhsDT - \sqrt{2 \cdot \left(\frac{lhsDT}{relA0} \right) \cdot (relV0 + NegativeArea_{-A+})} \quad (2.22)$$

The change in relative displacement from time t_i to time [t_i plus $DTzeroV$] is equal to the labeled positive area between the quadratic relative velocity curve and the time-line. At time [t_i plus $DTzeroV$] the structural displacement increases in magnitude from $relD0$ to $relDmid$. The relative velocity at time [t_i plus $DTzeroV$], expressed in terms of $DTzeroV$, is

$$relVmid = relV0 + \frac{1}{2} \cdot DTzeroV \cdot (relA0 + relA_{mid}) \quad (2.23)$$

with the relative acceleration at time [t_i plus $DTzeroV$] equal to

$$relA_{mid} = relA0 + \left(\frac{relA1 - relA0}{DT} \right) \cdot DTzeroV \quad (2.24)$$

The change in relative displacement from time t_i to time [t_i plus $DTzeroV$] is equal to the labeled positive area between the quadratic relative velocity curve and the time-line. At time [t_i plus $DTzeroV$] the structural displacement increases in magnitude from $relD0$ to $relDmid$.

$$relDmid = relD0 + DTzeroV \cdot relV0 + \frac{(DTzeroV)^2}{6} \cdot (2 \cdot relA0 + relA_{mid}) \quad (2.25)$$

The structure remains at rest with zero relative velocity and with no additional permanent relative displacement from time [t_i plus $DTzeroV$] until time [t_i plus $lhsDT$] when the relative acceleration of the structure begins (again). At time [t_i plus $lhsDT$] the structure begins to develop further permanent displacement as a result of the positive relative reacceleration of the structure. The positive (labeled) triangular area between the

time-line and the linear relative acceleration line, shown in the right-hand side of the top figure, equals the change in relative velocity and with the structure at rest, consequently, the value for relative velocity at time t_{i+1} (labeled $relV1$ in the lower relative velocity figure) is

$$relV1 = \frac{1}{2} \bullet rhsDT \bullet (0 + relA1) \quad (2.26)$$

The change in structural displacement from time [t_i plus $lhsDT$] to time t_{i+1} is equal to the integral of the positive relative velocity, as depicted in the middle two, right-hand side $relV$ -figures. The top $relV$ figure is a computational figure, and the bottom $relV$ figure is the $relV$ curve-shift figure that properly accounts for zero structural relative velocity over time increment $DTzeroD$, with an insert detailed, curve-shift figure for $relV$ shown of this computational $relV$ figure in Figure 2.3. The permanent relative structural displacement increases in value from $relDmid$ to $relD1$, as depicted in the bottom figure.

$$relD1 = relDmid + rhsDT \bullet 0 + \frac{(rhsDT)^2}{6} \bullet (2 \bullet 0 + relA1) \quad (2.27)$$

2.2.4 Negative relative accelerations $relA0$ and $relA1$ at times t_i and t_{i+1}

Next, consider a structure in motion (i.e., with a positive value for relative velocity) at time t_i but with the Figure 2.4 case of a negative values for relative acceleration computed at time steps t_i and t_{i+1} .¹

The first step is to determine if the structure, which is in motion at time t_i , comes to rest during the time step DT .

The negative area between the negative portion of the linear acceleration line and the time-line over the Figure 2.4 time increment DT is

$$NegativeArea_{-A-} = \frac{1}{2} \bullet DT \bullet (relA0 + relA1) \quad (2.28)$$

¹ Again, note the assumption of a linear variation in relative acceleration over the time step DT shown in Figure 2.4.

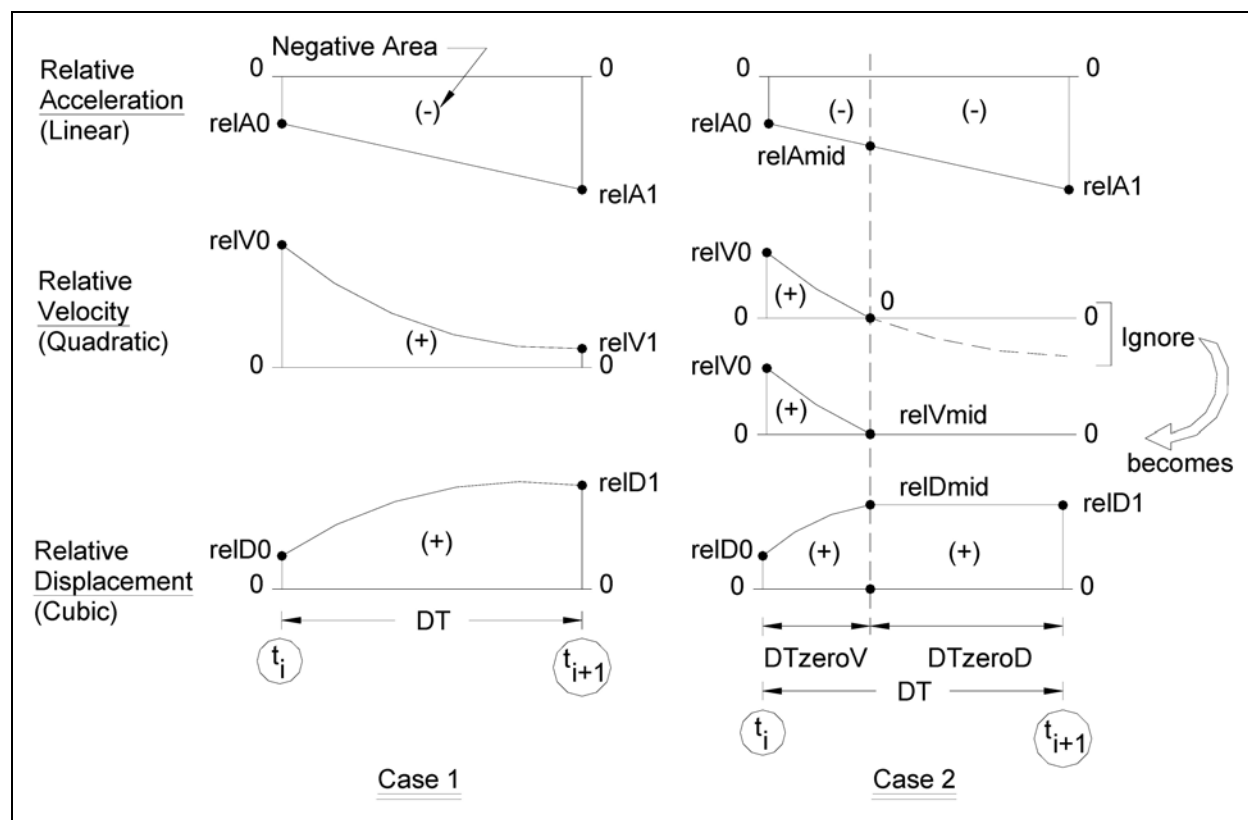


Figure 2.4. Two possible outcomes for the case of negative relative accelerations at times t_i and t_{i+1} .

There are two possible outcomes for the Figure 2.4 step-by-step numerical solution for relative velocity and relative displacement at time t_{i+1} , depending upon the magnitude of $relV0$ relative to the magnitude of Equation 2.28 $NegativeArea_{-A-}$. These possible scenarios are depicted by two columns of figures in Figure 2.4, labeled as Case 1 and Case 2 figure groups.

2.2.4.1 Case 1

This case results when the positive value for relative velocity at time t_i is greater than the magnitude of $NegativeArea_{-A-}$ (i.e., the negative area between the negative portion of the linear acceleration line and the time-line over the Figure 2.4 time step DT). The three left-hand side figures in Figure 2.4 are used to describe the Case 1 step-by-step solution scheme: The top figure describes the relative acceleration, the middle figure describes the relative velocity, and the lower figure describes the permanent relative structural displacement.

The top Case 1 figure depicts the case of a (labeled) negative area between the linear relative deceleration line and the time-line (i.e., $NegativeArea_{-A}$ by Equation 2.28), being of less magnitude than the positive value for relative velocity at time t_i (designated $relV0$). Consequently, the structure will remain in motion during the entire time step DT . At the time step DT after time t_i , the negative deceleration area reduces the value of relative velocity from the positive value of magnitude $relV0$ at time t_i to a smaller magnitude value at time [t_i plus DT], as shown in this figure. The relative velocity at time [t_i plus DT] is

$$relV1 = relV0 + \frac{1}{2} \bullet DT \bullet (relA0 + relV1) \quad (2.29)$$

The change in relative displacement from time t_i to time [t_i plus DT] is equal to the labeled positive area between the quadratic relative velocity curve and the time-line. At time [t_i plus DT] the structural displacement increases in magnitude from $relD0$ to $relD1$.

$$relD1 = relD0 + DT \bullet relV0 + \frac{(DT)^2}{6} \bullet (2 \bullet relA0 + relA1) \quad (2.30)$$

2.2.4.2 Case 2

This case results when the positive value for relative velocity at time t_i is less than the magnitude of $NegativeArea_{-A}$ (i.e., the negative area between the negative portion of the linear acceleration line and the time-line over the portion of the Figure 2.4 time increment labeled $lhsDT$). The four right-hand side figures in Figure 2.4 are used to describe the Case 2 step-by-step solution scheme. From the top to bottom, one figure describes the relative acceleration, two figures describe the relative velocity, and one figure describes the permanent relative structural displacement.

The top, right-hand side, Case 2 figure depicts the case of a (labeled) negative area between the linear relative deceleration line and the time-line (i.e., $NegativeArea_{-A}$ by Equation 2.28), being of greater magnitude than the positive value for relative velocity at time t_i (designated $relV0$). Consequently, the structure will come to rest before time t_{i+1} is achieved. At an increment in time DT_{zeroV} after time t_i , a portion of the negative deceleration area reduces the value of relative velocity from the positive

value of magnitude $relV0$ at time t_i to a value of 0 at time $[t_i$ plus $DTzeroV]$, as shown in this figure. At time $[t_i$ plus $DTzeroV]$ the relative acceleration is

$$relAmid = relA0 + DTzeroV \cdot \left(\frac{relA1 - relA0}{DT} \right) \quad (2.31)$$

where $DTzeroV$ is the time increment shown in Figure 2.4. The Figure 2.4 negative relative deceleration area below time increment $DTzeroV$ is

$$AreaTrapezoid_{A-} = \frac{1}{2} \cdot DTzeroV \cdot (relA0 + relAmid) \quad (2.32)$$

Introducing Equation 2.31, Equation 2.32 becomes

$$AreaTrapezoid_{A-} = \left\{ \begin{array}{l} \frac{1}{2} \cdot DTzeroV \cdot relA0 \\ + \frac{DTzeroV}{2} \\ \cdot \left[relA0 + DTzeroV \cdot \left(\frac{relA1 - relA0}{DT} \right) \right] \end{array} \right\} \quad (2.33)$$

This simplifies to

$$AreaTrapezoid_{A-} = DTzeroV \cdot relA0 + \frac{(DTzeroV)^2}{2} \cdot \left(\frac{relA1 - relA0}{DT} \right) \quad (2.34)$$

The change in rotation from time t_i to time $[t_i$ plus $DTzeroV]$ is equal to the labeled positive area between the quadratic relative velocity curve and the time-line. At time $[t_i$ plus $DTzeroV]$ the structural displacement increases in magnitude from $relD0$ to $relDmid$. The relative velocity at time $[t_i$ plus $DTzeroV]$ is

$$relVmid = relV0 + AreaTrapezoid_{A-} \quad (2.35)$$

With a value for $relVmid$ equal to zero, Equation 2.35 becomes

$$0 = \left[\frac{1}{2} \cdot \left(\frac{relA1 - relA0}{DT} \right) \right] \cdot (DTzeroV)^2 + relA0 \cdot DTzeroV + relV0 \quad (2.36)$$

This quadratic equation has a general solution of

$$DTzeroV = \frac{-relA0 \pm \sqrt{(relA0)^2 - 4 \cdot \left[\frac{1}{2} \cdot \left(\frac{relA1 - relA0}{DT} \right) \right] \cdot relV0}}{2 \cdot \left[\frac{1}{2} \cdot \left(\frac{relA1 - relA0}{DT} \right) \right]} \quad (2.37)$$

Even though this solution provides for two possible values for $DTzeroV$, only the positive value is assigned to $DTzeroV$ in program Newmark.

The change in displacement from time t_i to time $[t_i \text{ plus } DTzeroV]$ is equal to the labeled positive area between the quadratic relative velocity curve and the time-line. At time $[t_i \text{ plus } DTzeroV]$ the relative structural displacement increases in magnitude from $relD0$ to $relDTmid$.

$$\begin{aligned} relDmid &= relD0 + DTzeroV \cdot relV0 \\ &+ \frac{(DTzeroV)^2}{6} \cdot (2 \cdot relA0 + relA_{mid}) \end{aligned} \quad (\text{bis 2.25})$$

The structure remains at rest with zero relative velocity and with no additional permanent displacement from time $[t_i \text{ plus } DTzeroV]$ until time $[t_i \text{ plus } DT]$. Consequently, at time t_{i+1} the permanent relative structural displacement is constant, as depicted in the bottom figure.

$$relD1 = relDmid \quad (2.38)$$

with the value for $relDmid$ given by Equation 2.25.

2.2.5 Positive relative acceleration $relA0$ at time t_i and negative relative acceleration $relA1$ at t_{i+1}

Next, consider a structure in motion (i.e., with a positive value for relative velocity) at time t_i , but with the Figure 2.5 case of a positive value for relative acceleration at time step t_i and negative value for relative acceleration

at the next time step of t_{i+1} .¹ The first step is to determine the time instant $[t_i$ plus $lhsDT$] at which the relative acceleration is equal to zero, as labeled in the figure. By linear interpolation, this time increment $lhsDT$ is

$$lhsDT = \left| relA0 \cdot \left(\frac{DT}{relA1 - relA0} \right) \right| \quad (\text{bis 2.6})$$

The positive area between the positive portion of the linear acceleration line and the time-line over the Figure 2.5 time increment $lhsDT$ is

$$PositiveArea_{+A-} = \frac{1}{2} \cdot lhsDT \cdot (relA0 + 0) \quad (2.39)$$

The Figure 2.5 time increment $rhsDT$ is given by

$$rhsDT = DT - lhsDT \quad (2.40)$$

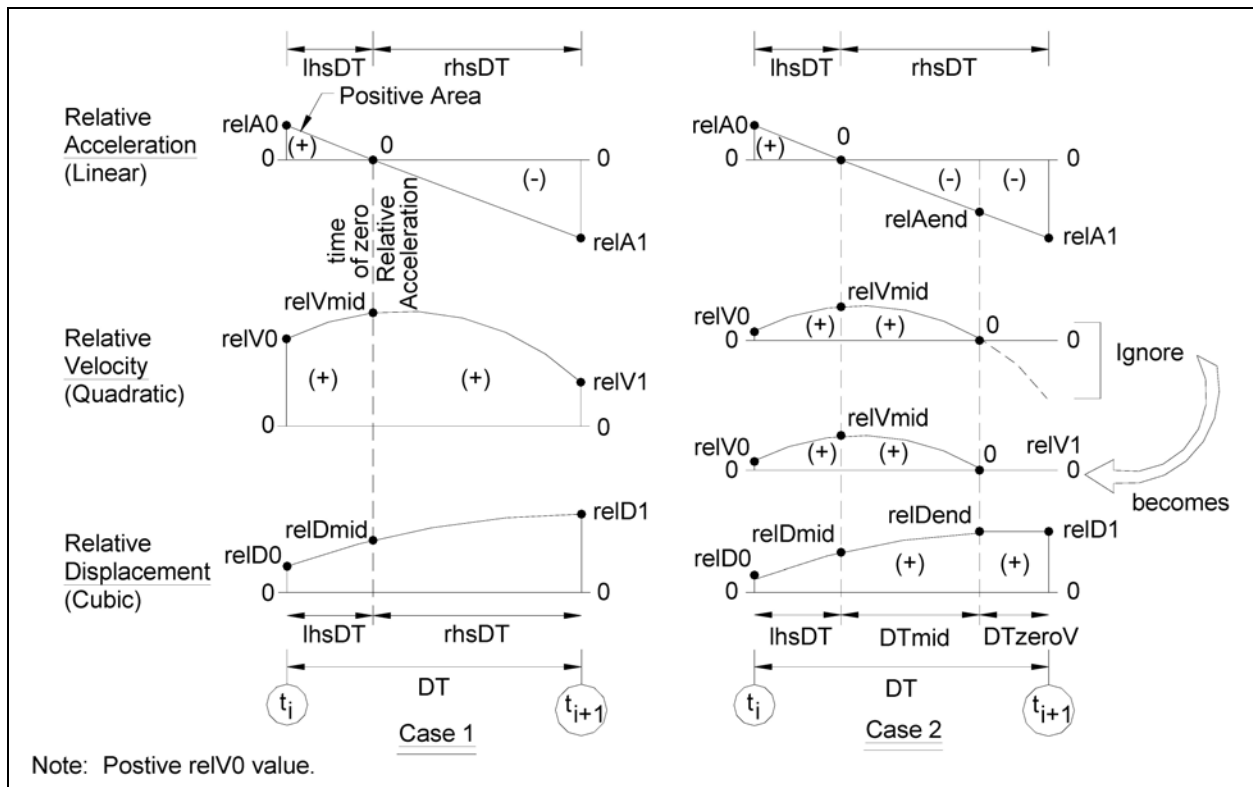


Figure 2.5. Two possible outcomes for the case of a positive relative acceleration at time t_i and a negative relative acceleration at time t_{i+1} .

¹ Again, observe the assumption of a linear variation in relative acceleration over the time step DT shown in Figure 2.5.

The negative area between the negative portion of the linear acceleration line and the time-line over the Figure 2.5 time increment $rhsDT$ is

$$NegativeArea_{+A-} = \frac{1}{2} \bullet rhsDT \bullet (0 + relA1) \quad (2.41)$$

There are two possible outcomes for the Figure 2.5 step-by-step numerical solution for relative velocity and relative displacement at time t_{i+1} , depending upon the magnitude of $relV0$ relative to the magnitude of the sum of the $PositiveArea_{+A-}$ plus the $NegativeArea_{+A-}$. These possible scenarios are depicted by two columns of figures in Figure 2.5, labeled as Case 1 and Case 2 figure groups.

2.2.5.1 Case 1

This case results if the $NegativeArea_{+A-}$ exceeds $PositiveArea_{+A-}$ but the positive value for relative velocity at time t_i is greater than the magnitude of the negative sum of $PositiveArea_{+A-}$ plus $NegativeArea_{+A-}$, or if the $NegativeArea_{+A-}$ is less than $PositiveArea_{+A-}$, consequently, the positive value for $relV0$ at time t_i will increase to a larger value of $relV1$ at time t_{i+1} (with an increase equal to the positive sum of $PositiveArea_{+A-}$ plus $NegativeArea_{+A-}$). The three left-hand side figures in Figure 2.5 are used to describe the Case 1 step-by-step solution scheme: The top figure describes the relative acceleration, the middle figure describes the relative velocity, and the lower figure describes the permanent relative structural displacement.

The top Case 1 figure depicts the case of a structure sliding during the entire time step DT because either the $NegativeArea_{+A-}$ exceeds $PositiveArea_{+A-}$ but the positive value for relative velocity at time t_i is greater than the magnitude of the sum of $PositiveArea_{+A-}$ plus $NegativeArea_{+A-}$, or because the $NegativeArea_{+A-}$ is less than $PositiveArea_{+A-}$. At the increment in time $lhsDT$ after time t_i , the positive acceleration area increases the value of relative velocity from the positive value of magnitude $relV0$ at time t_i to a larger magnitude value at time $[t_i$ plus $lhsDT]$, as shown in this figure. The relative velocity at time $[t_i$ plus $lhsDT]$ is

$$relVmid = relV0 + \frac{1}{2} \bullet lhsDT \bullet (relA0 + 0) \quad (\text{bis 2.8})$$

The change in displacement from time t_i to time $[t_i \text{ plus } lhsDT]$ is equal to the labeled positive area between the quadratic relative velocity curve and the time-line. At time $[t_i \text{ plus } lhsDT]$ the structural displacement increases in magnitude from $relD0$ to $relDmid$.

$$relDmid = relD0 + lhsDT \bullet relV0 + \frac{(lhsDT)^2}{6} \bullet (2 \bullet relA0 + 0) \quad (\text{bis 2.9})$$

The structure continues in motion, with positive relative velocity and with additional permanent relative displacement after time $[t_i \text{ plus } lhsDT]$, when the relative acceleration of the structure is positive. At time $[t_i \text{ plus } lhsDT]$, the magnitude of the structure's relative velocity begins to decrease in magnitude as a result of the relative deceleration of the structure. The negative (labeled) triangular area between the time-line and the linear relative deceleration line, shown in the top Case 1 figure, equals the change in relative velocity and for the structure. Consequently, the value for relative velocity at time t_{i+1} (labeled $relV1$ in the Case 1 middle figure) is

$$relV1 = relVmid + \frac{1}{2} \bullet rhsDT \bullet (0 + relA1) \quad (\text{bis 2.10})$$

The change in structural displacement from time $[t_i \text{ plus } lhsDT]$ to time t_{i+1} is equal to the integral of the positive relative velocity of the middle $relV$ -figure. The permanent relative structural displacement increases in value from $relDmid$ to $relD1$, as depicted in the bottom figure.

$$relD1 = relDmid + rhsDT \bullet relVmid + \frac{(rhsDT)^2}{6} \bullet (2 \bullet 0 + relA1) \quad (\text{bis 2.11})$$

2.2.5.2 Case 2

This case results when the $NegativeArea_{+A-}$ exceeds $PositiveArea_{+A-}$ and the positive value for relative velocity at time t_i is less than the magnitude of the sum of $PositiveArea_{+A-}$ plus $NegativeArea_{+A-}$. The four right-hand side figures in Figure 2.5 are used to describe the Case 2 step-by-step solution scheme. From the top to bottom, one figure describes the relative acceleration, two figures describe the relative velocity, and one figure describes the permanent relative structural displacement.

The top, right-hand side, Case 2 figure depicts the case of the sum of a (labeled) positive triangular area between the linear relative deceleration line and the time-line (i.e., $PositiveArea_{+A-}$ by Equation 2.39) plus a (labeled) negative triangular area between the linear relative deceleration line and the time-line (i.e., $NegativeArea_{+A-}$ by Equation 2.41), being negative and of greater magnitude than the positive value for relative velocity at time t_i (designated $relV0$). Consequently, the structure will come to rest before time t_{i+1} is achieved.

At time [t_i plus $lhsDT$], the structure's relative velocity increases in magnitude from $relV0$ to $relVmid$. The relative velocity at time [t_i plus $lhsDT$] is

$$relVmid = relV0 + \frac{1}{2} \bullet lhsDT \bullet (relA0 + 0) \quad (\text{bis 2.8})$$

with the relative acceleration at time [t_i plus $lhsDT$] equal to zero.

The change in displacement from time t_i to time [t_i plus $lhsDT$] is equal to the labeled positive area between the quadratic relative velocity curve and the time-line. At time [t_i plus $lhsDT$], the structural displacement increases in magnitude from $relD0$ to $relDmid$.

$$relDmid = relD0 + lhsDT \bullet relV0 + \frac{(lhsDT)^2}{6} \bullet (2 \bullet relA0 + 0) \quad (2.42)$$

At an increment in time [$lhsDT + DTmid$] after time t_i , a portion of the negative deceleration area reduces the value of relative velocity from the positive value of magnitude $relVmid$ at time [t_i plus $lhsDT$] to a value of 0 at time [t_i plus ($lhsDT + DTmid$)], as shown in this figure. At time [t_i plus ($lhsDT + DTmid$)], the relative acceleration is

$$relAend = DTmid \bullet \left(\frac{relA1}{rhsDT} \right) \quad (2.43)$$

where $DTmid$ is the time increment shown in Figure 2.5. The Figure 2.5 negative relative acceleration area below time increment $DTmid$ is

$$AreaTriangle_{+A-} = \frac{1}{2} \bullet DTmid \bullet (0 + relAend) \quad (2.44)$$

The Figure 2.5 negative relative acceleration area below time increment DT_{zeroV} is

$$AreaTrapezoid_{+A-} = \frac{1}{2} \bullet DT_{zeroV} \bullet (relA_{end} + relA_1) \quad (2.45)$$

Thus, the total Figure 2.5 negative relative acceleration area below time increment $rhsDT$ is

$$NegativeArea_{+A-} = AreaTrapezoid_{+A-} + AreaTriangle_{+A-} \quad (2.46)$$

With the relative velocity at time $[t_i \text{ plus } (lhsDT + DT_{mid})]$ equal to zero,

$$0 = relV_{mid} + AreaTriangle_{+A-} \quad (2.47)$$

By introducing Equations 2.8, 2.39, 2.43, and 2.44, and solving for DT_{mid} , Equation 2.47 becomes

$$DT_{mid} = \sqrt{-2 \bullet \left(\frac{rhsDT}{relA_1} \right) \bullet (relV_0 + PositiveArea_{+A-})} \quad (2.48)$$

At time $[t_i \text{ plus } (lhsDT + DT_{mid})]$, the relative structural displacement comes to rest with

$$\begin{aligned} relD_{end} &= relD_{mid} + DT_{mid} \bullet relV_{mid} \\ &+ \frac{(DT_{mid})^2}{6} \bullet (2 \bullet 0 + relA_{end}) \end{aligned} \quad (2.49)$$

The structure remains at rest with zero relative velocity and with no additional permanent relative displacement from time $[t_i \text{ plus } (lhsDT + DT_{mid})]$ until time t_{i+1} . The permanent relative structural displacement at this time t_{i+1} is

$$relD_1 = relD_{end} \quad (2.50)$$

2.2.6 Starting the program Newmark analysis and the initiation of structural translation during a DT time step

Start of the step-by-step time-history analysis: The numerical formulation used in the step-by-step time-history analysis by program Newmark assumes that the structure is at rest at the start of the analysis (i.e., at time t_i equal to 0 and with $i = 1$). Consequently, relative acceleration, relative velocity and relative displacement are equal to zero as an initial boundary condition at the first time step (i.e., with $i = 1$). Recall the relative acceleration at time t_i is equal to the difference between the horizontal ground acceleration value at time t_i minus the constant value of critical acceleration (i.e., maximum transmissible acceleration or yield acceleration).

Initiation of structural displacement during the first DT time step: At the end of the first DT time step, at time increment t_2 (i.e., t_{i+1} and with $i = 1$ so the subscript $i + 1$ becomes 2), a relative acceleration value is computed by program Newmark. If a positive value for relative acceleration is computed at time increment t_2 then the system is in motion (i.e., sliding) during this first time step DT .

However, if a negative value for relative acceleration is computed and the system has been at rest and with zero relative acceleration at time $t_i = 0$ (i.e., t_i and for $i = 1$) then the system is at rest at time t_2 . This means that the correct value for relative acceleration is zero at time t_2 .

Initiation of structural displacement during a DT time step: A structure is at rest at the beginning of any DT time step (designated time t_i in Figures 2.1 through 2.5) when relative velocity and relative displacement are equal to zero. At all DT time steps other than the first time step, the values at time t_i for relative acceleration, relative velocity and relative displacement were computed during the previous time step and then assigned as known values for this next time step. The step-by-step numerical procedure implemented in program Newmark allows for structural displacement to initiate during any DT time step during earthquake shaking. This will occur for a structure at rest at time t_i , i.e., the start of the time step, when a positive value is computed for relative acceleration at time t_{i+1} . The numerical procedure outlined in Figure 2.2 allows for the computation of relative velocity and relative displacement at time t_{i+1} for this case.

2.2.7 Cessation of structural translation

A structure is in motion at the start of any DT time step (designated time t_i in Figures 2.1 through 2.5) when relative velocity (i.e., $relV$) is nonzero. The step-by-step numerical procedure implemented in program Newmark allows for structural translation (i.e., sliding) to terminate during any DT time step during earthquake shaking. This occurs when the deceleration of the structure is sufficiently large during time step DT . The applicable numerical procedures are labeled as Case 2 in Figures 2.4 and 2.5.

In the case of structural translation decelerating and with negative values for relative acceleration at times t_i and t_{i+1} during time step DT , the relative velocity at time t_{i+1} (designated $relV1$) and the relative structural displacement at time t_{i+1} (designated $relD1$) are made using the Case 2 approach outlined in Figure 2.4. Note the relative velocity reduces to zero at a time increment $DTzeroV$ after time t_i . The structure remains at rest and with zero relative velocity over time increment $DTzeroD$, as shown in this figure.

In the case of structural translation decelerating and with a positive value for relative acceleration at time t_i and a negative value for relative acceleration at time t_{i+1} during time step DT , the relative velocity at time t_{i+1} (designated $relV1$) and the relative structural displacement at time t_{i+1} (designated $relD1$) are made using the Case 2 approach outlined in Figure 2.5. Note the relative velocity reduces to zero at a time increment $[lhsDT + DTmid]$ after time t_i . The structure remains at rest and with zero relative velocity over time increment $DTzeroV$, as shown in this figure.

Note that structural translation can begin again at a later point in time, as described in the subsection 2.2.6 paragraph entitled “Starting the program Newmark analysis and the initiation of structural translation during a DT time step.”

3 Regression Analysis

3.1 Introduction

This chapter describes three formulations for developing simplified non-dimensionalized permanent displacement relationships. These relationships as illustrated in Table 3.1 are described in detail at each following section, respectively. The derivations of these mean estimates, together with their standard error terms, also determine the 68 percent prediction intervals and 95 percent probability of non-exceedance upper bound estimates.

Table 3.1. Forms of simplified non-dimensionalized permanent displacement relationships.

Equation Form Three Three-term Regression Analysis	$\frac{d_m \cdot k_m g}{v_m^2} = \beta_1 \cdot \exp\left(\beta_2 \cdot \frac{k_c}{k_m}\right) \cdot \left(\frac{k_c}{k_m}\right)^{\beta_3}$
Equation Form Two Two-term Regression Analysis, Linear in Natural Logarithm Transformation	$\frac{d_m \cdot k_m g}{v_m^2} = \beta_1 \cdot \exp\left(\beta_2 \cdot \frac{k_c}{k_m}\right)$
Equation Form One Two-term Regression Analysis, Linear in Common Logarithm Transformation	$\frac{d_m \cdot k_m g}{v_m^2} = \beta_4 \cdot \left(\frac{k_c}{k_m}\right)^{\beta_5}$

3.2 Three-term regression analysis (Equation Form Three)

As noted earlier, Newmark (1965) first proposed the sliding block theory to estimate the permanent displacement of a sliding soil mass subjected to earthquake loading. Cai and Bathurst (1995) presented several simplified permanent displacement relationships that were developed by themselves as well as by others [e.g., Newmark (1965); Franklin and Chang (1977); Richards and Elms (1979); Whitman and Liao (1985a, 1985b); etc.], all of which are based on the Newmark sliding block method of analysis. These simplified permanent seismic displacement relationships use values of peak acceleration and peak velocity as a means to characterize earthquake demands on earthen and/or earth retaining structures founded on soil. All were derived using acceleration time-history records recorded on soil sites.

This subsection discusses one general form of a simplified permanent displacement relationship first proposed by Cai and Bathurst (1995).

One form of a simplified permanent seismic displacement relationship attributed to Cai and Bathurst (1995) and for a soil site, is of the form,

$$d_m = 35 \cdot \frac{v_m^2}{k_m g} \cdot \exp\left(-6.91 \cdot \frac{k_c}{k_m}\right) \cdot \left(\frac{k_c}{k_m}\right)^{-0.38} \quad (3.1)$$

Newmark (1965) introduced the peak ground acceleration and the peak ground velocity as characteristic soil parameters. Collecting these parameters, along with the permanent seismic displacement, the left-hand side becomes what is termed a non-dimensionalized displacement, which for the Cai and Bathurst relationship becomes,

$$\frac{d_m \cdot k_m g}{v_m^2} = 35 \cdot \exp\left(-6.91 \cdot \frac{k_c}{k_m}\right) \cdot \left(\frac{k_c}{k_m}\right)^{-0.38} \quad (3.2)$$

When discussing nonlinear regression, Equation 3.2 may be written in the general form of

$$y = \beta_1 \cdot \exp(\beta_2 \cdot x) \cdot x^{\beta_3} \quad (3.3)$$

with

$$y = \frac{d_m \cdot k_m g}{v_m^2}; \quad \text{non-dimensionalized displacement, and}$$

$$x = \frac{k_c}{k_m}; \quad \text{critical acceleration ratio}$$

where:

- d_m = permanent displacement
- $k_m g$ = maximum horizontal ground acceleration
- v_m = maximum ground velocity
- k_c = maximum transmissible acceleration capacity

for which β_1 , β_2 , and β_3 are constants and the equation is nonlinear in β_2 .

The form of Equation 3.3 is now $[x, y]$ as compared to the original form

$$\left[\frac{k_c}{k_m}, \frac{d_m \bullet k_m \mathcal{G}}{v_m^2} \right] \text{ of Equation 3.2.}$$

Taking the natural log (\ln) of both sides, Equation 3.3 becomes

$$\ln(y) = \ln(\beta_1) + \beta_2 \bullet x + \beta_3 \bullet \ln(x) \quad (3.4)$$

which simplifies to

$$\ln(y) = \beta_1^* + \beta_2 \bullet x + \beta_3 \bullet \ln(x) \quad (3.5)$$

with β_1^* equal to $\ln(\beta_1)$, or $\beta_1 = \exp(\beta_1^*)$.

The transformation of Equation 3.3 to Equations 3.4 and 3.5 resulted in the altered form of the equation from (x, y) to $(x, \ln(y))$ or specifically, (x, y^*) with $y^* = \ln(y)$, such that Equation 3.5 becomes,

$$y^* = \beta_1^* + \beta_2 \bullet x + \beta_3 \bullet \ln(x) \quad (3.6)$$

From Equation 3.6, the set of basis functions $(1, x, \ln(x))$ have a nonlinear term, $\ln(x)$; however, the parameters $(\beta_1^*, \beta_2, \text{ and } \beta_3)$ are constant and not part of any nonlinear term.

Regression models which are a linear function of the parameters are called linear regression models. Therefore, a linear regression analysis can be applied to solve for these constant parameters.

The least squares fitting method is one of the simplest and most common applied forms of linear regression. This method will be used to estimate the parameters which will minimize the sum of squares of the y-distance from the specified, or produce the least possible value of S ,

$$S = \sum_{i=1}^N e_i^2 = \sum_{i=1}^N \left[y_i^* - (\beta_1^* + \beta_2 x_i + \beta_3 x_i^*) \right]^2 \quad (3.7)$$

with

N = the total number of non-dimensionalized displacement terms
 $x^* = \ln(x)$.

We can estimate the parameters by taking the partial derivatives of Equation 3.7 with respect to β_1^* , β_2 , and β_3 , and setting the resultant equal to zero.

$$\begin{aligned}\frac{\partial S}{\partial \beta_1} &= \sum_{i=1}^N 2 \left[y_i^* - (\beta_1^* + \beta_2 x_i + \beta_3 x_i^*) \right] (-1) = 0 \\ \frac{\partial S}{\partial \beta_2} &= \sum_{i=1}^N 2 \left[y_i^* - (\beta_1^* + \beta_2 x_i + \beta_3 x_i^*) \right] (-x_i) = 0 \\ \frac{\partial S}{\partial \beta_3} &= \sum_{i=1}^N 2 \left[y_i^* - (\beta_1^* + \beta_2 x_i + \beta_3 x_i^*) \right] (-x_i^*) = 0\end{aligned}\quad (3.8)$$

The estimates of β_1^* , β_2 , and β_3 are then represented by 3 linear equations in 3 unknowns,

$$\begin{aligned}\beta_1^*(N) + \beta_2 \sum_{i=1}^N x_i + \beta_3 \sum_{i=1}^N x_i^* &= \sum_{i=1}^N y_i^* \\ \beta_1^* \sum_{i=1}^N x_i + \beta_2 \sum_{i=1}^N (x_i)^2 + \beta_3 \sum_{i=1}^N x_i x_i^* &= \sum_{i=1}^N x_i y_i^* \\ \beta_1^* \sum_{i=1}^N x_i^* + \beta_2 \sum_{i=1}^N x_i x_i^* + \beta_3 \sum_{i=1}^N (x_i^*)^2 &= \sum_{i=1}^N x_i^* y_i^*\end{aligned}\quad (3.9)$$

The linear system of Equation 3.9 can be reduced to the equivalent system expressed in matrix form, $M \cdot \beta = Y$, with matrix M , vector Y , and solving for vector β ,

$$\underbrace{\begin{bmatrix} N & \sum_{i=1}^N x_i & \sum_{i=1}^N x_i^* \\ \sum_{i=1}^N x_i & \sum_{i=1}^N (x_i)^2 & \sum_{i=1}^N x_i x_i^* \\ \sum_{i=1}^N x_i^* & \sum_{i=1}^N x_i x_i^* & \sum_{i=1}^N (x_i^*)^2 \end{bmatrix}}_M \cdot \underbrace{\begin{bmatrix} \beta_1^* \\ \beta_2 \\ \beta_3 \end{bmatrix}}_{\beta} = \underbrace{\begin{bmatrix} \sum_{i=1}^N y_i^* \\ \sum_{i=1}^N x_i y_i^* \\ \sum_{i=1}^N x_i^* y_i^* \end{bmatrix}}_Y \quad (3.10)$$

The solution for $\beta = [\beta_1^*, \beta_2, \text{ and } \beta_3]$ to the linear system $M \cdot \beta = Y$ can be determined with Cramer's formulas in terms of determinants. Solving for third order determinants, we have,

$$\beta_1^* = \frac{D_1}{D} \quad \beta_2 = \frac{D_2}{D} \quad \beta_3 = \frac{D_3}{D} \quad (3.11)$$

where D is the determinant of the matrix M and D_1, D_2, D_3 are each obtained by replacing the first, second and third columns of D , respectively, with the elements of the column Y . The determinants D, D_1, D_2 , and D_3 of the system can now be simply expressed as follows,

$$\begin{aligned}
 D = N \cdot & \left(\sum_{i=1}^N (x_i)^2 \cdot \sum_{i=1}^N (x_i^*)^2 - \sum_{i=1}^N x_i x_i^* \cdot \sum_{i=1}^N x_i x_i^* \right) \\
 & - \sum_{i=1}^N x_i \cdot \left(\sum_{i=1}^N x_i \cdot \sum_{i=1}^N (x_i^*)^2 - \sum_{i=1}^N x_i x_i^* \cdot \sum_{i=1}^N x_i^* \right) \\
 & + \sum_{i=1}^N x_i^* \cdot \left(\sum_{i=1}^N x_i \cdot \sum_{i=1}^N x_i x_i^* - \sum_{i=1}^N (x_i)^2 \cdot \sum_{i=1}^N x_i^* \right) \quad (3.12)
 \end{aligned}$$

$$\begin{aligned}
D_1 = & \sum_{i=1}^N y_i^* \cdot \left(\sum_{i=1}^N (x_i)^2 \cdot \sum_{i=1}^N (x_i^*)^2 - \sum_{i=1}^N x_i x_i^* \cdot \sum_{i=1}^N x_i x_i^* \right) \\
& - \sum_{i=1}^N x_i y_i^* \cdot \left(\sum_{i=1}^N x_i \cdot \sum_{i=1}^N (x_i^*)^2 - \sum_{i=1}^N x_i x_i^* \cdot \sum_{i=1}^N x_i^* \right) \\
& + \sum_{i=1}^N x_i^* y_i^* \cdot \left(\sum_{i=1}^N x_i \cdot \sum_{i=1}^N x_i x_i^* - \sum_{i=1}^N (x_i)^2 \cdot \sum_{i=1}^N x_i^* \right)
\end{aligned} \tag{3.13}$$

$$\begin{aligned}
D_2 = & - \sum_{i=1}^N y_i^* \cdot \left(\sum_{i=1}^N x_i \cdot \sum_{i=1}^N (x_i^*)^2 - \sum_{i=1}^N x_i^* \cdot \sum_{i=1}^N x_i x_i^* \right) \\
& + \sum_{i=1}^N x_i y_i^* \cdot \left(N \cdot \sum_{i=1}^N (x_i^*)^2 - \sum_{i=1}^N x_i^* \cdot \sum_{i=1}^N x_i^* \right) \\
& - \sum_{i=1}^N x_i^* y_i^* \cdot \left(N \cdot \sum_{i=1}^N x_i x_i^* - \sum_{i=1}^N x_i \cdot \sum_{i=1}^N x_i^* \right)
\end{aligned} \tag{3.14}$$

$$\begin{aligned}
D_3 = & \sum_{i=1}^N y_i^* \cdot \left(\sum_{i=1}^N x_i \cdot \sum_{i=1}^N x_i x_i^* - \sum_{i=1}^N x_i^* \cdot \sum_{i=1}^N (x_i)^2 \right) \\
& - \sum_{i=1}^N x_i y_i^* \cdot \left(N \cdot \sum_{i=1}^N x_i x_i^* - \sum_{i=1}^N x_i^* \cdot \sum_{i=1}^N x_i \right) \\
& + \sum_{i=1}^N x_i^* y_i^* \cdot \left(N \cdot \sum_{i=1}^N (x_i)^2 - \sum_{i=1}^N x_i \cdot \sum_{i=1}^N x_i \right)
\end{aligned} \tag{3.15}$$

From Cramer's rule (Equation 3.11), the coefficients, β_1^* , β_2^* , and β_3^* can now be determined. These parameters were originally estimated with the assumption that the sums of many independent and identically-distributed random variables possess a finite variance. With this in mind,

the residual error term or the variance, Equation 3.7, can be applied to determine the error in the estimates, the standard error (*Std. error*), defined as square root of the ratio of the square of the difference and the difference between N data points and the number of parameters (3),

$$Std. error = \sqrt{\frac{\sum_{i=1}^N [y_i^* - (\beta_1^* + \beta_2 x_i + \beta_3 x_i^*)]^2}{N-3}} \quad (3.16)$$

Typically, the smaller the *Std. error*, the more accurate the parameter estimation. As can be noted, the *Std. error* term will tend to get smaller with the increase in the number of data points. A 95 percent probability of non-exceedance will be used as an upper bound estimate. For a normally distributed variable, this value can be calculated by taking the product of the *Std. error* and 1.65, specifically from Equation 3.6 we can show that,

$$y^* = \beta_1^* + \beta_2 \cdot x + \beta_3 \cdot \ln(x) + 1.65 \cdot Std. error \quad (3.17)$$

Recalling that $\beta_1^* = \ln(\beta_1)$ and $y^* = \ln(y)$; taking the exponential of both sides of Equation 3.6 and the residual error term, reintroduces a form of Equation 3.3, namely,

$$y = \beta_1 \cdot \exp(\beta_2 \cdot x) \cdot x^{\beta_3} \cdot \exp(1.65 \cdot Std. error) \quad (3.18)$$

with $\beta_1 = \exp(\beta_1^*)$.

Finally, restoring to the original form of $\left[\frac{k_c}{k_m}, \frac{d_m \cdot k_m g}{v_m^2} \right]$ gives us the non-dimensionalized displacement equation for a 95 percent probability of non-exceedance,

$$\frac{d_m \cdot k_m g}{v_m^2} = \beta_1 \cdot \exp\left(\beta_2 \cdot \frac{k_c}{k_m}\right) \cdot \left(\frac{k_c}{k_m}\right)^{\beta_3} \cdot \exp(1.65 \cdot Std. error) \quad (3.19)$$

and the non-dimensionalized displacement equation of the mean of the estimate as presented in row one of Table 3.1,

$$\frac{d_m \bullet k_m \mathcal{G}}{v_m^2} = \beta_1 \bullet \exp\left(\beta_2 \bullet \frac{k_c}{k_m}\right) \bullet \left(\frac{k_c}{k_m}\right)^{\beta_3} \quad (3.20)$$

The estimate and its *Std. error* can also be used to construct prediction intervals about the mean estimate. These prediction intervals reflect ranges that limit the average of the estimated value with a known probability for a known distribution (a normal distribution for the transformed coordinate system in this case). For a selected N data set that is normally distributed, there is approximately a 68 percent probability that the average result will fall between one *Std. error* above the mean estimate and one *Std. error* below the mean estimate. The 68 percent prediction interval can be determined by modifying Equation 3.6 and adding/subtracting the *Std. error* as follows,

$$y^* = \beta_1^* + \beta_2 \bullet x + \beta_3 \bullet \ln(x) \pm \textit{Std. error} \quad (3.21)$$

or specifically,

$$y^* = \beta_1^* + \beta_2 \bullet x + \beta_3 \bullet \ln(x) + \textit{Std. error} \quad (3.21a)$$

and

$$y^* = \beta_1^* + \beta_2 \bullet x + \beta_3 \bullet \ln(x) - \textit{Std. error} \quad (3.21b)$$

Recalling that $\beta_1^* = \ln(\beta_1)$ and $y^* = \ln(y)$; taking the exponential of both sides of Equations 3.21a and 3.21b reintroduces a form of Equation 3.3, namely,

$$y = \beta_1 \bullet \exp(\beta_2 \bullet x) \bullet x^{\beta_3} \bullet \exp(\textit{Std. error}) \quad (3.22a)$$

and

$$y = \beta_1 \bullet \exp(\beta_2 \bullet x) \bullet x^{\beta_3} \bullet \exp(-\textit{Std. error}) \quad (3.22b)$$

with $\beta_1 = \exp(\beta_1^*)$.

Finally, restoring to the original form of $\left[\frac{k_c}{k_m}, \frac{d_m \bullet k_m g}{v_m^2} \right]$ gives us the non-dimensionalized displacement equations

$$\frac{d_m \bullet k_m g}{v_m^2} = \beta_1 \bullet \exp\left(\beta_2 \bullet \frac{k_c}{k_m}\right) \bullet \left(\frac{k_c}{k_m}\right)^{\beta_3} \bullet \exp(\text{Std. error}) \quad (3.23a)$$

$$\frac{d_m \bullet k_m g}{v_m^2} = \beta_1 \bullet \exp\left(\beta_2 \bullet \frac{k_c}{k_m}\right) \bullet \left(\frac{k_c}{k_m}\right)^{\beta_3} \bullet \exp(-\text{Std. error}) \quad (3.23b)$$

such that, there is a 68 percent probability that the mean of the estimate will fall between the 68 percent prediction intervals of Equations 3.23a and 3.23b.

3.3 Two-term regression analysis, linear in natural logarithm transformation (Equation Form Two)

A second form of a simplified permanent seismic displacement relationship attributed to Wong (1982) [reported in Whitman and Liao (1985)] for a soil site, is of the following form,

$$d_m = 37 \bullet \frac{v_m^2}{k_m g} \bullet \exp\left(-9.4 \bullet \frac{k_c}{k_m}\right) \quad (3.24)$$

Recall that Newmark (1965) introduced the peak ground acceleration and the peak ground velocity as characteristic soil parameters. Collecting these parameters, along with the permanent seismic displacement, the left-hand side becomes what is termed a non-dimensionalized displacement, which for the Wong relationship becomes,

$$\frac{d_m \bullet k_m g}{v_m^2} = 37 \bullet \exp\left(-9.4 \bullet \frac{k_c}{k_m}\right) \quad (3.25)$$

When discussing nonlinear regression, Equation 3.25 may be written in the general form of

$$y = \beta_1 \bullet \exp(\beta_2 \bullet x) \quad (3.26)$$

with

$$y = \frac{d_m \cdot k_m g}{v_m^2}; \quad \text{non-dimensionalized displacement, and}$$

$$x = \frac{k_c}{k_m}; \quad \text{critical acceleration ratio}$$

where:

$$d_m = \text{permanent displacement,}$$

$$k_m g = \text{maximum horizontal ground acceleration}$$

$$v_m = \text{maximum ground velocity}$$

$$k_c = \text{maximum transmissible acceleration capacity}$$

for which β_1 and β_2 are constants and the equation is nonlinear in β_2 .

The form of Equation 3.26 is now $[x, y]$ as compared to the original form $\left[\frac{k_c}{k_m}, \frac{d_m \cdot k_m g}{v_m^2} \right]$ of Equation 3.25.

Taking the natural log (ln) of both sides, Equation 3.26 becomes

$$\ln(y) = \ln(\beta_1) + \beta_2 \cdot x \quad (3.27)$$

which simplifies to

$$\ln(y) = \beta_1^* + \beta_2 \cdot x \quad (3.28)$$

with β_1^* equal to $\ln(\beta_1)$, or $\beta_1 = \exp(\beta_1^*)$.

The transformation of Equation 3.26 to Equations 3.27 and 3.28 resulted in the altered form of the equation from (x, y) to $(x, \ln(y))$ or specifically, (x, y^*) with $y^* = \ln(y)$, such that Equation 3.28 becomes,

$$y^* = \beta_1^* + \beta_2 \cdot x \quad (3.29)$$

From Equation 3.29, the set of basis functions $(1, x)$ are linear and the parameters $(\beta_1^*$ and $\beta_2)$ are constant. A linear regression analysis can be applied to solve for these constant parameters.

The least squares fitting method will be used to estimate the parameters $(\beta_1^*$ and $\beta_2)$ which will minimize the sum of squares of the distance from the specified curve, or produce the least possible value of S ,

$$S = \sum_{i=1}^N e_i^2 = \sum_{i=1}^N \left[y_i^* - (\beta_1^* + \beta_2 x_i) \right]^2 \quad (3.30)$$

with

$N =$ the total number of non-dimensionalized displacement terms.

We can estimate the parameters by taking the partial derivatives of Equation 3.30 with respect to β_1^* and β_2 , and setting the resultant equal to zero.

$$\frac{\partial S}{\partial \beta_1^*} = \sum_{i=1}^N 2 \left[y_i^* - (\beta_1^* + \beta_2 x_i) \right] (-1) = 0 \quad (3.31)$$

$$\frac{\partial S}{\partial \beta_2} = \sum_{i=1}^N 2 \left[y_i^* - (\beta_1^* + \beta_2 x_i) \right] (-x_i) = 0$$

The estimates of β_1^* and β_2 are then represented by 2 linear equations in 2 unknowns,

$$\beta_1^* (N) + \beta_2 \sum_{i=1}^N x_i = \sum_{i=1}^N y_i^* \quad (3.32)$$

$$\beta_1^* \sum_{i=1}^N x_i + \beta_2 \sum_{i=1}^N x_i^2 = \sum_{i=1}^N x_i y_i^*$$

The solution for β_1^* and β_2 to the linear system of Equation 3.32 can be numerically computed by applying the formula,

$$\beta_2 = \frac{\sum_{i=1}^N (x_i \cdot y_i^*) - \frac{\left(\sum_{i=1}^N x_i \right) \cdot \left(\sum_{i=1}^N y_i^* \right)}{N}}{\sum_{i=1}^N x_i^2 - \frac{\left(\sum_{i=1}^N x_i \right)^2}{N}}$$

or (3.33)

$$\frac{\sum_{i=1}^N \left[(x_i - \bar{x}) \cdot (y_i^* - \bar{y}^*) \right]}{\sum_{i=1}^N (x_i - \bar{x})^2}$$

$$\beta_1^* = \bar{y}^* - \beta_2 \bar{x} \quad (3.34)$$

with

$$\bar{y}^* = \frac{\sum_{i=1}^N y_i^*}{N}; \text{ the mean of } y^*$$

$$\bar{x} = \frac{\sum_{i=1}^N x_i}{N}; \text{ the mean of } x.$$

The parameters β_1^* and β_2 were originally estimated with the assumption that the sums of many independent and identically-distributed random variables possess a finite variance. With this in mind, the residual error term or the variance, Equation 3.30 can be applied to determine the error in the estimates, the standard error (*Std. error*), defined as the square root of the ratio of the square of the difference and the difference between N data points and the number of parameters (2),

$$\text{Std. error} = \sqrt{\frac{\sum_{i=1}^N \left[y_i^* - (\beta_1^* + \beta_2 x_i) \right]^2}{N-2}} \quad (3.35)$$

Typically, the smaller the *Std. error*, the more accurate the parameter estimation. As can be noted, the *Std. error* term will tend to get smaller with the increase in the number of data points. A 95 percent probability of non-exceedance will be used as an upper bound estimate. For a normally distributed variable, this value can be calculated by taking the product of the *Std. error* and 1.65, specifically from Equation 3.29 we can show that,

$$y^* = \beta_1^* + \beta_2 \bullet x + 1.65 \bullet \text{Std. error} \quad (3.36)$$

Recalling that $\beta_1^* = \ln(\beta_1)$ and $y^* = \ln(y)$; taking the exponential of both sides of Equation 3.29 and the residual error term, reintroduces a form of Equation 3.26, namely,

$$y = \beta_1 \bullet \exp(\beta_2 \bullet x) \bullet \exp(1.65 \bullet \text{Std. error}) \quad (3.37)$$

with $\beta_1 = \exp(\beta_1^*)$.

Finally, restoring to the original form of $\left[\frac{k_c}{k_m}, \frac{d_m \bullet k_m g}{v_m^2} \right]$ gives us the non-dimensionalized displacement equation for a 95 percent probability of non-exceedance,

$$\frac{d_m \bullet k_m g}{v_m^2} = \beta_1 \bullet \exp\left(\beta_2 \bullet \frac{k_c}{k_m}\right) \bullet \exp(1.65 \bullet \text{Std. error}) \quad (3.38)$$

and the non-dimensionalized displacement equation of the mean of the estimate, as presented in row two of Table 3.1,

$$\frac{d_m \bullet k_m g}{v_m^2} = \beta_1 \bullet \exp\left(\beta_2 \bullet \frac{k_c}{k_m}\right) \quad (3.39)$$

The estimate and its *Std. error* can also be used to construct prediction intervals about the mean estimate. These prediction intervals reflect ranges that limit the average of the estimated value with a known probability for a known distribution (a normal distribution for the transformed coordinate system in this case). For a selected N data set that is normally distributed, there is approximately a 68 percent probability that the average result will fall between one *Std. error* above the mean estimate

and one *Std. error* below the mean estimate. The 68 percent prediction interval can be determined by modifying Equation 3.39 and adding/subtracting the *Std. error* as follows,

$$y^* = \beta_1^* + \beta_2 \bullet x \pm \textit{Std. error} \quad (3.40)$$

or specifically,

$$y^* = \beta_1^* + \beta_2 \bullet x + \textit{Std. error} \quad (3.40a)$$

and

$$y^* = \beta_1^* + \beta_2 \bullet x - \textit{Std. error} \quad (3.40b)$$

Recalling that $\beta_1^* = \ln(\beta_1)$ and $y^* = \ln(y)$; taking the exponential of both sides of Equations 3.40a and 3.40b reintroduces a form of Equation 3.26, namely,

$$y = \beta_1 \bullet \exp(\beta_2 \bullet x) \bullet \exp(\textit{Std. error}) \quad (3.41a)$$

and

$$y = \beta_1 \bullet \exp(\beta_2 \bullet x) \bullet \exp(-\textit{Std. error}) \quad (3.41b)$$

with $\beta_1 = \exp(\beta_1^*)$.

Finally, restoring to the original form of $\left[\frac{k_c}{k_m}, \frac{d_m \bullet k_m g}{v_m^2} \right]$ gives us the non-dimensionalized displacement equations

$$\frac{d_m \bullet k_m g}{v_m^2} = \beta_1 \bullet \exp\left(\beta_2 \bullet \frac{k_c}{k_m}\right) \bullet \exp(\textit{Std. error}) \quad (3.42a)$$

$$\frac{d_m \bullet k_m g}{v_m^2} = \beta_1 \bullet \exp\left(\beta_2 \bullet \frac{k_c}{k_m}\right) \bullet \exp(-\textit{Std. error}) \quad (3.42b)$$

such that, there is a 68 percent probability that the mean of the estimate will fall between the 68 percent prediction intervals of Equations 3.42a and 3.42b.

3.4 Two-term regression analysis, linear in common logarithm transformation (Equation Form One)

A third form of a simplified permanent seismic displacement relationship attributed to Richards and Elms (1979) for a soil site, is of the following form,

$$d_m = 0.087 \cdot \frac{v_m^2}{k_m g} \cdot \left(\frac{k_c}{k_m} \right)^{-4} \quad (3.43)$$

Recall that Newmark (1965) introduced the peak ground acceleration and the peak ground velocity as characteristic soil parameters. Collecting these parameters, along with the permanent seismic displacement, the left-hand side becomes what is termed a non-dimensionalized displacement, which for the Richards and Elms relationship becomes,

$$\frac{d_m \cdot k_m g}{v_m^2} = 0.087 \cdot \left(\frac{k_c}{k_m} \right)^{-4} \quad (3.44)$$

When discussing nonlinear regression, this Equation 3.44 may be written in the general form of

$$y = \beta_4 \cdot x^{\beta_5} \quad (3.45)$$

with

$$y = \frac{d_m \cdot k_m g}{v_m^2}; \quad \text{non-dimensionalized displacement, and}$$

$$x = \frac{k_c}{k_m}; \quad \text{critical acceleration ratio}$$

where:

$$d_m = \text{permanent displacement,}$$

$$k_m g = \text{maximum horizontal ground acceleration}$$

v_m = maximum ground velocity
 k_c = maximum transmissible acceleration capacity

for which β_4 and β_5 are constants.

The form of Equation 3.45 is now $[x, y]$ as compared to the original form $\left[\frac{k_c}{k_m}, \frac{d_m \bullet k_m g}{v_m^2} \right]$ of Equation 3.2.

Taking the common log (\log_{10} or \log) of both sides, Equation 3.45 becomes

$$\log(y) = \log(\beta_4) + \beta_5 \bullet \log(x) \quad (3.46)$$

which simplifies to

$$\log(y) = \beta_4^{**} + \beta_5 \bullet \log(x) \quad (3.47)$$

with β_4^{**} equal to $\log(\beta_4)$, or $\beta_4 = 10^{(\beta_4^{**})}$.

The transformation of Equation 3.45 to Equations 3.46 and 3.47 resulted in the altered form of the equation from (x, y) to $(x, \log(y))$ or specifically, (x, y^{**}) with $y^{**} = \log(y)$, such that Equation 3.47 becomes,

$$y^{**} = \beta_4^{**} + \beta_5 \bullet \log(x) \quad (3.48)$$

From Equation 3.48, the set of basis functions $(1, \log(x))$ have a nonlinear term, $\log(x)$; however, the parameters β_4^{**} and β_5 are constant and not part of any nonlinear term. Regression models which are a linear function of the parameters are called linear regression models. Therefore, a linear regression analysis can be applied to solve for these constant parameters.

The least squares fitting method will be used to estimate the parameters β_4^{**} and β_5 which will minimize the sum of squares of the distance from the specified curve, or produce the least possible value of S ,

$$S = \sum_{i=1}^N e_i^2 = \sum_{i=1}^N \left[y_i^{**} - (\beta_4^{**} + \beta_5 \bullet x_i^{**}) \right]^2 \quad (3.49)$$

with

N = the total number of non-dimensionalized displacement terms.
 $\mathbf{x}^{**} = \log(\mathbf{x})$.

We can estimate the parameters by taking the partial derivatives of Equation 3.49 with respect to β_4^{**} and β_5 , and setting the resultant equal to zero.

$$\frac{\partial \mathcal{S}}{\partial \beta_4^{**}} = \sum_{i=1}^N 2 \left[y_i^{**} - (\beta_4^{**} + \beta_5 \bullet \mathbf{x}_i^{**}) \right] (-1) = 0 \quad (3.50)$$

$$\frac{\partial \mathcal{S}}{\partial \beta_5} = \sum_{i=1}^N 2 \left[y_i^{**} - (\beta_4^{**} + \beta_5 \bullet \mathbf{x}_i^{**}) \right] (-\mathbf{x}_i^{**}) = 0$$

The estimates of β_4^{**} and β_5 are then represented by 2 linear equations in 2 unknowns,

$$\beta_4^{**} (N) + \beta_5 \sum_{i=1}^N \mathbf{x}_i^{**} = \sum_{i=1}^N y_i^{**} \quad (3.51)$$

$$\beta_4^{**} \sum_{i=1}^N \mathbf{x}_i^{**} + \beta_5 \sum_{i=1}^N (\mathbf{x}_i^{**})^2 = \sum_{i=1}^N \mathbf{x}_i^{**} \bullet y_i^{**}$$

The solution for β_4^{**} and β_5 to the linear system of Equation 3.51 can be numerically computed by applying the formulae,

$$\beta_5 = \frac{\sum_{i=1}^N (x_i^{**} \cdot y_i^{**}) - \frac{\left(\sum_{i=1}^N x_i^{**} \right) \cdot \left(\sum_{i=1}^N y_i^{**} \right)}{N}}{\sum_{i=1}^N (x_i^{**})^2 - \frac{\left(\sum_{i=1}^N x_i^{**} \right)^2}{N}}$$

or (3.52)

$$= \frac{\sum_{i=1}^N \left[(x_i^{**} - \bar{x}^{**}) \cdot (y_i^{**} - \bar{y}^{**}) \right]}{\sum_{i=1}^N (x_i^{**} - \bar{x}^{**})^2}$$

$$\beta_4^{**} = \bar{y}^{**} - \beta_5 \bar{x}^{**} \quad (3.53)$$

with

$$\bar{y}^{**} = \frac{\sum_{i=1}^N y_i^{**}}{N}; \quad \text{the mean of } y^{**}$$

$$\bar{x}^{**} = \frac{\sum_{i=1}^N x_i^{**}}{N}; \quad \text{the mean of } x^{**}$$

The parameters β_4^{**} and β_5 were originally estimated with the assumption that the sums of many independent and identically-distributed random variables possess a finite variance. With this in mind, the residual error term or the variance, Equation 3.49 can be applied to determine the error in the estimates, the standard error (*Std. error*), defined as the square root of the ratio of the square of the difference and the difference between N data points and the number of parameters (2),

$$\text{Std. error} = \sqrt{\frac{\sum_{i=1}^N \left[y_i^{**} - (\beta_4^{**} + \beta_5 x_i^{**}) \right]^2}{N-2}} \quad (3.54)$$

Typically, the smaller the *Std. error*, the more accurate the parameter estimation. As can be noted, the *Std. error* term will tend to get smaller with the increase in the number of data points. A 95 percent probability of non-exceedance will be used as an upper bound estimate. For a normally distributed variable, this value can be calculated by taking the product of the *Std. error* and 1.65, specifically from Equation 3.48 we can show that,

$$y^{**} = \beta_4^{**} + \beta_5 \cdot \log(x) + 1.65 \cdot \text{Std. error} \quad (3.55)$$

Recalling that $\beta_4^{**} = \log(\beta_4)$ and $y^{**} = \log(y)$; taking the antilog of both sides of Equation 3.55 with the residual error term, reintroduces a form of Equation 3.45, namely,

$$y = \beta_4 \cdot x^{\beta_5} \cdot 10^{(1.65 \cdot \text{Std. error})} \quad (3.56)$$

with $\beta_4 = 10^{(\beta_4^{**})}$.

Finally, restoring to the original form of $\left[\frac{k_c}{k_m}, \frac{d_m \cdot k_m g}{v_m^2} \right]$ gives us the non-dimensionalized displacement equation for a 95 percent probability of non-exceedance,

$$\frac{d_m \cdot k_m g}{v_m^2} = \beta_4 \cdot \left(\frac{k_c}{k_m} \right)^{\beta_5} \cdot 10^{(1.65 \cdot \text{Std. error})} \quad (3.57)$$

and the non-dimensionalized displacement equation of the mean of the estimate, as presented in row three of Table 3.1,

$$\frac{d_m \cdot k_m g}{v_m^2} = \beta_4 \cdot \left(\frac{k_c}{k_m} \right)^{\beta_5} \quad (3.58)$$

The estimate and its *Std. error* can also be used to construct prediction intervals about the mean estimate. These prediction intervals reflect ranges that limit the average of the estimated value with a known probability for a known distribution (a normal distribution for the transformed coordinate system in this case). For a selected N data set that is normally distributed, there is approximately a 68 percent probability that the

average result will fall between one *Std. error* above the mean estimate and one *Std. error* below the mean estimate. The 68 percent prediction interval can be determined by modifying Equation 3.48 and adding/subtracting the *Std. error* as follows,

$$y^{**} = \beta_4^{**} + \beta_5 \bullet \log(x) \pm \textit{Std. error} \quad (3.59)$$

or specifically,

$$y^{**} = \beta_4^{**} + \beta_5 \bullet \log(x) + \textit{Std. error} \quad (3.59a)$$

and

$$y^{**} = \beta_4^{**} + \beta_5 \bullet \log(x) - \textit{Std. error} \quad (3.59b)$$

Recalling that $\beta_4^{**} = \log(\beta_4)$ and $y^{**} = \log(y)$; taking the antilog of both sides of Equations 3.59a and 3.59b reintroduces a form of Equation 3.45, namely,

$$y = \beta_4 \bullet x^{\beta_5} \bullet 10^{\textit{Std. error}} \quad (3.60a)$$

and

$$y = \beta_4 \bullet x^{\beta_5} \bullet 10^{-\textit{Std. error}} \quad (3.60b)$$

with $\beta_4 = 10^{(\beta_4^{**})}$.

Finally, restoring to the original form of $\left[\frac{k_c}{k_m}, \frac{d_m \bullet k_m g}{v_m^2} \right]$ gives us the non-dimensionalized displacement equations

$$\frac{d_m \bullet k_m g}{v_m^2} = \beta_4 \bullet \left(\frac{k_c}{k_m} \right)^{\beta_5} \bullet 10^{\textit{Std. error}} \quad (3.61a)$$

$$\frac{d_m \bullet k_m g}{v_m^2} = \beta_4 \bullet \left(\frac{k_c}{k_m} \right)^{\beta_5} \bullet 10^{-\textit{Std. error}} \quad (3.61b)$$

such that, there is a 68 percent probability that the mean of the estimate will fall between the 68 percent prediction intervals of Equations 3.61a and 3.61b.

4 Regression results for ground motions recorded on rock

4.1 Introduction

This chapter discusses the regression analysis of the permanent displacement of rock acceleration time histories.

A rock site acceleration time-history database developed for use with the permanent displacement regression analysis involved selecting, documenting, processing, and archiving engineering significant data from rock or stiff soil sites. One goal was to collect sufficient data to capture the inherent variability of earthquake ground response. Practically, this goal is not fully realizable due to the limited data set compared to an ideal complete set of data which would represent all combinations of tectonic settings, earthquake sizes, source to site distances, and site conditions. For example, large magnitude earthquake data at near distances, while increasing as strong ground motion monitoring is improving, is still limited resulting from the rareness of large earthquakes coupled with near field recording sites. This limited data aspect is the rationale for including stiff soil site records to build a sufficiently large rock site data set to support robust analyses applicable to a reasonable range of engineering significant situations with insight into its variability. Conversely, since the effort to build a large data set from a limited basis may tend to create bias, in order to counteract this data from different earthquakes, in different regions at a spread of ranges were selected.

To manage the data collection and follow-on analysis, three data sets were developed applicable for nominally small (Magnitude 5), medium (Magnitude 6), and large (Magnitude 7) earthquake sizes. The overall size range for the three sets was set at $M_w = 4.9$ at the low end and open ended for large size earthquakes. These three datasets are completely described within Tables 4.1, 4.2, and 4.3, respectively. The largest earthquake magnitude is $M_w = 8.1$ for these data. Table 4.4 describes the classifications of the three data sets. This cutoff on the low end was necessary based on the number of available records from the more frequent small magnitude events and the engineering significance of strong ground motions.

In addition to a minimum magnitude restriction in the data search, an additional lower bound constraint was set at $0.007 g$ for the peak ground acceleration. The magnitude boundaries between the three earthquake data sets was arbitrary in the sense that there is not an implied physical basis for these separations at or near these magnitude boundaries of 4.9, 6.1, and 6.9, but were chosen based on populating a sufficient number in each set. In this respect, one should not expect to find different results in using data from either set near the dividing magnitudes.

Important to the documentation and use of these data are the definitions for the parameters of earthquake magnitude and site conditions. Interestingly, earthquake magnitude is not a simple data parameter because of the historical development of various earthquake magnitude scales and now backwards application of new magnitude scales to historical events. Earthquake magnitude scale to assess the size of an earthquake was initially based on resulting levels of damage before seismic instrumentation was developed to measure ground motions. The initial use of the damage-based Mercalli Intensity scale had evolved to determinations based on measured response of earthquake accelerographs and most recently to current use of a magnitude scale based on a mechanical concept based energy released, estimated on the area of the ruptured crust and the strength of crust. This current preferred scale in engineering seismology is the moment magnitude scale (M_w) and necessarily involves backwards assignment to historical data collected prior to its accepted and now routine use. Table 4.5 is provided to illustrate this backward application and how the assigned earthquake magnitudes have changed for a few historically significant earthquakes.

The M_w is a standard magnitude scale that is completely independent of the type of instrument such as Richter (M) and surface wave (M_s), which are indirect estimations of strain energy based on measured displacement amplitudes of seismic waves of certain periods and at certain distances from sources. The M_w is a more direct measure of energy since it is based on calculated frictional resistance over the area of fault slippage.

Table 4.1. Master accelerograph table of magnitude 6.9 – 8.1.

M7 Master Accelerograph Table																								
Set	Rec#	Filename	Mw	Distance (hyp) km	PGA		PGV		PGD		Ratio 1		Ratio 2		AI 95%	Duration bracketed	Site Class	Region	Comp	deg	Setting & Mech	Earthquake	Date	Station
					+	-	+	-	Lin Disp		vm/km		d*km/vm ²											
					g%		cm/s		cm		in./s/%g													
1	1	101_lpg1_090a.dat	7.0	33	0.442	-0.418	27.0	-33.8	8.50	-2.90	24.1	31.8	5.04	1.04	151	9.7	Rock(a)	WUS	H1	90	XX-RO-17	Loma Prieta	10/18/1989	Gilroy Array #1
	2	102_lpg1_000a.dat	7.0	33	0.435	-0.375	32.5	-11.2	4.28	-9.49	29.4	11.8	1.73	27.71	95	13.2	Rock(a)	WUS	H2	0	XX-RO-17	Loma Prieta	10/18/1989	Gilroy Array #1
	3	103_lpg1_0upa.dat	7.0	33	0.178	-0.210	8.3	-15.3	8.29	-3.79	18.4	28.6	20.99	3.36	26	4.3	Rock(a)	WUS	V	UP	XX-RO-17	Loma Prieta	10/18/1989	Gilroy Array #1
2	4	104_hmjt_360a.dat	7.1	52	0.168	-0.190	14.0	-23.2	5.40	-5.00	32.8	48.1	4.54	1.73	56	13.1	Rock(w/s)	WUS	H1	360	MF-SS-05	Hector Mine	10/16/1999	Joshua Tree Fire Sta
	5	105_hmjt_090a.dat	7.1	52	0.102	-0.146	17.6	-17.1	7.00	-5.00	68.1	46.1	2.25	2.46	31	12.5	Rock(w/s)	WUS	H2	90	MF-SS-05	Hector Mine	10/16/1999	Joshua Tree Fire Sta
	6	106_hmjt_0upa.dat	7.1	52	0.102	-0.121	9.0	-8.0	4.12	-4.16	34.7	25.9	5.10	7.77	27	14.0	Rock(w/s)	WUS	V	UP	MF-SS-05	Hector Mine	10/16/1999	Joshua Tree Fire Sta
3	7	107_lpld_000a.dat	7.1	26	0.388	-0.442	38.0	-84.3	12.03	-16.01	38.6	75.1	3.17	0.98	168	6.7	Rock	WUS	H1	0	XX-RO-17	Loma Prieta	10/18/1989	Lexington Dam -Abut
	8	108_lpld_090a.dat	7.1	26	0.297	-0.409	31.9	-95.5	32.44	-10.98	42.3	91.9	9.27	0.48	158	7.1	Rock	WUS	H2	90	XX-RO-17	Loma Prieta	10/18/1989	Lexington Dam -Abut
	9	109_lpld_0upa.dat	7.1	26	0.117	-0.133	25.9	-16.8	11.86	-16.77	87.1	49.8	2.03	7.74	18	5.2	Rock	WUS	V	UP	XX-RO-17	Loma Prieta	10/18/1989	Lexington Dam -Abut
4	10	110_inut_075a.dat	7.0	34	0.310	-0.224	15.8	-18.7	1.57	-2.32	20.1	32.8	1.90	1.46	87	8.3	Rock	India	H1	0	XX-XX-10	Uttarakshi, India	10/19/1991	IIT Roorkee, India
	11	111_inut_345a.dat	7.0	34	0.227	-0.242	17.1	-9.6	1.82	-3.51	29.6	15.6	1.38	9.06	68	8.9	Rock	India	H2	345	XX-XX-10	Uttarakshi, India	10/19/1991	IIT Roorkee, India
	12	112_inut_0upa.dat	7.0	34	0.189	-0.197	13.2	-7.6	2.93	-2.12	27.6	15.2	3.10	7.04	48	10.4	Rock	India	V	V	XX-XX-10	Uttarakshi, India	10/19/1991	IIT Roorkee, India
5	13	113_dz65_00xa.dat	7.1	23	0.496	-0.332	15.5	-16.5	1.58	-2.24	12.3	19.6	3.22	2.67	180	21.2	Rock	Turkey	H1	EW	XX-SS-10	Duzce, Turkey	11/12/1999	LEDO Sta 6500
	14	114_dz65_00ya.dat	7.1	23	0.619	-0.920	39.0	-27.1	2.76	-3.05	24.8	11.6	1.10	3.74	885	23.8	Rock	Turkey	H2	NS	XX-SS-10	Duzce, Turkey	11/12/1999	LEDO Sta 6501
	15	115_dz65_0upa.dat	7.1	23	0.182	-0.151	5.0	-5.3	1.32	-1.55	10.8	13.8	9.36	8.23	39	17.3	Rock	Turkey	V	V	XX-SS-10	Duzce, Turkey	11/12/1999	LEDO Sta 6502
6	16	116_kbku_000a.dat	6.9	31	0.290	-0.239	42.3	-54.8	8.92	-13.59	57.5	90.2	1.41	1.06	110	9.5	Rock	Japan	H1	0	XX-SS-18	Kobe, Japan	1/16/1995	Kobe University
	17	117_kbku_090a.dat	6.9	31	0.310	-0.196	34.2	-20.2	7.17	-6.21	43.5	40.6	1.86	2.92	74	7.4	Rock	Japan	H2	90	XX-SS-18	Kobe, Japan	1/16/1995	Kobe University
	18	118_kbku_0upa.dat	6.9	31	0.380	-0.324	16.5	-20.2	5.17	-6.55	17.1	24.5	7.06	5.12	59	6.8	Rock	Japan	V	UP	XX-SS-18	Kobe, Japan	1/16/1995	Kobe University
7	19	119_kbch_000a.dat	6.9	65	0.079	-0.093	5.9	-4.8	1.83	-2.90	29.4	20.3	4.08	11.51	11	6.2	Rock	Japan	H1	0	XX-SS-18	Kobe, Japan	1/20/1995	Chihaya
	20	120_kbch_090a.dat	6.9	65	0.102	-0.108	3.4	-4.7	0.83	-1.08	13.0	17.1	7.25	5.19	14	8.5	Rock	Japan	H2	90	XX-SS-18	Kobe, Japan	1/20/1995	Chihaya
	21	121_kbch_0upa.dat	6.9	65	0.067	-0.080	2.0	-2.4	1.14	-1.52	11.5	12.0	19.46	20.35	8	8.7	Rock	Japan	V	UP	XX-SS-18	Kobe, Japan	1/20/1995	Chihaya
8	22	122_lpuc_000a.dat	7.0	66	0.120	-0.157	17.2	-13.1	6.78	-5.20	56.6	33.1	2.68	4.62	26	9.8	Rock	WUS	H1	0	XX-RO-17	Loma Prieta	10/18/1989	Up. Crystal Spr Pulgas
	23	123_lpuc_090a.dat	7.0	66	0.083	-0.086	10.3	-14.1	4.54	-5.85	48.9	64.3	3.46	2.49	16	7.8	Rock	WUS	H2	90	XX-RO-17	Loma Prieta	10/18/1989	Up. Crystal Spr Pulgas
	24	124_lpuc_0upa.dat	7.0	66	0.041	-0.061	6.2	-4.3	2.51	-2.22	58.9	27.9	2.67	7.14	5	2.9	Rock	WUS	V	UP	XX-RO-17	Loma Prieta	10/18/1989	Up. Crystal Spr Pulgas
9	25	125_saak_090a.dat	7.1	79	0.208	-0.173	5.0	-4.6	0.70	-0.57	9.5	10.5	5.69	4.53	22	9.2	Rock	Alaska	H1	90	XX-XX-43	Southeast Alaska	5/2/1971	Adak AK Naval Base
	26	126_saak_180a.dat	7.1	79	0.099	-0.117	3.2	-2.2	0.38	-0.57	13.0	7.5	3.48	13.10	6	3.7	Rock	Alaska	H2	180	XX-XX-43	Southeast Alaska	5/2/1971	Adak AK Naval Base
	27	127_saak_0upa.dat	7.1	79	0.065	-0.063	2.0	-2.6	0.77	-0.51	12.4	16.3	11.75	4.61	4	1.1	Rock	Alaska	V	UP	XX-XX-43	Southeast Alaska	5/2/1971	Adak AK Naval Base
10	28	128_cmppt_090a.dat	7.0	16	1.040	-1.017	37.5	-42.4	12.59	-25.15	14.2	16.4	9.11	13.96	217	34.2	Rock	WUS	H2	90	XX-RV-10	Cape Mendocino	4/25/1992	Cape Mendocino - Petrolia
	29	129_cmppt_000a.dat	7.0	16	1.498	-0.494	38.2	-129.2	11.80	-54.21	10.0	103.0	11.89	1.57	543	37.9	Rock	WUS	H1	180	XX-RV-10	Cape Mendocino	4/25/1992	Cape Mendocino - Petrolia
	30	130_cmppt_0upa.dat	7.0	16	0.514	-0.755	70.0	-54.7	133.42	-13.94	53.6	28.5	13.73	3.45	125	7.9	Rock	WUS	V	UP	XX-RV-10	Cape Mendocino	4/25/1992	Cape Mendocino - Petrolia
11	31	131_inbb_360a.dat	7.3	46	0.170	-0.192	14.0	-10.9	7.86	-9.44	32.3	22.4	6.71	14.89	56.64	25.1	Rock	WUS	H1	360	XX-SS-05	Landers	6/28/1992	Big Bear Lake - Civic Center
	32	132_inbb_270a.dat	7.3	46	0.165	-0.116	7.2	-7.6	3.43	-3.31	17.3	25.8	10.55	6.52	50.35	21.6	Rock	WUS	H2	270	XX-SS-05	Landers	6/28/1992	Big Bear Lake - Civic Center
	33	133_inbb_0upa.dat	7.3	46	0.064	-0.081	4.0	-4.1	1.18	-1.54	24.3	20.2	4.72	7.10	13.29	15.6	Rock	WUS	V	UP	XX-SS-05	Landers	6/28/1992	Big Bear Lake - Civic Center
12	34	134_tbir_190a.dat	7.4	18	0.401	-0.277	16.5	-25.0	9.86	-8.78	16.2	35.5	14.30	3.83	152.85	36.9	Rock	Iran	H1	190	XX-XX-XX	Tabas, Iran	9/16/1978	Ministry of Housing & Urban Dev.
	35	135_tbir_080a.dat	7.4	18	0.371	-0.290	24.5	-24.4	22.29	-23.32	25.9	33.1	13.58	11.15	160.34	36.8	Rock	Iran	H2	80	XX-XX-XX	Tabas, Iran	9/16/1978	Ministry of Housing & Urban Dev.
	36	136_tbir_0upa.dat	7.4	18	0.180	-0.189	12.1	-10.7	10.22	-6.28	26.4	22.3	12.38	10.17	84.9	35.7	Rock	Iran	V	UP	XX-XX-XX	Tabas, Iran	9/16/1978	Ministry of Housing & Urban Dev.

M7 Master Accelerograph Table																								
Set	Rec#	Filename	Mw	Distance (hyp) km	PGA		PGV		PGD		Ratio 1		Ratio 2		AI 95%	Duration bracketed	Site Class	Region	Comp	deg	Setting & Mech	Earthquake	Date	Station
					+	-	+	-	+	-	+	-	+	-										
					g%		cm/s		cm		in./s/%g													
13	37	137_elob_180a.dat	7.6	109	0.428	-0.404	35.7	-38.4	8.68	-4.12	32.8	37.4	2.86	1.11	346.19	33.7	Rock	El Salvador	H1	180	XX-XX-60	El Salvador	1/13/2001	Observatorio
	38	138_elob_090a.dat	7.6	109	0.349	-0.379	24.6	-26.1	4.63	-5.82	27.7	27.1	2.62	3.17	225.96	31.0	Rock	El Salvador	H2	90	XX-XX-60	El Salvador	1/13/2001	Observatorio
	39	139_elob_0upa.dat	7.6	109	0.253	-0.306	13.0	-11.6	6.33	-5.38	20.2	14.9	9.28	12.07	156.2	33.9	Rock	El Salvador	V	UP	XX-XX-60	El Salvador	1/13/2001	Observatorio
14	40	140_elism_360a.dat	7.6	80	0.581	-0.881	26.6	-27.8	4.06	-5.95	18.0	12.4	3.26	6.65	866.49	33.3	Rock	El Salvador	H1	360	XX-XX-60	El Salvador	1/13/2001	Santiago de Maria
	41	141_elism_090a.dat	7.6	80	0.646	-0.716	40.4	-40.1	8.41	-6.70	24.6	22.0	3.27	2.93	1057.8	35.2	Rock	El Salvador	H2	90	XX-XX-60	El Salvador	1/13/2001	Santiago de Maria
	42	142_elism_0upa.dat	7.6	80	0.440	-0.402	14.0	-16.1	6.88	-4.66	12.5	15.7	15.18	7.10	302	31.1	Rock	El Salvador	V	UP	XX-XX-60	El Salvador	1/13/2001	Santiago de Maria
15	43	143_itst_000a.dat	6.9	32	0.251	-0.231	36.4	-27.7	10.61	-11.37	57.2	47.2	1.97	3.36	107.28	17.3	Rock	Iprina, Italy	H1	0	XX-XX-9.5	Iprina, Italy	11/23/1980	ENEL, Struno, Italy
	44	144_itst_270a.dat	6.9	32	0.287	-0.358	49.2	-51.8	17.54	-32.36	67.5	57.0	2.04	4.23	127.08	23.7	Rock	Iprina, Italy	H2	270	XX-XX-9.5	Iprina, Italy	11/23/1980	ENEL, Struno, Italy
	45	145_itst_0upa.dat	6.9	32	0.260	-0.166	16.7	-25.6	10.29	-6.36	25.3	60.8	9.41	1.58	46.52	11.6	Rock	Iprina, Italy	V	UP	XX-XX-9.5	Iprina, Italy	11/23/1980	ENEL, Struno, Italy
16	46	146_itba_000a.dat	6.9	25	0.133	-0.139	22.1	-15.8	7.96	-9.24	65.2	44.6	2.14	5.07	30.35	9.1	Rock	Iprina, Italy	H1	0	XX-XX-9.5	Iprina, Italy	11/23/1980	ENEL, Bagnoli, Italy
	47	147_itba_270a.dat	6.9	25	0.202	-0.177	31.9	-17.8	9.59	-9.24	62.1	39.5	1.87	5.07	38.97	10.6	Rock	Iprina, Italy	H2	270	XX-XX-9.5	Iprina, Italy	11/23/1980	ENEL, Bagnoli, Italy
	48	148_itba_0upa.dat	6.9	25	0.108	-0.090	11.8	-14.1	4.80	-5.75	43.0	61.9	3.65	2.54	15.66	7.2	Rock	Iprina, Italy	V	UP	XX-XX-9.5	Iprina, Italy	11/23/1980	ENEL, Bagnoli, Italy
17	49	149_itbi_000a.dat	6.9	25	0.061	-0.100	23.4	-14.4	14.03	-12.65	152.2	56.7	1.52	5.96	16.91	9.9	Rock	Iprina, Italy	H1	0	XX-XX-9.5	Iprina, Italy	11/23/1980	ENEL, Bisaccia, Italy
	50	150_itbi_270a.dat	6.9	25	0.083	-0.057	11.9	-12.5	2.89	-2.93	56.6	86.9	1.65	1.04	12.46	2.1	Rock	Iprina, Italy	H2	270	XX-XX-9.5	Iprina, Italy	11/23/1980	ENEL, Bisaccia, Italy
	51	151_itbi_0upa.dat	6.9	25	0.055	-0.067	14.1	-11.6	11.12	-9.09	100.9	68.1	3.02	4.46	10.49	0.8	Rock	Iprina, Italy	V	UP	XX-XX-9.5	Iprina, Italy	11/23/1980	ENEL, Bisaccia, Italy
18	52	152_tasm_0ewa.dat	7.3	73	0.112	-0.136	13.5	-9.5	5.90	-4.77	47.3	27.4	3.57	7.11	28.95	9.1	Rock	Taiwan	H1	EW	XX-XX-15	Smart, Taiwan	11/14/1986	Smart, Taiwan
	53	153_tasm_0nsa.dat	7.3	73	0.139	-0.143	12.4	-10.5	3.43	-6.06	35.2	29.0	3.02	7.67	33.87	37.6	Rock	Taiwan	H2	NS	XX-XX-15	Smart, Taiwan	11/14/1986	Smart, Taiwan
	54	154_tasm_0dna.dat	7.3	73	0.042	-0.052	4.8	-5.4	1.96	-3.05	45.3	40.8	3.49	5.33	6.44	0.0	Rock	Taiwan	V	DN	XX-XX-15	Smart, Taiwan	11/14/1986	Smart, Taiwan
19	55	155_tach_45ea.dat	7.6	78	0.401	-0.474	36.6	-32.7	21.51	-50.39	35.9	27.1	6.32	21.95	125.55	21.7	Rock	Taiwan	H1	E	XX-XX-6.8	ChiChi	9/20/1999	ChiChi, Taiwan
	56	156_tach_45na.dat	7.6	78	0.512	-0.250	27.8	-39.1	13.59	-14.20	21.4	61.5	8.81	2.28	105.88	14.2	Rock	Taiwan	H2	N	XX-XX-6.8	ChiChi	9/20/1999	ChiChi, Taiwan
	57	157_tach_45va.dat	7.6	78	0.181	-0.361	21.4	-15.9	12.43	-22.90	46.6	17.3	4.81	32.27	33.95	12.6	Rock	Taiwan	V	V	XX-XX-6.8	ChiChi	9/20/1999	ChiChi, Taiwan
20	58	158_tach_71ea.dat	7.6	17	0.567	-0.524	37.6	-44.5	13.76	-12.62	26.1	33.4	5.40	3.28	839.55	58.2	Rock	Taiwan	H1	E	XX-XX-6.8	ChiChi	9/20/1999	ChiChi, Taiwan
	59	159_tach_71na.dat	7.6	17	0.567	-0.655	47.0	-69.4	48.34	-49.53	32.6	41.7	12.17	6.60	855.32	58.7	Rock	Taiwan	H2	N	XX-XX-6.8	ChiChi	9/20/1999	ChiChi, Taiwan
	60	160_tach_71va.dat	7.6	17	0.449	-0.348	31.3	-34.8	23.33	-31.34	27.4	39.4	10.50	8.83	248.74	30.0	Rock	Taiwan	V	V	XX-XX-6.8	ChiChi	9/20/1999	ChiChi, Taiwan
21	61	261_mhlu_000a.dat	8.1	84	0.164	-0.169	21.6	-21.0	22.52	-14.68	51.8	48.9	7.78	5.53	91.67	31.8	Rock	Mexico	H1	N00W	Su-IT-27	Michoacan	9/19/1985	La Union, Mexico
	62	262_mhli_090a.dat	8.1	84	0.151	-0.141	10.3	-13.2	8.59	-5.23	27.0	36.8	11.88	4.16	81.12	31.8	Rock	Mexico	H2	N90W	Su-IT-27	Michoacan	9/19/1985	La Union, Mexico
	63	263_mhlu_0upa.dat	8.1	84	0.107	-0.132	14.4	-15.0	13.15	-16.03	52.8	44.8	6.69	9.20	36.94	23.7	Rock	Mexico	V	V	Su-IT-27	Michoacan	9/19/1985	La Union, Mexico
22	64	264_pich_000a.dat	7.8	84	0.259	-0.205	9.6	-11.7	3.72	-2.76	14.6	22.5	10.31	4.06	140.48	23.2	Rock	Chile	H1	0	Su-IT-33	Valparaiso	3/3/1985	Pichemu, Chile
	65	265_pich_090a.dat	7.8	84	0.151	-0.178	12.4	-12.4	3.63	-3.92	32.5	27.5	3.47	4.43	76.65	22.5	Rock	Chile	H2	90	Su-IT-33	Valparaiso	3/3/1985	Pichemu, Chile
	66	266_pich_0upa.dat	7.8	84	0.107	-0.121	5.1	-5.9	1.95	-1.77	18.8	19.3	7.81	5.95	24.04	18.2	Rock	Chile	V	UP	Su-IT-33	Valparaiso	3/3/1985	Pichemu, Chile
23	67	267_pach_140a.dat	7.8	84	0.231	-0.230	12.4	-11.3	1.67	-1.88	21.1	19.4	2.47	3.31	254.62	59.1	Rock	Chile	H	140	Su-IT-33	Valparaiso	3/3/1985	Papudo Chile
	68	268_pach_0upa.dat	7.8	84	0.197	-0.177	6.2	-5.2	1.17	-1.12	12.5	11.6	5.79	7.22	93.93	50.3	Rock	Chile	V	UP	Su-IT-33	Valparaiso	3/3/1985	Papudo Chile

Table 4.2. Master accelerograph table of magnitude 6.1 – 6.8 earthquakes.

M6 Master Accelerograph Table																								
Set	Rec#	Filename	Mw	Distance (hyp) km	PGA		PGV		PGD		Ratio 1		Ratio 2		AI 0.95	Duration bracketed	Site Class	Region	Comp	deg	Setting & Mech	Earthquake	date	Station
					+	-	+	-	Lin Disp		vm/km		d*km/vm^2											
					g%		cm/s		cm		in./s/%g													
24	69	301_bbrc_090a.dat	6.5	70	0.051	-0.043	3.0	-3.4	0.51	-0.61	23.2	31.1	2.82	2.20	6	0	Rock(a)	WUS	H1	90	XX-RO-13	Big Bear	6/28/1992	Rancho Cucamonga - Deer Canyon
	70	302_bbrc_180a.dat	6.5	70	0.032	-0.029	2.0	-1.9	0.43	-0.32	24.4	26.2	3.48	2.46	2	0	Rock(a)	WUS	H2	180	XX-RO-13	Big Bear	6/28/1992	Rancho Cucamonga - Deer Canyon
	71	303_bbrc_Oupa.dat	6.5	70	0.021	-0.017	1.2	-1.1	0.20	-0.21	22.5	25.2	2.86	2.97	1	0	Rock(a)	WUS	V	UP	XX-RO-13	Big Bear	6/28/1992	Rancho Cucamonga - Deer Canyon
25	72	304_clpv_065a.dat	6.4	33	0.161	-0.147	13.3	-16.2	3.32	-2.94	32.7	43.4	2.94	1.62	35	9	Rock(a)	WUS	H1	65	MF-SS-05	Coalinga	5/2/1983	Parkfield Vineyard Canyon
26	73	305_clsc_045a.dat	6.4	34	0.166	-0.158	14.9	-16.1	4.18	-2.58	35.2	40.1	3.08	1.54	26	7	Rock(a)	WUS	H1	45	XX-RO-13	Coalinga	5/2/1983	Slack Canyon
	74	306_clsc_315a.dat	6.4	34	0.111	-0.153	11.7	-13.3	2.64	-2.71	41.6	34.2	2.10	2.30	21	4	Rock(a)	WUS	H2	315	XX-RO-13	Coalinga	5/2/1983	Slack Canyon
	75	307_clsc_Oupa.dat	6.4	34	0.044	-0.053	5.4	-6.8	2.05	-2.45	48.3	50.8	3.02	2.73	4	0	Rock(a)	WUS	V	UP	XX-RO-13	Coalinga	5/2/1983	Slack Canyon
27	76	308_vmcp_045a.dat	6.3	34	0.291	-0.621	31.8	-24.9	12.82	-7.10	43.0	15.8	3.62	6.98	177	13	Rock(a)	Mexico	H1	45	XX-XX-11	Victoria, Mexico	6/9/1980	UNAMUCSD Cerro Prieto
	77	309_vmcp_315a.dat	6.3	34	0.294	-0.587	19.9	-16.8	9.43	-7.77	26.7	11.3	6.86	15.78	90	12	Rock(a)	Mexico	H2	315	XX-XX-11	Victoria, Mexico	6/9/1980	UNAMUCSD Cerro Prieto
	78	310_vmcp_Oupa.dat	6.3	34	0.244	-0.304	12.1	-10.6	3.61	-4.81	19.5	13.8	5.90	12.69	47	10	Rock(a)	Mexico	V	UP	XX-XX-11	Victoria, Mexico	6/9/1980	UNAMUCSD Cerro Prieto
28	79	311_bbsv_090a.dat	6.5	40	0.059	-0.056	1.9	-1.9	0.23	-0.34	12.9	13.2	3.56	5.25	5	0	Rock	WUS	H	90	XX-RO-13	Big Bear	6/28/1992	Silent Valley - Poppet Flag
	80	312_bbsv_360a.dat	6.5	40	0.057	-0.070	2.1	-2.0	0.30	-0.29	14.2	11.5	3.98	4.87	7	6	Rock	WUS	H2	360	XX-RO-13	Big Bear	6/28/1992	Silent Valley - Poppet Flag
	81	313_bbsv_Oupa.dat	6.5	40	0.044	-0.047	1.3	-1.4	0.27	-0.18	11.6	11.8	6.96	4.07	4	0	Rock	WUS	V	UP	XX-RO-13	Big Bear	6/28/1992	Silent Valley - Poppet Flag
29	82	314_mhgg_067a.dat	6.2	39	0.114	-0.089	3.1	-3.6	0.83	-0.88	10.7	15.9	9.57	6.01	5	3	Rock	WUS	H1	67	XX-SS-09	Morgan Hill	4/24/1984	Gilroy, Gailan Coll
	83	315_mhgg_337a.dat	6.2	39	0.095	-0.069	2.9	-2.7	0.71	-0.94	11.9	15.1	8.02	9.06	5	3	Rock	WUS	H2	337	XX-SS-09	Morgan Hill	4/24/1984	Gilroy, Gailan Coll
	84	316_mhgg_Oupa.dat	6.2	39	0.115	-0.082	2.2	-1.9	0.25	-0.26	7.6	9.3	5.69	5.44	2	0	Rock	WUS	V	UP	XX-SS-09	Morgan Hill	4/24/1984	Gilroy, Gailan Coll
30	85	317_pspf_000a.dat	6.1	28	0.107	-0.139	3.9	-2.8	0.56	-0.47	14.5	7.9	3.80	8.36	9	2	Rock	WUS	H1	0	XX-SS-11	N.Palm Springs	7/8/1986	Silent Valley - Poppet Flat
	86	318_pspf_090a.dat	6.1	28	0.110	-0.113	3.6	-4.0	0.47	-0.80	12.7	13.8	3.97	5.65	5	2	Rock	WUS	H2	90	XX-SS-11	N.Palm Springs	7/8/1986	Silent Valley - Poppet Flat
	87	319_pspf_Oupa.dat	6.1	28	0.074	-0.095	2.3	-2.9	0.44	-0.46	12.4	12.2	5.92	4.96	4	1	Rock	WUS	V	UP	XX-SS-11	N.Palm Springs	7/8/1986	Silent Valley - Poppet Flat
31	88	320_sflh_111a.dat	6.6	24	0.161	-0.192	5.6	-5.4	0.88	-0.90	13.6	11.1	4.46	5.81	22	8	Rock	WUS	H1	111	XX-RO-13	San Fernando	2/9/1971	Lake Hughes
	89	321_sflh_201a.dat	6.6	24	0.153	-0.152	8.4	-7.9	0.66	-1.88	21.6	20.6	1.41	4.42	19	6	Rock	WUS	H2	201	XX-RO-13	San Fernando	2/9/1971	Lake Hughes
	90	322_sflh_dwna.dat	6.6	24	0.141	-0.164	6.4	-4.0	0.79	-0.87	17.8	9.7	2.70	8.65	17	6	Rock	WUS	V	DN	XX-RO-13	San Fernando	2/9/1971	Lake Hughes
32	91	323_sfol_180a.dat	6.6	39	0.079	-0.089	5.3	-3.9	0.78	-0.83	26.5	17.4	2.15	4.70	10	7	Rock	WUS	H1	180	XX-RO-13	San Fernando	2/9/1971	Pasadena - Old Seismo Lab
	92	324_sfol_270a.dat	6.6	39	0.202	-0.180	9.8	-10.8	2.40	-2.06	19.0	23.7	4.99	3.10	30	7	Rock	WUS	H2	270	XX-RO-13	San Fernando	2/9/1971	Pasadena - Old Seismo Lab
	93	325_sfol_dwna.dat	6.6	39	0.076	-0.091	4.3	-3.9	1.36	-1.01	22.3	16.9	5.46	5.92	6	2	Rock	WUS	V	DN	XX-RO-13	San Fernando	2/9/1971	Pasadena - Old Seismo Lab
33	94	326_sfpd_164a.dat	6.6	12	1.229	-0.788	38.8	-49.1	12.08	-2.71	12.4	24.5	9.68	0.87	391	10	Rock	WUS	H2	164	XX-RO-13	San Fernando	2/9/1971	Pacoima Dam
	95	327_sfpd_254a.dat	6.6	12	1.585	-0.848	43.2	-54.9	5.64	-5.15	10.7	25.5	4.69	1.42	786	24	Rock	WUS	H1	254	XX-RO-13	San Fernando	2/9/1971	Pacoima Dam
	96	328_sfpd_dwna.dat	6.6	12	1.124	-1.285	103.5	-68.4	22.94	-12.60	36.3	21.0	2.36	3.39	677	24	Rock	WUS	V	DN	XX-RO-13	San Fernando	2/9/1971	Pacoima Dam
34	97	329_nrgp_270a.dat	6.7	25	0.271	-0.289	24.9	-26.5	3.92	-3.53	36.2	36.1	1.68	1.42	137	15	Rock	WUS	H1	270	XX-XX-18	Northridge	1/17/1994	Griffith Park Observatory
	98	330_nrgp_360a.dat	6.7	25	0.129	-0.164	13.5	-10.4	2.39	-1.82	41.3	25.1	1.65	2.68	37	11	Rock	WUS	H2	360	XX-XX-18	Northridge	1/17/1994	Griffith Park Observatory
	99	331_nrgp_Oupa.dat	6.7	25	0.134	-0.116	5.6	-9.6	1.55	-1.61	16.4	32.4	6.59	2.00	18	8	Rock	WUS	V	UP	XX-XX-18	Northridge	1/17/1994	Griffith Park Observatory
35	100	332_nrbh_060a.dat	6.7	23	0.085	-0.073	3.6	-3.2	1.40	-1.45	16.5	17.6	9.17	9.81	6	3	Rock	WUS	H1	60	XX-XX-18	Northridge	1/17/1994	Burbank - Howard Rd
	101	333_nrbh_330a.dat	6.7	23	0.120	-0.095	6.9	-9.5	2.29	-1.86	22.5	39.7	5.72	1.90	19	7	Rock	WUS	H2	330	XX-XX-18	Northridge	1/17/1994	Burbank - Howard Rd
	102	334_nrbh_Oupa.dat	6.7	23	0.150	-0.163	8.5	-6.6	1.70	-1.75	22.4	15.9	3.43	6.45	30	8	Rock	WUS	V	UP	XX-XX-18	Northridge	1/17/1994	Burbank - Howard Rd
36	103	335_nrmw_000a.dat	6.7	46	0.085	-0.087	3.4	-2.7	0.52	-0.57	15.9	12.1	3.67	6.88	9	7	Rock	WUS	H1	0	XX-XX-18	Northridge	1/17/1994	Mt. Wilson - CIT Seismic Stn
	104	336_nrmw_090a.dat	6.7	46	0.234	-0.169	6.5	-7.3	0.54	-0.70	11.0	16.9	2.90	2.19	27	7	Rock	WUS	H2	90	XX-XX-18	Northridge	1/17/1994	Mt. Wilson - CIT Seismic Stn
	105	337_nrmw_Oupa.dat	6.7	46	0.119	-0.135	5.7	-3.4	0.45	-0.42	18.9	9.9	1.62	4.87	20	9	Rock	WUS	V	UP	XX-XX-18	Northridge	1/17/1994	Mt. Wilson - CIT Seismic Stn
37	106	338_nrpd_175a.dat	6.7	20	0.187	-0.191	14.1	-9.6	1.29	-1.26	29.7	19.9	1.19	2.54	27	8	Rock	WUS	H1	175	XX-XX-18	Northridge	1/17/1994	Pacoima Dam - Down Stream
	107	339_nrpd_265a.dat	6.7	20	0.353	-0.415	45.1	-17.6	4.98	-4.92	50.2	16.7	0.85	6.46	84	7	Rock	WUS	H2	265	XX-XX-18	Northridge	1/17/1994	Pacoima Dam - Down Stream
	108	340_nrpd_Oupa.dat	6.7	20	0.434	-0.373	30.9	-10.8	4.04	-4.46	28.1	11.4	1.80	14.05	66	5	Rock	WUS	V	UP	XX-XX-18	Northridge	1/17/1994	Pacoima Dam - Down Stream

M6 Master Accelerograph Table																								
Set	Rec#	Filename	Mw	Distance (hyp) km	PGA		PGV		PGD		Ratio 1		Ratio 2		AI 0.95	Duration bracketed	Site Class	Region	Comp	deg	Setting & Mech	Earthquake	date	Station
					+	-	+	-	Lin Disp		+	-	+	-										
									g%	cm/s														
38	109	341_nrp_x_104a.dat	6.7	20	1.226	-0.977	112.6	-55.2	31.74	-35.01	36.1	22.3	3.01	11.00	800	34	Rock	WUS	H1	104	XX-XX-18	Northridge	1/17/1994	Pacoima Dam - Upper Left
	110	342_nrp_x_194a.dat	6.7	20	0.849	-1.160	54.1	-43.4	11.65	-5.03	25.1	14.7	3.31	3.04	687	33	Rock	WUS	H2	194	XX-XX-18	Northridge	1/17/1994	Pacoima Dam - Upper Left
	111	343_nrp_x_0upa.dat	6.7	20	0.650	-0.699	52.5	-56.4	18.51	-13.24	31.8	31.8	4.27	2.85	385	32	Rock	WUS	V	UP	XX-XX-18	Northridge	1/17/1994	Pacoima Dam - Upper Left
39	112	344_nrvr_000a.dat	6.7	38	0.091	-0.077	5.0	-6.1	1.17	-1.61	21.7	31.4	4.12	3.23	9	3	Rock	WUS	H1	0	XX-XX-18	Northridge	1/17/1994	Vasquez Rocks Park
	113	345_nrvr_090a.dat	6.7	38	0.140	-0.151	18.4	-9.3	1.46	-2.88	51.9	24.3	0.59	4.90	34	8	Rock	WUS	H2	90	XX-XX-18	Northridge	1/17/1994	Vasquez Rocks Park
	114	346_nrvr_0upa.dat	6.7	38	0.139	-0.128	11.1	-10.8	2.88	-2.86	31.3	33.4	3.21	3.06	29	8	Rock	WUS	V	UP	XX-XX-18	Northridge	1/17/1994	Vasquez Rocks Park
40	115	347_nrwa_095a.dat	6.7	19	0.069	-0.106	3.1	-3.6	1.11	-0.71	17.7	13.5	7.82	5.59	8	6	Rock	WUS	H1	95	XX-XX-18	Northridge	1/17/1994	LA - Wonderland Ave
	116	348_nrwa_185a.dat	6.7	19	0.094	-0.112	5.7	-8.7	1.43	-1.80	23.9	30.3	4.04	2.64	13	6	Rock	WUS	H2	185	XX-XX-18	Northridge	1/17/1994	LA - Wonderland Ave
	117	349_nrwa_0upa.dat	6.7	19	0.172	-0.087	11.8	-11.1	1.24	-2.80	27.1	50.0	1.49	1.94	18	6	Rock	WUS	V	UP	XX-XX-18	Northridge	1/17/1994	LA - Wonderland Ave
41	118	350_omnz_130a.dat	6.2	89	0.065	-0.080	4.0	-4.0	0.30	-0.38	24.5	19.5	1.17	1.88	8	4	Rock	New Zealand	H1	130	XX-XX-36	Ormond	8/10/1993	Maraenui, NZ
	119	351_omnz_040a.dat	6.2	89	0.093	-0.107	3.7	-5.2	0.23	-0.34	15.6	19.0	1.53	1.33	11	5	Rock	New Zealand	H2	40	XX-XX-36	Ormond	8/10/1993	Maraenui, NZ
	120	352_omnz_0upa.dat	6.2	89	0.039	-0.040	1.2	-1.1	0.16	-0.17	12.3	10.7	4.07	5.72	4	0	Rock	New Zealand	V	UP	XX-XX-36	Ormond	8/10/1993	Maraenui, NZ
42	121	353_vall_100a.dat	6.2	65	0.147	-0.191	12.0	-13.4	1.27	-1.36	32.1	27.7	1.27	1.41	61	17	Rock	Chile	H1	100	XX-XX-50	Valparaiso A Shock	3/3/1985	Llolleo, Chile
	122	354_vall_010a.dat	6.2	65	0.163	-0.186	10.9	-10.8	1.50	-1.07	26.4	22.8	2.02	1.68	65	24	Rock	Chile	H2	10	XX-XX-50	Valparaiso A Shock	3/3/1985	Llolleo, Chile
	123	355_vall_0upa.dat	6.2	65	0.137	-0.121	4.5	-4.6	0.71	-0.86	12.9	15.1	4.71	4.79	28	14	Rock	Chile	V	UP	XX-XX-50	Valparaiso A Shock	3/3/1985	Llolleo, Chile
43	124	356_cigo_290a.dat	6.6	17	0.199	-0.145	19.8	-22.9	2.84	-5.25	39.2	62.1	1.42	1.43	26	4	Rock	India	H1	290	XX-XX-15	Chamoli	3/28/1993	Gopeshwar, India
	125	357_cigo_020a.dat	6.6	17	0.205	-0.360	44.9	-28.5	12.39	-4.16	86.1	31.2	1.24	1.80	72	10	Rock	India	H2	20	XX-XX-15	Chamoli	3/28/1993	Gopeshwar, India
	126	358_cigo_0upa.dat	6.6	17	0.157	-0.151	6.9	-7.6	1.65	-3.25	17.5	19.7	5.26	8.44	22	6	Rock	India	V	UP	XX-XX-15	Chamoli	3/28/1993	Gopeshwar, India
44	127	359_cigo_000a.dat	6.6	75	0.064	-0.073	3.2	-3.5	0.86	-0.74	19.7	18.8	5.24	4.36	10	6	Rock	India	H1	0	XX-XX-15	Chamoli	3/28/1993	Ghansiali, India
	128	360_cigo_090a.dat	6.6	75	0.081	-0.084	3.7	-4.2	1.25	-0.84	17.9	19.8	7.32	3.87	13	7	Rock	India	H2	90	XX-XX-15	Chamoli	3/28/1993	Ghansiali, India
	129	361_cigo_0upa.dat	6.6	75	0.035	-0.040	2.1	-1.5	0.34	-0.39	24.4	15.3	2.52	6.36	3	0	Rock	India	V	UP	XX-XX-15	Chamoli	3/28/1993	Ghansiali, India
45	130	362_tknz_130a.dat	6.3	68	0.066	-0.084	2.3	-3.4	0.22	-0.21	13.6	15.8	2.73	1.50	6	2	Rock	New Zealand	H1	130	XX-XX-12	Offshore Te Kuha	12/15/1994	Maraenui, NZ
	131	363_tknz_040a.dat	6.3	68	0.086	-0.079	3.6	-4.3	0.22	-0.37	16.5	21.5	1.42	1.54	8	3	Rock	New Zealand	H2	40	XX-XX-12	Offshore Te Kuha	12/15/1994	Maraenui, NZ
	132	364_tknz_0upa.dat	6.3	68	0.035	-0.034	0.9	-1.2	0.12	-0.13	10.5	13.9	4.87	2.99	2	0	Rock	New Zealand	V	UP	XX-XX-12	Offshore Te Kuha	12/15/1994	Maraenui, NZ
46	133	365_nrmn_270a.dat	6.7	19	0.162	-0.147	7.3	-7.3	1.73	-2.04	17.7	19.6	5.17	5.49	28	9	Rock	WUS	H	270	XX-XX-18	Northridge	1/17/1994	Monte Nido Fire Station
	134	366_nrmn_360a.dat	6.7	19	0.178	-0.179	6.8	-8.4	3.17	-2.54	15.0	18.5	12.01	6.30	31	9	Rock	WUS	H2	360	XX-XX-18	Northridge	1/17/1994	Monte Nido Fire Station
	135	367_nrmn_0upa.dat	6.7	19	0.125	-0.118	3.4	-3.8	1.56	-0.96	10.8	12.8	16.25	7.50	17	10	Rock	WUS	V	UP	XX-XX-18	Northridge	1/17/1994	Monte Nido Fire Station
47	136	368_iibi_000a.dat	6.2	22	0.035	-0.049	4.5	-3.3	0.46	-0.52	50.8	26.5	0.78	2.31	3	0	Rock	Italy	H1	0	XX-XX-07	Irpinia	11/23/1980	Bagnoli Irpinio
	137	369_iibi_270a.dat	6.2	22	0.031	-0.058	3.1	-3.5	0.67	-0.56	39.8	23.8	2.08	2.57	2	0	Rock	Italy	H2	270	XX-XX-07	Irpinia	11/23/1980	Bagnoli Irpinio
	138	370_iibi_0upa.dat	6.2	22	0.032	-0.024	2.2	-2.9	0.73	-0.70	27.6	46.5	4.59	2.01	1	0	Rock	Italy	V	UP	XX-XX-07	Irpinia	11/23/1980	Bagnoli Irpinio
48	139	371_iist_000a.dat	6.2	27	0.056	-0.071	3.4	-3.3	0.73	-0.91	23.9	18.6	3.46	5.70	7	2	Rock	Italy	H1	0	XX-XX-07	Irpinia	11/23/1980	Sturno
	140	372_iist_270a.dat	6.2	27	0.071	-0.077	4.4	-4.4	0.69	-0.73	24.5	22.3	2.46	2.91	7	2	Rock	Italy	H2	270	XX-XX-07	Irpinia	11/23/1980	Sturno
	141	373_iist_0upa.dat	6.2	27	0.032	-0.037	2.2	-2.4	0.40	-0.39	26.7	25.8	2.66	2.45	1	0	Rock	Italy	V	UP	XX-XX-07	Irpinia	11/23/1980	Sturno
49	142	374_sffd_056a.dat	6.6	29	0.071	-0.060	4.7	-3.8	0.41	-0.68	25.8	25.1	1.31	2.71	4	1	Rock	WUS	H1	56	XX-RO-13	San Fernando	2/9/1971	Fairmont Dam
	143	375_sffd_326a.dat	6.6	29	0.109	-0.092	6.4	-5.1	0.98	-1.08	23.3	22.0	2.53	3.68	5	2	Rock	WUS	H2	326	XX-RO-13	San Fernando	2/9/1971	Fairmont Dam
	144	376_sffd_0upa.dat	6.6	29	0.039	-0.034	3.5	-2.9	0.73	-0.62	35.7	32.7	2.23	2.57	2	0	Rock	WUS	V	UP	XX-RO-13	San Fernando	2/9/1971	Fairmont Dam
50	145	377_ivcp_147a.dat	6.5	25	0.162	-0.169	11.6	-10.6	4.10	-4.26	28.1	24.8	4.87	6.24	110	34	Rock	WUS	H1	147	XX-RO-10	Imperial Valley	10/15/1979	Cerro Prieto
	146	378_ivcp_237a.dat	6.5	25	0.148	-0.157	15.6	-18.6	8.04	-7.36	41.7	46.7	4.77	3.27	120	41	Rock	WUS	H2	237	XX-RO-10	Imperial Valley	10/15/1979	Cerro Prieto
	147	379_ivcp_0dna.dat	6.5	25	0.175	-0.212	6.7	-6.7	2.12	-3.26	15.0	12.5	8.20	14.92	68	24	Rock	WUS	V	DN	XX-RO-10	Imperial Valley	10/15/1979	Cerro Prieto
51	148	380_kgz_00la.dat	6.4	18	0.215	-0.147	9.2	-9.3	1.66	-1.47	16.8	25.0	4.16	2.44	25	5	Rock	Greece	H1	L	XX-RO-13	Kozani, Greece	05/13/1995	ITSK Kozani

M6 Master Accelerograph Table																								
Set	Rec#	Filename	Mw	Distance (hyp) km	PGA		PGV		PGD		Ratio 1		Ratio 2		AI 0.95	Duration bracketed	Site Class	Region	Comp	deg	Setting & Mech	Earthquake	date	Station
					+	-	+	-	Lin Disp		vm/km		d*km/vm^2											
					g%		cm/s		cm		in./s/%g													
	149	381_kgkz_00ta.dat	6.4	18	0.139	-0.125	4.6	-6.7	0.54	-0.36	13.1	21.1	3.46	0.98	18	4	Rock	Greece	H2	T	XX-RO-13	Kozani, Greece	05/13/1995	ITSAK Kozani
	150	382_kgkz_Oupa.dat	6.4	18	0.092	-0.072	4.3	-3.6	0.53	-0.58	18.2	19.6	2.63	3.19	6	4	Rock	Greece	V	UP	XX-RO-13	Kozani, Greece	05/13/1995	ITSAK Kozani
52	151	383_sfsa_003a.dat	6.6	46	0.151	-0.140	4.7	-4.2	1.64	-2.35	12.3	12.0	10.97	17.86	25	11	Rock	WUS	H1	3	XX-RO-13	San Fernando	2/9/1971	Santa Anita Dam
	152	384_sfsa_273a.dat	6.6	46	0.212	-0.160	4.1	-6.1	2.98	-2.19	7.7	14.9	36.09	9.35	27	8	Rock	WUS	H2	273	XX-RO-13	San Fernando	2/9/1971	Santa Anita Dam
	153	385_sfsa_0dna.dat	6.6	46	0.063	-0.056	2.6	-3.9	1.79	-1.64	16.4	27.7	16.25	5.80	5	3	Rock	WUS	V	DN	XX-RO-13	San Fernando	2/9/1971	Santa Anita Dam
53	153	386_cc71_71na.dat	6.2	21	0.195	-0.191	13.2	-11.8	0.90	-1.54	26.8	24.3	0.98	2.07	32	64	Rock	Taiwan	H1	71N	XX-XX-08	Chi-Chi	09/20/1999	TCU071
	154	387_cc71_71ea.dat	6.2	21	0.351	-0.380	13.0	-12.0	1.68	-1.72	14.5	12.4	3.45	4.49	63	11	Rock	Taiwan	H2	71E	XX-XX-08	Chi-Chi	09/20/1999	TCU071
	155	388_cc71_71va.dat	6.2	21	0.139	-0.143	2.9	-3.8	0.71	-1.16	8.2	10.5	11.43	11.18	11	3	Rock	Taiwan	V	71V	XX-XX-08	Chi-Chi	09/20/1999	TCU071
54	156	389_cc12_02na.dat	6.2	61	0.064	-0.040	3.7	-2.7	0.71	-0.76	22.5	26.5	3.35	4.07	3	0	Rock	Taiwan	H1	102N	XX-XX-08	Chi-Chi	09/20/1999	TCU102
	157	390_cc12_02ea.dat	6.2	61	0.042	-0.030	4.2	-4.3	1.29	-1.64	39.4	56.3	2.98	2.61	3	0	Rock	Taiwan	H2	102E	XX-XX-08	Chi-Chi	09/20/1999	TCU102
	158	391_cc12_02va.dat	6.2	61	0.028	-0.029	3.2	-2.9	1.03	-0.95	46.0	39.5	2.66	3.25	1	0	Rock	Taiwan	V	102V	XX-XX-08	Chi-Chi	09/20/1999	TCU102
55	159	392_mhg6_000a.dat	6.2	36	0.201	-0.222	8.7	-11.4	2.48	-2.18	17.1	20.2	6.42	3.66	34	8	Rock	WUS	H1	0	XX-SS-09	Morgan Hill	4/24/1984	Gilroy Array # 6
	160	393_mhg6_090a.dat	6.2	36	0.259	-0.292	23.0	-36.7	6.17	-4.25	34.9	49.5	2.97	0.90	78	10	Rock	WUS	H2	90	XX-SS-09	Morgan Hill	4/24/1984	Gilroy Array # 6
	161	394_mhg6_0upa.dat	6.2	36	0.405	-0.302	9.0	-14.0	1.89	-1.26	8.7	18.3	9.28	1.90	30	5	Rock	WUS	V	UP	XX-SS-09	Morgan Hill	4/24/1984	Gilroy Array # 6
56	162	395_mhsj_270a.dat	6.2	58	0.070	-0.081	6.5	-6.1	2.52	-2.59	36.8	29.7	4.06	5.52	17	9	Rock	WUS	H1	270	XX-SS-09	Morgan Hill	4/24/1984	San Justo Dam
	163	396_mhsj_360a.dat	6.2	58	0.070	-0.061	4.7	-5.1	1.86	-1.28	26.6	33.2	5.72	2.92	9	5	Rock	WUS	H2	360	XX-SS-09	Morgan Hill	4/24/1984	San Justo Dam
	164	397_mhsj_0upa.dat	6.2	58	0.030	-0.033	2.2	-1.7	0.50	-0.41	28.6	19.9	3.14	4.71	2	0	Rock	WUS	V	UP	XX-SS-09	Morgan Hill	4/24/1984	San Justo Dam
57	165	398_bbsf_090a.dat	6.5	71	0.172	-0.171	2.6	-3.0	0.17	-0.18	5.9	6.9	4.43	3.31	45	18	Rock	WUS	H1	90	XX-RO-13	Big Bear	6/28/1992	Sage Fire Station
	166	399_bbsf_180a.dat	6.5	71	0.165	-0.165	2.7	-2.5	0.16	-0.16	6.3	5.9	3.76	4.10	50	21	Rock	WUS	H2	360	XX-RO-13	Big Bear	6/28/1992	Sage Fire Station
	167	400_bbsf_0upa.dat	6.5	71	0.112	-0.118	1.7	-1.8	0.16	-0.14	5.9	5.9	6.35	5.03	25	22	Rock	WUS	V	UP	XX-RO-13	Big Bear	6/28/1992	Sage Fire Station
58	168	40a_nqhh_180a.dat	6.8	56	0.104	-0.104	17.1	-15.7	7.36	-9.32	64.6	59.4	2.57	3.85	37	17	Rock	WUS	H1	180	XX-XX-XX	Nisqually	2/28/2001	Howard Hanson Dam, L abut
	169	40b_nqhh_270a.dat	6.8	56	0.078	-0.106	20.9	-23.6	11.73	-8.27	105.6	88.0	2.05	1.53	36	17	Rock	WUS	H2	270	XX-XX-XX	Nisqually	2/28/2001	Howard Hanson Dam, L abut
	170	40c_nqhh_0upa.dat	6.8	56	0.048	-0.067	11.7	-11.7	9.00	-5.29	96.7	69.1	3.06	2.53	12	0	Rock	WUS	V	UP	XX-XX-XX	Nisqually	2/28/2001	Howard Hanson Dam, L abut
59	171	40d_cvpl_070a.dat	6.4	20	0.168	-0.100	5.0	-4.2	1.42	-1.40	11.6	16.3	9.56	7.94	12	6	Rock	WUS	H1	70	XX-SS-10	Chalfant Valley	7/21/1986	Bishop CA - Paradise Lodge
	172	40e_cvpl_160a.dat	6.4	20	0.117	-0.147	7.9	-11.1	3.01	-2.32	26.5	29.6	5.56	2.73	18	9	Rock	WUS	H2	160	XX-SS-10	Chalfant Valley	7/21/1986	Bishop CA - Paradise Lodge
	173	40f_cvpl_0upa.dat	6.4	20	0.091	-0.087	5.5	-4.8	1.13	-1.06	24.0	21.8	3.29	3.90	11	7	Rock	WUS	V	UP	XX-SS-10	Chalfant Valley	7/21/1986	Bishop CA - Paradise Lodge
60	174	40g_cvlc_009a.dat	6.4	29	0.159	-0.101	4.1	-7.3	0.76	-0.67	10.2	28.5	7.05	1.24	12	3	Rock	WUS	H1	9	XX-SS-10	Chalfant Valley	7/21/1986	Lake Crowley, Shelborn Residence
	175	40h_cvlc_099a.dat	6.4	29	0.070	-0.092	5.0	-3.6	0.53	-0.64	28.4	15.5	1.42	4.41	9	4	Rock	WUS	H2	99	XX-SS-10	Chalfant Valley	7/21/1986	Lake Crowley, Shelborn Residence
	176	40i_cvlc_0upa.dat	6.4	29	0.078	-0.081	3.0	-2.6	0.22	-0.35	15.1	12.4	1.89	4.31	7	4	Rock	WUS	V	UP	XX-SS-10	Chalfant Valley	7/21/1986	Lake Crowley, Shelborn Residence
61	177	40j_cvml_290a.dat	6.4	43	0.049	-0.041	2.1	-2.9	0.33	-0.33	17.0	27.3	3.54	1.65	3	0	Rock	WUS	H1	290	XX-SS-10	Chalfant Valley	7/21/1986	Mammoth Lakes Sheriff Sta
	178	40k_cvml_020a.dat	6.4	43	0.031	-0.042	2.3	-1.7	0.31	-0.35	29.1	16.5	1.79	4.67	2	0	Rock	WUS	H2	20	XX-SS-10	Chalfant Valley	7/21/1986	Mammoth Lakes Sheriff Sta
	179	40m_cvml_0upa.dat	6.4	43	0.020	-0.025	1.4	-1.6	0.22	-0.25	26.3	25.3	2.35	2.31	1	0	Rock	WUS	V	UP	XX-SS-10	Chalfant Valley	7/21/1986	Mammoth Lakes Sheriff Sta

Table 4.3. Master accelerograph table of magnitude 4.9 – 6.1 earthquakes.

M6 Master Accelerograph Table																								
Set	Rec#	Filename	Mw	Distance (hyp) km	PGA		PGV		PGD		Ratio 1		Ratio 2		AI 0.95	Duration bracketed	Site Class	Region	Comp	deg	Setting & Mech	Earthquake	date	Station
					+	-	+	-	Lin Disp		vm/km		d*km/vm^2											
					g%		cm/s		+	-	+	-	+	-										
48	167	401_wnmc_000a.dat	6.0	41	0.0832	-0.089	3.91	-3.94	0.518	-0.388	18.506	17.381	2.764	2.186	9.470	4.260	Rock(a)	WUS	H1	0	XX-XX-15	Whittier Narrows	10/1/1987	Mill Creek
	168	402_wnmc_090a.dat	6.0	41	0.0706	-0.065	3.02	-3.24	0.315	-0.244	16.828	19.508	2.394	1.491	6.680	4.240	Rock(a)	WUS	H2	90	XX-XX-15	Whittier Narrows	10/1/1987	Mill Creek
	169	403_wnmc_0upa.dat	6.0	41	0.0397	-0.036	1.16	-1.51	0.100	-0.083	11.548	16.504	2.881	1.275	2.183	0.000	Rock(a)	WUS	V	UP	XX-XX-15	Whittier Narrows	10/1/1987	Mill Creek
49	170	404_wnkr_090a.dat	6.0	20	0.106	-0.112	6.81	-8.01	0.895	-0.992	25.314	28.060	2.004	1.703	7.862	3.206	Rock(a)	WUS	H1	90	XX-XX-15	Whittier Narrows	10/1/1987	Pasadena - Kresge Lab
	171	405_wnkr_360a.dat	6.0	20	0.0892	-0.079	3.76	-3.60	0.275	-0.216	16.578	17.943	1.706	1.292	4.411	1.806	Rock(a)	WUS	H2	360	XX-XX-15	Whittier Narrows	10/1/1987	Pasadena - Kresge Lab
	172	406_wnkr_0upa.dat	6.0	20	0.0536	-0.081	3.34	-2.21	0.372	-0.297	24.525	10.802	1.755	4.795	2.921	2.116	Rock(a)	WUS	V	UP	XX-XX-15	Whittier Narrows	10/1/1987	Pasadena - Kresge Lab
50	173	407_wnmw_000a.dat	6.0	24	0.1047	-0.123	3.32	-3.25	0.372	-0.311	12.507	10.380	3.457	3.559	13.176	6.761	Rock(a)	WUS	H1	0	XX-XX-15	Whittier Narrows	10/1/1987	Mt. Wilson
	174	408_wnmw_090a.dat	6.0	24	0.1429	-0.186	4.22	-4.61	0.206	-0.186	11.618	9.759	1.620	1.592	23.500	6.911	Rock(a)	WUS	H2	90	XX-XX-15	Whittier Narrows	10/1/1987	Mt. Wilson
	175	409_wnmw_0upa.dat	6.0	24	0.097	-0.119	3.25	-2.30	0.195	-0.254	13.201	7.617	1.753	5.586	10.204	7.286	Rock(a)	WUS	V	UP	XX-XX-15	Whittier Narrows	10/1/1987	Mt. Wilson
51	176	410_wnvr_000a.dat	6.0	56	0.0461	-0.06	2.11	-1.89	0.116	-0.072	18.068	12.375	1.168	1.198	2.436	0.566	Rock(a)	WUS	H1	0	XX-XX-15	Whittier Narrows	10/1/1987	Vasquez Rock Park
	177	411_wnvr_090a.dat	6.0	56	0.0582	-0.06	1.52	-2.34	0.110	-0.088	10.250	15.381	2.731	0.945	2.506	0.876	Rock(a)	WUS	H2	90	XX-XX-15	Whittier Narrows	10/1/1987	Vasquez Rock Park
	178	412_wnvr_0upa.dat	6.0	56	0.0394	-0.034	0.90	-1.07	0.069	-0.089	8.960	12.339	3.330	2.603	1.059	0.000	Rock(a)	WUS	V	UP	XX-XX-15	Whittier Narrows	10/1/1987	Vasquez Rock Park
52	179	413_w2mw_000a.dat	5.3	23	0.1576	-0.097	5.72	-3.63	0.212	-0.245	14.286	14.788	1.002	1.763	6.153	0.886	Rock(a)	WUS	H1	0	XX-XX-13	Whittier Narrows II	10/4/1987	Mt. Wilson
	180	414_w2mw_090a.dat	5.3	23	0.1424	-0.115	4.57	-4.54	0.197	-0.126	12.634	15.556	1.317	0.687	7.216	0.716	Rock(a)	WUS	H2	90	XX-XX-13	Whittier Narrows II	10/4/1987	Mt. Wilson
	181	415_w2mw_0upa.dat	5.3	23	0.0863	-0.072	2.20	-1.76	0.138	-0.156	10.028	9.615	2.419	3.579	2.393	0.596	Rock(a)	WUS	V	UP	XX-XX-13	Whittier Narrows II	10/4/1987	Mt. Wilson
53	182	416_psar_270a.dat	6.1	47	0.1017	-0.104	5.18	-4.69	0.299	-0.635	20.044	17.831	1.111	2.933	7.603	2.950	Rock	WUS	H1	270	XX-XX-11	N. Palm Springs	7/8/1986	Red Mountain
	183	417_psar_360a.dat	6.1	47	0.1292	-0.107	3.17	-3.43	0.266	-0.458	9.676	12.666	3.347	4.064	6.634	4.370	Rock	WUS	H2	360	XX-XX-11	N. Palm Springs	7/8/1986	Red Mountain
	184	418_psar_0upa.dat	6.1	47	0.06	-0.072	2.22	-1.64	0.166	-0.215	14.571	9.026	1.980	5.598	2.009	0.215	Rock	WUS	V	UP	XX-XX-11	N. Palm Springs	7/8/1986	Red Mountain
54	185	419_pssr_270a.dat	6.1	50	0.0966	-0.106	2.56	-2.02	0.109	-0.102	10.431	7.510	1.578	2.590	5.593	3.105	Rock	WUS	H1	270	XX-XX-11	N. Palm Springs	7/8/1986	Santa Rosa Mountain
	186	420_pssr_360a.dat	6.1	50	0.1026	-0.08	1.32	-2.23	0.051	-0.103	5.079	10.963	2.946	1.633	4.114	1.730	Rock	WUS	H2	360	XX-XX-11	N. Palm Springs	7/8/1986	Santa Rosa Mountain
	187	421_pssr_0upa.dat	6.1	50	0.0464	-0.051	1.21	-1.45	0.087	-0.097	10.248	11.183	2.723	2.300	2.036	0.000	Rock	WUS	V	UP	XX-XX-11	N. Palm Springs	7/8/1986	Santa Rosa Mountain
55	188	422_psat_270a.dat	6.1	61	0.0679	-0.11	6.21	-6.54	0.710	-0.634	36.009	23.482	1.226	1.595	5.371	1.431	Rock	WUS	H1	270	XX-XX-11	N. Palm Springs	7/8/1986	Anza - Tule Canyon
	189	423_psat_360a.dat	6.1	61	0.0952	-0.07	7.51	-5.10	0.559	-0.707	31.039	28.784	0.926	1.860	5.256	0.845	Rock	WUS	H2	360	XX-XX-11	N. Palm Springs	7/8/1986	Anza - Tule Canyon
	190	424_psat_0upa.dat	6.1	61	0.0309	-0.049	2.62	-2.26	0.295	-0.238	33.355	18.251	1.304	2.224	1.476	0.000	Rock	WUS	V	UP	XX-XX-11	N. Palm Springs	7/8/1986	Anza - Tule Canyon
56	191	425_pswb_000a.dat	6.1	61	0.0702	-0.055	1.59	-1.94	0.196	-0.176	8.923	14.002	5.327	2.498	2.906	1.826	Rock	WUS	H1	0	XX-XX-11	N. Palm Springs	7/8/1986	Winchester Bergman Ranch
	192	426_pswb_090a.dat	6.1	61	0.0844	-0.093	1.76	-1.61	0.287	-0.290	8.216	6.847	7.657	10.139	4.089	2.501	Rock	WUS	H2	90	XX-XX-11	N. Palm Springs	7/8/1986	Winchester Bergman Ranch
	193	427_pswb_0upa.dat	6.1	61	0.062	-0.072	1.55	-1.51	0.221	-0.244	9.846	8.270	5.599	7.539	2.583	1.286	Rock	WUS	V	UP	XX-XX-11	N. Palm Springs	7/8/1986	Winchester Bergman Ranch
57	194	428_pslm_162a.dat	6.1	80	0.0517	-0.062	1.43	-1.51	0.074	-0.082	10.901	9.652	1.837	2.166	2.606	1.195	Rock	WUS	H2	162	XX-XX-11	N. Palm Springs	7/8/1986	Lake Mathews Dike Toe
	195	429_pslm_252a.dat	6.1	80	0.0404	-0.046	0.74	-0.74	0.021	-0.033	7.264	6.343	1.475	2.662	1.777	0.000	Rock	WUS	H1	252	XX-XX-11	N. Palm Springs	7/8/1986	Lake Mathews Dike Toe
	196	430_pslm_0upa.dat	6.1	80	0.0305	-0.039	0.52	-0.47	0.014	-0.016	6.706	4.725	1.509	2.745	0.979	0.000	Rock	WUS	V	UP	XX-XX-11	N. Palm Springs	7/8/1986	Lake Mathews Dike Toe
58	197	431_bccp_161a.dat	5.5	7	1.3882	-1.144	47.20	-43.19	10.083	-11.280	13.386	14.868	6.162	6.783	334.327	8.345	Rock	WUS	H1	161	XX-XX-06	Baja California	2/7/1987	Cerro Prieto
	198	432_bccp_251a.dat	5.5	7	0.6687	-0.891	52.21	-65.76	7.844	-5.713	30.740	29.076	1.887	1.154	295.650	10.340	Rock	WUS	H2	251	XX-XX-06	Baja California	2/7/1987	Cerro Prieto
	199	433_bccp_0upa.dat	5.5	7	0.5402	-0.59	18.03	-28.85	2.520	-1.185	13.139	19.263	4.108	0.824	172.894	6.735	Rock	WUS	V	UP	XX-XX-06	Baja California	2/7/1987	Cerro Prieto
59	200	434_hmfb_000a.dat	6.0	6	0.0323	-0.047	0.67	-0.47	0.018	-0.023	8.217	3.995	1.268	4.619	0.179	0.000	Rock	WUS	H1	0	XX-XX-XX	Helena, Montana	10/31/1935	Helena Federal Bldg.
	201	435_hmfb_090a.dat	6.0	6	0.0414	-0.027	0.65	-0.18	0.044	-0.038	6.177	2.640	4.274	31.520	0.118	0.000	Rock	WUS	H2	90	XX-XX-XX	Helena, Montana	10/31/1935	Helena Federal Bldg.
	202	436_hmfb_0upa.dat	6.0	6	0.0117	-0.01	0.21	-0.30	0.055	-0.038	6.983	12.018	14.508	4.079	0.038	0.000	Rock	WUS	V	UP	XX-XX-XX	Helena, Montana	10/31/1935	Helena Federal Bldg.

M6 Master Accelerograph Table																								
Set	Rec#	Filename	Mw	Distance (hyp) km	PGA		PGV		PGD		Ratio 1		Ratio 2		AI 0.95	Duration bracketed	Site Class	Region	Comp	deg	Setting & Mech	Earthquake	date	Station
					+	-	+	-	Lin Disp		+	-	+	-										
					g%		cm/s		cm		in./s/%g		d*km/vm^2											
60	203	437_s7gg_010a.dat	5.3	14	0.0934	-0.095	3.91	-2.16	0.187	-0.181	16.468	8.936	1.124	3.620	2.704	0.426	Rock	WUS	H1	10	XX-XX-08	San Francisco	3/22/1957	Golden Gate Park
	204	438_s7gg_100a.dat	5.3	14	0.1118	-0.101	4.14	-4.58	0.432	-0.310	14.569	17.864	2.766	1.464	4.978	1.611	Rock	WUS	H2	100	XX-XX-08	San Francisco	3/22/1957	Golden Gate Park
	205	439_s7gg_0upa.dat	5.3	14	0.0305	-0.047	1.09	-1.08	0.181	-0.134	14.118	9.020	4.525	5.334	0.667	0.000	Rock	WUS	V	UP	XX-XX-08	San Francisco	3/22/1957	Golden Gate Park
61	206	440_smcd_155a.dat	5.6	22	0.2963	-0.302	13.00	-14.87	1.604	-2.004	17.267	19.388	2.760	2.684	39.092	4.139	Rock	WUS	H1	155	XX-XX-12	Sierra Madre	6/28/1991	Cogswell Dam - Right Abutment
	207	441_smcd_065a.dat	5.6	22	0.2641	-0.212	9.55	-7.99	0.579	-0.940	14.244	14.827	1.642	3.063	27.867	3.039	Rock	WUS	H2	65	XX-XX-12	Sierra Madre	6/28/1991	Cogswell Dam - Right Abutment
	208	442_smcd_0upa.dat	5.6	22	0.1665	-0.228	6.09	-6.56	0.772	-0.445	14.394	11.347	3.400	2.311	19.435	3.379	Rock	WUS	V	UP	XX-XX-12	Sierra Madre	6/28/1991	Cogswell Dam - Right Abutment
62	209	443_hhg1_157a.dat	5.1	13	0.1054	-0.061	2.55	-2.71	0.089	-0.128	9.533	17.556	1.405	1.042	3.065	1.235	Rock	WUS	H1	157	XX-XX-06	Hollister	11/28/1974	Gillroy Array # 1
	210	444_hhg1_247a.dat	5.1	13	0.1325	-0.084	3.99	-2.71	0.128	-0.168	11.859	12.673	1.045	1.886	4.168	1.100	Rock	WUS	H2	247	XX-XX-06	Hollister	11/28/1974	Gillroy Array # 1
63	211	445_oror_037a.dat	5.9	14	0.0775	-0.092	2.03	-3.70	0.169	-0.168	10.302	15.854	3.121	1.104	3.230	0.600	Rock	WUS	H1	37	XX-XX-06	Orville	8/1/1975	Oroville Seismograph
	212	446_oror_307a.dat	5.9	14	0.0684	-0.072	2.84	-2.49	0.223	-0.214	16.364	13.548	1.853	2.446	3.581	1.425	Rock	WUS	H2	307	XX-XX-06	Orville	8/1/1975	Oroville Seismograph
64	213	447_clcd_160a.dat	5.7	11	0.1402	-0.157	10.80	-8.20	0.809	-1.306	30.332	20.505	0.953	2.999	17.005	3.162	Rock	WUS	H1	160	XX-XX-10	Coyote Lake	8/6/1979	Coyote Lake Dam(SW ABUT)
	214	448_clcd_250a.dat	5.7	11	0.2791	-0.259	14.18	-20.29	2.331	-1.896	20.002	30.839	3.173	1.170	32.313	3.992	Rock	WUS	H2	250	XX-XX-10	Coyote Lake	8/6/1979	Coyote Lake Dam(SW ABUT)
	215	449_clcd_0upa.dat	5.7	11	0.1212	-0.071	6.44	-4.16	0.384	-0.674	20.896	23.117	1.103	2.704	5.218	2.612	Rock	WUS	V	UP	XX-XX-10	Coyote Lake	8/6/1979	Coyote Lake Dam(SW ABUT)
65	216	450_c7cm_030a.dat	5.2	37	0.085	-0.115	2.29	-3.10	0.092	-0.096	10.589	10.622	1.460	1.119	7.892	2.660	Rock	WUS	H1	30	XX-XX-21	Northern California	8/6/1979	Cape Mendocino
	217	451_c7cm_120a.dat	5.2	37	0.1473	-0.179	4.90	-4.60	0.158	-0.121	13.097	10.121	0.950	1.006	10.688	2.645	Rock	WUS	H2	120	XX-XX-21	Northern California	8/6/1979	Cape Mendocino
	218	452_c7cm_0dna.dat	5.2	37	0.0265	-0.024	0.76	-0.82	0.035	-0.039	11.274	13.652	1.568	1.331	0.702	0.000	Rock	WUS	V	DN	XX-XX-21	Northern California	8/6/1979	Cape Mendocino
66	219	453_lccs_095a.dat	5.3	21	0.0708	-0.059	1.80	-1.62	0.098	-0.115	9.993	10.914	2.114	2.503	1.638	0.686	Rock	WUS	H1	95	XX-XX-08	Lytle Creek	9/12/1970	Cedar Springs - Allen Ranch
	220	454_lccs_185a.dat	5.3	21	0.0503	-0.046	1.14	-1.20	0.048	-0.058	8.935	10.228	1.825	1.804	1.065	0.001	Rock	WUS	H2	185	XX-XX-08	Lytle Creek	9/12/1970	Cedar Springs - Allen Ranch
67	221	455_lcdc_090a.dat	5.3	22	0.1321	-0.146	3.19	-3.33	0.153	-0.181	9.504	8.981	1.946	2.333	8.230	1.630	Rock	WUS	H1	90	XX-XX-08	Lytle Creek	9/12/1970	Devils Canyon
	222	456_lcdc_180a.dat	5.3	22	0.1213	-0.151	4.54	-5.60	0.172	-0.228	14.754	14.598	0.988	1.077	9.388	2.030	Rock	WUS	H2	180	XX-XX-08	Lytle Creek	9/12/1970	Devils Canyon
	223	457_lcdc_0dna.dat	5.3	22	0.0837	-0.08	1.64	-1.73	0.074	-0.101	7.702	8.534	2.258	2.636	1.945	0.260	Rock	WUS	V	DN	XX-XX-08	Lytle Creek	9/12/1970	Devils Canyon
68	224	458_lcsa_003a.dat	5.3	46	0.03	-0.042	0.94	-1.64	0.047	-0.095	12.362	15.260	1.566	1.461	0.642	0.000	Rock	WUS	H1	3	XX-XX-08	Lytle Creek	9/12/1970	Santa Anita Dam
	225	459_lcsa_273a.dat	5.3	46	0.0178	-0.018	0.40	-0.50	0.040	-0.035	8.868	10.817	4.360	2.514	0.288	0.000	Rock	WUS	H2	273	XX-XX-08	Lytle Creek	9/12/1970	Santa Anita Dam
	226	460_lcsa_0dna.dat	5.3	46	0.013	-0.013	0.20	-0.27	0.011	-0.011	6.204	8.307	3.358	1.788	0.073	0.000	Rock	WUS	V	DN	XX-XX-08	Lytle Creek	9/12/1970	Santa Anita Dam
69	227	461_dtdt_00la.dat	5.3	9	0.2234	-0.199	7.88	-6.72	0.537	-0.459	13.891	13.297	1.894	1.983	16.996	2.630	Rock	Turkey	H1	L	XX-XX-07	Dursunbery, Turkey	7/18/1979	Dursunbery
	228	462_dtdt_00ta.dat	5.3	9	0.3662	-0.168	8.11	-10.18	0.577	-0.743	8.714	23.858	3.151	1.181	20.120	2.360	Rock	Turkey	H2	T	XX-XX-07	Dursunbery, Turkey	7/18/1979	Dursunbery
	229	463_dtdt_00va.dat	5.3	9	0.127	-0.102	5.72	-4.01	0.309	-0.308	17.733	15.411	1.177	1.928	7.085	2.010	Rock	Turkey	V	V	XX-XX-07	Dursunbery, Turkey	7/18/1979	Dursunbery
70	230	464_itiz_00la.dat	5.3	6	0.3297	-0.41	12.46	-10.34	0.452	-0.388	14.877	9.931	0.942	1.460	31.661	1.160	Rock	Turkey	H	L	XX-XX-05	Izmir, Turkey	12/16/1977	Izmir
	231	465_itiz_00ta.dat	5.3	6	0.1345	-0.146	3.75	-5.33	0.291	-0.203	10.967	14.369	2.737	1.025	5.812	0.720	Rock	Turkey	H2	T	XX-XX-05	Izmir, Turkey	12/16/1977	Izmir
	232	466_itiz_00va.dat	5.3	6	0.0707	-0.075	1.61	-2.38	0.065	-0.061	8.967	12.507	1.743	0.796	2.028	1.540	Rock	Turkey	V	V	XX-XX-05	Izmir, Turkey	12/16/1977	Izmir
71	233	467_fisr_000a.dat	5.9	18	0.0554	-0.06	4.82	-4.41	1.130	-0.918	34.222	29.082	2.646	2.762	2.958	1.885	Rock	Italy	H1	0	XX-XX-04	Friuli, Italy	9/15/1976	San Rocco
	234	468_fisr_270a.dat	5.9	18	0.1244	-0.134	7.62	-6.27	1.242	-1.994	24.107	18.378	2.610	6.678	7.940	3.175	Rock	Italy	H2	270	XX-XX-04	Friuli, Italy	9/15/1976	San Rocco
	235	469_fisr_0upa.dat	5.9	18	0.0585	-0.05	3.99	-6.23	1.987	-1.309	26.835	49.207	7.171	1.650	2.087	0.020	Rock	Italy	V	UP	XX-XX-04	Friuli, Italy	9/15/1976	San Rocco
72	236	470_f2sr_0nsa.dat	5.5	21	0.0282	-0.029	1.41	-2.33	0.478	-0.431	19.750	31.576	6.610	2.257	0.502	0.000	Rock	Italy	H1	NS	XX-XX-06	Friuli, Italy	9/11/1976	San Rocco
	237	471_f2sr_0wea.dat	5.5	21	0.0718	-0.045	3.59	-4.31	0.812	-0.543	19.704	38.087	4.426	1.279	1.863	0.091	Rock	Italy	H2	WE	XX-XX-06	Friuli, Italy	9/11/1976	San Rocco
	238	472_f2sr_0upa.dat	5.5	21	0.0102	-0.013	1.36	-1.82	0.295	-0.336	52.679	54.365	1.584	1.311	0.227	0.000	Rock	Italy	V	UP	XX-XX-06	Friuli, Italy	9/11/1976	San Rocco

M6 Master Accelerograph Table																								
Set	Rec#	Filename	Mw	Distance (hyp) km	PGA		PGV		PGD		Ratio 1		Ratio 2		AI 0.95	Duration bracketed	Site Class	Region	Comp	deg	Setting & Mech	Earthquake	date	Station
					+	-	+	-	Lin Disp		+	-	+	-										
					g%		cm/s		cm		in./s/%g		d*km/vm^2											
73	239	473_hmcc_180a.dat	6.0	6	0.1498	-0.116	4.58	-5.77	1.040	-0.770	12.030	19.557	7.295	2.635	6.430	1.740	Rock(a)	WUS	H1	180	XX-SS-06	Helena, Montana	10/31/1935	USGS Carroll College
	240	474_hmcc_270a.dat	6.0	6	0.1731	-0.107	9.98	-16.43	2.335	-2.184	22.690	60.571	3.982	0.847	9.300	1.560	Rock(a)	WUS	H2	270	XX-SS-06	Helena, Montana	10/31/1935	USGS Carroll College
	241	475_hmcc_0dna.dat	6.0	6	0.1024	-0.098	5.54	-7.24	2.247	-1.428	21.312	28.984	7.343	2.629	3.020	1.520	Rock(a)	WUS	V	DN	XX-SS-06	Helena, Montana	10/31/1935	USGS Carroll College
74	242	476_cosb_000a.dat	5.4	16	0.0437	-0.028	4.49	-5.12	2.285	-1.683	40.532	71.523	4.843	1.773	1.698	0.000	Rock	WUS	H1	0	XX-RX-02	Coalinga 03	6/11/1983	CDMG Sulphur Baths
	243	477_cosb_090a.dat	5.4	16	0.0335	-0.037	4.40	-4.48	1.641	-1.278	51.737	47.793	2.785	2.308	1.542	0.000	Rock	WUS	H2	90	XX-RX-02	Coalinga 03	6/11/1983	CDMG Sulphur Baths
	244	478_cosb_0upa.dat	5.4	16	0.0273	-0.034	2.90	-3.51	1.197	-1.472	41.850	41.243	3.805	3.921	1.260	0.000	Rock	WUS	V	UP	XX-RX-02	Coalinga 03	6/11/1983	CDMG Sulphur Baths
75	245	479_lvmt_265a.dat	5.4	18	0.198	-0.149	6.11	-11.69	0.677	-1.017	12.159	30.928	3.516	1.086	16.978	2.761	Rock	WUS	H1	265	XX-SS-15	Livermore 02	1/27/1980	Morgan Terr Park
	246	480_lvmt_355a.dat	5.4	18	0.2511	-0.252	9.77	-9.18	1.299	-1.105	15.328	14.321	3.349	3.244	33.727	2.256	Rock	WUS	H2	355	XX-SS-15	Livermore 02	1/27/1980	Morgan Terr Park
	247	481_lvmt_0upa.dat	5.4	18	0.0778	-0.066	4.08	-2.85	0.390	-0.288	20.636	17.055	1.791	2.285	3.173	0.506	Rock	WUS	V	UP	XX-SS-15	Livermore 02	1/27/1980	Morgan Terr Park
76	248	482_c2sb_000a.dat	5.2	17	0.0441	-0.055	2.17	-1.83	0.214	-0.192	19.348	13.058	1.972	3.092	1.698	0.016	Rock	WUS	H1	0	XX-RX-09	Coalinga 04	7/9/1983	CDMG Sulphur Baths
	249	483_c2sb_090a.dat	5.2	17	0.0376	-0.075	1.45	-1.26	0.120	-0.153	15.157	6.642	2.113	7.099	1.668	0.026	Rock	WUS	H2	90	XX-RX-09	Coalinga 04	7/9/1983	CDMG Sulphur Baths
	250	484_c2sb_0upa.dat	5.2	17	0.0316	-0.042	0.99	-0.97	0.091	-0.088	12.299	9.242	2.893	3.768	0.874	0.000	Rock	WUS	V	UP	XX-RX-09	Coalinga 04	7/9/1983	CDMG Sulphur Baths
77	251	485_c3sb_000a.dat	5.8	15	0.1412	-0.101	5.47	-4.29	0.693	-0.791	15.252	16.707	3.207	4.258	9.477	2.846	Rock	WUS	H1	0	XX-RX-07	Coalinga 05	7/22/1983	CDMG Sulphur Baths
	252	486_c3sb_090a.dat	5.8	15	0.1034	-0.127	6.24	-3.58	0.543	-0.656	23.764	11.074	1.414	6.388	9.621	3.816	Rock	WUS	H2	90	XX-RX-07	Coalinga 05	7/22/1983	CDMG Sulphur Baths
	253	487_c3sb_0upa.dat	5.8	15	0.0823	-0.082	3.03	-4.07	0.608	-0.687	14.481	19.629	5.352	3.323	5.169	2.031	Rock	WUS	V	UP	XX-RX-07	Coalinga 05	7/22/1983	CDMG Sulphur Baths
78	254	488_c4sb_000a.dat	4.9	14	0.039	-0.034	1.42	-1.56	0.139	-0.205	14.349	18.171	2.634	2.798	0.561	0.000	Rock	WUS	H1	0	XX-RX-08	Coalinga 06	7/22/1983	CDMG Sulphur Baths
	255	489_c4sb_090a.dat	4.9	14	0.0212	-0.03	0.75	-0.96	0.108	-0.158	13.913	12.537	4.000	5.056	0.403	0.000	Rock	WUS	H2	90	XX-RX-08	Coalinga 06	7/22/1983	CDMG Sulphur Baths
	256	490_c4sb_0upa.dat	4.9	14	0.0284	-0.029	0.89	-1.12	0.116	-0.170	12.386	14.996	4.026	3.919	0.481	0.000	Rock	WUS	V	UP	XX-RX-08	Coalinga 06	7/22/1983	CDMG Sulphur Baths
79	257	491_nibv_0ewa.dat	5.9	36	0.0194	-0.023	1.03	-1.02	0.092	-0.085	20.989	17.363	1.632	1.862	0.876	0.000	Rock	Italy	H1	EW	XX-NX-06	Norcia, Italy	9/19/1979	Bevagna, Italy
	258	492_nibv_0onsa.dat	5.9	36	0.0381	-0.04	2.18	-2.06	0.294	-0.412	22.569	20.420	2.303	3.785	1.372	0.000	Rock	Italy	H2	NS	XX-NX-06	Norcia, Italy	9/19/1979	Bevagna, Italy
	259	493_nibv_0upa.dat	5.9	36	0.0203	-0.025	0.67	-0.90	0.064	-0.064	13.007	14.381	2.809	1.909	0.707	0.000	Rock	Italy	V	UP	XX-NX-06	Norcia, Italy	9/19/1979	Bevagna, Italy
80	260	494_nics_0ewa.dat	5.9	7	0.1996	-0.169	11.50	-8.40	1.679	-1.455	22.689	19.559	2.485	3.417	17.033	3.720	Rock	Italy	H1	EW	XX-NX-06	Norcia, Italy	9/19/1979	Cascia, Italy
	261	495_nics_0onsa.dat	5.9	7	0.1327	-0.161	8.47	-6.17	0.621	-0.614	25.131	15.054	1.127	2.553	23.091	4.180	Rock	Italy	H2	NS	XX-NX-06	Norcia, Italy	9/19/1979	Cascia, Italy
	262	496_nics_0upa.dat	5.9	7	0.1457	-0.135	3.78	-4.09	0.428	-0.256	10.217	11.964	4.279	2.018	11.543	4.390	Rock	Italy	V	UP	XX-NX-06	Norcia, Italy	9/19/1979	Cascia, Italy
81	263	497_c5sb_000a.dat	5.2	15	0.1518	-0.143	8.49	-7.01	1.267	-0.911	22.019	19.274	2.617	2.601	6.723	1.711	Rock	WUS	H1	0	XX-RX-08	Coalinga 07	7/25/1983	CDMG Sulphur Baths
	264	498_c5sb_090a.dat	5.2	15	0.1662	-0.23	8.17	-10.89	0.762	-0.699	19.355	18.671	1.860	1.327	11.531	1.256	Rock	WUS	H2	90	XX-RX-08	Coalinga 07	7/25/1983	CDMG Sulphur Baths
	265	499_c5sb_0upa.dat	5.2	15	0.1191	-0.139	2.95	-6.45	0.325	-0.314	9.759	18.234	4.357	1.030	7.169	1.411	Rock	WUS	V	UP	XX-RX-08	Coalinga 07	7/25/1983	CDMG Sulphur Baths
82	266	500_c6sb_000a.dat	5.2	20	0.0139	-0.013	0.64	-0.54	0.064	-0.061	18.135	16.464	2.121	2.630	0.207	0.000	Rock	WUS	H	0	XX-SS-07	Coalinga 08	9/9/1983	CDMG Sulphur Baths
	267	501_c6sb_090a.dat	5.2	20	0.0165	-0.011	0.54	-0.63	0.041	-0.059	12.800	21.985	2.272	1.631	0.193	0.000	Rock	WUS	H2	90	XX-SS-07	Coalinga 08	9/9/1983	CDMG Sulphur Baths
	268	502_c6sb_0upa.dat	5.2	20	0.0157	-0.011	0.53	-0.61	0.039	-0.036	13.267	21.787	2.151	1.039	0.241	0.000	Rock	WUS	V	UP	XX-SS-07	Coalinga 08	9/9/1983	CDMG Sulphur Baths
83	269	503_clga_230a.dat	5.7	15	0.1026	-0.08	2.63	-3.37	0.353	-0.484	10.076	16.609	5.150	3.331	5.761	1.837	Rock	WUS	H1	230	XX-SS-10	Coyote	8/6/1979	Gilroy Array # 1
	270	504_clga_320a.dat	5.7	15	0.1163	-0.132	6.52	-8.25	0.888	-1.523	22.092	24.517	2.378	2.908	7.186	1.767	Rock	WUS	H2	320	XX-SS-10	Coyote	8/6/1979	Gilroy Array # 1
	271	505_clga_0upa.dat	5.7	15	0.061	-0.072	2.04	-2.53	0.407	-0.337	13.173	13.860	5.840	3.707	3.208	2.567	Rock	WUS	V	UP	XX-SS-10	Coyote	8/6/1979	Gilroy Array # 1
84	272	506_clg6_230a.dat	5.7	9	0.3334	-0.434	49.21	-17.74	6.519	-7.697	58.100	16.098	0.880	10.403	69.690	3.957	Rock	WUS	H1	230	XX-SS-10	Coyote	8/6/1979	Gilroy Array # 6
	273	507_clg6_320a.dat	5.7	9	0.2617	-0.316	24.47	-21.13	3.849	-2.058	36.818	26.316	1.649	1.429	61.161	5.562	Rock	WUS	H2	320	XX-SS-10	Coyote	8/6/1979	Gilroy Array # 6
	274	508_clg6_0upa.dat	5.7	9	0.1359	-0.146	11.91	-12.80	3.959	-2.913	34.480	34.533	3.724	2.544	14.119	3.467	Rock	WUS	V	UP	XX-SS-10	Coyote	8/6/1979	Gilroy Array # 6

M6 Master Accelerograph Table																								
Set	Rec#	Filename	Mw	Distance (hyp) km	PGA		PGV		PGD Lin Disp		Ratio 1 vm/km		Ratio 2 d*km/vm^2		AI 0.95	Duration bracketed	Site Class	Region	Comp	deg	Setting & Mech	Earthquake	date	Station
					+	-	+	-	+	-	+	-	+	-										
					g%		cm/s		cm		in./s/%g													
85	275	509_mlmc_117a.dat	4.9	11	0.0784	-0.075	1.46	-1.62	0.102	-0.087	7.340	8.515	3.683	2.426	2.700	1.326	Rock	WUS	H	117	XX-XX-08	Mammoth Lakes 09	6/11/1980	USC McGee Creek
	276	510_mlmc_207a.dat	4.9	11	0.1936	-0.211	2.97	-2.21	0.077	-0.085	6.046	4.121	1.659	3.614	9.212	0.701	Rock	WUS	H2	207	XX-XX-08	Mammoth Lakes 09	6/11/1980	USC McGee Creek
	277	511_mlmc_0upa.dat	4.9	11	0.0904	-0.066	0.74	-0.76	0.035	-0.024	3.234	4.509	5.599	2.758	1.847	0.946	Rock	WUS	V	UP	XX-XX-08	Mammoth Lakes 09	6/11/1980	USC McGee Creek
86	278	512_azpf_045a.dat	5.2	19	0.1099	-0.086	1.71	-2.49	0.105	-0.110	6.141	11.419	3.844	1.492	2.417	1.000	Rock	WUS	H	45	XX-SS-14	Anza	2/25/1980	Pinyon Flat
	279	513_azpf_135a.dat	5.2	19	0.107	-0.131	3.22	-5.11	0.492	-0.368	11.834	15.331	4.988	1.814	3.095	0.835	Rock	WUS	H2	135	XX-SS-14	Anza	2/25/1980	Pinyon Flat
	280	514_azpf_0upa.dat	5.2	19	0.0459	-0.042	0.81	-1.11	0.064	-0.085	6.905	10.318	4.458	2.864	1.206	0.000	Rock	WUS	V	UP	XX-SS-14	Anza	2/25/1980	Pinyon Flat
87	281	515_scsl_234a.dat	6.0	76	0.036	-0.035	2.68	-2.94	0.655	-0.973	29.232	33.030	3.233	3.866	1.646	0.000	Rock	WUS	H	234	XX-XX-XX	Southern Cal	11/22/1952	San Luis Obispo
	282	516_scsl_324a.dat	6.0	76	0.0441	-0.054	2.57	-3.33	0.531	-0.470	22.951	24.490	3.469	2.227	2.083	0.021	Rock	WUS	H2	324	XX-XX-XX	Southern Cal	11/22/1952	San Luis Obispo
	283	517_scsl_0upa.dat	6.0	76	0.0275	-0.021	2.37	-1.60	0.671	-0.411	33.814	30.543	3.236	3.247	0.574	0.000	Rock	WUS	V	UP	XX-XX-XX	Southern Cal	11/22/1952	San Luis Obispo
88	284	518_aztv_045a.dat	5.2	16	0.1283	-0.131	3.92	-2.80	0.166	-0.123	12.015	8.396	1.360	2.030	3.993	0.625	Rock	WUS	H	45	XX-SS-14	Anza	2/25/1980	Terwilliger Valley
	285	519_aztv_135a.dat	5.2	16	0.0805	-0.079	1.67	-1.64	0.064	-0.064	8.181	8.223	1.803	1.824	1.980	0.705	Rock	WUS	H2	135	XX-SS-14	Anza	2/25/1980	Terwilliger Valley
	286	520_aztv_0upa.dat	5.2	16	0.0678	-0.066	1.66	-1.29	0.057	-0.057	9.656	7.662	1.367	2.226	1.479	0.640	Rock	WUS	V	UP	XX-SS-14	Anza	2/25/1980	Terwilliger Valley
89	287	521_bb7r_090a.dat	4.9	33	0.0113	-0.011	0.31	-0.31	0.063	-0.067	10.699	11.048	7.399	7.667	0.094	0.000	Rock	WUS	H	90	XX-SS-06	Big Bear City	2/22/2003	Seven Oaks Dam Right Abut
	288	522_bb7r_360a.dat	4.9	33	0.013	-0.012	0.45	-0.43	0.089	-0.091	13.686	14.132	5.553	5.789	0.115	0.000	Rock	WUS	H2	360	XX-SS-06	Big Bear City	2/22/2003	Seven Oaks Dam Right Abut
	289	523_bb7r_0upa.dat	4.9	33	0.0081	-0.008	0.27	-0.23	0.020	-0.029	13.357	11.073	2.138	4.442	0.065	0.000	Rock	WUS	V	UP	XX-SS-06	Big Bear City	2/22/2003	Seven Oaks Dam Right Abut
90	290	524_bb7d_090a.dat	4.9	33	0.027	-0.031	0.77	-0.66	0.073	-0.081	11.251	8.462	3.260	5.558	0.633	0.000	Rock	WUS	H	90	XX-SS-06	Big Bear City	2/22/2003	Seven Oaks Dam Downstream
	291	525_bb7d_360a.dat	4.9	33	0.0419	-0.03	0.77	-0.86	0.072	-0.081	7.268	11.231	4.958	3.228	0.648	0.000	Rock	WUS	H2	360	XX-SS-06	Big Bear City	2/22/2003	Seven Oaks Dam Downstream
	292	526_bb7d_0upa.dat	4.9	33	0.0125	-0.012	0.22	-0.25	0.021	-0.024	6.875	8.123	5.488	4.613	0.143	0.000	Rock	WUS	V	UP	XX-SS-06	Big Bear City	2/22/2003	Seven Oaks Dam Downstream
91	293	527_bbsb_111a.dat	4.9	41	0.0064	-0.007	0.41	-0.33	0.055	-0.083	25.002	18.420	2.081	5.211	0.078	0.000	Rock	WUS	H	111	XX-SS-06	Big Bear City	2/22/2003	San Bernardino - Del Rosa
	294	528_bbsb_021a.dat	4.9	41	0.0082	-0.008	0.38	-0.36	0.093	-0.123	18.173	19.237	5.234	6.740	0.087	0.000	Rock	WUS	H2	21	XX-SS-06	Big Bear City	2/22/2003	San Bernardino - Del Rosa
	295	529_bbsb_0upa.dat	4.9	41	0.0062	-0.007	0.19	-0.24	0.036	-0.045	11.835	14.053	6.198	5.280	0.047	0.000	Rock	WUS	V	UP	XX-SS-06	Big Bear City	2/22/2003	San Bernardino - Del Rosa
92	296	530_lzat_0nsa.dat	5.8	19	0.0933	-0.061	3.33	-3.29	0.417	-0.437	14.059	21.150	3.437	2.425	5.515	2.111	Rock	Italy	H	NS	XX-XX-14	Lazio-Abruzzo	5/7/1984	ENEL 99999 Atina, Italy
	297	531_lzat_0wea.dat	5.8	19	0.1135	-0.07	3.77	-4.00	0.345	-0.337	13.084	22.446	2.700	1.450	4.677	1.252	Rock	Italy	H2	WE	XX-XX-14	Lazio-Abruzzo	5/7/1984	ENEL 99999 Atina, Italy
	298	532_lzat_0upa.dat	5.8	19	0.0757	-0.046	1.75	-2.03	0.234	-0.263	9.105	17.227	5.656	2.910	3.096	0.035	Rock	Italy	V	UP	XX-XX-14	Lazio-Abruzzo	5/7/1984	ENEL 99999 Atina, Italy
93	299	533_h4ss_205a.dat	5.5	14	0.0439	-0.044	5.32	-5.03	1.266	-0.847	47.688	45.232	1.925	1.437	2.270	0.000	Rock	WUS	H	205	XX-SS-09	Hollister-04	1/26/1980	SAGO South - Surface
	300	534_h4ss_295a.dat	5.5	14	0.0615	-0.09	4.96	-9.26	1.500	-1.698	31.735	40.546	3.683	1.745	4.619	1.276	Rock	WUS	H2	295	XX-SS-09	Hollister-04	1/26/1980	SAGO South - Surface
	301	535_h4ss_0upa.dat	5.5	14	0.0305	-0.053	3.27	-3.38	0.529	-0.388	42.260	25.143	1.477	1.764	1.692	0.026	Rock	WUS	V	UP	XX-SS-09	Hollister-04	1/26/1980	SAGO South - Surface
94	302	536_pgpk_0nsa.dat	5.0	176	0.1499	-0.157	8.04	-8.03	0.541	-0.496	21.116	20.171	1.230	1.183	19.937	4.311	Rock	Greece	H	NS	XX-XX-81	Pelekanada	10/10/1984	ITSAK Pelekanada, Greece
	303	537_pgpk_0wea.dat	5.0	176	0.1489	-0.168	7.80	-6.29	0.532	-0.481	20.638	14.750	1.274	2.001	20.317	3.814	Rock	Greece	H2	WE	XX-XX-81	Pelekanada	10/10/1984	ITSAK Pelekanada, Greece
	304	538_pgpk_0upa.dat	5.0	176	0.0834	-0.102	2.87	-2.93	0.175	-0.159	13.553	11.377	1.734	1.840	9.199	4.755	Rock	Greece	V	UP	XX-XX-81	Pelekanada	10/10/1984	ITSAK Pelekanada, Greece
95	305	539_dgkv_0nsa.dat	5.2	48	0.0398	-0.049	2.25	-1.83	0.105	-0.106	22.230	14.849	0.807	1.504	1.836	0.000	Rock	Greece	H	NS	XX-SS-14	Drama	11/9/1985	ITSAK Kavala
	306	540_dgkv_0wea.dat	5.2	48	0.0387	-0.036	1.37	-1.20	0.082	-0.065	13.958	13.145	1.648	1.605	1.374	0.000	Rock	Greece	H2	WE	XX-SS-14	Drama	11/9/1985	ITSAK Kavala
	307	541_dgkv_0upa.dat	5.2	48	0.0491	-0.031	1.51	-1.11	0.090	-0.071	12.093	14.185	1.899	1.757	0.791	0.000	Rock	Greece	V	UP	XX-SS-14	Drama	11/9/1985	ITSAK Kavala
96	308	542_cc38_00ea.dat	5.9	64	0.009	-0.007	0.60	-0.75	0.131	-0.140	26.097	43.212	3.239	1.664	0.111	0.000	Rock	Taiwan	H	E	XX-XX-08	Chi-Chi	9/20/1999	CWB HWA 038, Taiwan
	309	543_cc38_00na.dat	5.9	64	0.0125	-0.01	1.03	-0.73	0.192	-0.164	32.429	27.915	2.223	3.128	0.154	0.000	Rock	Taiwan	H2	N	XX-XX-08	Chi-Chi	9/20/1999	CWB HWA 038, Taiwan
	310	544_cc38_00va.dat	5.9	64	0.0085	-0.007	0.68	-0.42	0.115	-0.104	31.511	24.380	2.060	3.918	0.106	0.000	Rock	Taiwan	V	V	XX-XX-08	Chi-Chi	9/20/1999	CWB HWA 038, Taiwan

M6 Master Accelerograph Table																								
Set	Rec#	Filename	Mw	Distance (hyp) km	PGA		PGV		PGD Lin Disp		Ratio 1 vm/km		Ratio 2 d*km/vm^2		AI 0.95	Duration bracketed	Site Class	Region	Comp	deg	Setting & Mech	Earthquake	date	Station
					+	-	+	-	+	-	+	-	+	-										
					g%		cm/s		cm		in./s/%g													
97	311	545_cc46_00na.dat	5.9	67	0.0253	-0.03	2.47	-2.40	0.275	-0.298	38.468	31.308	1.116	1.531	0.817	0.000	Rock	Taiwan	H	N	XX-XX-08	Chi-Chi	9/20/1999	CWB HWA 046, Taiwan
	312	546_cc46_00wa.dat	5.9	67	0.0263	-0.027	1.92	-1.82	0.231	-0.260	28.684	26.315	1.624	2.095	0.856	0.000	Rock	Taiwan	H2	W	XX-XX-08	Chi-Chi	9/20/1999	CWB HWA 046, Taiwan
	313	547_cc46_00va.dat	5.9	67	0.0149	-0.015	1.37	-1.18	0.197	-0.217	36.216	30.836	1.532	2.304	0.265	0.000	Rock	Taiwan	V	V	XX-XX-08	Chi-Chi	9/20/1999	CWB HWA 046, Taiwan
98	314	548_cc31_00ea.dat	5.9	112	0.0159	-0.016	0.85	-0.71	0.095	-0.082	21.048	17.572	2.064	2.527	0.343	0.000	Rock	Taiwan	H	E	XX-XX-08	Chi-Chi	9/20/1999	CWB ILA 031, Taiwan
	315	549_cc31_00na.dat	5.9	112	0.0194	-0.017	2.02	-1.68	0.235	-0.241	40.997	39.993	1.099	1.385	0.539	0.000	Rock	Taiwan	H2	N	XX-XX-08	Chi-Chi	9/20/1999	CWB ILA 031, Taiwan
	316	550_cc31_00va.dat	5.9	112	0.0087	-0.01	0.79	-0.94	0.131	-0.150	35.684	37.050	1.790	1.658	0.114	0.000	Rock	Taiwan	V	V	XX-XX-08	Chi-Chi	9/20/1999	CWB ILA 031, Taiwan
99	317	551_cc45_00ea.dat	5.9	68	0.0236	-0.024	1.32	-2.85	0.475	-0.366	22.027	47.419	6.308	1.047	0.472	0.000	Rock	Taiwan	H	E	XX-XX-08	Chi-Chi	9/20/1999	CWB TCU 045, Taiwan
	318	552_cc45_00na.dat	5.9	68	0.022	-0.019	1.41	-1.30	0.163	-0.200	25.179	27.417	1.770	2.165	0.549	0.000	Rock	Taiwan	H2	N	XX-XX-08	Chi-Chi	9/20/1999	CWB TCU 045, Taiwan
	319	553_cc45_00va.dat	5.9	68	0.0116	-0.01	0.68	-0.90	0.125	-0.181	23.052	36.107	3.066	2.145	0.151	0.000	Rock	Taiwan	V	V	XX-XX-08	Chi-Chi	9/20/1999	CWB TCU 045, Taiwan
100	320	554_cc71_00ea.dat	5.9	24	0.1011	-0.099	6.29	-4.74	0.722	-0.788	24.482	18.891	1.809	3.400	10.902	4.978	Rock	Taiwan	H	E	XX-XX-08	Chi-Chi	9/20/1999	CWB TCU 071, Taiwan
	321	555_cc71_00na.dat	5.9	24	0.0551	-0.058	2.78	-2.92	0.323	-0.250	19.868	19.695	2.255	1.683	4.779	2.753	Rock	Taiwan	H2	N	XX-XX-08	Chi-Chi	9/20/1999	CWB TCU 071, Taiwan
	322	556_cc71_00va.dat	5.9	24	0.0267	-0.026	1.40	-1.29	0.212	-0.257	20.648	19.466	2.838	3.947	1.163	0.000	Rock	Taiwan	V	V	XX-XX-08	Chi-Chi	9/20/1999	CWB TCU 071, Taiwan
101	323	557_smmw_000a.dat	0.0	0	0.276	-0.187	13.54	-9.93	0.714	-1.777	19.314	20.949	1.054	3.300	37.110	3.879	Rock	WUS	H	0	XX-XX-12	Sierra Madre	6/28/1991	CDMG Mt. Wilson
	324	558_smmw_090a.dat	0.0	0	0.2001	-0.198	7.79	-6.25	0.756	-1.067	15.319	12.428	2.449	5.300	29.797	3.659	Rock	WUS	H2	90	XX-XX-12	Sierra Madre	6/28/1991	CDMG Mt. Wilson
	325	559_smmw_0upa.dat	0.0	0	0.2372	-0.194	4.34	-5.74	0.731	-0.646	7.199	11.627	9.039	3.738	24.572	3.699	Rock	WUS	V	UP	XX-XX-12	Sierra Madre	6/28/1991	CDMG Mt. Wilson
102	326	560_n6gp_00Ea.dat	5.3	24	0.0286	-0.032	2.31	-2.01	0.213	-0.253	31.735	24.868	1.123	1.950	1.017	0.000	Rock	WUS	H	0	XX-XX-13	Northridge	3/20/1994	Griffith Park Observatory
	327	561_n6gp_90Wa.dat	5.3	24	0.0529	-0.056	2.39	-2.19	0.169	-0.235	17.762	15.400	1.536	2.694	2.416	1.680	Rock	WUS	H2	90	XX-XX-13	Northridge	3/20/1994	Griffith Park Observatory
	328	562_n6gp_0upa.dat	5.3	24	0.021	-0.027	1.14	-1.33	0.056	-0.109	21.394	19.442	0.883	1.622	0.543	0.000	Rock	WUS	V	UP	XX-XX-13	Northridge	3/20/1994	Griffith Park Observatory
103	329	563_sms2_000a.dat	5.7	32	0.0885	-0.119	5.04	-3.29	0.339	-0.504	22.448	10.887	1.155	5.433	4.170	0.462	Rock	WUS	H	0	XX-XX-12	Little Skull Mtn, NV	6/29/1992	USGS Station # 2 NTS Control Point
	330	564_sms2_270a.dat	5.7	32	0.0906	-0.057	3.24	-4.66	0.475	-0.636	14.080	32.013	4.023	1.647	2.564	0.552	Rock	WUS	H2	270	XX-XX-12	Little Skull Mtn, NV	6/29/1992	USGS Station # 2 NTS Control Point
	331	565_sms2_0upa.dat	5.7	32	0.0502	-0.07	2.61	-2.31	0.237	-0.253	20.507	13.061	1.705	3.245	1.543	0.447	Rock	WUS	V	UP	XX-XX-12	Little Skull Mtn, NV	6/29/1992	USGS Station # 2 NTS Control Point
104	332	566_sms8_000a.dat	5.7	100	0.0123	-0.011	0.51	-0.52	0.095	-0.099	16.116	18.179	4.499	4.033	0.190	0.000	Rock	WUS	H	0	XX-XX-12	Little Skull Mtn, NV	6/29/1992	USGS Station # 8 Death Valley
	333	567_sms8_270a.dat	5.7	100	0.0129	-0.009	0.43	-0.40	0.094	-0.097	13.067	17.535	6.513	5.288	0.157	0.000	Rock	WUS	H2	270	XX-XX-12	Little Skull Mtn, NV	6/29/1992	USGS Station # 8 Death Valley
	334	568_sms8_0upa.dat	5.7	100	0.0088	-0.007	0.26	-0.30	0.098	-0.086	11.735	16.740	12.281	6.506	0.103	0.000	Rock	WUS	V	UP	XX-XX-12	Little Skull Mtn, NV	6/29/1992	USGS Station # 8 Death Valley
105	335	569_cagi_020a.dat	5.4	15	0.0006	-6E-04	0.03	-0.02	0.003	-0.003	17.675	15.114	2.456	3.445	0.000	0.000	Rock	India	H	20	XX-XX-10	Chamoli Aftershock	3/28/1996	Gopershwar, India
	336	570_cagi_290a.dat	5.4	15	0.0004	-2E-04	0.02	-0.03	0.004	-0.003	15.900	46.943	5.777	0.977	0.000	0.000	Rock	India	H2	290	XX-XX-10	Chamoli Aftershock	3/28/1996	Gopershwar, India
	337	571_cagi_00va.dat	5.4	15	0.0004	-5E-04	0.01	-0.01	0.004	-0.002	10.493	10.374	11.461	6.518	0.000	0.000	Rock	India	V	V	XX-XX-10	Chamoli Aftershock	3/28/1996	Gopershwar, India
106	338	572_ibui_087a.dat	6.0	78	0.0015	-0.002	0.04	-0.03	0.005	-0.008	9.196	6.430	5.396	17.757	0.001	0.000	Rock	India	H	87	XX-XX-XX	India-Burma Border	5/8/1997	Ummulong, India
	339	573_ibui_357a.dat	6.0	78	0.0009	-0.001	0.02	-0.02	0.006	-0.010	7.784	9.480	16.465	16.220	0.001	0.000	Rock	India	H2	357	XX-XX-XX	India-Burma Border	5/8/1997	Ummulong, India
	340	574_ibui_00va.dat	6.0	78	0.0002	-3E-04	0.01	-0.01	0.003	-0.003	13.468	10.216	11.339	14.892	0.000	0.000	Rock	India	V	V	XX-XX-XX	India-Burma Border	5/8/1997	Ummulong, India
107	341	575_n2s1_010a.dat	5.4	Unknown	0.2286	-0.138	6.73	-4.04	0.412	-0.325	11.600	11.545	2.037	2.691	7.098	3.910	Rock	Canada	H	10	XX-XX-10	Nahanni	12/23/1985	Nahanni, NWT - Station #1
	342	576_n2s1_280a.dat	5.4	Unknown	0.0894	-0.058	3.12	-3.14	0.397	-0.360	13.757	21.221	3.564	2.087	3.140	1.260	Rock	Canada	H2	280	XX-XX-10	Nahanni	12/23/1985	Nahanni, NWT - Station #1
	343	577_n2s1_0upa.dat	5.4	Unknown	0.1122	-0.082	4.60	-1.84	0.369	-0.328	16.138	8.832	1.922	7.808	2.959	0.445	Rock	Canada	V	UP	XX-XX-10	Nahanni	12/23/1985	Nahanni, NWT - Station #1
108	344	578_n1s3_270a.dat	5.7	Unknown	0.0876	-0.09	2.08	-1.19	0.395	-0.370	9.351	5.212	7.845	23.053	2.120	0.835	Rock	Canada	H	270	XX-XX-10	Nahanni	12/25/1985	Nahanni, NWT - Station #3
	345	579_n1s3_360a.dat	5.7	Unknown	0.0942	-0.105	1.11	-1.17	0.140	-0.143	4.625	4.396	10.583	10.693	2.550	1.180	Rock	Canada	H2	360	XX-XX-10	Nahanni	12/25/1985	Nahanni, NWT - Station #3
	346	580_n1s3_0upa.dat	5.7	Unknown	0.0631	-0.074	1.19	-1.55	0.283	-0.380	7.441	8.232	12.295	11.503	1.684	0.910	Rock	Canada	V	UP	XX-XX-10	Nahanni	12/25/1985	Nahanni, NWT - Station #3

Table 4.4. Sets of earthquake time-history data classified by moment magnitude ranges.

Earthquake Magnitude	Magnitude 7	Magnitude 6	Magnitude 5
Moment Magnitude range (Mw)	6.90 – 8.10	6.90 – 8.10	4.85 – 6.06
Average Moment Magnitude (Mw)	7.25	7.25	5.57
No. sets (set id range)	23 (1-23)	23 (1-23)	61 (48-108)
H or H1	23	23	61
H2	22	22	61
V	23	23	58
TOTAL TH's	68	68	180

Table 4.5. Comparison between the Richter and Moment Magnitude Scales.

Earthquake	Richter Scale	Moment Magnitude
New Madrid, MO, 1812	8.7	8.1
San Francisco, CA, 1906	8.3	7.7
Prince William, AK, 1964	8.4	9.2
Northridge, CA, 1994	6.4	6.7

The criteria for selection of “rock” data were records that were assigned a rock site classification, and where more site information was available, the site’s V_{s30} (average shear wave velocity (V_s) in the upper 30 m). Records were accepted if V_{s30} exceeded 600 meters per second (m/s) to insure “rock” records using an upper bound site class C to avoid stiff soil sites. A V_{s30} of 760 m/s is an unweathered rock and including only down to 600 m/s allows weathered rock, but voids highly weathered rock or stiff soil sites which start at 360 m/s. Also, records were selected based on instrument housing as free-field, or less preferred, but acceptable, one-story structures.

The records selected were all instrument corrected records. The further processing included a baseline correction based on the procedure, “baseline,” a PC-based algorithm developed by Norm Abrahamson that uses a polynomial fit to remove any baseline shift from the earthquake acceleration time-history. The baseline shift is usually an artifact introduced by the data collection process. Since the application of this data is to estimate permanent displacements, it was important that this artifact be removed so that the data doesn’t include an initial undesirable permanent

component of displacement. The specifics of the parameters used in the processing were use of 5th order polynomial, 50 zeros padded at the end of each record, and a 10 second taper. All records received identical processing. Visual data quality checks involved reviewing time-histories and response spectra to be sure that all data appeared free-field and rock-like in nature. All response spectra were plotted together to identify any large deviations from the full population data set. The sources of these data were predominately from the Pacific Earthquake Engineering Research Center (PEER) database and Consortium of Strong-ground motion Observations Systems (COSMOS) virtual data center. 4.2 Regression results of earthquakes covering the Moment Magnitude (M_w) range of 6.9 – 8.1 (Magnitude 7)

This section will discuss the results from regression analyses of the non-dimensionalized displacement relationships described by Equations 3.20, 3.39, and 3.58 previously derived in Chapter 3. The values for the coefficients summarized by the above mentioned equations and the standard error terms, as well as the probabilistic measures of Equation Forms One, Two and Three as shown in Table 4.6, will be discussed in Sections 4.2.1, 4.2.2, and 4.2.3. These regression analyses were performed for baseline corrected acceleration time histories recorded on rock with a M_w range of 6.9 to 8.1 and an average M_w of 7.3.

Table 4.6. Values for the regression equations constants for Moment Magnitude (M_w) range of 6.9 – 8.1 (Magnitude 7).

Coefficients and <i>Std. Error</i>	Equation Form One	Equation Form Two	Equation Form Three
β_1		70.146	66.727
β_2		-9.200	-9.134
β_3			-0.018
β_4	-0.124		
β_5	-2.076		
<i>Std. Error</i>	1.428	0.932	0.932

4.2.1 Three-term regression results

The standard error term (*Std. error*) for this regression analysis was determined to be 0.93 for both the non-dimensionalized displacement as well as the standardized displacement for earthquakes of Magnitude 7. This non-dimensionalized three-term displacement equation is identified as

Equation Form Three with the coefficients and *Std. error* terms summarized in column four of Table 4.6.

4.2.1.1 Mean relationships

The regression analysis of the 23 sets of Magnitude 7 acceleration time histories resulted in the mean non-dimensionalized displacement relationship of

$$\frac{d_m \bullet k_m g}{v_m^2} = 66.7 \bullet \exp\left(-9.13 \bullet \frac{k_c}{k_m}\right) \bullet \left(\frac{k_c}{k_m}\right)^{-0.018} \quad (4.1)$$

where:

- d_m = permanent displacement
- $k_m g$ = peak (positive) rock acceleration expressed in units of length per sec², consistent with units of d_m (length) and v_m (length per sec)
- v_m = peak (positive) ground velocity of the earthquake
- k_c = critical acceleration expressed as a fraction of g
- k_m = peak (positive) rock acceleration expressed as a fraction of g .

This mean relationship is shown in yellow in Figure 4.1.

By a second independent regression analysis, the mean standardized maximum displacement (d_s) in units of inches was derived for the standardized velocity, $v_s = 29.92$ in./sec (0.76 m/sec) and the standardized acceleration $k_s = 0.5 g$ (193.04 in./sec² : 4.90 m/sec²)

$$d_s = 309.5 \bullet \exp\left(-9.13 \bullet \frac{k_c}{k_m}\right) \bullet \left(\frac{k_c}{k_m}\right)^{-0.018} \quad (4.2)$$

The standardized maximum displacement (d_s) can be converted to the permanent displacement (d_m) by the following transformation (Franklin and Chang 1977),

$$d_m = d_s \bullet \left[\left(\frac{k_s}{v_s^2} \right) \bullet \left(\frac{v_m^2}{k_m} \right) \right] \quad (4.3)$$

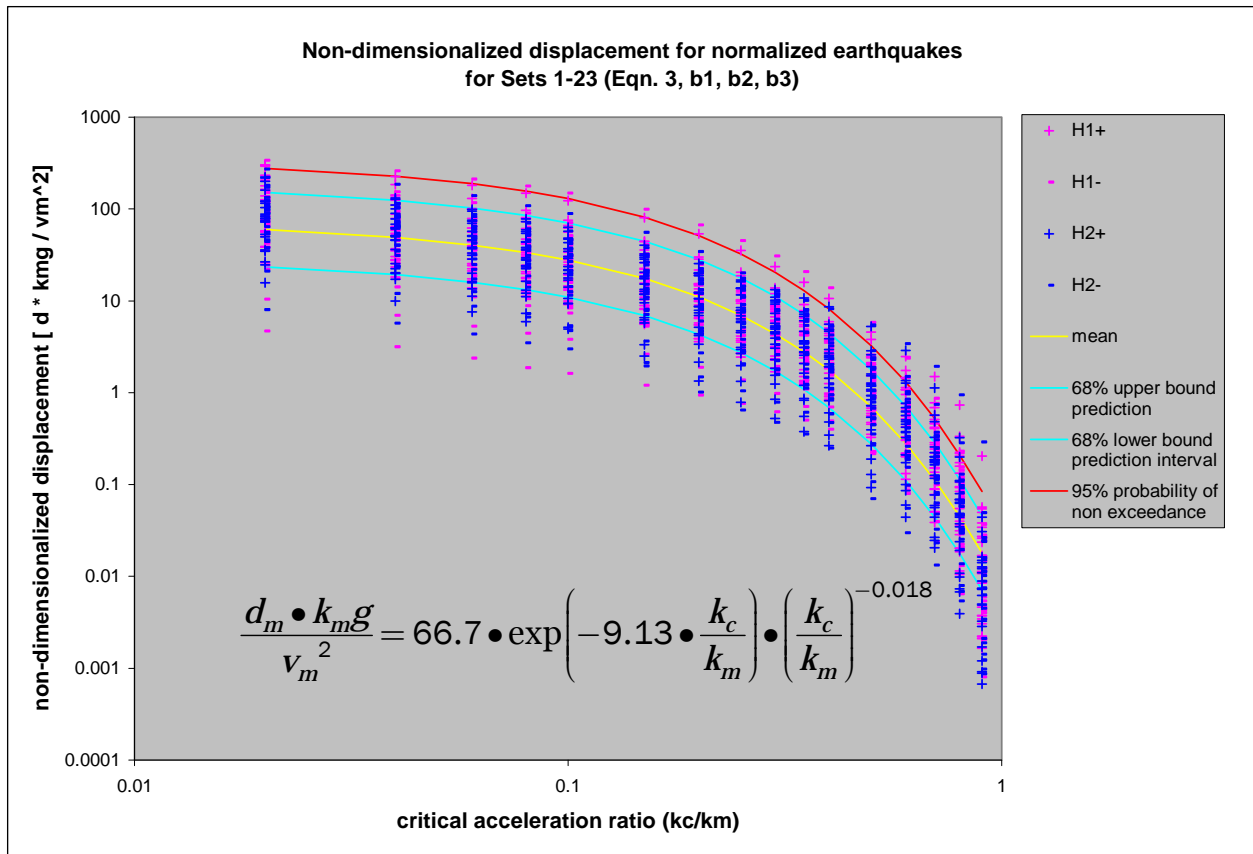


Figure 4.1. Non-dimensionalized displacements with the mean, 68 percent prediction intervals and 95 percent probability of non-exceedance curves.

where:

- k_s = standardized acceleration expressed as a fraction of g (0.5)
- v_s = standardized velocity (29.92 in./sec).

The mean permanent displacement is derived by introducing Equation 4.2 into Equation 4.3.

$$d_m = 309.5 \cdot \exp\left(-9.13 \cdot \frac{k_c}{k_m}\right) \cdot \left(\frac{k_c}{k_m}\right)^{-0.018} \cdot \left[0.216 \cdot \left(\frac{v_m^2}{k_m \cdot g}\right)\right] \quad (4.4)$$

where the right-hand-side term $k_m g$ is the peak (positive) rock acceleration expressed in units of length per sec².

Note that Equation 4.4 is the same as Equation 4.1, indicating consistent results from both regression analyses.

4.2.1.2 Ninety-five percent probability of non-exceedance

The regression analysis of the 23 sets of Magnitude 7 rock acceleration time histories resulted in the non-dimensionalized displacement for 95 percent probability of non-exceedance of

$$\frac{d_m \bullet k_m g}{v_m^2} = 66.7 \bullet \exp\left(-9.13 \bullet \frac{k_c}{k_m}\right) \bullet \left(\frac{k_c}{k_m}\right)^{-0.018} \bullet 4.64 \quad (4.5)$$

The 95 percent probability of non-exceedance is shown in red in Figure 4.1.

By the second independent regression analysis, the standardized maximum displacement (d_s) in units of inches, derived using $v_s = 29.92$ in./sec and $k_s = 0.5 g$, is

$$d_s = 309.5 \bullet \exp\left(-9.13 \bullet \frac{k_c}{k_m}\right) \bullet \left(\frac{k_c}{k_m}\right)^{-0.018} \bullet 4.64 \quad (4.6)$$

The corresponding permanent displacement is

$$d_m = 309.5 \bullet \exp\left(-9.13 \bullet \frac{k_c}{k_m}\right) \bullet \left(\frac{k_c}{k_m}\right)^{-0.018} \bullet 4.64 \bullet \left[0.216 \bullet \left(\frac{v_m^2}{k_m \bullet g}\right)\right] \quad (4.7)$$

Note that Equation 4.7 is the same as Equation 4.5, indicating consistent results from both regression analyses,

4.2.1.3 Sixty-eight percent prediction intervals

The regression analysis of the 23 sets of Magnitude 7 rock acceleration time histories resulted in the non-dimensionalized displacement relationships for the 68 percent prediction intervals of

$$\frac{d_m \bullet k_m g}{v_m^2} = 66.7 \bullet \exp\left(-9.13 \bullet \frac{k_c}{k_m}\right) \bullet \left(\frac{k_c}{k_m}\right)^{-0.018} \bullet 2.53 \quad (4.8a)$$

$$\frac{d_m \bullet k_m g}{v_m^2} = 66.7 \bullet \exp\left(-9.13 \bullet \frac{k_c}{k_m}\right) \bullet \left(\frac{k_c}{k_m}\right)^{-0.018} \bullet 0.39 \quad (4.8b)$$

The 68 percent prediction intervals are shown in blue in Figure 4.1.

By the second independent regression analysis, the standardized maximum displacements (d_s) in units of inches, derived using $v_s = 29.92$ in./sec and $k_s = 0.5 g$, are

$$d_s = 309.5 \cdot \exp\left(-9.13 \cdot \frac{k_c}{k_m}\right) \cdot \left(\frac{k_c}{k_m}\right)^{-0.018} \cdot 2.53 \quad (4.9a)$$

$$d_s = 309.5 \cdot \exp\left(-9.13 \cdot \frac{k_c}{k_m}\right) \cdot \left(\frac{k_c}{k_m}\right)^{-0.018} \cdot 0.39 \quad (4.9b)$$

Introducing Equation 4.3, the corresponding permanent displacements are

$$d_m = 309.5 \cdot \exp\left(-9.13 \cdot \frac{k_c}{k_m}\right) \cdot \left(\frac{k_c}{k_m}\right)^{-0.018} \cdot 2.53 \cdot \left[0.216 \cdot \left(\frac{v_m^2}{k_m \cdot g}\right)\right] \quad (4.10a)$$

$$d_m = 309.5 \cdot \exp\left(-9.13 \cdot \frac{k_c}{k_m}\right) \cdot \left(\frac{k_c}{k_m}\right)^{-0.018} \cdot 0.39 \cdot \left[0.216 \cdot \left(\frac{v_m^2}{k_m \cdot g}\right)\right] \quad (4.10b)$$

where the right-hand-side term $k_m g$ is the peak (positive) rock acceleration expressed in units of length per sec².

Note that Equations 4.10a and 4.10b are the same as Equations 4.8a and 4.8b, indicating consistent results from both regression analyses.

4.2.2 Two-term regression results, linear in natural logarithm transformation

The standard error term (*Std. error*) for this regression analysis was determined to be 0.93 for both the non-dimensionalized displacement as well as the standardized displacement for earthquakes of Magnitude 7. This non-dimensionalized two-term displacement equation is identified as Equation Form Two with the coefficients and *Std. error* terms summarized in column three of Table 4.6.

4.2.2.1 Mean relationships

The regression analysis of the 23 sets of Magnitude 7 rock acceleration time histories resulted in the mean non-dimensionalized displacement relationship of

$$\frac{d_m \bullet k_m g}{v_m^2} = 70.1 \bullet \exp\left(-9.2 \bullet \frac{k_c}{k_m}\right) \tag{4.11}$$

where the left-hand-side term $k_m g$ is the peak (positive) rock acceleration expressed in units of length per sec², consistent with units of d_m (length) and v_m (length per sec) in which d_m is the permanent displacement, v_m is the peak (positive) ground velocity of the earthquake and k_c is the critical acceleration expressed as a fraction of g . The right hand side term k_m is the peak (positive) rock acceleration expressed as a fraction of g .

This mean relationship is shown in yellow in Figure 4.2.

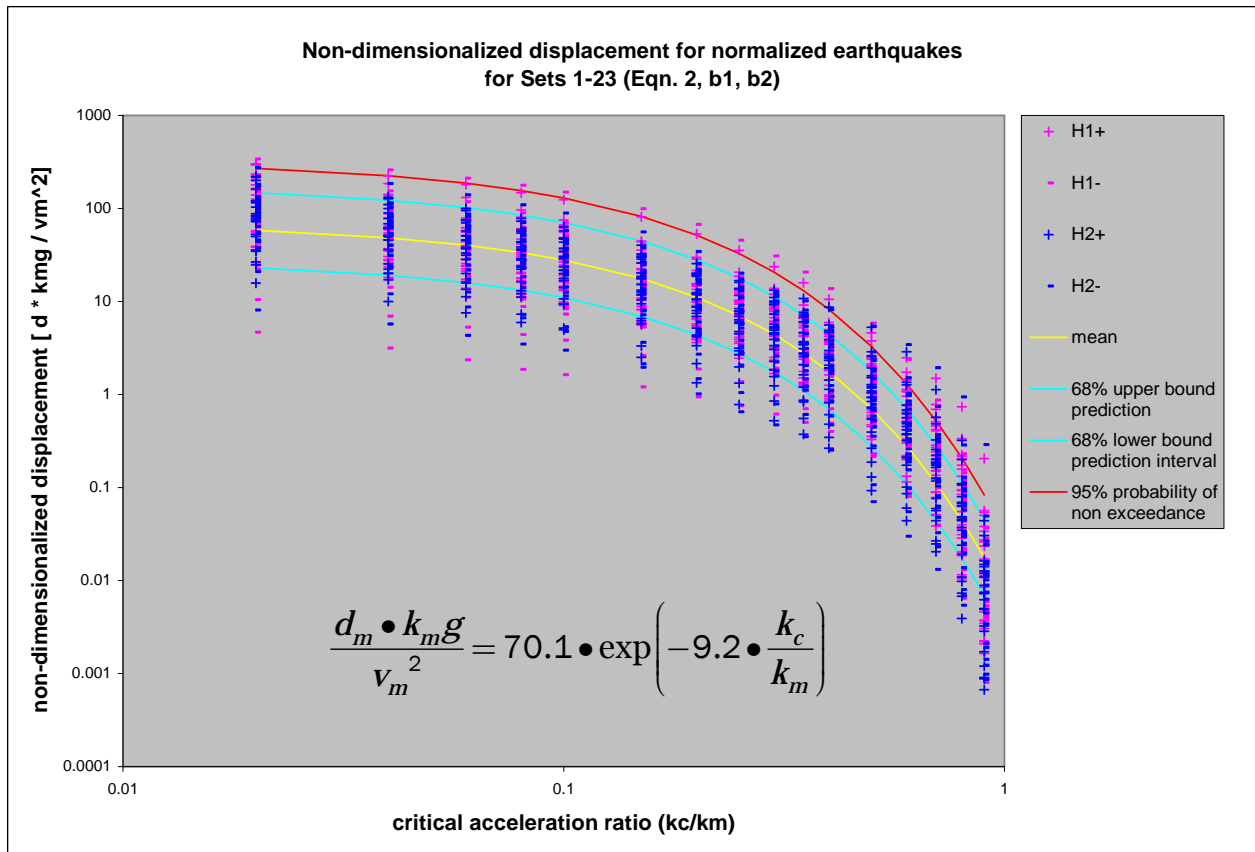


Figure 4.2. Non-dimensionalized displacements with the mean, 68 percent prediction intervals and 95 percent probability of non-exceedance curves.

By a second independent regression analysis, the mean standardized maximum displacement (d_s) in units of inches was derived for the standardized velocity, $v_s = 29.92$ in./sec (0.76 m/sec) and the standardized acceleration $k_s = 0.5 g$ (193.04 in./sec² : 4.90 m/sec²)

$$d_s = 325.3 \bullet \exp\left(-9.2 \bullet \frac{k_c}{k_m}\right) \quad (4.12)$$

The standardized maximum displacement (d_s) can be converted to the permanent displacement (d_m) by the following transformation,

$$d_m = d_s \bullet \left[\left(\frac{k_s}{v_s^2} \right) \bullet \left(\frac{v_m^2}{k_m} \right) \right] \quad (\text{bis 4.3})$$

where:

k_s = standardized acceleration expressed as a fraction of g (0.5)

v_s = standardized velocity (29.92 in./sec).

The mean permanent displacement is derived by introducing Equation 4.12 into Equation 4.3.

$$d_m = 325.3 \bullet \exp\left(-9.2 \bullet \frac{k_c}{k_m}\right) \bullet \left[0.216 \bullet \left(\frac{v_m^2}{k_m \bullet g} \right) \right] \quad (4.13)$$

where the right-hand-side term $k_m g$ is the peak (positive) rock acceleration expressed in units of length per sec².

Note that Equation 4.13 is the same as Equation 4.11, indicating consistent results from both regression analyses.

4.2.2.2 Ninety-five percent probability of non-exceedance

The regression analysis of the 23 sets of Magnitude 7 rock acceleration time histories resulted in the non-dimensionalized displacement for 95 percent probability of non-exceedance of

$$\frac{d_m \bullet k_m g}{v_m^2} = 70.1 \bullet \exp\left(-9.2 \bullet \frac{k_c}{k_m}\right) \bullet 4.64 \quad (4.14)$$

The 95 percent probability of non-exceedance is shown in red in Figure 4.2.

By the second, independent regression analysis, the standardized maximum displacement (d_s) in units of inches, derived using $v_s = 29.92$ in./sec and $k_s = 0.5 g$, is

$$d_s = 325.3 \bullet \exp\left(-9.2 \bullet \frac{k_c}{k_m}\right) \bullet 4.64 \quad (4.15)$$

The corresponding permanent displacement is

$$d_m = 325.3 \bullet \exp\left(-9.2 \bullet \frac{k_c}{k_m}\right) \bullet 4.64 \bullet \left[0.216 \bullet \left(\frac{v_m^2}{k_m \bullet g}\right)\right] \quad (4.16)$$

where the right-hand-side term $k_m g$ is the peak (positive) rock acceleration expressed in units of length per sec².

Note that Equation 4.16 is the same as Equation 4.14, indicating consistent results from both regression analyses.

4.2.2.3 Sixty-eight percent prediction intervals

The regression analysis of the 23 sets of Magnitude 7 rock acceleration time histories resulted in the non-dimensionalized displacement relationships for the 68 percent prediction intervals of

$$\frac{d_m \bullet k_m g}{v_m^2} = 70.1 \bullet \exp\left(-9.2 \bullet \frac{k_c}{k_m}\right) \bullet 2.53 \quad (4.17a)$$

$$\frac{d_m \bullet k_m g}{v_m^2} = 70.1 \bullet \exp\left(-9.2 \bullet \frac{k_c}{k_m}\right) \bullet 0.39 \quad (4.17b)$$

The 68 percent prediction intervals are shown in blue in Figure 4.2.

By the second independent regression analysis, the standardized maximum displacements (d_s) in units of inches, derived using $v_s = 29.92$ in./sec and $k_s = 0.5 g$, are

$$d_s = 325.3 \bullet \exp\left(-9.2 \bullet \frac{k_c}{k_m}\right) \bullet 2.53 \quad (4.18a)$$

$$d_s = 325.3 \bullet \exp\left(-9.2 \bullet \frac{k_c}{k_m}\right) \bullet 0.39 \quad (4.18b)$$

Introducing Equation 4.3, the corresponding permanent displacements are

$$d_m = 325.3 \bullet \exp\left(-9.2 \bullet \frac{k_c}{k_m}\right) \bullet 2.53 \bullet \left[0.216 \bullet \left(\frac{v_m^2}{k_m \bullet g}\right)\right] \quad (4.19a)$$

$$d_m = 325.3 \bullet \exp\left(-9.2 \bullet \frac{k_c}{k_m}\right) \bullet 0.39 \bullet \left[0.216 \bullet \left(\frac{v_m^2}{k_m \bullet g}\right)\right] \quad (4.19b)$$

where the right-hand-side term $k_m g$ is the peak (positive) rock acceleration expressed in units of length per sec².

Note that Equations 4.19a and 4.19b are the same as Equations 4.17a and 4.17b, indicating consistent results from both regression analyses.

4.2.3 Two-term regression results, linear in common logarithm transformation

The standard error term (*Std. error*) for this regression analysis was determined to be 1.43 for both the non-dimensionalized displacement as well as the standardized displacement for earthquakes of Magnitude 7. This non-dimensionalized two-term displacement equation is identified as Equation Form One with the coefficients and *Std. error* terms summarized in column two of Table 4.6.

4.2.3.1 Mean relationships

The regression analysis of the 23 sets of Magnitude 7 rock acceleration time histories resulted in the mean non-dimensionalized displacement relationship of

$$\frac{d_m \cdot k_m g}{v_m^2} = 0.124 \cdot \left(\frac{k_c}{k_m} \right)^{-2.08} \tag{4.20}$$

where:

- d_m = permanent displacement
- $k_m g$ = peak (positive) rock acceleration expressed in units of length per sec², consistent with units of d_m (length) and v_m (length per sec)
- v_m = peak (positive) ground velocity of the earthquake
- k_c = critical acceleration expressed as a fraction of g
- k_m = peak (positive) rock acceleration expressed as a fraction of g .

This mean relationship is shown in yellow in Figure 4.3.

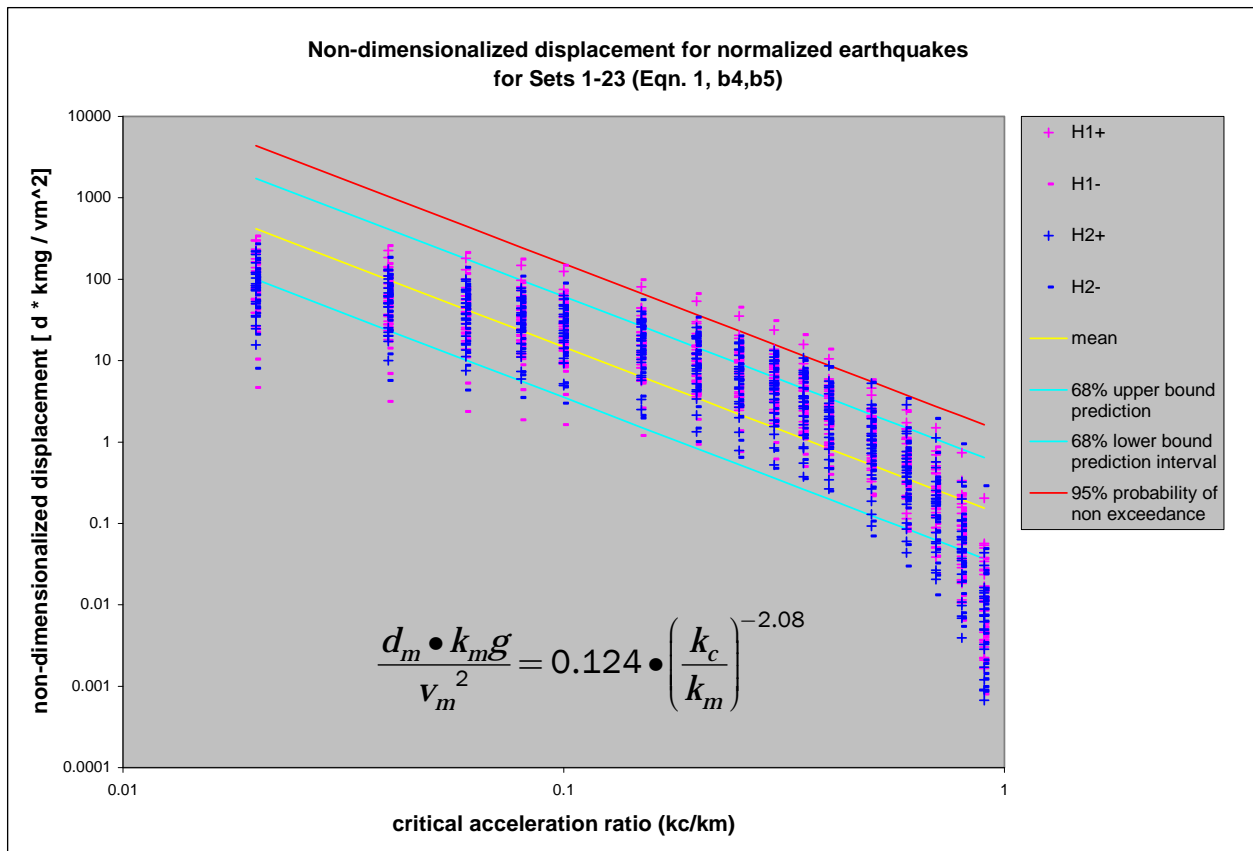


Figure 4.3. Non-dimensionalized displacements with the mean, 68 percent prediction intervals and 95 percent probability of non-exceedance curves.

By a second independent regression analysis, the mean standardized maximum displacement (d_s) in units of inches was derived for the standardized velocity, $v_s = 29.92$ in./sec (0.76 m/sec) and the standardized acceleration $k_s = 0.5 g$ (193.04 in./sec² : 4.90 m/sec²)

$$d_s = 0.573 \cdot \left(\frac{k_c}{k_m} \right)^{-2.08} \quad (4.21)$$

The standardized maximum displacement (d_s) can be converted to the permanent displacement (d_m) by the following transformation,

$$d_m = d_s \cdot \left[\left(\frac{k_s}{v_s^2} \right) \cdot \left(\frac{v_m^2}{k_m} \right) \right] \quad (\text{bis 4.3})$$

where:

k_s = standardized acceleration expressed as a fraction of g (0.5)

v_s = standardized velocity (29.92 in./sec).

The mean permanent displacement is derived by introducing Equation 4.21 into Equation 4.3.

$$d_m = 0.573 \cdot \left(\frac{k_c}{k_m} \right)^{-2.08} \cdot \left[0.216 \cdot \left(\frac{v_m^2}{k_m \cdot g} \right) \right] \quad (4.22)$$

where the right-hand-side term $k_m g$ is the peak (positive) rock acceleration expressed in units of length per sec².

Note that Equation 4.22 is the same as Equation 4.20, indicating consistent results from both regression analyses.

4.2.3.2 Ninety-five percent probability of non-exceedance

The regression analysis of the 23 sets of Magnitude 7 rock acceleration time histories resulted in the non-dimensionalized displacement for 95 percent probability of non-exceedance of

$$\frac{d_m \bullet k_m g}{v_m^2} = 0.124 \bullet \left(\frac{k_c}{k_m} \right)^{-2.08} \bullet 2.78 \quad (4.23)$$

The 95 percent probability of non-exceedance is shown in red in Figure 4.3.

By the second independent regression analysis, the standardized maximum displacement (d_s) in units of inches, derived using $v_s = 29.92$ in./sec and $k_s = 0.5 g$, is

$$d_s = 0.573 \bullet \left(\frac{k_c}{k_m} \right)^{-2.08} \bullet 2.78 \quad (4.24)$$

Introducing Equation 4.3, the corresponding permanent displacement is

$$d_m = 0.573 \bullet \left(\frac{k_c}{k_m} \right)^{-2.08} \bullet 2.78 \bullet \left[0.216 \bullet \left(\frac{v_m^2}{k_m \bullet g} \right) \right] \quad (4.25)$$

where the right-hand-side term $k_m g$ is the peak (positive) rock acceleration expressed in units of length per sec².

Note that Equation 4.25 is the same as Equation 4.23, indicating consistent results from both regression analyses.

4.2.3.3 Sixty-eight percent prediction intervals

The regression analysis of the 23 sets of Magnitude 7 rock acceleration time histories resulted in the non-dimensionalized displacement relationships for the 68 percent prediction intervals of

$$\frac{d_m \bullet k_m g}{v_m^2} = 0.124 \bullet \left(\frac{k_c}{k_m} \right)^{-2.08} \bullet 1.86 \quad (4.26a)$$

$$\frac{d_m \bullet k_m g}{v_m^2} = 0.124 \bullet \left(\frac{k_c}{k_m} \right)^{-2.08} \bullet 0.538 \quad (4.26b)$$

The 68 percent prediction intervals are shown in blue in Figure 4.3.

By the second independent regression analysis, the standardized maximum displacements (d_s) in units of inches, derived using $v_s = 29.92$ in./sec and $k_s = 0.5$ g, are

$$d_s = 325.3 \cdot \exp\left(-9.2 \cdot \frac{k_c}{k_m}\right) \cdot 1.86 \quad (4.27a)$$

$$d_s = 325.3 \cdot \exp\left(-9.2 \cdot \frac{k_c}{k_m}\right) \cdot 0.538 \quad (4.27b)$$

Introducing Equation 4.3, the corresponding permanent displacements are,

$$d_m = 325.3 \cdot \exp\left(-9.2 \cdot \frac{k_c}{k_m}\right) \cdot 1.86 \cdot \left[0.216 \cdot \left(\frac{v_m^2}{k_m \cdot g}\right)\right] \quad (4.28a)$$

$$d_m = 325.3 \cdot \exp\left(-9.2 \cdot \frac{k_c}{k_m}\right) \cdot 0.538 \cdot \left[0.216 \cdot \left(\frac{v_m^2}{k_m \cdot g}\right)\right] \quad (4.28b)$$

where the right-hand-side term $k_m g$ is the peak (positive) rock acceleration expressed in units of length per sec².

Note that Equations 4.28a and 4.28b are the same as Equations 4.26a and 4.26b, indicating consistent results from both regression analyses.

4.2.4 Comparison of regression results of all three forms of the simplified non-dimensionalized displacement relationships

The three forms of regression analysis (discussed in Sections 4.2.1, 4.2.2, and 4.2.3), namely, the three-term regression analysis (identified as eqn3 in Figure 4.4), the two-term, linear in Natural Logarithm Transformation (eqn2 in Figure 4.4) and the two-term, linear in common logarithm transformation (eqn1 in Figure 4.4) will have their results compared and evaluated.

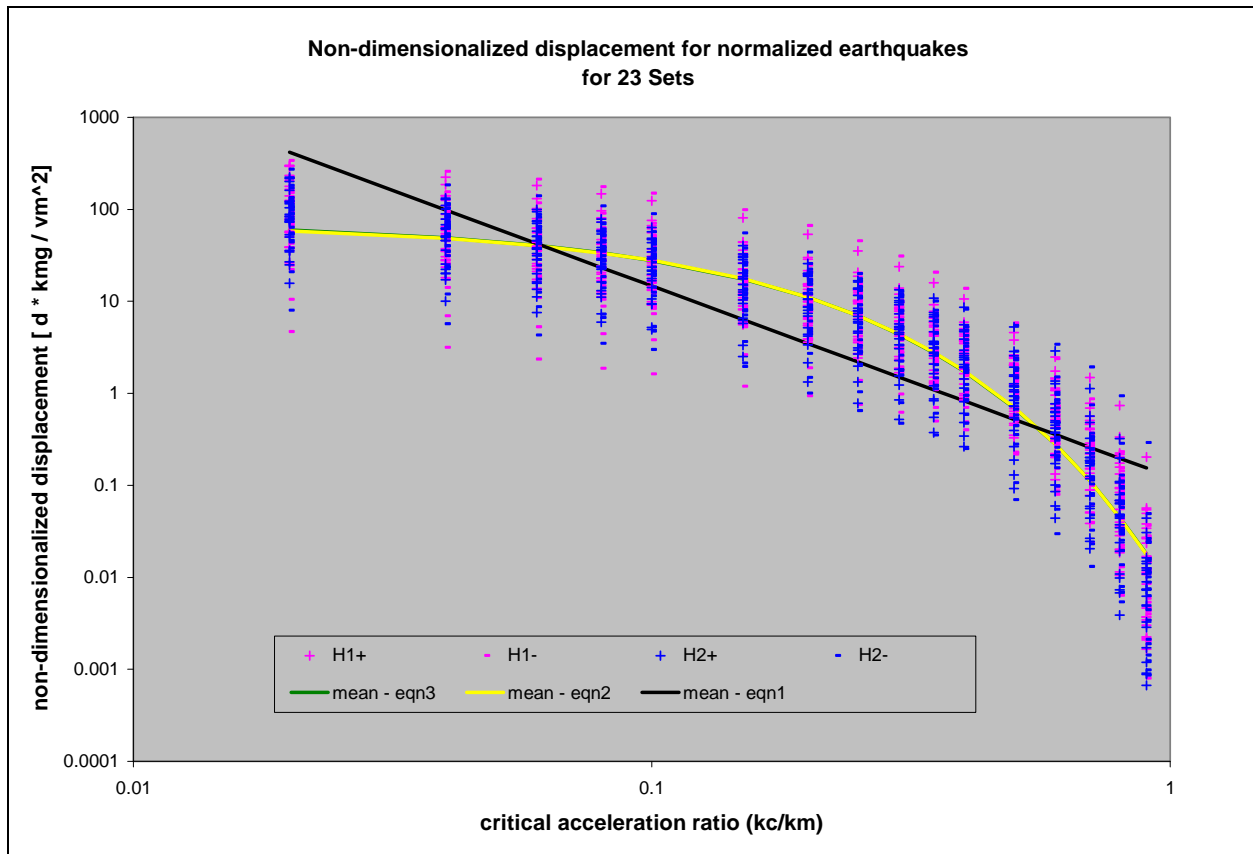


Figure 4.4. Non-dimensionalized displacements and comparisons of the means of the three regression analysis equations for Magnitude 7 earthquakes.

One method of comparison will be the *Std. error* term determined from the error in the estimates. The *Std. error* for eqn3 is 0.93, for eqn2, 0.93 and for eqn1, equal to 1.43 when transformed to a natural logarithm from a common logarithm standard error value of 0.62. These results show that eqn3 and eqn2 have a more accurate estimate as compared to eqn1, and that eqn3 and eqn2 have practically equal values.

Another comparison is the mean relationships as illustrated in Figure 4.4. As can be seen, eqn2 and eqn3 follow the shape of the data and are positioned at the center of the data points while eqn1 does not. Note also that the mean curves of eqn2 and eqn3 are almost superimposing each other, which show the similarity of the results.

Lastly, given the small value of the exponent for the (k_c/k_m) term of eqn3 (-0.018), this explains the comparable results of eqn2 and eqn3.

4.3 Regression results of earthquakes covering the Moment Magnitude (M_w) range of 6.1 – 6.8 (Magnitude 6)

This subsequent section will discuss the results from regression analyses of the non-dimensionalized displacement relationships described by Equations 3.20, 3.39, and 3.58 previously derived in chapter three. The values for the coefficients summarized by the above mentioned equations and the standard error terms, as well as the probabilistic measures of Equation Forms One, Two and Three, as documented in Table 4.7, will be discussed in Sections 4.2.1, 4.2.2, and 4.2.3. These regression analyses were performed for baseline corrected acceleration time histories recorded on rock with a M_w range of 6.1 to 6.8 and an average M_w of 6.5.

Table 4.7. Values for the regression equations constants for Moment Magnitude (M_w) range of 6.1 – 6.8 (Magnitude 6).

Coefficients and <i>Std. Error</i>	Equation Form One	Equation Form Two	Equation Form Three
β_1		78.618	71.851
β_2		-9.121	-9.003
β_3			-0.032
β_4	-0.146		
β_5	-2.060		
<i>Std. Error</i>	1.328	0.792	0.792

4.3.1 Three-term regression results

The standard error term (*Std. error*) for this regression analysis was determined to be 0.79 for both the non-dimensionalized displacement as well as the standardized displacement for earthquakes of Magnitude 6. This non-dimensionalized three-term displacement equation is identified as Equation Form Three with the coefficients and *Std. error* terms summarized in column four of Table 4.7.

4.3.1.1 Mean relationships

The regression analysis of the 38 sets of Magnitude 6 rock acceleration time histories resulted in the mean non-dimensionalized displacement relationship of

$$\frac{d_m \cdot k_m g}{v_m^2} = 71.9 \cdot \exp\left(-9.00 \cdot \frac{k_c}{k_m}\right) \cdot \left(\frac{k_c}{k_m}\right)^{-0.032} \tag{4.29}$$

where:

- d_m = permanent displacement
- $k_m g$ = peak (positive) rock acceleration expressed in units of length per sec², consistent with units of d_m (length) and v_m (length per sec)
- v_m = peak (positive) ground velocity of the earthquake
- k_c = critical acceleration expressed as a fraction of g
- k_m = peak (positive) rock acceleration expressed as a fraction of g .

This mean relationship is shown in yellow in Figure 4.5.

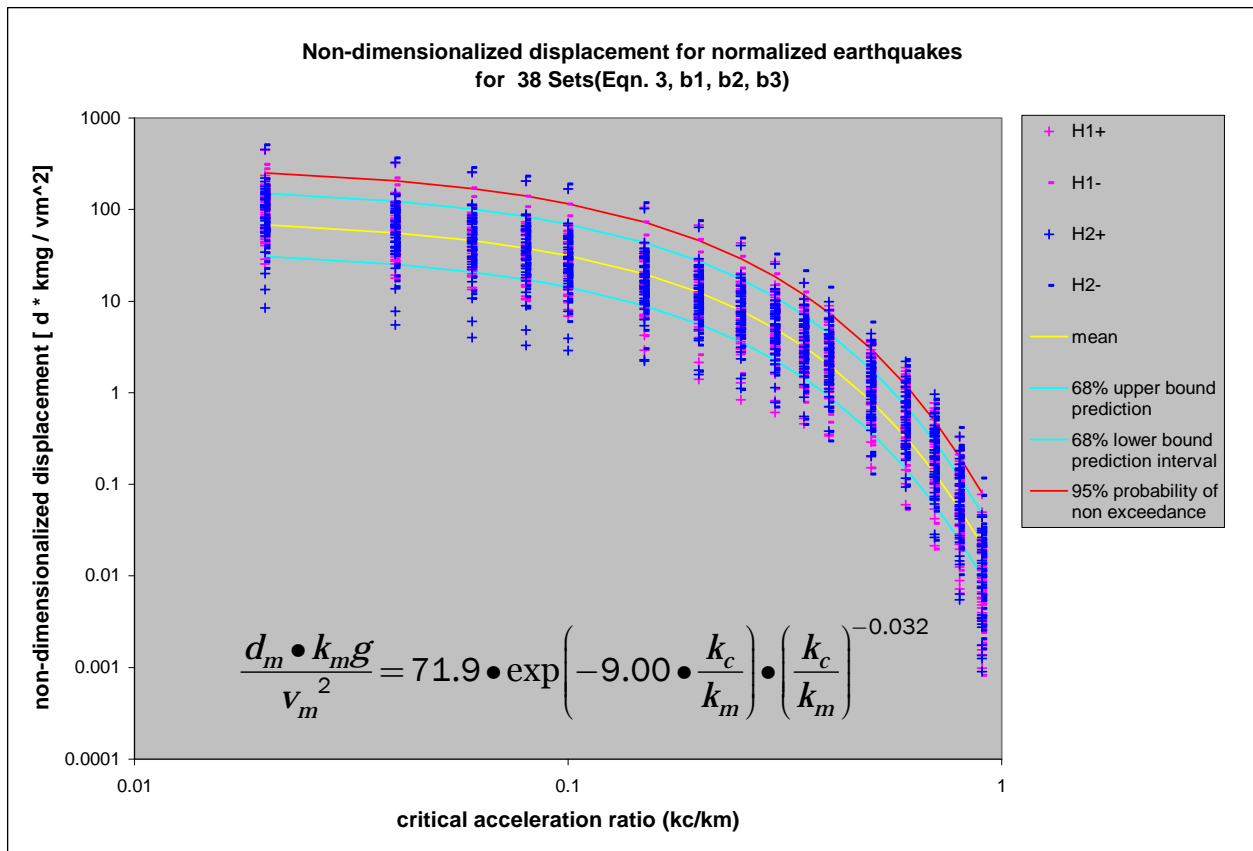


Figure 4.5. Non-dimensionalized displacements with the mean, 68 percent prediction intervals and 95 percent probability of non-exceedance curves.

By a second independent regression analysis, the mean standardized maximum displacement (d_s) in units of inches was derived for the standardized velocity, $v_s = 29.92$ in./sec (0.76 m/sec) and the standardized acceleration $k_s = 0.5 g$ (193.04 in./sec² : 4.90 m/sec²)

$$d_s = 333.22 \cdot \exp\left(-9.00 \cdot \frac{k_c}{k_m}\right) \cdot \left(\frac{k_c}{k_m}\right)^{-0.032} \quad (4.30)$$

The standardized maximum displacement (d_s) can be converted to the permanent displacement (d_m) by the following transformation,

$$d_m = d_s \cdot \left[\left(\frac{k_s}{v_s^2} \right) \cdot \left(\frac{v_m^2}{k_m} \right) \right] \quad (\text{bis. 4.3})$$

where:

k_s = standardized acceleration expressed as a fraction of g (0.5)

v_s = standardized velocity (29.92 in./sec).

The mean permanent displacement is derived by introducing Equation 4.30 into Equation 4.3.

$$d_m = 333.22 \cdot \exp\left(-9.00 \cdot \frac{k_c}{k_m}\right) \cdot \left(\frac{k_c}{k_m}\right)^{-0.032} \cdot \left[0.216 \cdot \left(\frac{v_m^2}{k_m \cdot g} \right) \right] \quad (4.31)$$

where the right-hand-side term $k_m g$ is the peak (positive) rock acceleration expressed in units of length per sec².

Note that Equation 4.31 is the same as Equation 4.29, indicating consistent results from both regression analyses.

4.3.1.2 Ninety-five percent probability of non-exceedance

The regression analysis of the 38 sets of Magnitude 6 rock acceleration time histories resulted in the non-dimensionalized displacement for 95 percent probability of non-exceedance of

$$\frac{d_m \cdot k_m g}{v_m^2} = 71.9 \cdot \exp\left(-9.00 \cdot \frac{k_c}{k_m}\right) \cdot \left(\frac{k_c}{k_m}\right)^{-0.032} \cdot 3.68 \quad (4.32)$$

The 95 percent probability of non-exceedance is shown in red in Figure 4.5.

By the second, independent regression analysis, the standardized maximum displacement (d_s) in units of inches, derived using $v_s = 29.92$ in./sec and $k_s = 0.5 g$, is

$$d_s = 333.2 \cdot \exp\left(-9.00 \cdot \frac{k_c}{k_m}\right) \cdot \left(\frac{k_c}{k_m}\right)^{-0.032} \cdot 3.68 \quad (4.33)$$

Introducing Equation 4.3, the corresponding permanent displacement is

$$d_m = 333.2 \cdot \exp\left(-9.00 \cdot \frac{k_c}{k_m}\right) \cdot \left(\frac{k_c}{k_m}\right)^{-0.032} \cdot 3.68 \cdot \left[0.216 \cdot \left(\frac{v_m^2}{k_m \cdot g}\right)\right] \quad (4.34)$$

where the right-hand-side term $k_m g$ is the peak (positive) rock acceleration expressed in units of length per sec².

Note that Equation 4.34 is the same as Equation 4.32, indicating consistent results from both regression analyses,

4.3.1.3 Sixty-eight percent prediction intervals

The regression analysis of the 38 sets of Magnitude 6 rock acceleration time histories resulted in the non-dimensionalized displacement relationships for the 68 percent prediction intervals of

$$\frac{d_m \cdot k_m g}{v_m^2} = 71.9 \cdot \exp\left(-9.00 \cdot \frac{k_c}{k_m}\right) \cdot \left(\frac{k_c}{k_m}\right)^{-0.032} \cdot 2.20 \quad (4.35a)$$

$$\frac{d_m \cdot k_m g}{v_m^2} = 71.9 \cdot \exp\left(-9.00 \cdot \frac{k_c}{k_m}\right) \cdot \left(\frac{k_c}{k_m}\right)^{-0.032} \cdot 0.45 \quad (4.35b)$$

The 68 percent prediction intervals are shown in blue in Figure 4.5.

By the second independent regression analysis, the standardized maximum displacements (d_s) in units of inches, derived using $v_s = 29.92$ in./sec and $k_s = 0.5$ g, are

$$d_s = 333.2 \cdot \exp\left(-9.00 \cdot \frac{k_c}{k_m}\right) \cdot \left(\frac{k_c}{k_m}\right)^{-0.032} \cdot 2.20 \quad (4.36a)$$

$$d_s = 333.2 \cdot \exp\left(-9.00 \cdot \frac{k_c}{k_m}\right) \cdot \left(\frac{k_c}{k_m}\right)^{-0.032} \cdot 0.454 \quad (4.36b)$$

Introducing Equation 4.3, the corresponding permanent displacements are

$$d_m = 333.2 \cdot \exp\left(-9.00 \cdot \frac{k_c}{k_m}\right) \cdot \left(\frac{k_c}{k_m}\right)^{-0.032} \cdot 2.20 \cdot \left[0.216 \cdot \left(\frac{v_m^2}{k_m \cdot g}\right)\right] \quad (4.37a)$$

$$d_m = 333.2 \cdot \exp\left(-9.00 \cdot \frac{k_c}{k_m}\right) \cdot \left(\frac{k_c}{k_m}\right)^{-0.032} \cdot 0.454 \cdot \left[0.216 \cdot \left(\frac{v_m^2}{k_m \cdot g}\right)\right] \quad (4.37b)$$

where the right-hand-side term $k_m g$ is the peak (positive) rock acceleration expressed in units of length per sec².

Note that Equations 4.37a and 4.37b are the same as Equations 4.35a and 4.35b, indicating consistent results from both regression analyses.

4.3.2 Two-term regression results, linear in natural logarithm transformation

The standard error term (*Std. error*) for this regression analysis was determined to be 0.79 for both the non-dimensionalized displacement as well as the standardized displacement for earthquakes of Magnitude 6. This non-dimensionalized two-term displacement equation is identified as Equation Form Two with the coefficients and *Std. error* terms summarized in column three of Table 4.7.

4.3.2.1 Mean relationships

The regression analysis of the 38 sets of Magnitude 6 rock acceleration time histories resulted in the mean non-dimensionalized displacement relationship of

$$\frac{d_m \bullet k_m g}{v_m^2} = 78.6 \bullet \exp\left(-9.12 \bullet \frac{k_c}{k_m}\right) \quad (4.38)$$

where:

- d_m = permanent displacement
- $k_m g$ = peak (positive) rock acceleration expressed in units of length per sec², consistent with units of d_m (length) and v_m (length per sec)
- v_m = peak (positive) ground velocity of the earthquake
- k_c = critical acceleration expressed as a fraction of g
- k_m = peak (positive) rock acceleration expressed as a fraction of g .

This mean relationship is shown in yellow in Figure 4.6.

By a second independent regression analysis, the mean standardized maximum displacement (d_s) in units of inches was derived for the standardized velocity, $v_s = 29.92$ in./sec (0.76 m/sec) and the standardized acceleration $k_s = 0.5 g$ (193.04 in./sec² : 4.90 m/sec²)

$$d_s = 364.6 \bullet \exp\left(-9.12 \bullet \frac{k_c}{k_m}\right) \quad (4.39)$$

The standardized maximum displacement (d_s) can be converted to the permanent displacement (d_m) by the following transformation,

$$d_m = d_s \bullet \left[\left(\frac{k_s}{v_s^2} \right) \bullet \left(\frac{v_m^2}{k_m} \right) \right] \quad (\text{bis } 4.3)$$

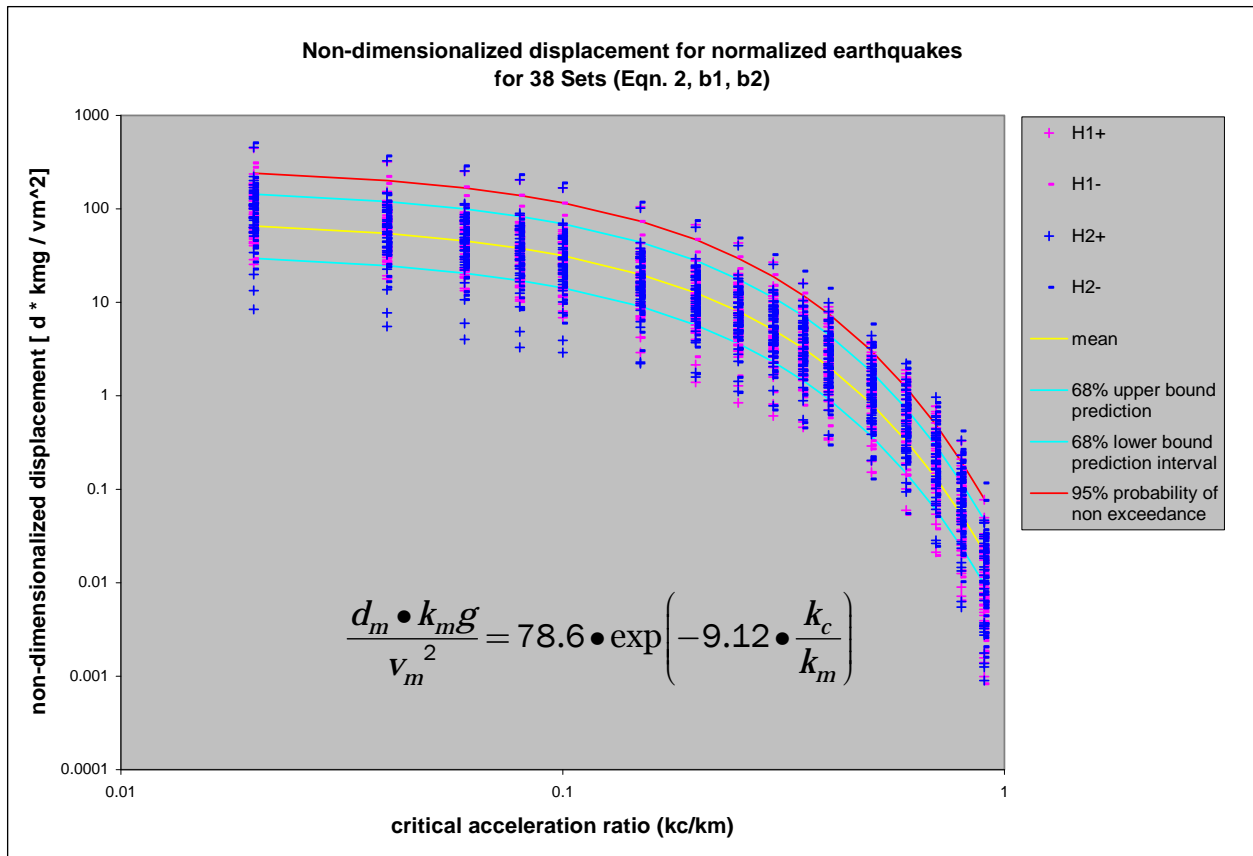


Figure 4.6. Non-dimensionalized displacements with the mean, 68 percent prediction intervals and 95 percent probability of non-exceedance curves.

where:

- k_s = standardized acceleration expressed as a fraction of g (0.5)
- v_s = standardized velocity (29.92 in./sec).

The mean permanent displacement is derived by introducing Equation 4.39 into Equation 4.3.

$$d_m = 364.6 \cdot \exp\left(-9.12 \cdot \frac{k_c}{k_m}\right) \cdot \left[0.216 \cdot \left(\frac{v_m^2}{k_m \cdot g}\right)\right] \quad (4.40)$$

where the right-hand-side term $k_m g$ is the peak (positive) rock acceleration expressed in units of length per sec².

Note that Equation 4.40 is the same as Equation 4.38, indicating consistent results from both regression analyses.

4.3.2.2 Ninety-five percent probability of non-exceedance

The regression analysis of the 38 sets of Magnitude 6 rock acceleration time histories resulted in the non-dimensionalized displacement for 95 percent probability of non-exceedance of

$$\frac{d_m \bullet k_m g}{v_m^2} = 78.6 \bullet \exp\left(-9.12 \bullet \frac{k_c}{k_m}\right) \bullet 3.68 \quad (4.41)$$

The 95 percent probability of non-exceedance is shown in red in Figure 4.6.

By the second, independent regression analysis, the standardized maximum displacement (d_s) in units of inches, derived using $v_s = 29.92$ in./sec and $k_s = 0.5$ g, is

$$d_s = 364.6 \bullet \exp\left(-9.12 \bullet \frac{k_c}{k_m}\right) \bullet 3.68 \quad (4.42)$$

Introducing Equation 4.3, the corresponding permanent displacement is

$$d_m = 364.6 \bullet \exp\left(-9.12 \bullet \frac{k_c}{k_m}\right) \bullet 3.68 \bullet \left[0.216 \bullet \left(\frac{v_m^2}{k_m \bullet g}\right)\right] \quad (4.43)$$

where the right-hand-side term $k_m g$ is the peak (positive) rock acceleration expressed in units of length per sec².

Note that Equation 4.43 is the same as Equation 4.41, indicating consistent results from both regression analyses.

4.3.2.3 Sixty-eight percent prediction intervals

The regression analysis of the 38 sets of Magnitude 6 rock acceleration time histories resulted in the non-dimensionalized displacement relationships for the 68 percent prediction intervals of

$$\frac{d_m \bullet k_m g}{v_m^2} = 78.6 \bullet \exp\left(-9.12 \bullet \frac{k_c}{k_m}\right) \bullet 2.20 \quad (4.44a)$$

$$\frac{d_m \bullet k_m g}{v_m^2} = 78.6 \bullet \exp\left(-9.12 \bullet \frac{k_c}{k_m}\right) \bullet 0.454 \quad (4.44b)$$

The 68 percent prediction intervals are shown in blue in Figure 4.6.

By the second independent regression analysis, the standardized maximum displacements (d_s) in units of inches, derived using $v_s = 29.92$ in./sec and $k_s = 0.5$ g, are

$$d_s = 364.6 \bullet \exp\left(-9.12 \bullet \frac{k_c}{k_m}\right) 2.20 \quad (4.45a)$$

$$d_s = 325.3 \bullet \exp\left(-9.2 \bullet \frac{k_c}{k_m}\right) \bullet 0.454 \quad (4.45b)$$

Introducing Equation 4.3, the corresponding permanent displacements are

$$d_m = 364.6 \bullet \exp\left(-9.12 \bullet \frac{k_c}{k_m}\right) \bullet 2.20 \bullet \left[0.216 \bullet \left(\frac{v_m^2}{k_m \bullet g}\right)\right] \quad (4.46a)$$

$$d_m = 364.6 \bullet \exp\left(-9.12 \bullet \frac{k_c}{k_m}\right) \bullet 0.454 \bullet \left[0.216 \bullet \left(\frac{v_m^2}{k_m \bullet g}\right)\right] \quad (4.46b)$$

where the right-hand-side term $k_m g$ is the peak (positive) rock acceleration expressed in units of length per sec².

Note that Equations 4.46a and 4.46b are the same as Equations 4.44a and 4.44b, indicating consistent results from both regression analyses.

4.3.3 Two-term regression results, linear in common logarithm transformation

The standard error term (*Std. error*) for this regression analysis was determined to be 1.33 for both the non-dimensionalized displacement as well as the standardized displacement for earthquakes of Magnitude 6. This non-dimensionalized two-term displacement equation is identified as Equation Form One with the coefficients and *Std. error* terms summarized in column two of Table 4.7.

4.3.3.1 Mean relationships

The regression analysis of the 38 sets of Magnitude 6 rock acceleration time histories resulted in the mean non-dimensionalized displacement relationship of

$$\frac{d_m \bullet k_m g}{v_m^2} = 0.146 \bullet \left(\frac{k_c}{k_m} \right)^{-2.06} \quad (4.47)$$

where:

- d_m = permanent displacement
- $k_m g$ = peak (positive) rock acceleration expressed in units of length per sec², consistent with units of d_m (length) and v_m (length per sec)
- v_m = peak (positive) ground velocity of the earthquake
- k_c = critical acceleration expressed as a fraction of g
- k_m = peak (positive) rock acceleration expressed as a fraction of g .

This mean relationship is shown in yellow in Figure 4.7.

By a second independent regression analysis, the mean standardized maximum displacement (d_s) in units of inches was derived for the standardized velocity, $v_s = 29.92$ in./sec (0.76 m/sec) and the standardized acceleration $k_s = 0.5 g$ (193.04 in./sec² : 4.90 m/sec²)

$$d_s = 0.676 \bullet \left(\frac{k_c}{k_m} \right)^{-2.06} \quad (4.48)$$

The standardized maximum displacement (d_s) can be converted to the permanent displacement (d_m) by the following transformation,

$$d_m = d_s \bullet \left[\left(\frac{k_s}{v_s^2} \right) \bullet \left(\frac{v_m^2}{k_m} \right) \right] \quad (\text{bis } 4.3)$$

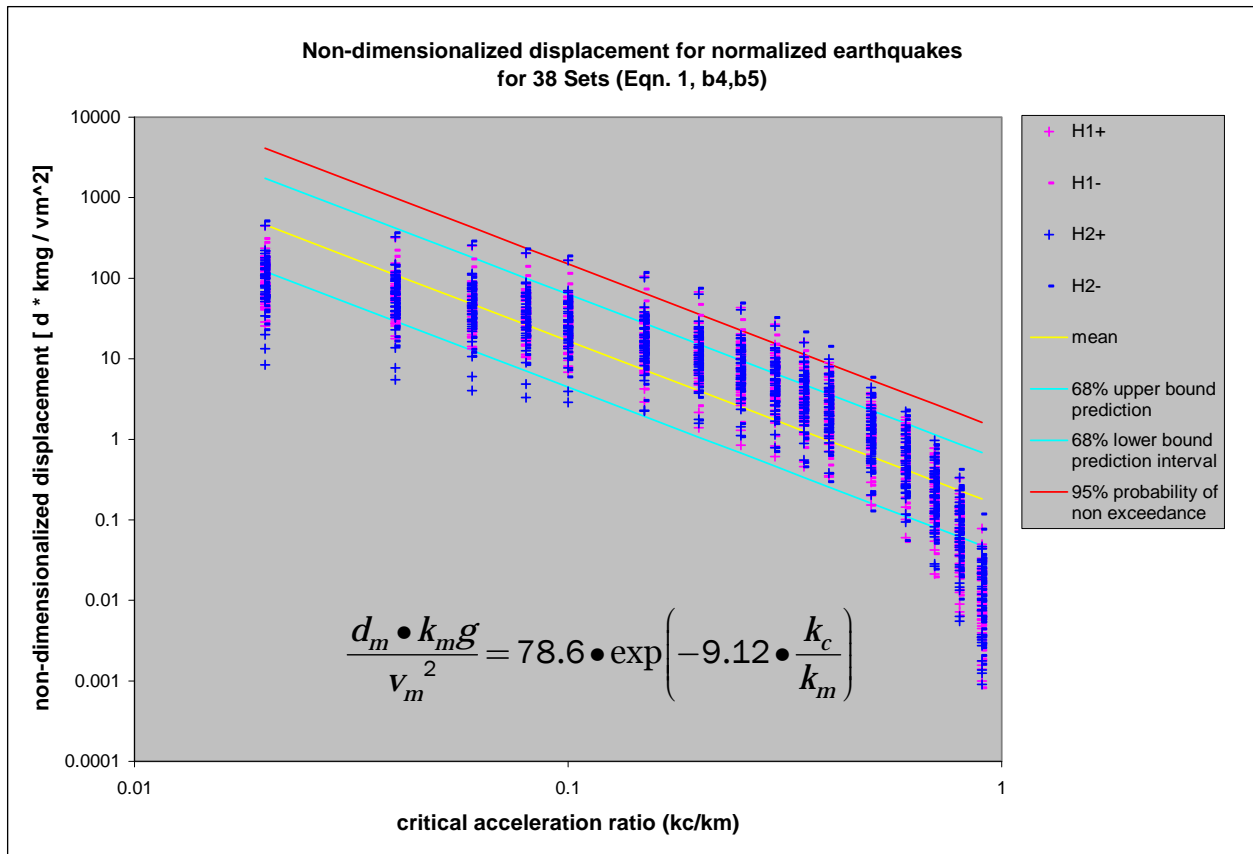


Figure 4.7. Non-dimensionalized displacements with the mean, 68 percent prediction intervals and 95 percent probability of non-exceedance curves.

where:

- k_s = standardized acceleration expressed as a fraction of g (0.5)
- v_s = standardized velocity (29.92 in./sec).

The mean permanent displacement is derived by introducing Equation 4.48 into Equation 4.3.

$$d_m = 0.676 \cdot \left(\frac{k_c}{k_m} \right)^{-2.06} \cdot \left[0.216 \cdot \left(\frac{v_m^2}{k_m \cdot g} \right) \right] \tag{4.49}$$

where the right-hand-side term $k_m g$ is the peak (positive) rock acceleration expressed in units of length per sec².

Note that Equation 4.49 is the same as Equation 4.47, indicating consistent results from both regression analyses.

4.3.3.2 Ninety-five percent probability of non-exceedance

The regression analysis of the 38 sets of Magnitude 6 rock acceleration time histories resulted in the non-dimensionalized displacement for 95 percent probability of non-exceedance of

$$\frac{d_m \bullet k_m g}{v_m^2} = 0.146 \bullet \left(\frac{k_c}{k_m} \right)^{-2.06} \bullet 2.60 \quad (4.50)$$

The 95 percent probability of non-exceedance is shown in red in Figure 4.7.

By the second, independent regression analysis, the standardized maximum displacement (d_s) in units of inches, derived using $v_s = 29.92$ in./sec and $k_s = 0.5 g$, is

$$d_s = 0.676 \bullet \left(\frac{k_c}{k_m} \right)^{-2.06} \bullet 2.60 \quad (4.51)$$

Introducing Equation 4.3, the corresponding permanent displacement is

$$d_m = 0.676 \bullet \left(\frac{k_c}{k_m} \right)^{-2.06} \bullet 2.60 \bullet \left[0.216 \bullet \left(\frac{v_m^2}{k_m \bullet g} \right) \right] \quad (4.52)$$

where the right-hand-side term $k_m g$ is the peak (positive) rock acceleration expressed in units of length per sec².

Note that Equation 4.52 is the same as Equation 4.50, indicating consistent results from both regression analyses.

4.3.3.3 Sixty-eight percent prediction intervals

The regression analysis of the 38 sets of Magnitude 6 rock acceleration time histories resulted in the non-dimensionalized displacement relationships for the 68 percent prediction intervals of

$$\frac{d_m \bullet k_m g}{v_m^2} = 0.146 \bullet \left(\frac{k_c}{k_m} \right)^{-2.06} \bullet 1.79 \quad (4.53a)$$

$$\frac{d_m \bullet k_m g}{v_m^2} = 0.146 \bullet \left(\frac{k_c}{k_m} \right)^{-2.06} \bullet 0.560 \quad (4.53b)$$

The 68 percent prediction intervals are shown in blue in Figure 4.7.

By the second independent regression analysis, the standardized maximum displacements (d_s) in units of inches, derived using $v_s = 29.92$ in./sec and $k_s = 0.5 g$, are

$$d_s = 0.676 \bullet \left(\frac{k_c}{k_m} \right)^{-2.06} \bullet 1.79 \quad (4.54a)$$

$$d_s = 0.676 \bullet \left(\frac{k_c}{k_m} \right)^{-2.06} \bullet 0.560 \quad (4.54b)$$

Introducing Equation 4.3, the corresponding permanent displacements are,

$$d_m = 0.676 \bullet \left(\frac{k_c}{k_m} \right)^{-2.06} \bullet 1.79 \bullet \left[0.216 \bullet \left(\frac{v_m^2}{k_m \bullet g} \right) \right] \quad (4.55a)$$

$$d_m = 0.676 \bullet \left(\frac{k_c}{k_m} \right)^{-2.06} \bullet 0.560 \bullet \left[0.216 \bullet \left(\frac{v_m^2}{k_m \bullet g} \right) \right] \quad (4.55b)$$

where the right-hand-side term $k_m g$ is the peak (positive) rock acceleration expressed in units of length per sec².

Note that Equations 4.55a and 4.55b are the same as Equations 4.53a and 4.53b, indicating consistent results from both regression analyses.

4.3.4 Comparison of regression results of all three forms of the simplified non-dimensionalized displacement relationships

The three forms of regression analysis (discussed in Sections 4.3.1, 4.3.2, and 4.3.3), namely, the three-term regression analysis (eqn3 in Figure 4.8), the two-term, linear in Natural Logarithm Transformation (eqn2 in Figure 4.8) and the two-term, linear in common logarithm transformation (eqn1 in Figure 4.8) will have their results compared and evaluated.

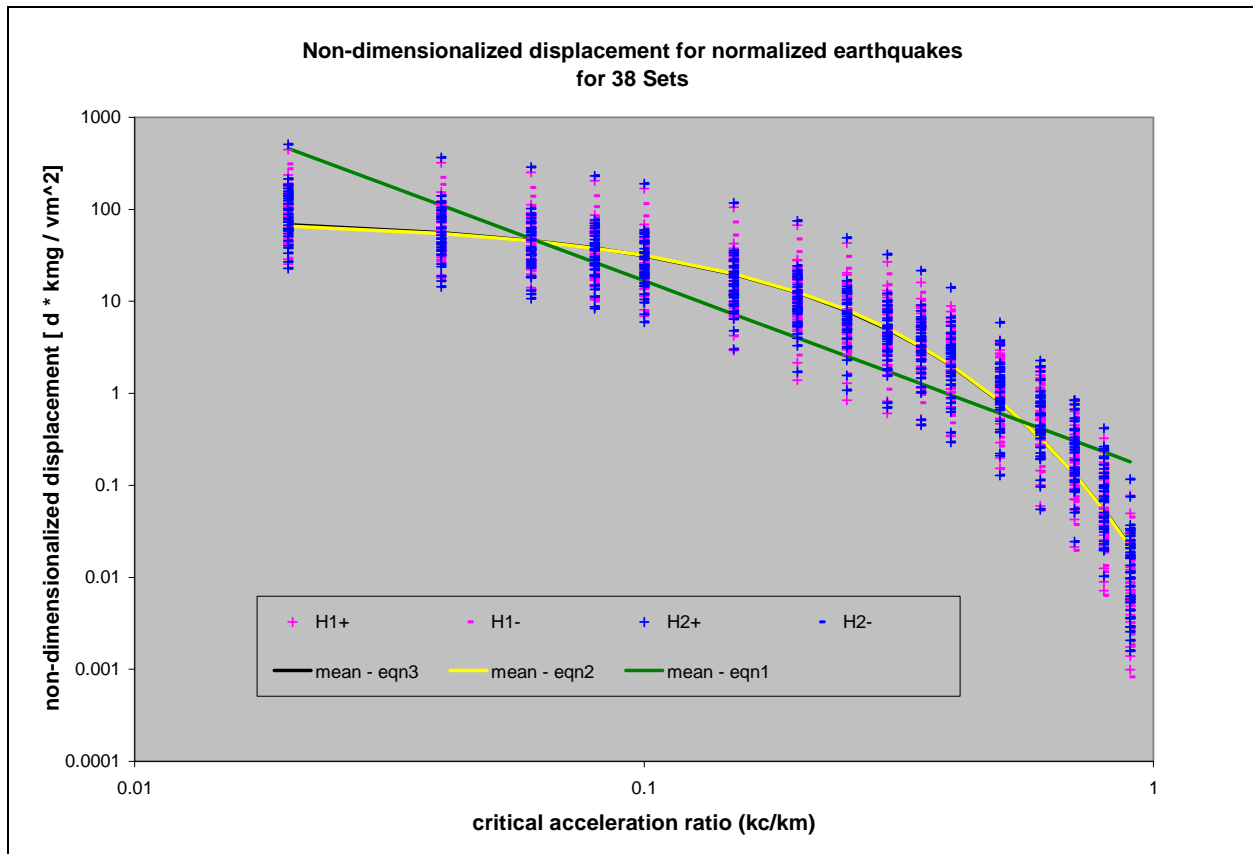


Figure 4.8. Non-dimensionalized displacements and comparisons of the means of the three regression analysis equations for Magnitude 6 earthquakes.

One method of comparison will be the *Std. error* term determined from the error in the estimates. The *Std. error* for eqn3 is 0.79, for eqn2, 0.79 and for eqn1, equal to 1.34 when transformed to a natural logarithm from a common logarithm standard error value of 0.58. These results show that eqn3 and eqn2 have a more accurate estimate as compared to eqn1, and that eqn3 and eqn2 have practically equal values.

Another comparison is the mean relationships as illustrated in Figure 4.8. As can be seen, eqn2 and eqn3 follow the shape of the data and are positioned at the center of the data points while eqn1 does not. Note also that the mean curves of eqn2 and eqn3 are almost superimposing each other which show the similarity of the results.

Lastly, given the small value of the exponent for the (k_c/k_m) term of eqn3 (-0.032), this explains the comparable results of eqn2 and eqn3.

4.4 Regression results of earthquakes covering the Moment Magnitude (M_w) range from 4.9 – 6.1 (Magnitude 5)

This subsequent section will discuss the results from regression analyses of the non-dimensionalized displacement relationships described by Equations 3.20, 3.39, and 3.58 previously derived in chapter three. The values for the coefficients summarized by the above mentioned equations and the standard error terms as well as the probabilistic measures of Equation Forms One, Two and Three, as documented in Table 4.8, will be discussed in Sections 4.4.1, 4.4.2, and 4.4.3. These regression analyses were performed for baseline corrected acceleration time histories recorded on rock with M_w range of 4.9 to 6.1 and an average M_w of 5.6.

Table 4.8. Values for the regression equations constants for Moment Magnitude (M_w) range of 4.9 – 6.1 (Magnitude 5).

Coefficients and <i>Std. Error</i>	Equation Form One	Equation Form Two	Equation Form Three
β_1		56.980	51.077
β_2		-8.579	-8.436
β_3			-0.039
β_4	-0.153		
β_5	-1.940		
<i>Std. Error</i>	1.242	0.738	0.738

4.4.1 Three-term regression results

The standard error term (*Std. error*) for this regression analysis was determined to be 0.74 for both the non-dimensionalized displacement as well as the standardized displacement for earthquakes of Magnitude 5. This non-dimensionalized three-term displacement equation is identified as Equation Form Three with the coefficients and *Std. error* terms summarized in column four of Table 4.8.

4.4.1.1 Mean relationships

The regression analysis of the 23 sets of Magnitude 5 rock acceleration time histories resulted in the mean non-dimensionalized displacement relationship of

$$\frac{d_m \bullet k_m g}{v_m^2} = 51.1 \bullet \exp\left(-8.44 \bullet \frac{k_c}{k_m}\right) \bullet \left(\frac{k_c}{k_m}\right)^{-0.039} \tag{4.56}$$

where:

- d_m = permanent displacement
- $k_m g$ = peak (positive) rock acceleration expressed in units of length per sec², consistent with units of d_m (length) and v_m (length per sec)
- v_m = peak (positive) ground velocity of the earthquake
- k_c = critical acceleration expressed as a fraction of g
- k_m = peak (positive) rock acceleration expressed as a fraction of g .

This mean relationship is shown in yellow in Figure 4.9.

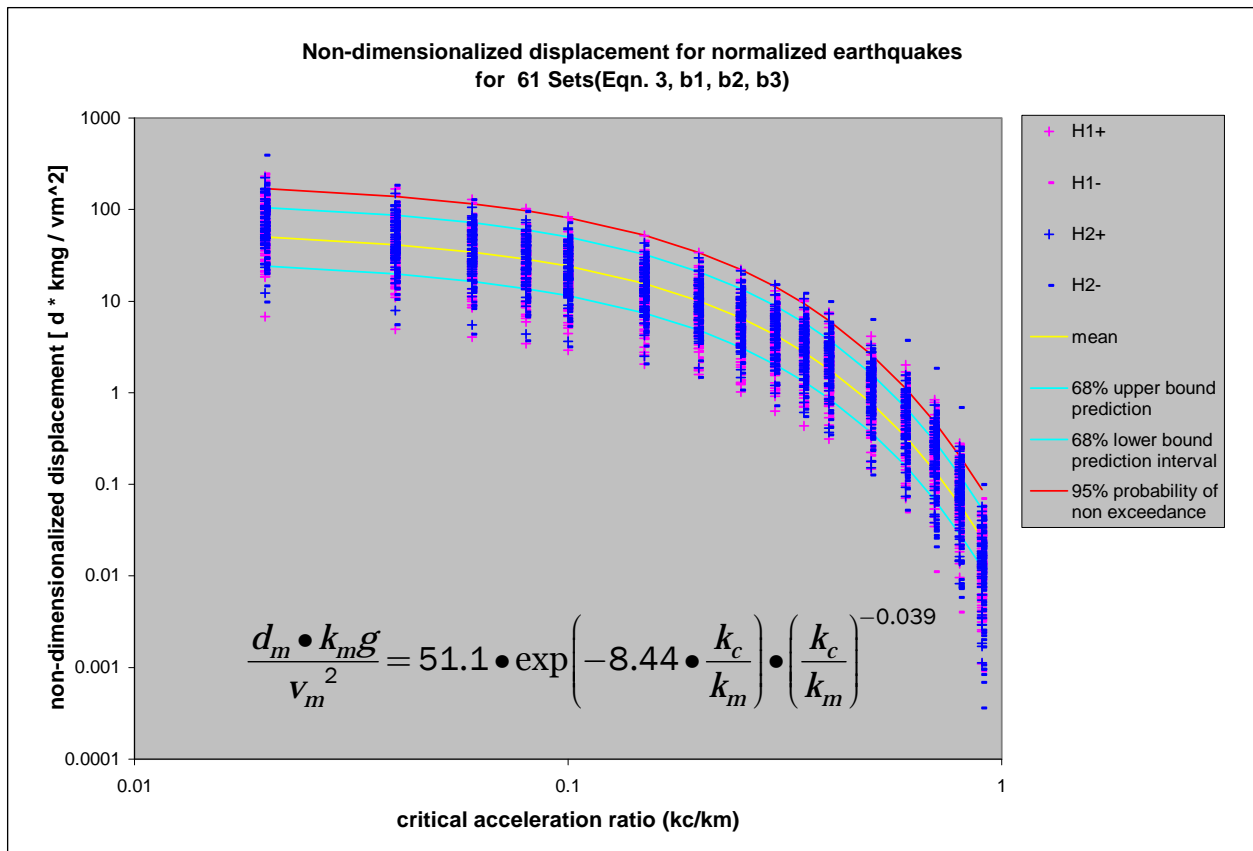


Figure 4.9. Non-dimensionalized displacements with the mean, 68 percent prediction intervals and 95 percent probability of non-exceedance curves.

By a second independent regression analysis, the mean standardized maximum displacement (d_s) in units of inches was derived for the standardized velocity, $v_s = 29.92$ in./sec (0.76 m/sec) and the standardized acceleration $k_s = 0.5 g$ (193.04 in./sec² : 4.90 m/sec²)

$$d_s = 236.9 \cdot \exp\left(-8.44 \cdot \frac{k_c}{k_m}\right) \cdot \left(\frac{k_c}{k_m}\right)^{-0.039} \quad (4.57)$$

The standardized maximum displacement (d_s) can be converted to the permanent displacement (d_m) by the following transformation,

$$d_m = d_s \cdot \left[\left(\frac{k_s}{v_s^2} \right) \cdot \left(\frac{v_m^2}{k_m} \right) \right] \quad (\text{bis 4.3})$$

where:

k_s = standardized acceleration expressed as a fraction of g (0.5)

v_s = standardized velocity (29.92 in./sec).

The mean permanent displacement is derived by introducing Equation 4.57 into Equation 4.3.

$$d_m = 236.9 \cdot \exp\left(-8.44 \cdot \frac{k_c}{k_m}\right) \cdot \left(\frac{k_c}{k_m}\right)^{-0.039} \cdot \left[0.216 \cdot \left(\frac{v_m^2}{k_m \cdot g} \right) \right] \quad (4.58)$$

where the right-hand-side term $k_m g$ is the peak (positive) rock acceleration expressed in units of length per sec².

Note that Equation 4.58 is the same as Equation 4.56, indicating consistent results from both regression analyses.

4.4.1.2 Ninety-five percent probability of non-exceedance

The regression analysis of the 61 sets of Magnitude 5 rock acceleration time histories resulted in the non-dimensionalized displacement for 95 percent probability of non-exceedance of

$$\frac{d_m \bullet k_m g}{v_m^2} = 51.1 \bullet \exp\left(-8.44 \bullet \frac{k_c}{k_m}\right) \bullet \left(\frac{k_c}{k_m}\right)^{-0.039} \bullet 3.39 \quad (4.59)$$

The 95 percent probability of non-exceedance is shown in red in Figure 4.9.

By the second, independent regression analysis, the standardized maximum displacement (d_s) in units of inches, derived using $v_s = 29.92$ in./sec and $k_s = 0.5$ g, is

$$d_s = 236.9 \bullet \exp\left(-8.44 \bullet \frac{k_c}{k_m}\right) \bullet \left(\frac{k_c}{k_m}\right)^{-0.039} \bullet 3.39 \quad (4.60)$$

Introducing Equation 4.3, the corresponding permanent displacement is

$$d_m = 236.9 \bullet \exp\left(-8.44 \bullet \frac{k_c}{k_m}\right) \bullet \left(\frac{k_c}{k_m}\right)^{-0.039} \bullet 3.39 \bullet \left[0.216 \bullet \left(\frac{v_m^2}{k_m \bullet g}\right)\right] \quad (4.61)$$

where the right-hand-side term $k_m g$ is the peak (positive) rock acceleration expressed in units of length per sec².

Note that Equation 4.61 is the same as Equation 4.59, indicating consistent results from both regression analyses.

4.4.1.3 Sixty-eight percent prediction intervals

The regression analysis of the 61 sets of Magnitude 5 rock acceleration time histories resulted in the non-dimensionalized displacement relationships for the 68 percent prediction intervals of

$$\frac{d_m \bullet k_m g}{v_m^2} = 51.1 \bullet \exp\left(-8.44 \bullet \frac{k_c}{k_m}\right) \bullet \left(\frac{k_c}{k_m}\right)^{-0.039} \bullet 2.10 \quad (4.62a)$$

$$\frac{d_m \bullet k_m g}{v_m^2} = 51.1 \bullet \exp\left(-8.44 \bullet \frac{k_c}{k_m}\right) \bullet \left(\frac{k_c}{k_m}\right)^{-0.039} \bullet 0.477 \quad (4.62b)$$

The 68 percent prediction intervals are shown in blue in Figure 4.9.

By the second independent regression analysis, the standardized maximum displacements (d_s) in units of inches, derived using $v_s = 29.92$ in./sec and $k_s = 0.5$ g, are

$$d_s = 236.9 \cdot \exp\left(-8.44 \cdot \frac{k_c}{k_m}\right) \cdot \left(\frac{k_c}{k_m}\right)^{-0.039} \cdot 2.10 \quad (4.63a)$$

$$d_s = 236.9 \cdot \exp\left(-8.44 \cdot \frac{k_c}{k_m}\right) \cdot \left(\frac{k_c}{k_m}\right)^{-0.039} \cdot 0.477 \quad (4.63b)$$

Introducing Equation 4.3, the corresponding permanent displacements are

$$d_m = 236.9 \cdot \exp\left(-8.44 \cdot \frac{k_c}{k_m}\right) \cdot \left(\frac{k_c}{k_m}\right)^{-0.039} \cdot 2.10 \cdot \left[0.216 \cdot \left(\frac{v_m^2}{k_m \cdot g}\right)\right] \quad (4.64a)$$

$$d_m = 236.9 \cdot \exp\left(-8.44 \cdot \frac{k_c}{k_m}\right) \cdot \left(\frac{k_c}{k_m}\right)^{-0.039} \cdot 0.477 \cdot \left[0.216 \cdot \left(\frac{v_m^2}{k_m \cdot g}\right)\right] \quad (4.64b)$$

where the right-hand-side term $k_m g$ is the peak (positive) rock acceleration expressed in units of length per sec²

Note that Equations 4.64a and 4.64b are the same as Equations 4.62a and 4.62b, indicating consistent results from both regression analyses.

4.4.2 Two-term regression results, linear in natural logarithm transformation

The standard error term (*Std. error*) for this regression analysis was determined to be 0.74 for both the non-dimensionalized displacement as well as the standardized displacement for earthquakes of Magnitude 5. This non-dimensionalized two-term displacement equation is identified as Equation Form Two with the coefficients and *Std. error* terms summarized in column three of Table 4.8.

4.4.2.1 Mean relationships

The regression analysis of the 61 sets of Magnitude 5 rock acceleration time histories resulted in the mean non-dimensionalized displacement relationship of

$$\frac{d_m \cdot k_m g}{v_m^2} = 57.0 \cdot \exp\left(-8.58 \cdot \frac{k_c}{k_m}\right) \quad (4.65)$$

where:

- d_m = permanent displacement
- $k_m g$ = peak (positive) rock acceleration expressed in units of length per sec², consistent with units of d_m (length) and v_m (length per sec)
- v_m = peak (positive) ground velocity of the earthquake
- k_c = critical acceleration expressed as a fraction of g
- k_m = peak (positive) rock acceleration expressed as a fraction of g .

This mean relationship is shown in yellow in Figure 4.10.

By a second independent regression analysis, the mean standardized maximum displacement (d_s) in units of inches was derived for the standardized velocity, $v_s = 29.92$ in./sec (0.76 m/sec) and the standardized acceleration $k_s = 0.5 g$ (193.04 in./sec² : 4.90 m/sec²)

$$d_s = 264.3 \cdot \exp\left(-8.58 \cdot \frac{k_c}{k_m}\right) \quad (4.66)$$

The standardized maximum displacement (d_s) can be converted to the permanent displacement (d_m) by the following transformation,

$$d_m = d_s \cdot \left[\left(\frac{k_s}{v_s^2} \right) \cdot \left(\frac{v_m^2}{k_m} \right) \right] \quad (\text{bis 4.3})$$

where:

- k_s = standardized acceleration expressed as a fraction of g (0.5)
- v_s = standardized velocity (29.92 in./sec).

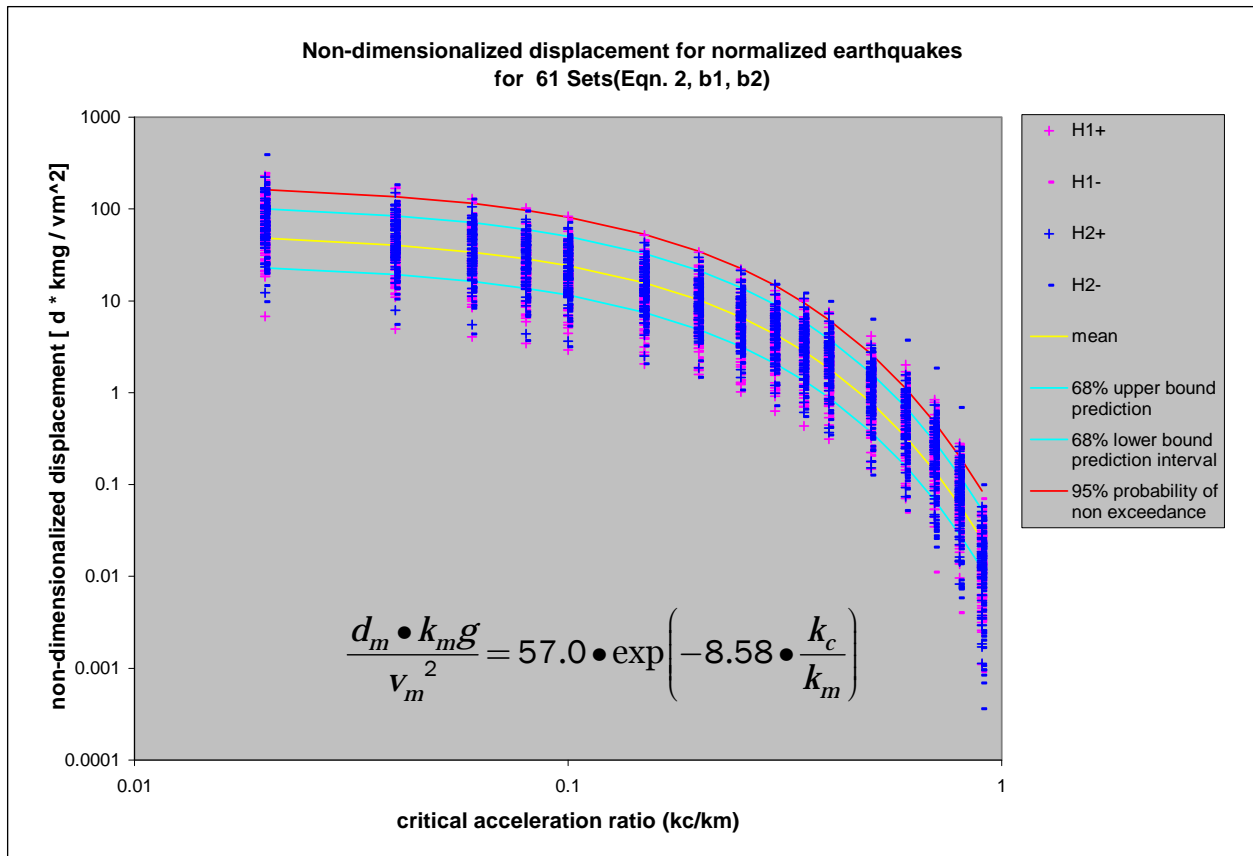


Figure 4.10. Non-dimensionalized displacements with the mean, 68 percent prediction intervals and 95 percent probability of non-exceedance curves.

The mean permanent displacement is derived by introducing Equation 4.66 into Equation 4.3.

$$d_m = 264.3 \cdot \exp\left(-8.58 \cdot \frac{k_c}{k_m}\right) \cdot \left[0.216 \cdot \left(\frac{v_m^2}{k_m \cdot g}\right)\right] \quad (4.67)$$

where the right-hand-side term $k_m g$ is the peak (positive) rock acceleration expressed in units of length per sec².

Note that Equation 4.67 is the same as Equation 4.65, indicating consistent results from both regression analyses.

4.4.2.2 Ninety-five percent probability of non-exceedance

The regression analysis of the 61 sets of Magnitude 5 rock acceleration time histories resulted in the non-dimensionalized displacement for 95 percent probability of non-exceedance of

$$\frac{d_m \bullet k_m g}{v_m^2} = 57.0 \bullet \exp\left(-8.58 \bullet \frac{k_c}{k_m}\right) \bullet 3.39 \quad (4.68)$$

The 95 percent probability of non-exceedance is shown in red in Figure 4.10.

By the second, independent regression analysis, the standardized maximum displacement (d_s) in units of inches, derived using $v_s = 29.92$ in./sec and $k_s = 0.5 g$, is

$$d_s = 264.3 \bullet \exp\left(-8.58 \bullet \frac{k_c}{k_m}\right) \bullet 3.39 \quad (4.69)$$

Introducing Equation 4.3, the corresponding permanent displacement is

$$d_m = 264.3 \bullet \exp\left(-8.58 \bullet \frac{k_c}{k_m}\right) \bullet 3.39 \bullet \left[0.216 \bullet \left(\frac{v_m^2}{k_m \bullet g}\right)\right] \quad (4.70)$$

where the right-hand-side term $k_m g$ is the peak (positive) rock acceleration expressed in units of length per sec².

Note that Equation 4.70 is the same as Equation 4.68, indicating consistent results from both regression analyses.

4.4.2.3 Sixty-eight percent prediction intervals

The regression analysis of the 61 sets of Magnitude 5 rock acceleration time histories resulted in the non-dimensionalized displacement relationships for the 68 percent prediction intervals of

$$\frac{d_m \bullet k_m g}{v_m^2} = 57.0 \bullet \exp\left(-8.58 \bullet \frac{k_c}{k_m}\right) \bullet 2.10 \quad (4.71a)$$

$$\frac{d_m \bullet k_m g}{v_m^2} = 57.0 \bullet \exp\left(-8.58 \bullet \frac{k_c}{k_m}\right) \bullet 0.477 \quad (4.71b)$$

The 68 percent prediction intervals are shown in blue in Figure 4.10.

By the second independent regression analysis, the standardized maximum displacements (d_s) in units of inches, derived using $v_s = 29.92$ in./sec and $k_s = 0.5$ g, are

$$d_s = 264.3 \cdot \exp\left(-8.58 \cdot \frac{k_c}{k_m}\right) \cdot 2.10 \quad (4.72a)$$

$$d_s = 264.3 \cdot \exp\left(-8.58 \cdot \frac{k_c}{k_m}\right) \cdot 0.477 \quad (4.72b)$$

Introducing Equation 4.3, the corresponding permanent displacements are

$$d_m = 264.3 \cdot \exp\left(-8.58 \cdot \frac{k_c}{k_m}\right) \cdot 2.10 \cdot \left[0.216 \cdot \left(\frac{v_m^2}{k_m \cdot g}\right)\right] \quad (4.73a)$$

$$d_m = 264.3 \cdot \exp\left(-8.58 \cdot \frac{k_c}{k_m}\right) \cdot 0.477 \cdot \left[0.216 \cdot \left(\frac{v_m^2}{k_m \cdot g}\right)\right] \quad (4.73b)$$

where the right-hand-side term $k_m g$ is the peak (positive) rock acceleration expressed in units of length per sec².

Note that Equations 4.73a and 4.73b are the same as Equations 4.71a and 4.71b, indicating consistent results from both regression analyses.

4.4.3 Two-term regression results, linear in common logarithm transformation

The standard error term (*Std. error*) for this regression analysis was determined to be 1.24 for both the non-dimensionalized displacement as well as the standardized displacement for earthquakes of Magnitude 5. This non-dimensionalized two-term displacement equation is identified as Equation Form One with the coefficients and *Std. error* terms summarized in column two of Table 4.8.

4.4.3.1 Mean relationships

The regression analysis of the 61 sets of Magnitude 5 rock acceleration time histories resulted in the mean non-dimensionalized displacement relationship of

$$\frac{d_m \bullet k_m g}{v_m^2} = 0.153 \bullet \left(\frac{k_c}{k_m} \right)^{-1.94} \quad (4.74)$$

where:

- d_m = permanent displacement
- $k_m g$ = peak (positive) rock acceleration expressed in units of length per sec², consistent with units of d_m (length) and v_m (length per sec)
- v_m = peak (positive) ground velocity of the earthquake
- k_c = critical acceleration expressed as a fraction of g
- k_m = peak (positive) rock acceleration expressed as a fraction of g .

This mean relationship is shown in yellow in Figure 4.11.

By a second independent regression analysis, the mean standardized maximum displacement (d_s) in units of inches was derived for the standardized velocity, $v_s = 29.92$ in./sec (0.76 m/sec) and the standardized acceleration $k_s = 0.5 g$ (193.04 in./sec² : 4.90 m/sec²)

$$d_s = 0.71 \bullet \left(\frac{k_c}{k_m} \right)^{-1.94} \quad (4.75)$$

The standardized maximum displacement (d_s) can be converted to the permanent displacement (d_m) by the following transformation,

$$d_m = d_s \bullet \left[\left(\frac{k_s}{v_s^2} \right) \bullet \left(\frac{v_m^2}{k_m} \right) \right] \quad (\text{bis } 4.3)$$

where:

- k_s = standardized acceleration expressed as a fraction of g (0.5)
- v_s = standardized velocity (29.92 in./sec).

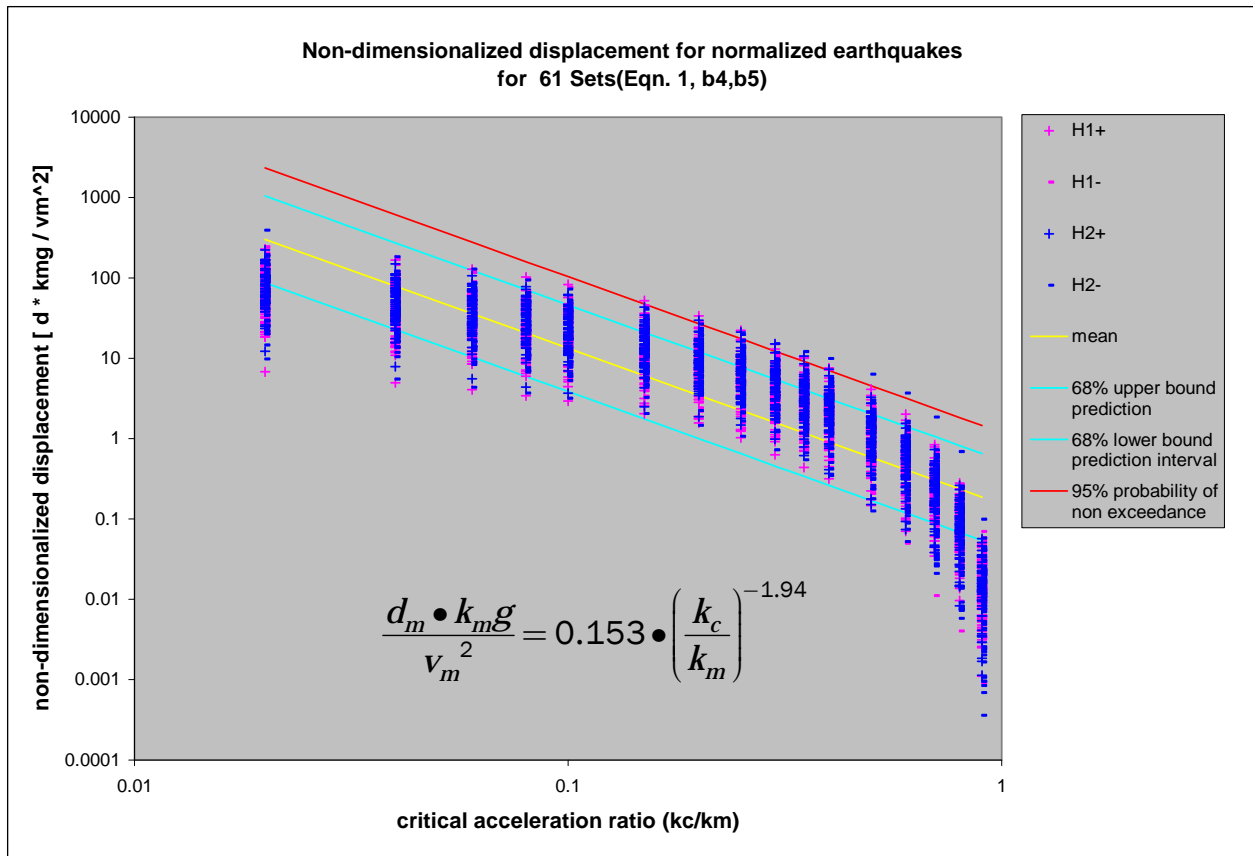


Figure 4.11. Non-dimensionalized displacements with the mean, 68 percent prediction intervals and 95 percent probability of non-exceedance curves.

The mean permanent displacement is derived by introducing Equation 4.74 into Equation 4.3.

$$d_m = 0.71 \cdot \left(\frac{k_c}{k_m} \right)^{-1.94} \cdot \left[0.216 \cdot \left(\frac{v_m^2}{k_m \cdot g} \right) \right] \tag{4.76}$$

where the right-hand-side term $k_m g$ is the peak (positive) rock acceleration expressed in units of length per sec².

Note that Equation 4.76 is the same as Equation 4.74, indicating consistent results from both regression analyses.

4.4.3.2 Ninety-five percent probability of non-exceedance

The regression analysis of the 61 sets of Magnitude 5 rock acceleration time histories resulted in the non-dimensionalized displacement for 95 percent probability of non-exceedance of

$$\frac{d_m \bullet k_m g}{v_m^2} = 0.153 \bullet \left(\frac{k_c}{k_m} \right)^{-1.94} \bullet 2.44 \quad (4.77)$$

The 95 percent probability of non-exceedance is shown in red in Figure 4.11.

By the second independent regression analysis, the standardized maximum displacement (d_s) in units of inches, derived using $v_s = 29.92$ in./sec and $k_s = 0.5$ g, is

$$d_s = 0.71 \bullet \left(\frac{k_c}{k_m} \right)^{-1.94} \bullet 2.44 \quad (4.78)$$

Introducing Equation 4.3, the corresponding permanent displacement is

$$d_m = 0.71 \bullet \left(\frac{k_c}{k_m} \right)^{-1.94} \bullet 2.44 \bullet \left[0.216 \bullet \left(\frac{v_m^2}{k_m \bullet g} \right) \right] \quad (4.79)$$

where the right-hand-side term $k_m g$ is the peak (positive) rock acceleration expressed in units of length per sec².

Note that Equation 4.79 is the same as Equation 4.77, indicating consistent results from both regression analyses.

4.4.3.3 Sixty-eight percent prediction intervals

The regression analysis of the 61 sets of Magnitude 5 rock acceleration time histories resulted in the non-dimensionalized displacement relationships for the 68 percent prediction intervals of

$$\frac{d_m \bullet k_m g}{v_m^2} = 0.153 \bullet \left(\frac{k_c}{k_m} \right)^{-1.94} \bullet 1.72 \quad (4.80a)$$

$$\frac{d_m \bullet k_m g}{v_m^2} = 0.153 \bullet \left(\frac{k_c}{k_m} \right)^{-1.94} \bullet 0.583 \quad (4.80b)$$

The 68 percent prediction intervals are shown in blue in Figure 4.11.

By the second independent regression analysis, the standardized maximum displacements (d_s) in units of inches, derived using $v_s = 29.92$ in./sec and $k_s = 0.5 g$, are

$$d_s = 0.71 \cdot \left(\frac{k_c}{k_m} \right)^{-1.94} \cdot 1.72 \quad (4.81a)$$

$$d_s = 0.71 \cdot \left(\frac{k_c}{k_m} \right)^{-1.94} \cdot 0.583 \quad (4.81b)$$

Introducing Equation 4.3, the corresponding permanent displacements are,

$$d_m = 0.71 \cdot \left(\frac{k_c}{k_m} \right)^{-1.94} \cdot 1.72 \cdot \left[0.216 \cdot \left(\frac{v_m^2}{k_m \cdot g} \right) \right] \quad (4.82a)$$

$$d_m = 0.71 \cdot \left(\frac{k_c}{k_m} \right)^{-1.94} \cdot 0.583 \cdot \left[0.216 \cdot \left(\frac{v_m^2}{k_m \cdot g} \right) \right] \quad (4.82b)$$

where the right-hand-side term $k_m g$ is the peak (positive) rock acceleration expressed in units of length per sec².

Note that Equations 4.82a and 4.82b are the same as Equations 4.80a and 4.80b, indicating consistent results from both regression analyses.

4.4.4 Comparison of regression results of all three forms of the simplified non-dimensionalized displacement relationships.

The three forms of regression analysis (discussed in Sections 4.4.1, 4.4.2, and 4.4.3), namely, the three-term regression analysis (identified as eqn3 in Figure 4.12), the two-term, linear in Natural Logarithm Transformation (eqn2 in Figure 4.12) and the two-term, linear in common logarithm transformation (eqn1 in Figure 4.12) will have their results compared and evaluated.

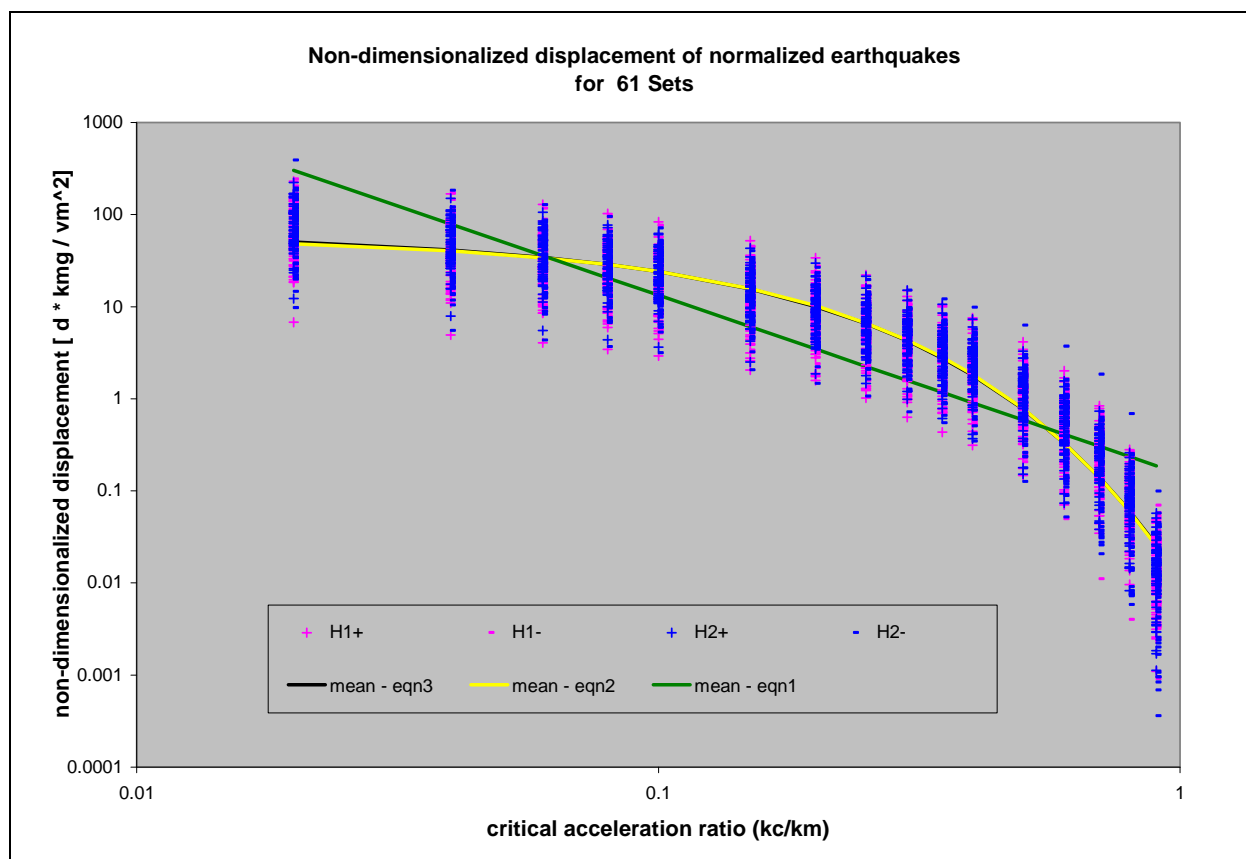


Figure 4.12. Non-dimensionalized displacements and comparisons of the means of the three regression analysis equations for Magnitude 5 earthquakes.

One method of comparison will be the *Std. error* term determined from the error in the estimates. The *Std. error* for eqn3 is 0.74, for eqn2, 0.74 and for eqn1, equal to 1.24 when transformed to a natural logarithm from a common logarithm standard error value of 0.54. These results show that eqn3 and eqn2 have a more accurate estimate as compared to eqn1, and that eqn3 and eqn2 have practically equal values.

Another comparison is the mean relationships as illustrated in Figure 4.12. As can be seen, eqn2 and eqn3 follow the shape of the data and are positioned at the center of the data points while eqn1 does not. Note also that the mean curves of eqn2 and eqn3 are almost superimposing each other, which show the similarity of the results.

Lastly, given the small value of the exponent for the (k_c/k_m) term of eqn3 (-0.039), this explains the comparable results of eqn2 and eqn3.

4.5 Special regression results of Equation Form Two of non-dimensionalized displacement relationships without differentiation of Moment Magnitude

This subsequent section will discuss the results from regression analyses of the non-dimensionalized displacement relationships described by Equation 3.39, previously derived in Chapter 3. The values for the coefficients summarized by the above-mentioned equation and the standard error terms as well as the probabilistic measures of Equation Form Two are documented in Table 4.9 and will be discussed in Sections 4.5.1, 4.5.2, and 4.5.3. The regression analysis was performed for baseline corrected acceleration time histories recorded on rock with M_w range of 4.9 to 8.1.

Table 4.9. Values for the regression Equation Form Two constants without differentiation of M_w .

Coefficients and <i>Std. Error</i>	Equation Form Two
β_1	64.439
β_2	-8.862
β_3	
β_4	
β_5	
<i>Std. Error</i>	0.800

The standard error term (*Std. error*) for this regression analysis was determined to be 0.80 for both the non-dimensionalized displacement as well as the standardized displacement. This non-dimensionalized two-term displacement equation is identified as Equation Form Two with the coefficients and *Std. error* terms summarized in column two of Table 4.9.

4.5.1. Mean relationships

The regression analysis of the 122 sets of Magnitude 5 – 7 rock acceleration time histories resulted in the mean non-dimensionalized displacement relationship of

$$\frac{d_m \bullet k_m g}{v_m^2} = 65.44 \bullet \exp\left(-8.86 \bullet \frac{k_c}{k_m}\right) \quad (4.83)$$

where:

- d_m = permanent displacement
- $k_m g$ = peak (positive) rock acceleration expressed in units of length per sec², consistent with units of d_m (length) and v_m (length per sec)
- v_m = peak (positive) ground velocity of the earthquake

k_c = critical acceleration expressed as a fraction of g
 k_m = peak (positive) rock acceleration expressed as a fraction of g .

This mean relationship is shown in yellow in Figure 4.13.

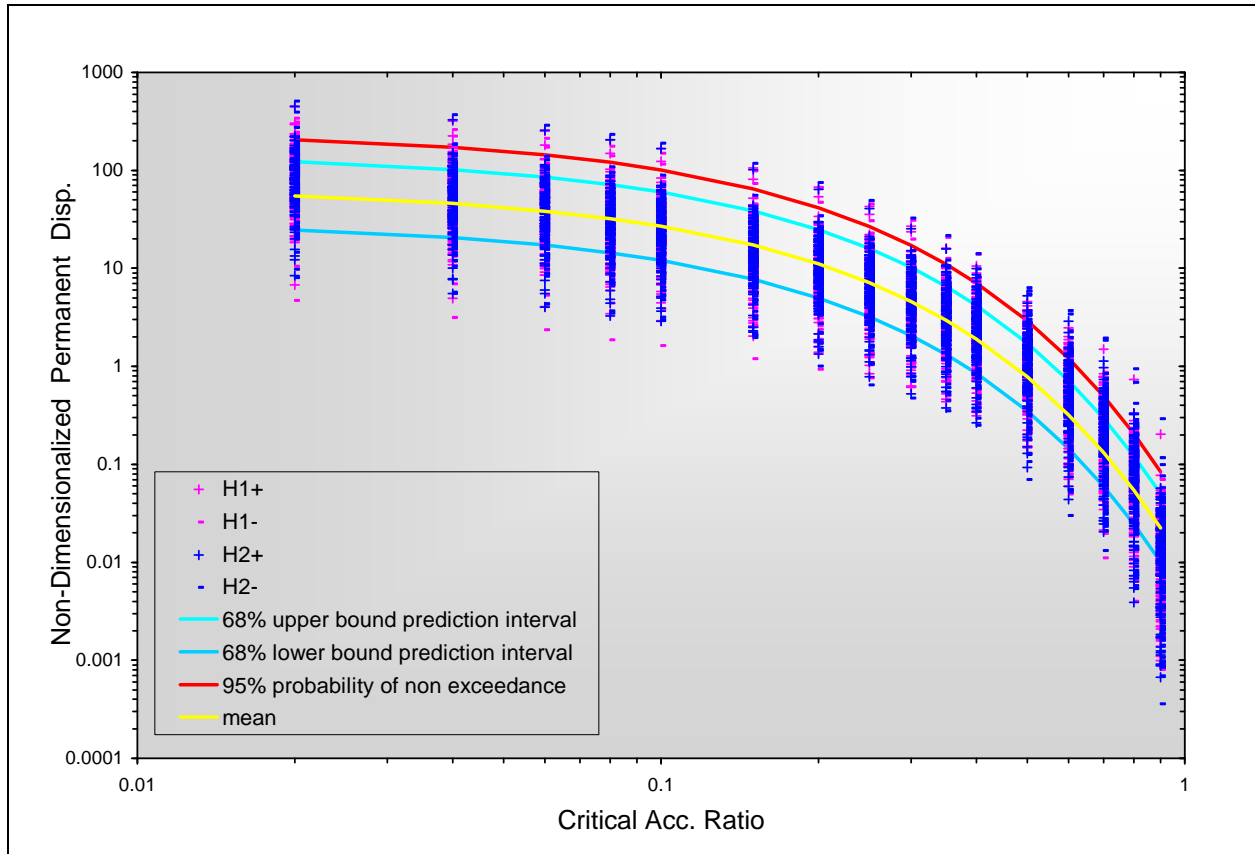


Figure 4.13. Non-dimensionalized displacements for normalized earthquakes without differentiation of Moment Magnitude (Equation Form Two).

By a second independent regression analysis, the mean standardized maximum displacement (d_s) in units of inches was derived for the standardized velocity, $v_s = 29.92$ in./sec (0.76 m/sec) and the standardized acceleration $k_s = 0.5 g$ (193.04 in./sec² : 4.90 m/sec²).

$$d_s = 303.484 \cdot \exp\left(-8.862 \cdot \frac{k_c}{k_m}\right) \tag{4.84}$$

The standardized maximum displacement (d_s) can be converted to the permanent displacement (d_m) by the following transformation,

$$d_m = d_s \cdot \left[\left(\frac{k_s}{v_s^2} \right) \cdot \left(\frac{v_m^2}{k_m} \right) \right] \quad (\text{bis 4.3})$$

where:

k_s = standardized acceleration expressed as a fraction of g (0.5)

v_s = standardized velocity (29.92 in./sec).

The mean permanent displacement is derived by introducing Equation 4.66 into Equation 4.3.

$$d_m = 303.484 \cdot \exp \left(-8.862 \cdot \frac{k_c}{k_m} \right) \cdot \left[0.216 \cdot \left(\frac{v_m^2}{k_m \cdot g} \right) \right] \quad (4.86)$$

where the right-hand-side term $k_m g$ is the peak (positive) rock acceleration expressed in units of length per sec².

Note that Equation 4.83 is the approximately the same as Equation 4.86, indicating consistent results from both regression analyses.

4.5.2 Ninety-five percent probability of non-exceedance

The regression analysis of the 122 sets of M_w 5 to 7 rock acceleration time histories resulted in the non-dimensionalized displacement for 95 percent probability of non-exceedance of

$$\frac{d_m \cdot k_m g}{v_m^2} = 65.44 \cdot \exp \left(-8.86 \cdot \frac{k_c}{k_m} \right) \cdot 3.75 \quad (4.87)$$

The 95 percent probability of non-exceedance is shown in red in Figure 4.13.

By the second, independent regression analysis, the standardized maximum displacement (d_s) in units of inches, derived using $v_s = 29.92$ in./sec and $k_s = 0.5 g$, is

$$d_s = 303.484 \cdot \exp \left(-8.86 \cdot \frac{k_c}{k_m} \right) \cdot 3.75 \quad (4.88)$$

Introducing Equation 4.3, the corresponding permanent displacement is

$$d_m = 303.484 \bullet \exp\left(-8.86 \bullet \frac{k_c}{k_m}\right) \bullet 3.75 \bullet \left[0.216 \bullet \left(\frac{v_m^2}{k_m \bullet g}\right)\right] \quad (4.89)$$

where the right-hand-side term $k_m g$ is the peak (positive) rock acceleration expressed in units of length per sec².

Note that Equation 4.89 is the approximately the same as Equation 4.87, indicating consistent results from both regression analyses.

4.5.3 Sixty-eight percent prediction intervals

The regression analysis of the 122 sets of Magnitude 5 - 7 rock acceleration time histories resulted in the non-dimensionalized displacement relationships for the 68 percent prediction intervals of

$$\frac{d_m \bullet k_m g}{v_m^2} = 65.44 \bullet \exp\left(-8.86 \bullet \frac{k_c}{k_m}\right) \bullet 2.23 \quad (4.90a)$$

$$\frac{d_m \bullet k_m g}{v_m^2} = 65.44 \bullet \exp\left(-8.86 \bullet \frac{k_c}{k_m}\right) \bullet 0.449 \quad (4.90b)$$

The 68 percent prediction intervals are shown in blue in Figure 4.13.

By the second independent regression analysis, the standardized maximum displacements (d_s) in units of inches, derived using $v_s = 29.92$ in./sec and $k_s = 0.5 g$, are

$$d_s = 303.484 \bullet \exp\left(-8.86 \bullet \frac{k_c}{k_m}\right) \bullet 2.23 \quad (4.91a)$$

$$d_s = 303.484 \bullet \exp\left(-8.86 \bullet \frac{k_c}{k_m}\right) \bullet 0.449 \quad (4.91b)$$

Introducing Equation 4.3, the corresponding permanent displacements are

$$d_m = 303.484 \cdot \exp\left(-8.86 \cdot \frac{k_c}{k_m}\right) \cdot 2.23 \cdot \left[0.216 \cdot \left(\frac{v_m^2}{k_m \cdot g}\right)\right] \quad (4.92a)$$

$$d_m = 303.484 \cdot \exp\left(-8.86 \cdot \frac{k_c}{k_m}\right) \cdot 0.449 \cdot \left[0.216 \cdot \left(\frac{v_m^2}{k_m \cdot g}\right)\right] \quad (4.92b)$$

where the right-hand-side term $k_m g$ is the peak (positive) rock acceleration expressed in units of length per sec².

Note that Equations 4.92a and 4.92b are approximately the same as Equations 4.90a and 4.90b, indicating consistent results from both regression analyses.

5 The Visual Modeler for Newmark – Newmark_{VM}

5.1 Introduction

This chapter provides guidance on the details of the Visual Modeler (Newmark_{VM}), the PC-based Graphical User Interface (GUI) to the program named Newmark. Newmark_{VM} gathers the necessary user specified information and provides a simple and expedient means of interpreting the results from a Newmark analysis (by executing Newmark, the FORTRAN engineering formulation discussed in Chapter 2). There will be discussions on how to perform and interpret the results of an analysis.

5.2 The Visual Modeling Environment

Newmark is a program that can perform a permanent sliding block displacement analysis given a baseline corrected rock site-specific acceleration time-history. Newmark can also conduct regression analyses for sets of rock founded acceleration time histories in order to develop up to three user selected forms of generalized equations of simplified permanent displacement relationships. The user has the option of performing one of two types of translational (i.e. sliding) analysis, either a single or deterministic analysis, or a multiple analysis that can include regression analyses.

At the onset of Newmark_{VM}, the user is automatically introduced to a graphical image representing the results obtained from a typical regression analysis computed by Newmark. In this case, evaluation of 122 sets of (rock) acceleration time histories ranging from earthquake magnitudes of 5 thru 7 were used for the multiple analyses. This image is included in the **Introduction** tab and shown in Figure 5.1. Directly above this tab are two drop down menus. The first, entitled **File**, provides an easy and convenient way to open an existing file, create a new file or save existing data to a file. These files are user created and have an “.nmk” extension. Opening an existing file will immediately replenish the data within all tabs and thereby allow the user to quickly run an analysis from previous data input. The second drop down menu above the **Introduction** tab is labeled **Analysis Type**; here the user is given the option to select the scenario of either a single analysis or multiple analyses that may apply regression.

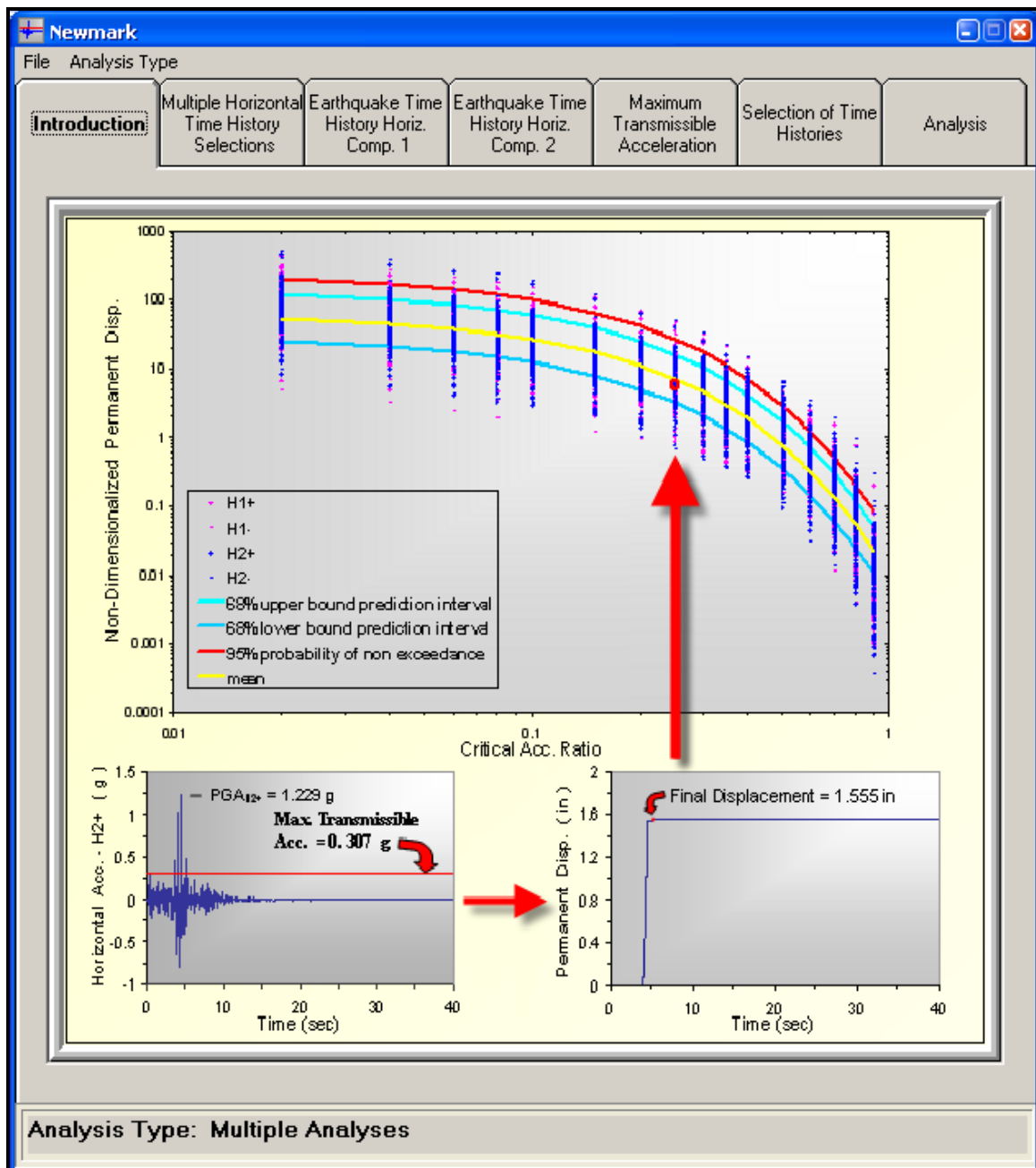


Figure 5.1. The **Introduction** tab features the process of a multiple analysis.

5.2.1 Significant Tabs relevant to an analysis

With a single analysis, the input data to Newmark falls into three different groups and Newmark_{VM} displays these groups with the following tabs available for user input

- Earthquake Time-History Horizontal Component 1 data
- Maximum Transmissible Acceleration values

- Analysis of specified data

Input data for a multiple or regression analyses falls into six different groups and the Newmark_{VM} displays these groups as tabs and available for user input

- Multiple Horizontal Time-History Selections menu
- Earthquake Time-History Horizontal Component 1 data
- Earthquake Time-History Horizontal Component 2 data
- Maximum Transmissible Acceleration values
- Selection of Time Histories for analysis
- Analysis of specified data

In order to perform multiple analyses, it is required that we consider only sets of acceleration time histories. A set is made up of two site-specific acceleration time-history files; each representing a horizontal component. If only one component is available for one or more sets of time histories, Newmark will acknowledge this fact and perform the analyses with the available time histories.

The following subsections of Section 5.2 are listed in the order as shown in the Newmark_{VM} tabs. Each subsection describes the function of each tab and identifies whether each tab relates to a single analysis, multiple analyses or both.

5.2.2 Multiple Horizontal Time-History Selections (Multiple Analyses only)

The function of this tab relates to the collection of sets of base-line corrected acceleration time histories as input and consists mainly of file handling. Figure 5.2 shows the many options necessary for the creation of a list of filenames relating to acceleration time histories for an analysis.

The user data entry within this tab will be described in a top-down manner. Data within this tab can be divided into subgroups and is described in the following two sections.

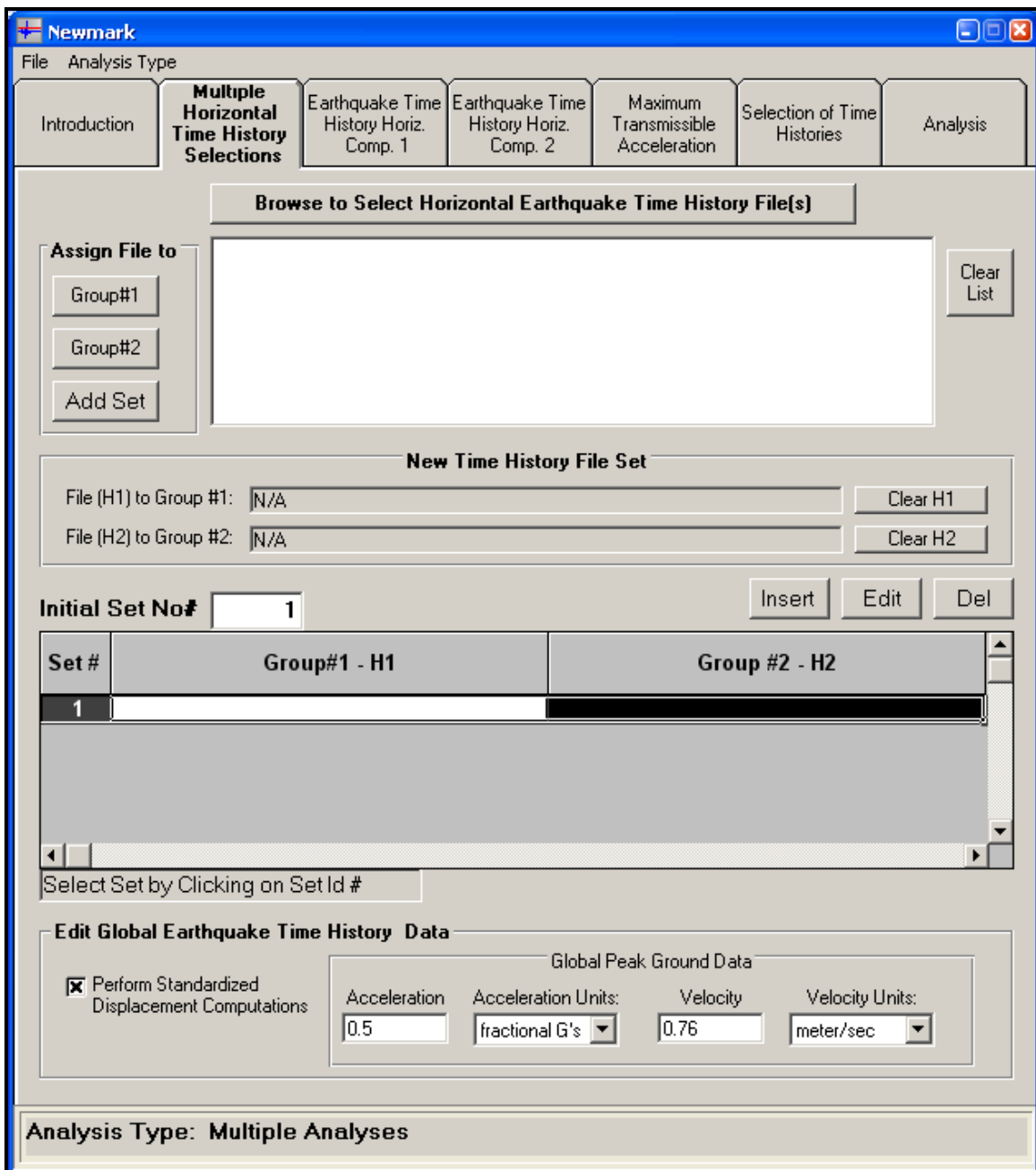


Figure 5.2. The **Multiple Horizontal Time-History Selections** tab ready for user input.

5.2.2.1 Selection of Horizontal Earthquake Time-History Files

The **Browse to Select Horizontal Earthquake Time-History File(s)** allows the user to gather all relative acceleration time-history files necessary for computing multiple analyses. Once selected, a file management screen will appear for the user to choose all relevant files. The pull-down menu on the left of the screen (Figure 5.3) gives the path (i.e., drive and directory) to the location of the files. The large center box shows a list

of files contained within the selected directory. The **Copy Selected** button at the right allows the selection of any or all files in the center box. If the user decides to start over or clear the list of files in the center box, the **Clear List** button on the upper right of the previous menu (Figure 5.2) is an option used to remove the selected files. Finally, when the user is satisfied with all files, the **OK** button is accepted and the original screen of Section 5.2.2 will appear with the list of all selected files.

From the list of previously selected acceleration time-history files, the user can start matching the sets, i.e. the horizontal components of these earthquake time histories need to belong to the same set. It is important to correctly pick the files that pertain to horizontal component 1 (group 1) and the files for horizontal component 2 (group 2). This is accomplished by the **Assign File to** frame or container located to the left in Figure 5.2 which contains 3 buttons. To select a set, use the following steps

1. Choose a file for group 1, by selecting the file listed in the center box and then pressing the **Group#1** button
2. This file will appear in the **File (H1) to Group #1:** box within the **New Time-History File Set** frame
3. If file in step 2 is incorrect, select **Clear H1** and start over with step 1
4. Choose a file for group 2, by selecting the file listed in the center box and then pressing the **Group#2** button
5. This group 2 file will appear in the **File (H1) to Group #2:** box within the **New Time-History File Set** frame
6. If file in step 5 is incorrect, select **Clear H2** and start over with step 4 for selection of group 2 files.
7. Select the **Add Set** button located in the **Assign File to** frame to create the set

Note: If there is no file pertaining to either group 1 or group 2, the user can take the default of **N/A** found within the **New Time-History File Set** frame.

After selecting the **Add Set** button, the new set will be added to a scroll-down list with a gray background, and each file will be located within its respective group number.

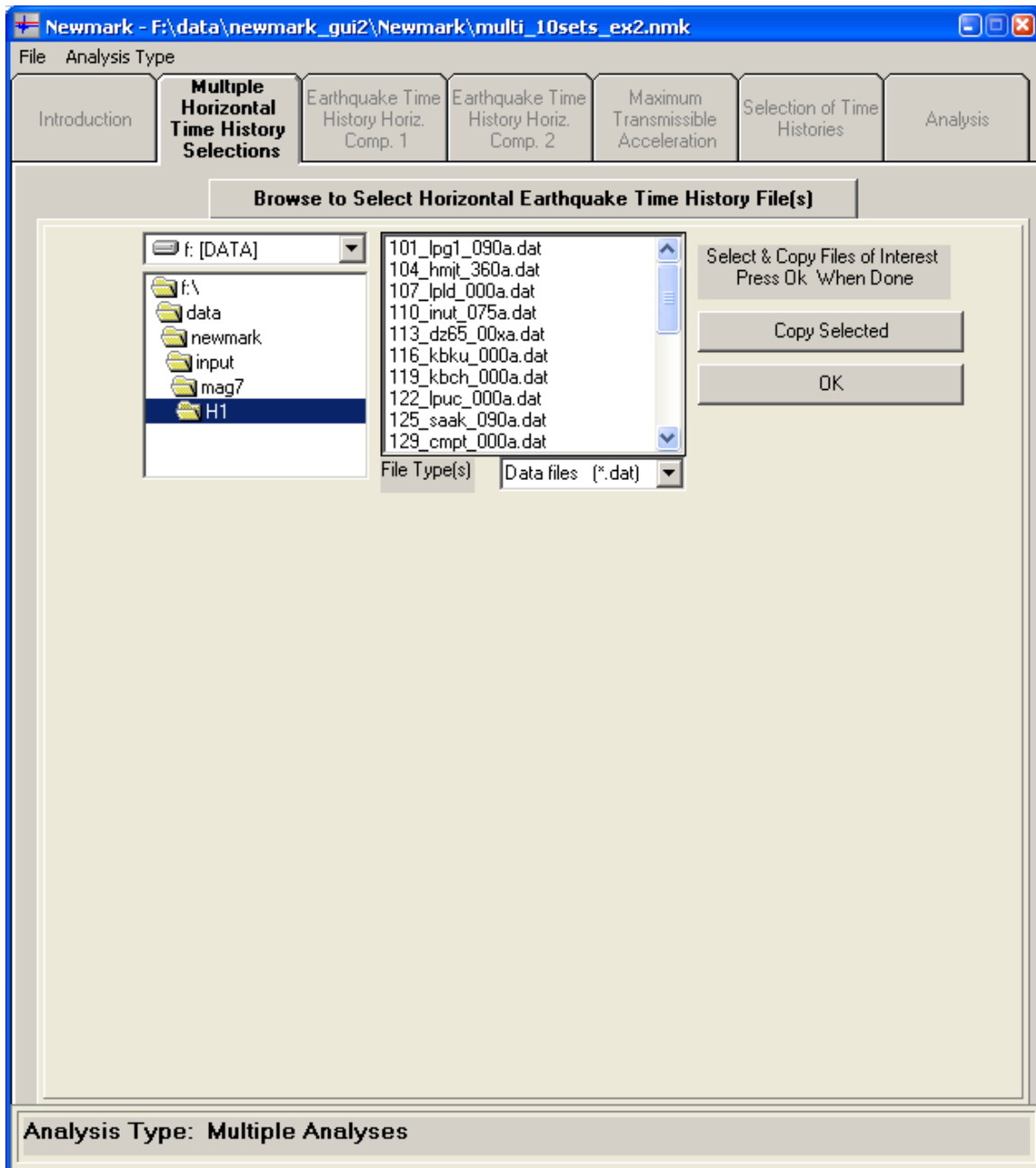


Figure 5.3. Selection of horizontal time-history files.

The first set is given a set number of 1 or the value of the **Initial Set No#** box. The addition of more sets will require the user to go over the above seven steps for each set. As a useful means for the management of these sets, buttons are included for inserting, editing and deleting sets.

The **Initial Set No#** box located above the gray scroll-down list allows the user to enter the set number of interest. This feature will automatically place that particular set at the top of the list.

5.2.2.2 Standardized Displacement Computations

At the lower portion of the **Multiple Horizontal Time-History Selections** tab is an option to perform standardized displacement computations. The global peak ground acceleration with its units and the peak velocity with its units can be provided as input. With the selection of this option, the resultant analysis will include the standardized displacement computations.

5.2.3 Earthquake Time-History Horizontal Component 1 and 2 input (Single Analysis or Multiple Analyses)

Both horizontal component 1 and horizontal component 2 time-history input follow the same input pattern. First an appropriate, base-line corrected acceleration time-history data file is selected for the Corps project by the user. Given the non-standardized nature of earthquake time-history data files, certain attributes need to be specified to correctly read the input (ASCII) data file. These attributes are entered in the Format section of the Earthquake Time-History (EQTH) tabs – Horizontal Comp. 1 and Horizontal Comp. 2. This is an exceptionally powerful tool for handling multiple format EQTH files. Figure 5.4 shows the horizontal component 1 earthquake time-history tab.

To work with the appropriate EQTH data file, the user must first specify a file to be read in. The user can type a specific filename or select a file using the **Find** button that exists on the **Earthquake Time-History Horz Comp. 1** tab in a single analysis case.

For multiple analyses there will be a dropdown menu next to the file name that allows the user to select which file to work with. The listed files can also be found in the gray shaded area within the **Multiple Horizontal Time-History Selections** tab. These time histories will be listed in Group#1 or Group#2 depending on whether the user is currently working in the **Earthquake Time Horz Comp. 1** or **Earthquake Time-History Horz Comp. 2** tabs. When working with the **Set #** combo box, located at the top right of the tab, the user can either enter the set number of interest or use the arrow buttons to increase/decrease the set number.

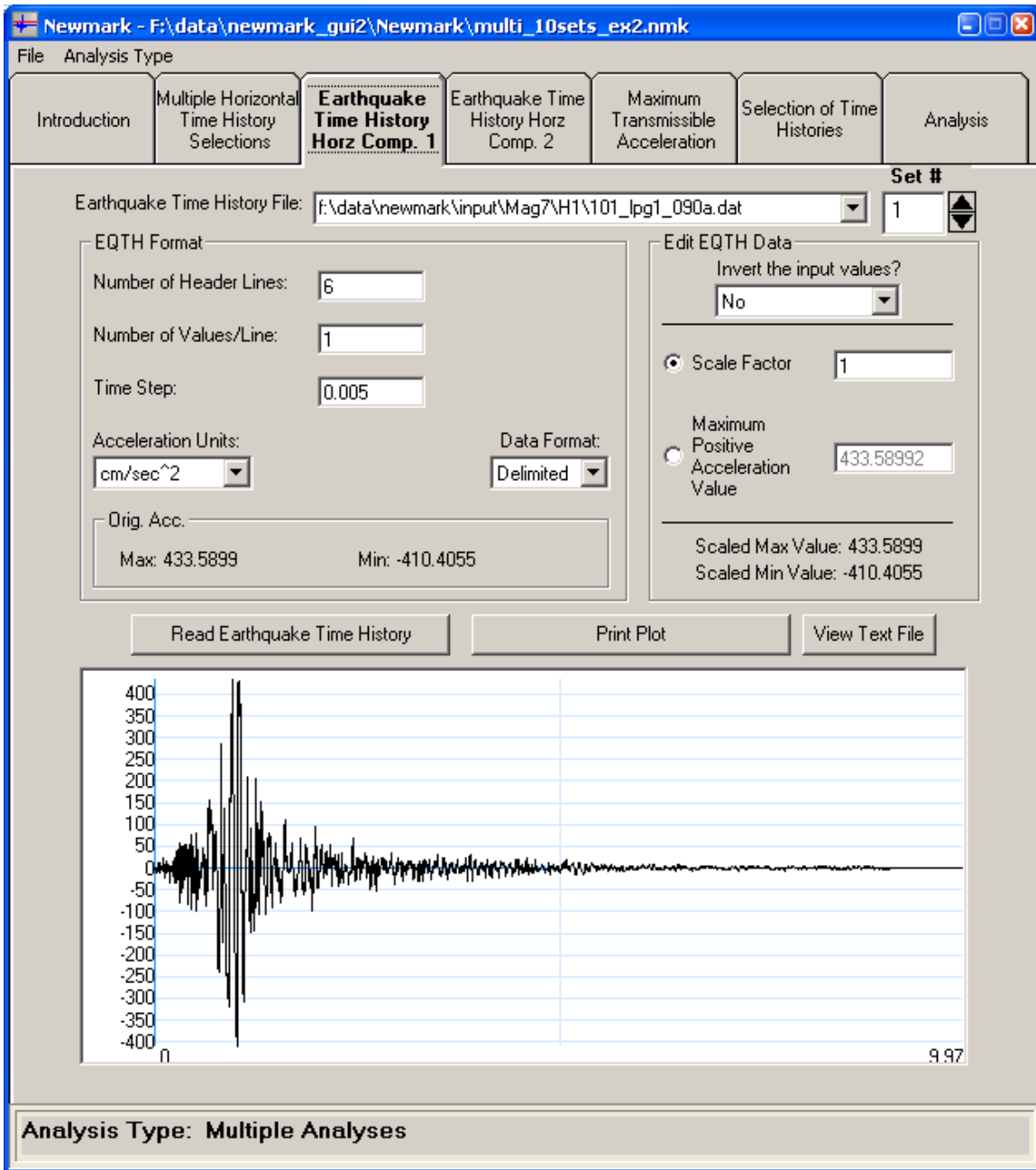


Figure 5.4. Horizontal earthquake time-history ground motion shown in the **Earthquake Time-History Horz Comp. 1** tab.

This set number matches the **Set #** found in the gray area within the **Multiple Horizontal Time-History Selections** tab. Selection of a particular set will update all relevant data within the current earthquake time-history tab, including the graph at the bottom of the form.

When a file has been selected, a format must be built. All specifications for reading a file are grouped in a frame labeled **EQTH Format**. To know what information to enter for reading the file, it will be beneficial to select the **View Text File** button and peruse the file to find each section of data.

The first block of data in each EQTH file is the number of header lines. Entering how many header lines there are allows the program to skip those lines. It is also important to know how many data samples are on each line. Entering the **Number of Values/Line** keeps the program from entering blank samples or ignoring samples. The value entered for **Time Step** should be the amount of time that occurs between samples, establishing the sampling frequency and the total time for the earthquake data.

Since Newmark works from the beginning of an earthquake, it is to be assumed that the first sample, time step 0, will have a value of 0.0 in whatever units chosen. If the EQTH file does not have this zero point, it will be accounted for in the software.

There is a combo box that allows the user to specify the units that the data were recorded in. NOTE: The horizontal component 1 EQTH file uses the same units as the Horizontal component 2 EQTH file. There is no way to mix and match EQTH units.

There is a second combo box that shows several options for a data format. These formats are displayed as if they were in a FORTRAN FORMAT statement. These are especially important in areas where data text may run together. In the **Data Format** pull-down menu, the **Delimited** option is the space.

After an EQTH format has been built for a particular file, the user can read in the Earthquake Time-History. After the button is pressed, the actual values of the maximum and minimum values for that file are displayed in the **Orig. Acc.** sub-frame of the **EQTH Format** frame. A plot of the input data is also displayed at the bottom of the tab. The **Edit EQTH Data** frame will also be enabled.

The **Edit EQTH Data** frame is a tool that allows the user to scale the EQTH data to values more appropriate for modeling the problem at hand. There is a combo-box that allows the user to invert the user specified

earthquake acceleration time-history values, which is valuable for determining whether the direction of peak values influence the computed (permanent displacement) results.

There are also two possible ways of scaling the input data, either by setting an absolute scale value to multiply the samples by or by setting an absolute maximum value for the positive peak value and scaling the other samples to match. To choose the scale method, click the radio button beside that option. Then, type in the value desired.

When this is done, the inactive choice will be updated with the related value. Also, the scaled minimum and maximum values will be displayed, and the data plot at the bottom of the form will reflect the changes.

If the user desires a hardcopy of the scaled data in the same format as at the bottom of the tab, there is a button labeled **Print Plot**.

If the user would like to view the raw data in its original format, there is a button labeled **View Text File**.

5.2.4 Maximum Transmissible Acceleration input (Single Analysis or Multiple Analyses)

To perform a Newmark sliding block analysis, a maximum transmissible acceleration (as described in Section 1.1.3.2 of this report) has to be specified with this value of acceleration at the incipient of displacement resulting in a factor of safety less than or equal to 1.0. Figure 5.5 allows for user input for either a single analysis or multiple analyses.

In a single analysis, the user has the option of providing the maximum transmissible acceleration (k_c) and its units or the ratio of k_c and the peak acceleration (k_m) as user input.

For multiple analyses, the maximum transmissible acceleration is given as a fraction of the peak acceleration. Multiple k_c/k_m values are necessary and the user has the option to add any values or accept the defaults (selected by the authors). The Multiple Analyses frame allows the user to modify the values by directly editing the existing 16 values; add additional values at the end of the list, delete and/or insert values.

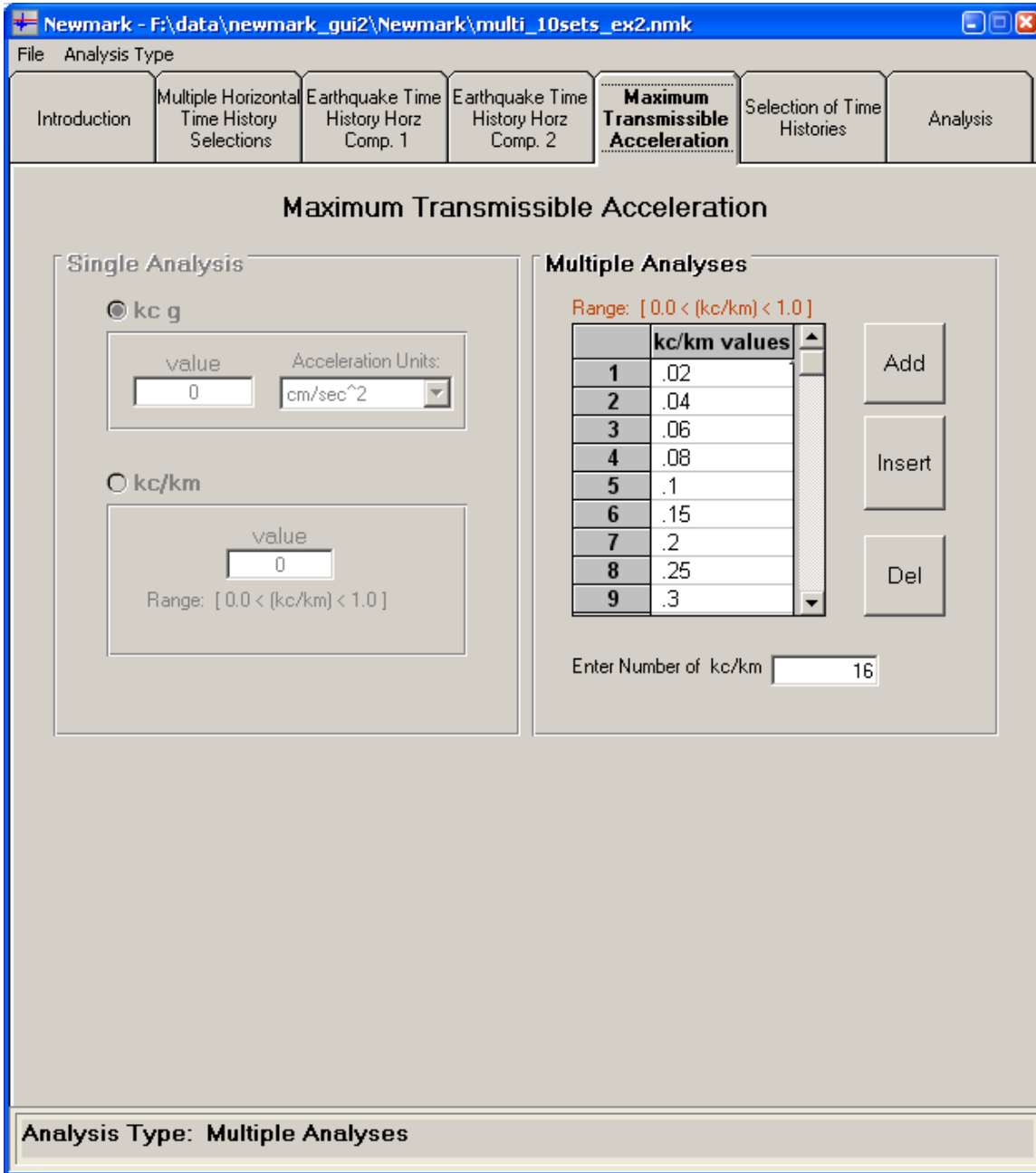


Figure 5.5. **Maximum Transmissible Acceleration** tab for multiple analyses data entry.

5.2.5 The Selection of Time Histories (Multiple Analyses)

This section summarizes a simple way of including all or excluding some files previously selected in the **Multiple Horizontal Time-History Selections** tab (Figure 5.6) for an analysis. The acceleration time histories (i.e. the horizontal component 1 (H1) and horizontal component 2 (H2)) chosen will be used for user specified regression analyses and

displayed after the completion of the execution of Newmark in the **Analysis** tab.

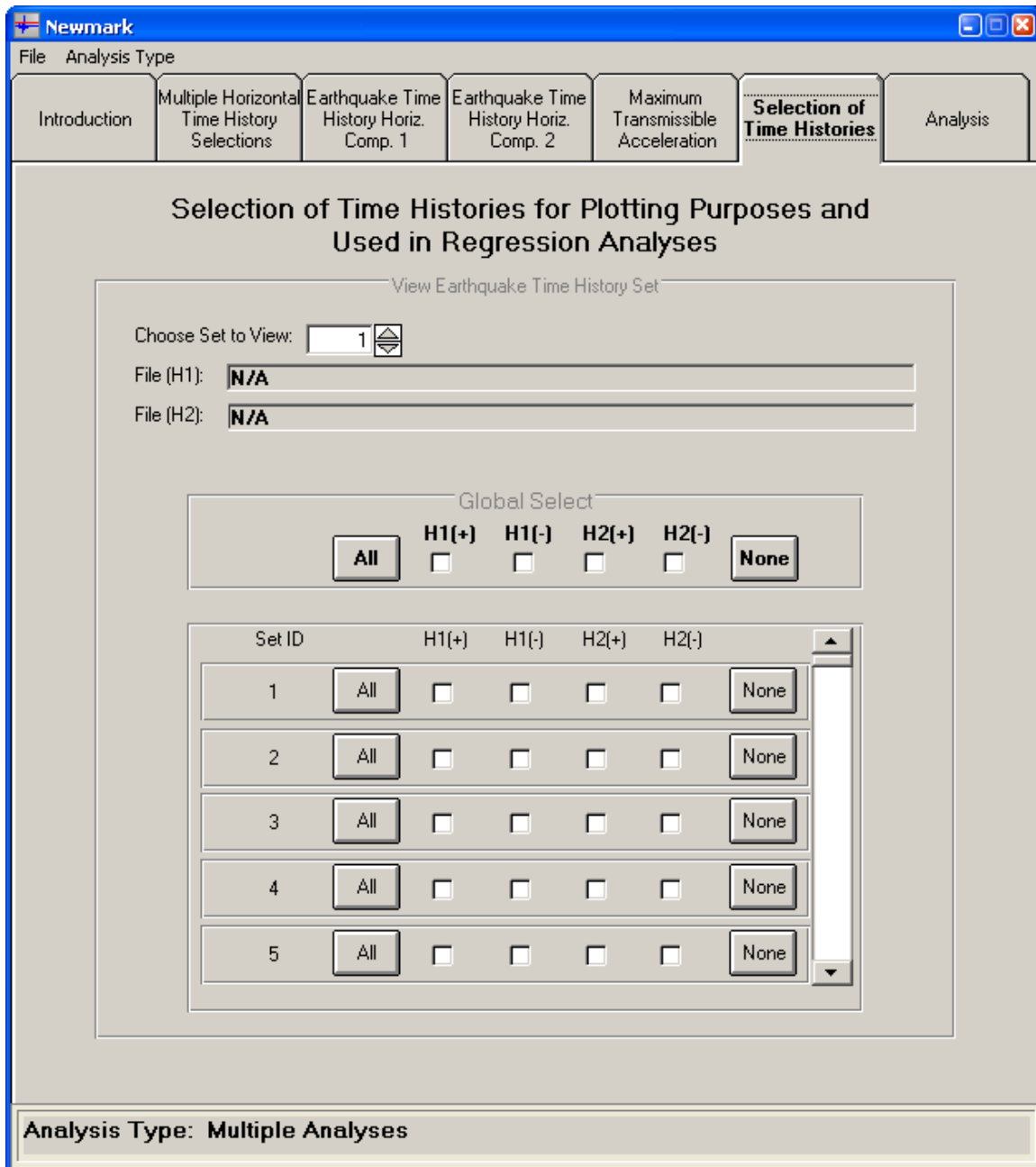


Figure 5.6. The **Selection of Time Histories** tab for data entry used for multiple analyses.

The first horizontal acceleration time-history set (i.e. H1 and H2) is displayed within the **View Earthquake Time-History Set** frame and each labeled by **File(H1):** and **File(H2):** for the respective horizontal components. If either component was not available there would be an **N/A** placed instead of the name of the file. There is also a **Choose Set to View**

entry/selection box with a default of 1 that allows the user to specify which set to list. This can be used to verify the files being used and is by no means a way of sorting the entire set of lists.

The earthquake time-history horizontal components **H1** and **H2** can further be evaluated by inverting the values of each horizontal component time-history. The reasoning for this is to determine whether the magnitudes of **H1** and/or **H2** have an effect on the resultant (permanent displacement) analysis. Therefore, a separate time-history was created that is the inverse of the original. Thus, **H1** is now **H1(+)**, with an **H1(-)** as its inverse. The same logic is applied for **H2**.

About the center of this tab, there is the **Global Select** frame which allows the user an easy way to select any of the possible four horizontal components in a vertical sense (i.e. the selection of the **H1(+)** button will mark all the **H1(+)** buttons listed vertically in the sub-frame directly below). This feature also applies for the **H1(-)**, **H2(+)**, **H2(-)** buttons.

There is an **All** button, which accepts all files, and a **None** button, which clears out the files previous selected and un-marks all of the buttons.

The sub-frame located beneath the **Global Select** frame is used for selecting time histories on a set-by-set basis. For set 1, the user can mark or unmark any of the 4 buttons, i.e., **H1(+)**, **H1(-)**, **H2(+)**, **H2(-)**. There is an **All** button which accepts all files in this set and a **None** button which un-marks all the buttons of the current set. The sliding bar to the right allows the user to view which sets are marked or unmarked.

5.2.6 Analysis results (Single Analysis or Multiple Analyses)

The Figure 5.7 **Analysis** tab can be divided into three sections: **Input Parameters**, **Run Newmark Analyzer** and **View Output**. The **Input Parameters** section allows the user to select the regression analysis type and also set the output units from an execution of Newmark. The **Run Newmark Analyzer** section is a button that will execute the Newmark program. The **View Output** section contains options for viewing the many outputs of the Newmark Analysis, including the **Regression Analysis** subsection that allows the user to view the data and the statistic parameters derived from a multiple analysis.

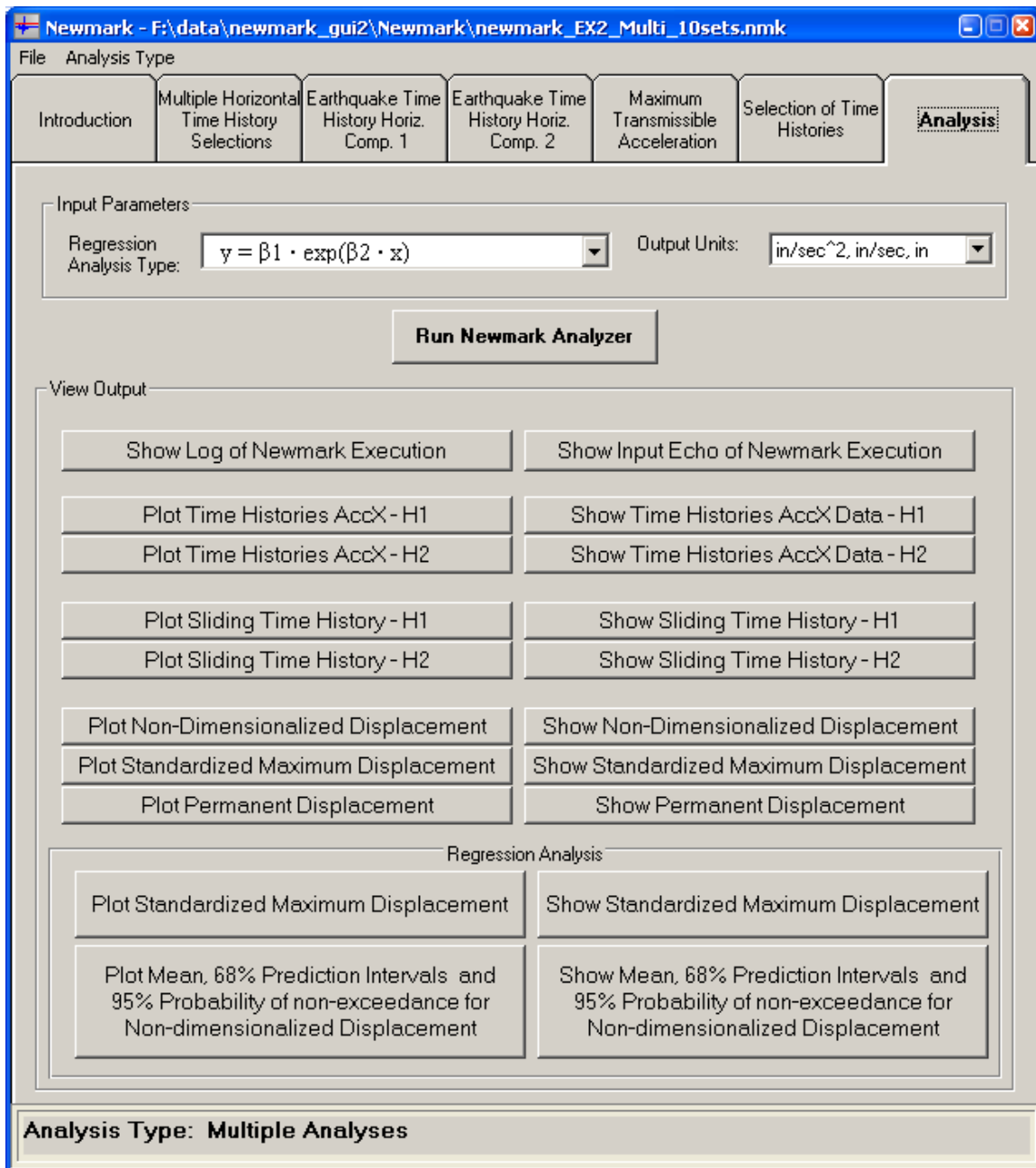


Figure 5.7. The **Analysis** tab used for all analyses.

In the **Input Parameters** frame of the **Analysis** tab, the user can select inputs from two combo boxes. The **Regression Analysis Type** combo box shows the option of no regression, performing regression analyses with three different forms of equations and the combinations of these equations.

Figure 5.8 shows a snapshot of the **Regression Analysis Type** combo box. Upon observation, Equation Form Type 2 (Chapter 3 - Table 3.1) is selected for the analysis. The second combo box in the **Input Parameters** frame is the Output Units box where the user has the option to select the resultant output units of the analysis.

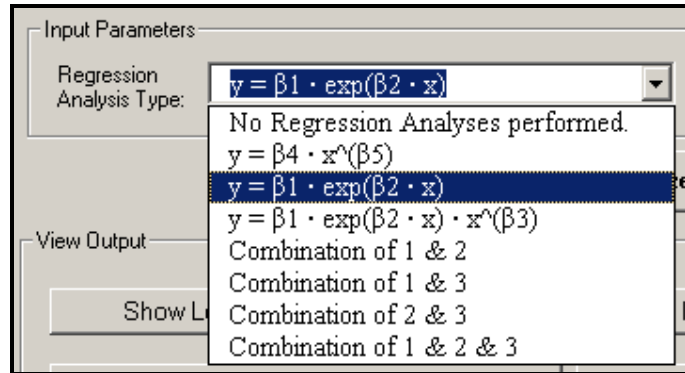


Figure 5.8. Single and combinations of three equations available for Regression Analyses.

Immediately prior to execution (or termination of an execution) of Newmark, it is a good idea to create a restart file containing all of the input information. This is accomplished by using the **File** drop-down menu with the save option which is located at the top left corner of the Newmark_{VM}. The file created has an “nmk” extension. This file may also be read in by the Newmark_{VM}, using this same file drop-down menu and will populate the same data contained within all tabs at a later point in time.

As soon as the **Run Newmark Analyzer** button is activated, a Newmark.in ASCII data input file, described in Appendix A, is created by the Newmark_{VM} and the FORTRAN engineering program, Newmark, is executed. Newmark creates the output and plot data files that are used in the **View Output** frame of the **Analysis** tab (Figure 5.7). Appendix B lists and summarizes the contents of these output and plot data files. The ASCII data file created by Newmark_{VM} becomes the input to FORTRAN Newmark.

A display will show (Figure 5.9) the stability analysis being performed by Newmark for each set of time histories. Note: A set of time histories represent two horizontal acceleration time histories, namely **H1** and **H2**. With each being represented as two separate calculations; namely; **H1(+)**, **H1(-)** and **H2(+)**, **H2(-)**. This process could take a minute or two, depending on the number of sets being evaluated (and the speed of the computer). Upon completion, the execution window disappears and a pop-up window waits for the user to select the OK button.

```

F:\data\newmark_gui2\Newmark\newmark.exe
Processing 4000 of 4995 time increments
Processing 4995 of 4995 time increments completed
4996 10.9826572414596 9.82823501162929
Processing 0 of 4995 time increments
Processing 1000 of 4995 time increments
Processing 2000 of 4995 time increments
Processing 3000 of 4995 time increments
Processing 4000 of 4995 time increments
Processing 4995 of 4995 time increments completed
4996 14.6435429886128 6.98413413116565
Processing 0 of 4995 time increments
Processing 1000 of 4995 time increments
Processing 2000 of 4995 time increments
Processing 3000 of 4995 time increments
Processing 4000 of 4995 time increments
Processing 4995 of 4995 time increments completed
4996 18.3044287357660 4.96039301379251
Processing 0 of 4995 time increments
Processing 1000 of 4995 time increments
Processing 2000 of 4995 time increments
Processing 3000 of 4995 time increments
Processing 4000 of 4995 time increments
Processing 4995 of 4995 time increments completed
4996 21.9653144829192 3.55179650737859

```

Figure 5.9. Illustrative example of Newmark during execution.

The focus now returns to the Analysis Tab and the View Output section. The user has many options available for viewing and evaluating the data by the selection of any particular button. There are logs of input and run-time data for the user to examine. The scaled horizontal time-history results of acceleration, velocity and displacement are readily available for inspection. A sliding block analysis with the given maximum transmissible acceleration will report the value of the cumulative (permanent) horizontal relative wall displacement. In the event where multiple sets were used in the analysis, another window will appear (Figure 5.10) to allow the user to view the output data pertaining to any set.

In a multiple analyses simulation, resultant non-dimensionalized, standardized if elected, and permanent displacement data for each time-history set will be available for evaluation. A similar form of Figure 5.10 will also be available for the viewing of these displacement results. Regression analyses can be performed when specified, with resultant data and statistical parameters available for assessment. Figure 5.11 shows a portion of the output data from an ASCII text file resulting from a regression analysis.

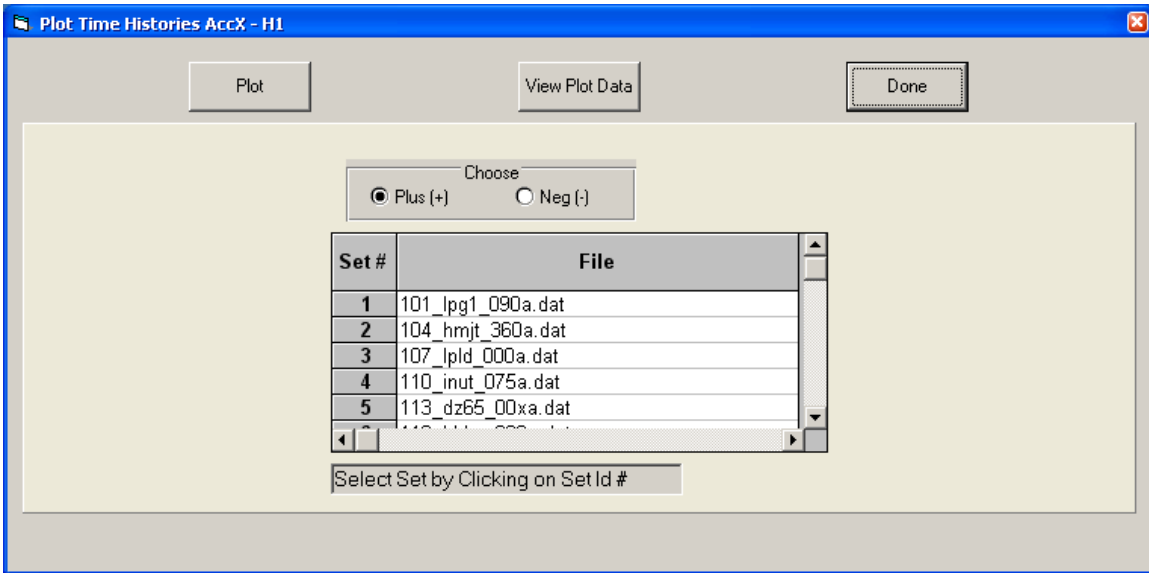


Figure 5.10. Resultant output data from multiple analyses.

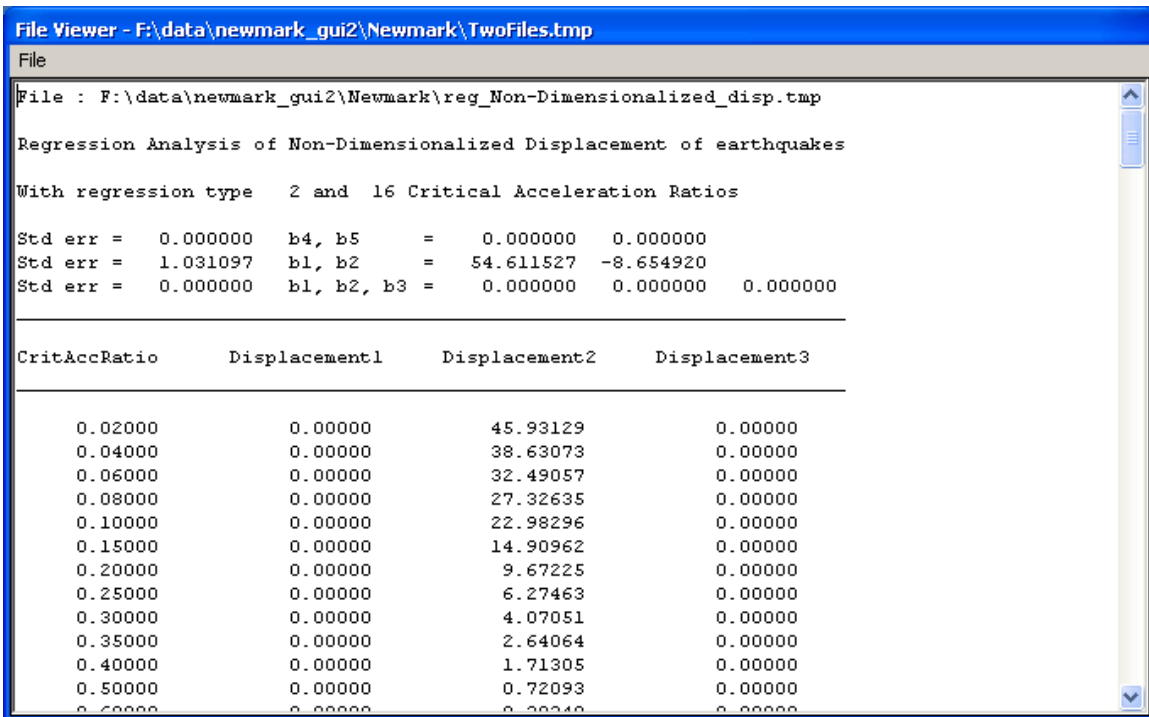


Figure 5.11. Resultant output data from a regression analysis.

5.3 Example 1 – Single Analysis or Sliding Block Analysis

In this first example, a single acceleration time-history is considered. The tabs that will be used for this example are described in Section 5.2.1. From the **File** pull-down menu, select **Open** and accept the file “single_analysis_kcg.nmk”. This particular horizontal earthquake time-history was recorded having a moment magnitude of 6.6. The next step is to decide on the maximum transmissible acceleration or critical acceleration used for this analysis. At the **Maximum Transmissible Acceleration** Tab, for a single analysis, select the **kc_g** option and enter a value of 0.3 with the **Acceleration Units** as fractional G. Finally, in the **Analysis** tab (Figure 5.12), set the Output Units to values of inches. Run the analysis by selecting the **Run Newmark Analyzer**.

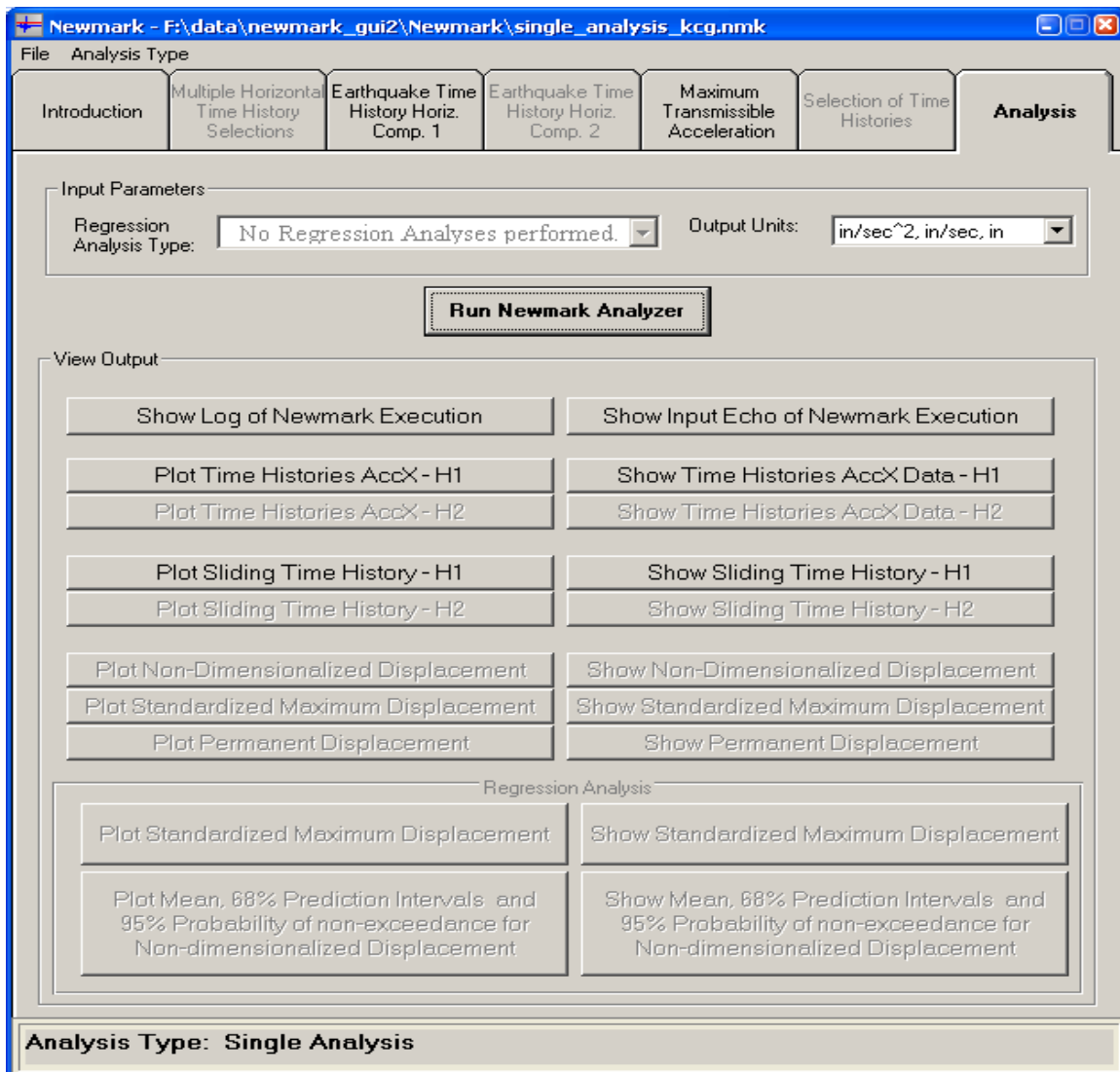


Figure 5.12. The **Analysis** tab for Example 1.

The results for the time-history permanent displacement analysis for this problem are shown in Figure 5.13. This figure is seen by activating the **Plot Sliding Time-History – H1** button on the **Analysis** tab. (Note the **Show Sliding Time-History – H1** button (or, equivalently, in the singlePLOTslideTH11.TMP1 ACSII output file) also reports the value for the cumulative (permanent) horizontal relative wall displacement). The first or upper figure is a plot of the horizontal acceleration time-history and the red line designates the maximum transmissible acceleration (or, equivalently, the yield acceleration) value of $0.3 g$. Permanent structural displacements start to occur the first time the acceleration trace plots above this red line. Observe that permanent wall translation starts at about 3.8 seconds after initial shaking and concludes by about 5 seconds out of a total of 38 seconds of ground shaking. The cumulative permanent displacement of the structural block is about 1.625 inches, which occurs over about 3 significant relative (structural) velocity and displacement pulses (refer to the second and third figure down from the top, respectively).

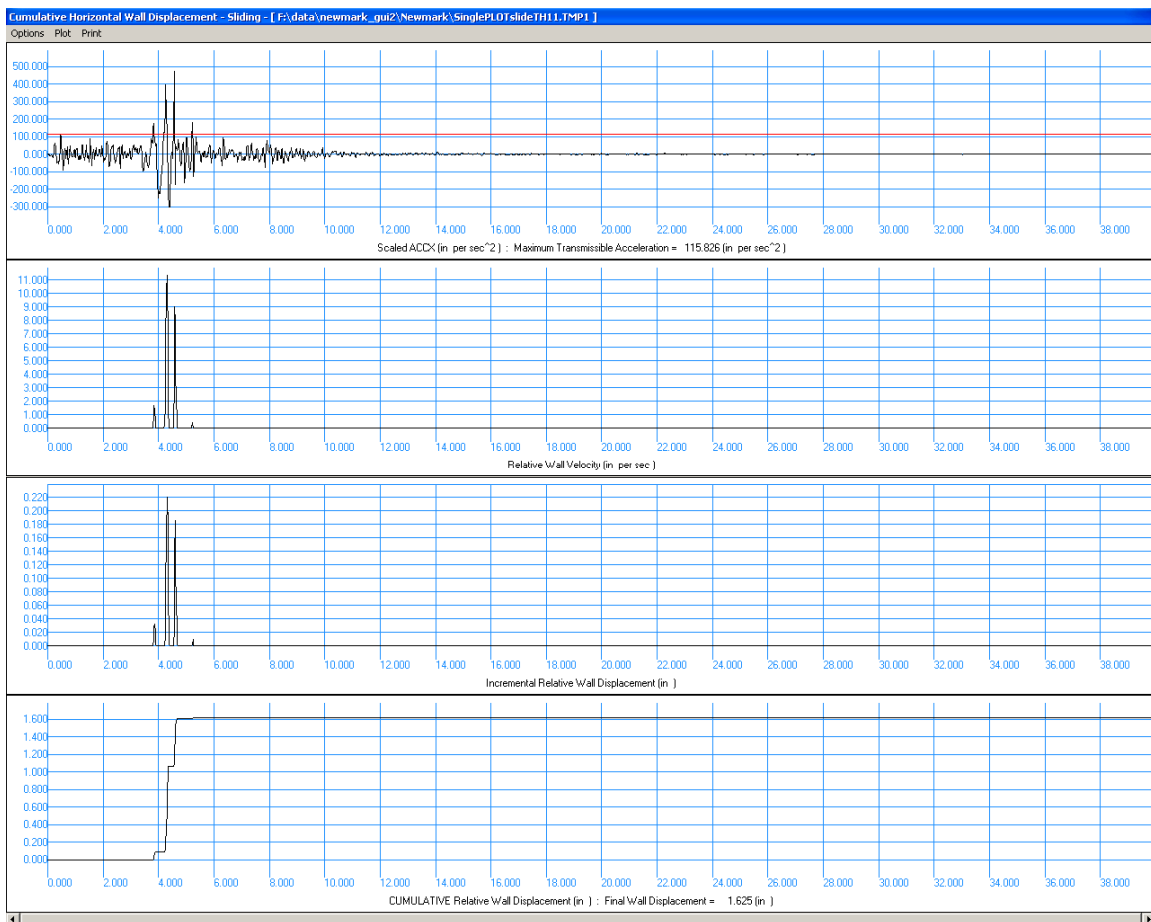


Figure 5.13. Sliding block time-history results for Example 1.

5.4 Example 2 – Multiple Analyses with Regression using Equation Form Two.

In this second example and with compactness in mind, a set of 10 pairs of baseline corrected acceleration time histories are considered. These sets of horizontal earthquake time histories were recorded on rock and for moment magnitudes in the 7 range.

Starting from the **File** pull-down menu, select **Open** and accept the file “multi_10sets_ex2.nmk”. From this input file, the user can browse through data within tabs two through four. Data entry and information regarding these tabs are listed within the multiple analyses segment of Section 5.2.1 and also in Sections 5.2.2 and 5.2.3. Please note that for this example, standardized displacement computations have not been requested.

The next step is to decide on the maximum transmissible acceleration or critical acceleration used for this analysis. From the **Maximum Transmissible Acceleration** tab and for multiple analyses, there are 16 k_c/k_m values listed. These values are the default and will be used for this example. At the **Selection of Time Histories** tab, all of the various combinations will be included for this example.

In the **Analysis** tab, the regression form type two expression is the equation of choice and the output units will be in inches, as shown in Figure 5.14.

After this selection, run the analysis by selecting the **Run Newmark Analyzer**.

The results for the time-history permanent displacement analysis for this example 2 can be seen for each individually time-history or set, by activating the **Plot Sliding Time-History – H1** or **Plot Sliding Time-History – H2** button on the **Analysis** tab. (Note the **Show Sliding Time-History – H1** button (or, equivalently, in the output ASCII texts file as described in Appendix B) also reports the value for the cumulative (permanent) horizontal relative structural displacement).

An observation from viewing the output of the non-dimensionalized displacement of set 1, Figure 5.15, shows for this analysis that the **H2(-)** graph has the largest magnitude.

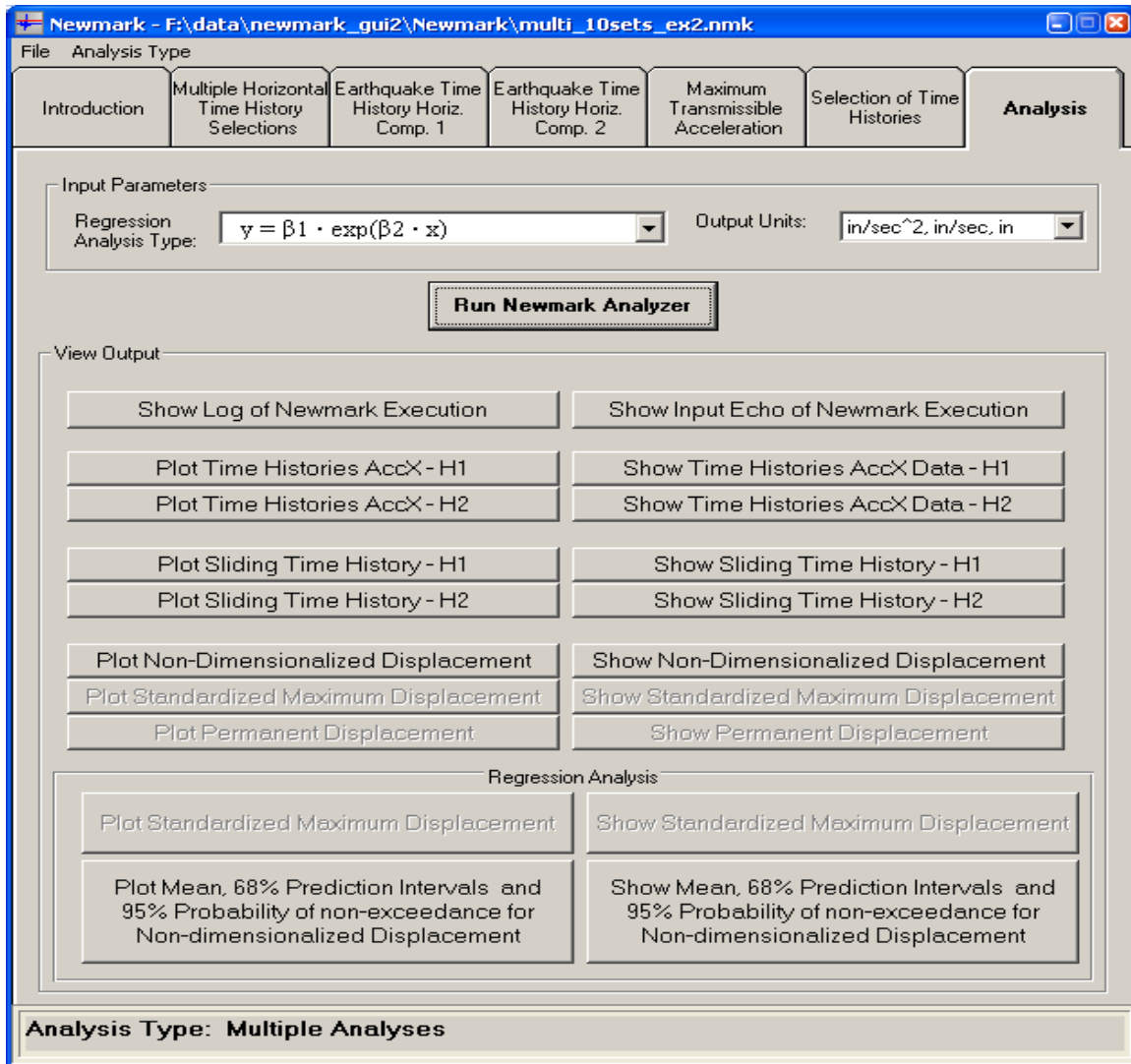


Figure 5.14. The **Analysis** tab for Example 2.

Upon inspection of the regression analysis for this example 2, Figure 5.16, shows that all of the data below a k_c/k_m value of 0.4 is contained below the curve representing the 95 percent probability of non-exceedance relationship. Some of the data greater than a k_c/k_m value of 0.4 does fall above the curve and lies above the 95 percent probability of non-exceedance relationship. An ideal data set would have a few data points falling above the 95 percent probability of non-exceedance relationship for all k_c/k_m data point values. This example illustrates the importance of including larger number of sets of horizontal time histories in order to more efficiently represent the data when performing a regression analysis. As a final note, observe the plotted data from the **Introduction** tab (Figure 5.1).

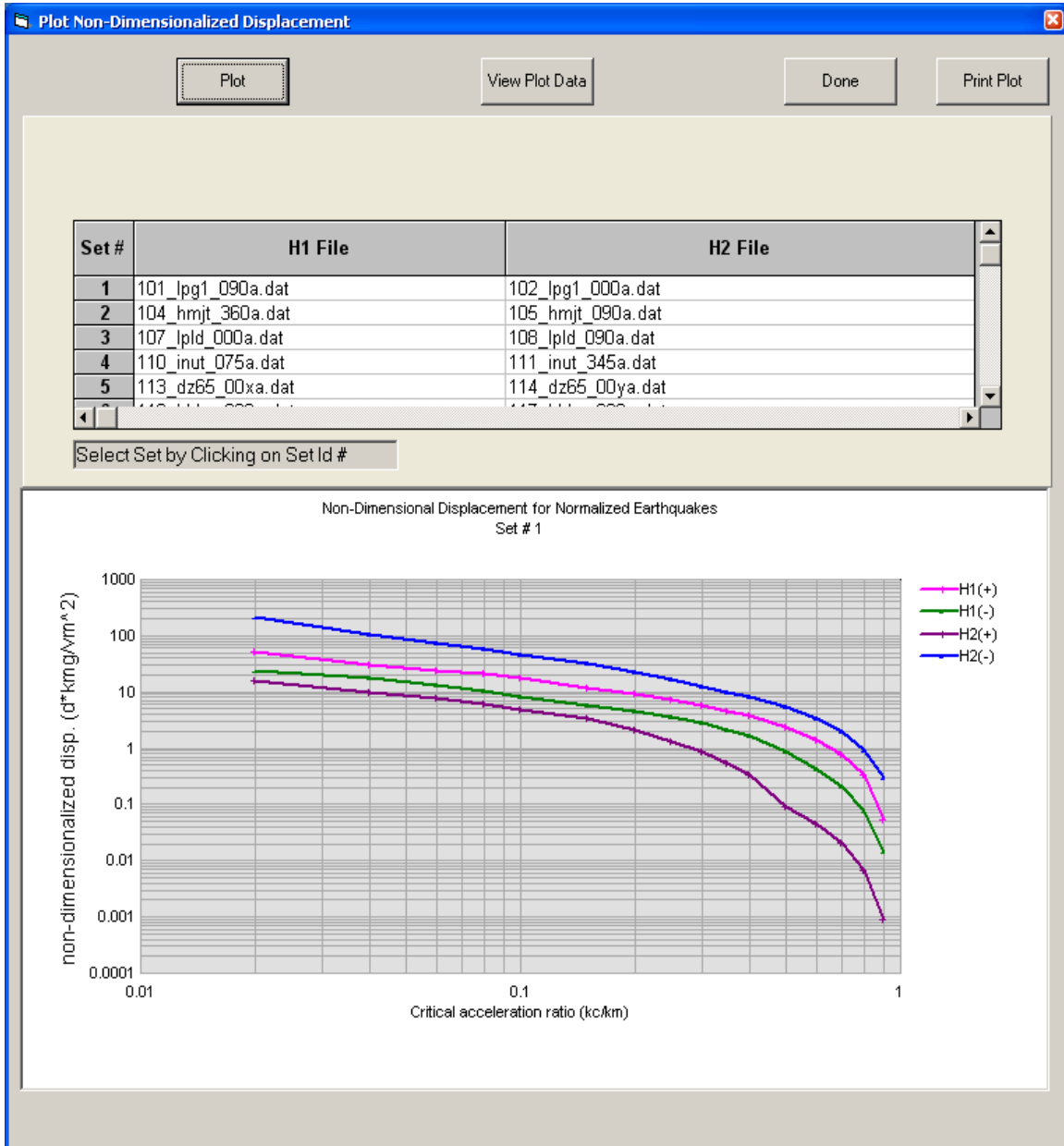


Figure 5.15. Non-dimensionalized earthquake displacements.

The authors of this report believe that the resultant plot from the regression analysis shows a reasonable data set base which results in reasonable statistical relationships for the 122 sets of horizontal earthquake time histories and over the entire range of k_c/k_m data point values.

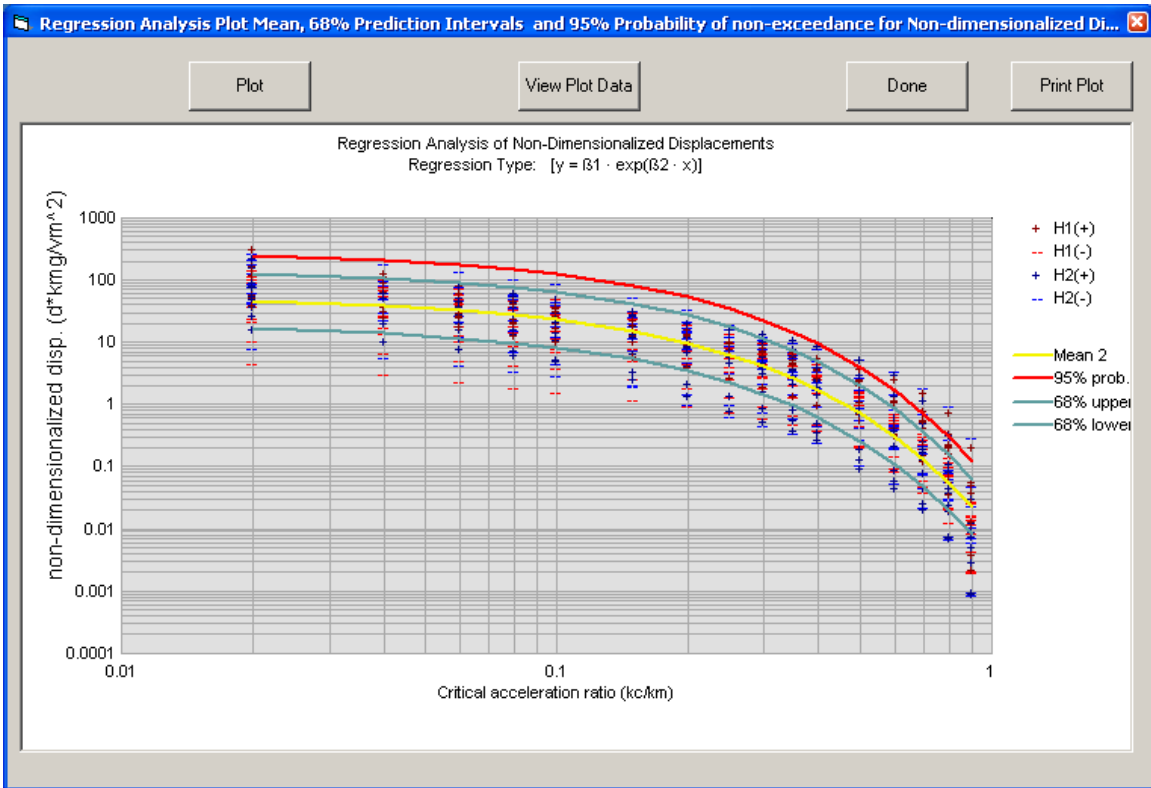


Figure 5.16. The mean, 68 percent prediction intervals and 95 percent probability of non-exceedance.

6 Conclusions and Recommendations

6.1 Introduction

This report describes the results of a series of numerical investigations using the PC-based software named Newmark that performs a permanent sliding block displacement analysis. The authors of this report note that baseline corrected acceleration time histories must be used in these permanent deformation analyses. Newmark can also perform regression analyses in order to develop up to three user selected forms of generalized equations of simplified permanent displacement relationships for sets of user defined acceleration time histories. In Chapter 4, a series of regression analyses were summarized for baseline corrected acceleration time histories recorded on rock for three earthquake moment magnitude M_w ranges of 4.85 to 6.06, 6.06 to 6.8, and 6.9 to 8.1, with average M_w values of 5.6, 6.5, and 7.3 for each of the three groups. An assessment discussed in Chapter 4 concluded that Equation Form Two, the two-term regression results for a form of equation that is linear in natural logarithm transformation, provides both the best fit to the (non-dimensionalized) permanent displacement data as well as the lowest order relationship without compromising accuracy. Lastly, as a special case established in Chapter 4, Equation Form Two regression results were evaluated for the entire 122 sets of baseline corrected acceleration time histories recorded on rock, without differentiation of M_w (group four). This chapter summarizes the probabilistic relationships derived from Equation Form Two of all four groups of earthquake magnitudes.

6.2 Ninety-five percent probability of non-exceedance

The next four subsections (6.2.1 – 6.2.4) report the 95 percent probability of non-exceedance relationships for each of the three magnitude groups with the last subsection, the fourth group, encompassing all three groups.

6.2.1 Non-dimensionalized displacements of 23 sets of Moment Magnitude 7 group.

The regression analysis of the 23 sets of Magnitude 7 rock acceleration time histories resulted in the non-dimensionalized displacement for 95 percent probability of non-exceedance of

$$\frac{d_m \bullet k_m g}{v_m^2} = 70.1 \bullet \exp\left(-9.2 \bullet \frac{k_c}{k_m}\right) \bullet 4.64 \quad (\text{bis 4.14})$$

where:

- d_m = permanent displacement
- $k_m g$ = peak (positive) rock acceleration expressed in units of length per sec², consistent with units of d_m (length) and v_m (length per sec)
- v_m = peak (positive) ground velocity of the earthquake
- k_c = critical acceleration expressed as a fraction of g
- k_m = peak (positive) rock acceleration expressed as a fraction of g .

The corresponding 95 percent probability of non-exceedance permanent displacement relationship is

$$d_m = 325.4 \bullet \left[\frac{v_m^2}{k_m \bullet g} \right] \bullet \exp\left(-9.2 \bullet \frac{k_c}{k_m}\right) \quad (6.1)$$

where the right-hand-side term $k_m g$ is the peak (positive) rock acceleration expressed in units of length per sec².

6.2.2 Non-dimensionalized displacements of 38 sets of Moment Magnitude 6 group

The regression analysis of the of the 38 sets of Magnitude 6 rock acceleration time histories resulted in the non-dimensionalized displacement for 95 percent probability of non-exceedance of

$$\frac{d_m \bullet k_m g}{v_m^2} = 78.6 \bullet \exp\left(-9.12 \bullet \frac{k_c}{k_m}\right) \bullet 3.68 \quad (\text{bis 4.41})$$

The corresponding 95 percent probability of non-exceedance permanent displacement relationship is

$$d_m = 289.5 \bullet \left[\frac{v_m^2}{k_m \bullet g} \right] \bullet \exp\left(-9.12 \bullet \frac{k_c}{k_m}\right) \quad (6.2)$$

where the right-hand-side term $k_m g$ is the peak (positive) rock acceleration expressed in units of length per sec².

6.2.3 Non-dimensionalized displacements of 66 sets of Moment Magnitude 5 group

The regression analysis of the 61 sets of Magnitude 5 rock acceleration time histories resulted in the non-dimensionalized displacement for 95 percent probability of non-exceedance of

$$\frac{d_m \bullet k_m g}{v_m^2} = 57.0 \bullet \exp\left(-8.58 \bullet \frac{k_c}{k_m}\right) \bullet 3.39 \quad (\text{bis 4.68})$$

The corresponding 95 percent probability of non-exceedance permanent displacement relationship is

$$d_m = 193.2 \bullet \left[\frac{v_m^2}{k_m \bullet g}\right] \bullet \exp\left(-8.58 \bullet \frac{k_c}{k_m}\right) \quad (6.3)$$

where the right-hand-side term $k_m g$ is the peak (positive) rock acceleration expressed in units of length per sec².

6.2.4 Non-dimensionalized displacements of 122 sets of Moment Magnitude 5 - 7 groups

The regression analysis of the 122 sets of all Magnitudes 5 - 7 of rock acceleration time histories resulted in the non-dimensionalized displacement for 95 percent probability of non-exceedance of

$$\frac{d_m \bullet k_m g}{v_m^2} = 65.44 \bullet \exp\left(-8.86 \bullet \frac{k_c}{k_m}\right) \bullet 3.75 \quad (\text{bis 4.87})$$

The corresponding 95 percent probability of non-exceedance permanent displacement relationship is

$$d_m = 245.4 \bullet \left[\frac{v_m^2}{k_m \bullet g}\right] \bullet \exp\left(-8.86 \bullet \frac{k_c}{k_m}\right) \quad (6.4)$$

where the right-hand-side term $k_m g$ is the peak (positive) rock acceleration expressed in units of length per sec².

The non-dimensionalized displacement relationships for the four earthquake magnitude groups are shown in Figure 6.1, plotted as function of the critical acceleration ratio k_c/k_m , with their corresponding values summarized in Table 6.1. Figure 6.1 and Table 6.1 show the resulting (95 percent probability of non-exceedance) non-dimensionalized permanent displacements. The Magnitude 7 relationship lies above the Magnitude 6 relationship which, in turn, lies above the Magnitude 5 relationship. The Magnitude 5 – 7 earthquake group of 122 rock ground motion sets falls above the Magnitude 5 relationship and below the Magnitude 6 relationship; this is possibly due to the fact that more than half of the data set resides within the Magnitude 5 relationship.

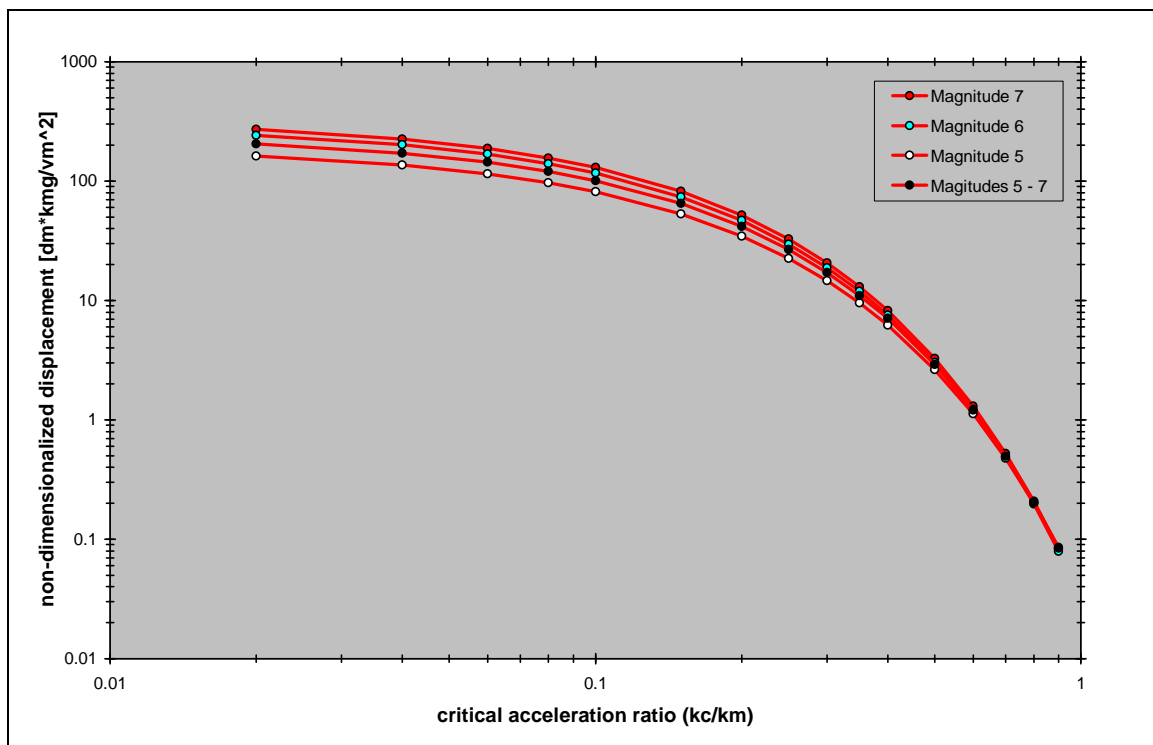


Figure 6.1. 95 percent probability of non-exceedance relationships of non-dimensionalized displacements of four magnitude groups.

Table 6.1. 95 percent probability percent of non-exceedance relationships of non-dimensionalized displacements of four magnitude groups.

$\frac{k_c}{k_m}$	Magnitude 5	Magnitude 6	Magnitude 7	Magnitude 5 - 7
0.02	162.2120	242.0580	271.6762	205.30615
0.04	136.6378	201.6964	226.0193	171.95999
0.06	115.0956	168.0649	188.0354	144.02997
0.08	96.9498	140.0412	156.4349	120.63639
0.1	81.6648	116.6902	130.1450	101.04243
0.15	53.1807	73.9574	82.1604	64.87351
0.2	34.6317	46.8736	51.8678	41.65154
0.25	22.5525	29.7081	32.7441	26.74205
0.3	14.6863	18.8288	20.6713	17.16953
0.35	9.5639	11.9335	13.0498	11.02356
0.4	6.2281	7.5634	8.2383	7.07759
0.5	2.6412	3.0382	3.2833	2.91751
0.6	1.1200	1.2204	1.3085	1.20265
0.7	0.4750	0.4902	0.5215	0.49576
0.8	0.2014	0.1969	0.2078	0.05456
0.9	0.0854	0.0791	0.0828	0.02249

6.3 Mean relationships

The next four subsections (6.3.1 – 6.3.4) report the mean relationships for each of the three magnitude groups with the last subsection, the fourth group, encompassing all three groups.

6.3.1 Non-dimensionalized displacements of 23 sets of Moment Magnitude group 7

The regression analysis of the 23 sets of Magnitude 7 rock acceleration time histories resulted in the mean non-dimensionalized displacement relationship of

$$\frac{d_m \bullet k_m g}{v_m^2} = 70.1 \bullet \exp\left(-9.2 \bullet \frac{k_c}{k_m}\right) \quad (\text{bis 4.11})$$

where:

- d_m = permanent displacement
- $k_m g$ = peak (positive) rock acceleration expressed in units of length per sec², consistent with units of d_m (length) and v_m (length per sec)
- v_m = peak (positive) ground velocity of the earthquake
- k_c = critical acceleration expressed as a fraction of g
- k_m = peak (positive) rock acceleration expressed as a fraction of g .

The corresponding mean permanent displacement relationship is

$$d_m = 70.1 \cdot \left[\frac{v_m^2}{k_m \cdot g} \right] \cdot \exp \left(-9.2 \cdot \frac{k_c}{k_m} \right) \quad (6.5)$$

where the right-hand-side term $k_m g$ is the peak (positive) rock acceleration expressed in units of length per sec².

6.3.2 Non-dimensionalized displacements of 38 sets of Moment Magnitude group 6

The regression analysis of the of the 38 sets of Magnitude 6 rock acceleration time histories resulted in the mean non-dimensionalized displacement relationship of

$$\frac{d_m \cdot k_m g}{v_m^2} = 78.6 \cdot \exp \left(-9.12 \cdot \frac{k_c}{k_m} \right) \quad (\text{bis 4.38})$$

The corresponding mean permanent displacement relationship is

$$d_m = 78.6 \cdot \left[\frac{v_m^2}{k_m \cdot g} \right] \cdot \exp \left(-9.12 \cdot \frac{k_c}{k_m} \right) \quad (6.6)$$

where the right-hand-side term $k_m g$ is the peak (positive) rock acceleration expressed in units of length per sec².

6.3.3 Non-dimensionalized displacements of 66 sets of Moment Magnitude group 5

The regression analysis of the 61 sets of Magnitude 5 rock acceleration time histories resulted in the mean non-dimensionalized displacement relationship of

$$\frac{d_m \bullet k_m g}{v_m^2} = 57.0 \bullet \exp\left(-8.58 \bullet \frac{k_c}{k_m}\right) \quad (\text{bis 4.65})$$

The corresponding mean permanent displacement relationship is

$$d_m = 57.0 \bullet \left[\frac{v_m^2}{k_m \bullet g} \right] \bullet \exp\left(-8.58 \bullet \frac{k_c}{k_m}\right) \quad (6.7)$$

where the right-hand-side term $k_m g$ is the peak (positive) rock acceleration expressed in units of length per sec².

6.3.4 Non-dimensionalized displacements of 122 sets of Moment Magnitude 5 – 7 groups

The regression analysis of the 122 sets of Magnitude 5 - 7 rock acceleration time histories resulted in the mean non-dimensionalized displacement relationship of

$$\frac{d_m \bullet k_m g}{v_m^2} = 65.44 \bullet \exp\left(-8.86 \bullet \frac{k_c}{k_m}\right) \quad (\text{bis 4.83})$$

The corresponding mean permanent displacement relationship is

$$d_m = 65.44 \bullet \left[\frac{v_m^2}{k_m \bullet g} \right] \bullet \exp\left(-8.86 \bullet \frac{k_c}{k_m}\right) \quad (6.8)$$

where the right-hand-side term $k_m g$ is the peak (positive) rock acceleration expressed in units of length per sec².

The non-dimensionalized displacement relationships for the four earthquake magnitude groups are shown in Figure 6.2, plotted as functions of the critical acceleration ratio k_c/k_m , with their corresponding values summarized in Table 6.2. The data contained in the table and the figure show the Magnitude 6 non-dimensionalized permanent displacement mean relationship to be greater than that for the Magnitude 5 relationship. However, the relationship for the Magnitude 7 relationship falls between the Magnitude 5 and 6 relationships. The authors of this report speculate that this may possibly be due to the smaller acceleration time-history data set used in the regression analysis for the Magnitude 7 earthquake group (23 sets) compared to the larger data sets used in the regression analyses for both the Magnitude 5 and 6 earthquake groups (61 sets and 38 sets, respectively). The Magnitude 5 – 7 earthquake group fits between these three groups.

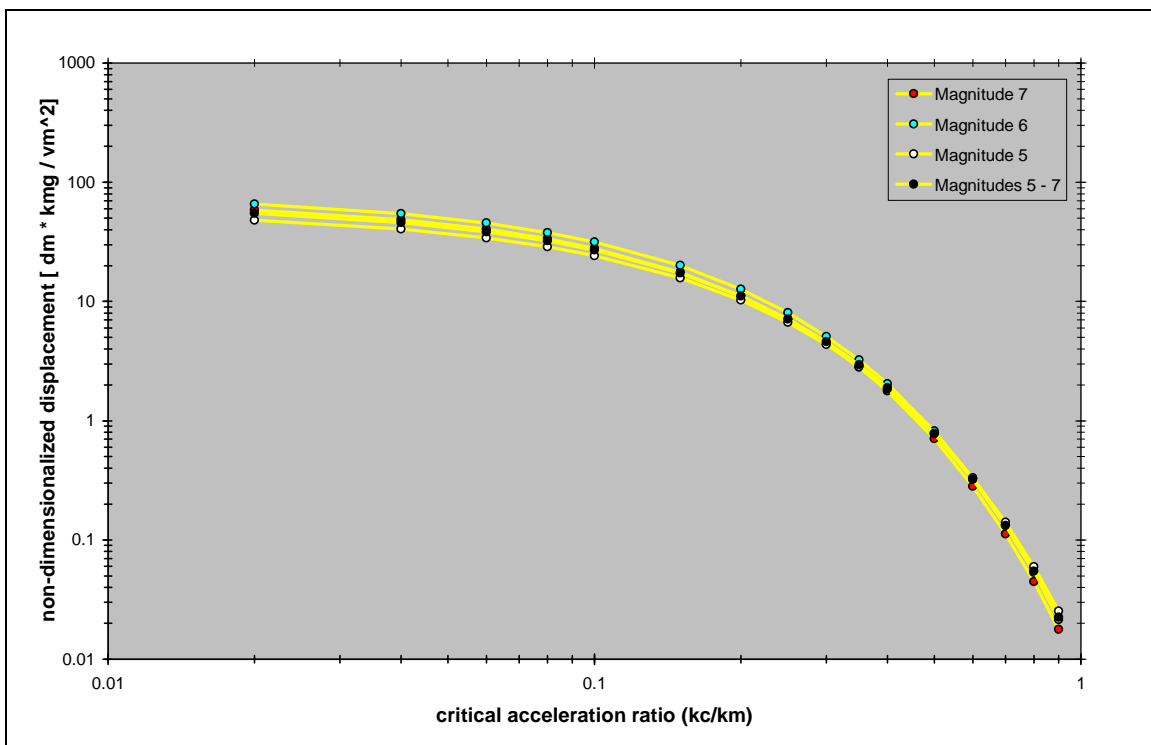


Figure 6.2. Mean relationships of non-dimensionalized displacements of all four magnitude groups.

Table 6.2. Mean relationships of non-dimensionalized displacements of all four magnitude groups.

$\frac{k_c}{k_m}$	Magnitude 5	Magnitude 6	Magnitude 7	Magnitude 5 - 7
0.02	47.9965	65.5091	58.3576	54.81028
0.04	40.4294	54.5859	48.5502	45.9079
0.06	34.0554	45.4841	40.3911	38.45147
0.08	28.6862	37.8999	33.6031	32.20612
0.1	24.1636	31.5803	27.9559	26.97515
0.15	15.7355	20.0154	17.6485	17.31918
0.2	10.2471	12.6856	11.1415	11.11965
0.25	6.6730	8.0400	7.0336	7.13929
0.3	4.3455	5.0957	4.4403	4.58372
0.35	2.8298	3.2296	2.8032	2.94294
0.4	1.8428	2.0469	1.7696	1.88949
0.5	0.7815	0.8222	0.7053	0.77888
0.6	0.3314	0.3303	0.2811	0.32107
0.7	0.1405	0.1327	0.1120	0.13235
0.8	0.0596	0.0533	0.0446	0.05456
0.9	0.0253	0.0214	0.0178	0.02249

6.4 Recommendations

As mentioned previously, the resultant mean non-dimensionalized displacement relationships of both Magnitude 5 and Magnitude 6 earthquake groups showed reasonable results. However, there was a noticeable magnitude influence in the Magnitude 7 earthquake group on the mean relationship. It is speculated that this may be due to an incomplete/limited data set of only 23 sets of baseline corrected acceleration time histories. Recall that there were 38 sets of Magnitude 6 and 61 sets of Magnitude 5 rock acceleration time histories used in this study. A recommendation would be the addition of supplemental data sets of the Magnitude 7 earthquake group as recorded rock acceleration time histories become available in the future with a repeat of the regression analysis for the Magnitude range 7 events.

References

- Ambraseys, N. N., and J. M. Menu. 1988. Earthquake-induced ground displacements. *Earthquake Engineering and Structural Dynamics*. 16:985–1006.
- American Society of Civil Engineers (ASCE) Standard. 1986. Seismic analysis of safety-related nuclear structures and commentary on Standard for Seismic Analysis of Safety Related Nuclear Structures. 004-98. New York: ASCE.
- Cai, Z., and R. J. Bathurst. 1996. Deterministic sliding block methods for estimating seismic displacements of earth structures. *Soil Dynamics and Earthquake Engineering* 15:255–268.
- Clough, G. W., and J. M. Duncan. 1969. *Finite element analyses of Port Allen and Old River Locks*. Contract Report S-69-6. Vicksburg, MS: U.S. Army Engineer Waterways Experiment Station.
- _____. 1991. Earth Pressures, Chapter 6. In *Foundation Engineering Handbook*, 2nd ed., ed. H. Y. Fang, 223–235. New York: Van Nostrand Reinhold.
- Ebeling, R. M. 1992. *Introduction to the computation of response spectrum for earthquake engineering*. Technical Report ITL-92-4. Vicksburg, MS: U.S. Army Engineer Waterways Experiment Station.
- Ebeling, R. M., and A. Chase. *Translational response of rock-founded gravity dams to earthquake ground motions using Corps DamSlip (CDSlip)* (in preparation). Vicksburg, MS: U.S. Army Engineer Research and Development Center.
- Ebeling, R. M., and E. E. Morrison. 1992. *The seismic design of waterfront retaining structures*. Technical Report ITL-92-11. Vicksburg, MS: U.S. Army Waterways Experiment Station.
- Ebeling, R. M., and R. L. Mosher. 1996. Red River U-Frame Lock No. 1, Backfill-structure-foundation interaction. *ASCE Journal of Geotechnical Engineering* 122(3):216–225.
- Ebeling, R. M., and R. E. Wahl. 1997. *Soil-structure-foundation interaction analysis of new roller-compacted concrete north lock wall at McAlpine Locks*. Technical Report ITL-97-5. Vicksburg, MS: U.S. Army Engineer Waterways Experiment Station.
- Ebeling, R. M., and B. C. White. 2006. *The rotational response of toe-restrained retaining walls to earthquake ground motions*. ERDC/ITL TR-06-2. Vicksburg, MS: U.S. Army Engineer Research and Development Center
- Ebeling, R. M., J. F. Peters, and G. W. Clough. 1992. *Users Guide for the incremental construction, soil-structure interaction program SOILSTRUCT*. Technical Report ITL-90-6. Vicksburg, MS: U.S. Army Waterways Experiment Station.

- Ebeling, R. M., R. L. Mosher, K. Abraham, and J. F. Peters. 1993. *Soil-structure interaction study of Red River Lock and Dam No. 1 subjected to sediment loading*. Technical Report ITL-93-3. Vicksburg, MS: U.S. Army Engineer Waterways Experiment Station.
- Ebeling, R. M., R. A. Green, and S. E. French. 1997a. *Accuracy of response of single-degree-of-freedom systems to ground motion*. Technical Report ITL-97-7. Vicksburg, MS: U.S. Army Engineer Waterways Experiment Station
- Ebeling, R. M., M. E. Pace, and E. E. Morrison. 1997b. *Evaluating the stability of existing massive concrete gravity structures founded on rock*. Technical Report REMR-CS-54. Vicksburg, MS: U.S. Army Engineer Waterways Experiment Station.
- Ebeling, R. M., J. F. Peters, and R. L. Mosher. 1997c. The role of non-linear deformation analyses in the design of a reinforced soil berm at Red River U-Frame Lock No. 1. *International Journal for Numerical and Analytical Methods in Geomechanics* 21:753–787.
- Ebeling, R. M., A. Chase, and B. C. White. 2007. *Translational response of toe-restrained retaining walls to earthquake ground motions using Corps WallSlip (CWSlip)*. ERDC/ITL TR-07-1. Vicksburg, MS: U.S. Army Engineer Research and Development Center.
- Franklin, A. G., and F. K. Chang. 1977. *Earthquake resistance of earth and rockfill dams: Report 5: Permanent displacement of earth embankments by Newmark sliding block analysis*. Miscellaneous Paper S-71-17. Vicksburg, MS: U.S. Army Waterways Experiment Station.
- Green, R. A., and R. M. Ebeling. 2002. *Seismic analysis of cantilever retaining walls, Phase I*. ERDC/ITL TR-02-3. Vicksburg, MS: U.S. Army Engineer Research and Development Center.
- Headquarters, U.S. Army Corps of Engineers. 1989. *Retaining and flood walls*. EM 1110-2-2502. Washington, DC.
- Headquarters, Department of the Army. 1995. *Earthquake design and evaluation for civil works projects*. ER 1110-2-1806. Washington, DC.
- _____. 2005. *Stability analysis of concrete structures*. EM 1110-2-2100. Washington, DC.
- Hynes-Griffin, M. E., and A. G. Franklin. 1984. *Rationalizing the seismic coefficient method*. Miscellaneous Paper GL-84-13. Vicksburg, MS: U.S. Army Engineer Waterways Experiment Station.
- Idriss, I. M. 1985. Evaluating seismic risk in engineering practice. In *Proceeding, 11th International Conference on Soil Mechanics and Foundation Engineering* 1:255–320.
- Lysmer, J., T. Udaka, C.-F. Tsai, and H. B. Seed. 1975. *FLUSH - A computer program for approximate 3-D analysis of soil-structure interaction problems*. Report No. EERC 75-30. Berkley, CA: Earthquake Engineering Research Center, University of California, Berkeley.

- Makdisi, F. I., and H. B. Seed. 1978. Simplified procedure for estimating dam and embankment earthquake-induced deformations. *Journal of the Geotechnical Engineering Division, ASCE*, 104(GT7):849–867.
- Mononobe, N., and H. Matsuo. 1929. On the determination of earth pressures during earthquakes. In *Proceedings, World Engineering Congress* 9:177–185.
- Newmark, N. 1965. Effects of earthquakes on dams and embankments. *Geotechnique* 15(2):139–160.
- Okabe, S. 1924. General theory of earth pressures and seismic stability of retaining walls. *Journal Japan Society of Civil Engineering* 10(6).
- _____. 1926. General theory of earth pressures. *Journal Japan Society of Civil Engineering* 12(1).
- Richards, R., Jr., and D. Elms. 1979. Seismic behavior of gravity retaining walls. *Journal of Geotechnical Engineering Division, ASCE*, 105(GT4):449–464.
- Schnabel, P. B., J. Lysmer, and H. B. Seed. 1972. *SHAKE: A computer program for earthquake response analysis of horizontally layered sites*. Report EERC-72-12. Berkeley, CA: Earthquake Engineering Research Center, University of California, Berkeley.
- Steedman, R. S., and X. Zeng. 1996. Rotation of large gravity walls on rigid foundations under seismic loading. In *Proceedings, Analysis and Design of Retaining Structures Against Earthquakes*. ASCE Geotechnical Special Publication No. 60. ed., S. Prakash, 38-56. Soil Dynamics Committee of the Geo-Institute of ASCE.
- Strom, R. W., and R. M. Ebeling. 2004. *Simplified methods used to estimate the limit state axial load capacity of spillway invert slabs*. ERDC/ITL TR-04-3. Vicksburg, MS: U.S. Army Engineer Research and Development Center.
- Whitman, R. V. 1990. Seismic design behavior of gravity retaining walls. *Proceedings of ASCE Specialty Conference on Design and Performance of Earth Retaining Structures*. Geotechnical Special Publication No. 25:817–842.
- Whitman, R. V., and S. Liao. 1985a. *Seismic design of retaining walls*. Miscellaneous Paper GL-85-1. Vicksburg, MS: U.S. Army Engineer Waterways Experiment Station.
- _____. 1985b. Seismic design of gravity retaining walls. *Proc. 8th World Conference on Earthquake Engineering, San Francisco* 3:533–540.
- _____. 2000. *Fifty years of soil dynamics*. Fifteenth Nabor Carrillo Lecture. Delivered during the XX National Meeting of Soil Mechanics, Oaxaca, Mexico, November 2000. 88 p.
- Wong, C. 1982. *Seismic analysis and improved seismic design procedure for gravity retaining walls*. Research Report 82-32. Cambridge, MA: Department of Civil Engineering, Massachusetts Institute of Technology.

Zeng, X., and R. S. Steedman. 2000. Rotating block method for seismic displacement of gravity walls. *ASCE Journal of Geotechnical and Geoenvironmental Engineering* 126(8):709–717.

Appendix A: Listing and Description of the Newmark ASCII Input Data File (file name: Newmark.in)

A.1 Introduction

This appendix lists and describes the contents of the ASCII input data file to the FORTRAN engineering computer program portion of Newmark. This input data file, always designated as Newmark.in, is created by the graphical user interface (GUI), the visual modeler portion of Newmark. The FORTRAN code of Newmark evolved from CorpsWallRotate_Wet (Ebeling et al. 2007)¹ which encompasses similar engineering concepts and computations.

The ASCII input data to Newmark is provided in 6 groups of data. They are as follows:

A.2 Group 1 – Designate the type of Newmark Analysis

KEY_NEWMARK_Analysis

with

- KEY_NEWMARK_Analysis = 1, Single Newmark analysis using one horizontal acceleration time-history.
- = 2, Multiple Newmark time history analyses using multiple acceleration time histories are required.

A.3 Group 2 – Designate global parameters and horizontal components with the input listed in two parts

¹Note: Part 1 will be skipped for a single Newmark analysis (KEY_NEWMARK_Analysis = 1)

Part 1: Key_GlobalAccVel

¹ All references cited in this appendix are included in the Reference section at the end of the main text.

Spga, SpgaUnits, Spgv, SpgvUnits

with

- Key_GlobalAccVel = 0, No Standardized displacement computations performed.
- Key_GlobalAccVel = 1, Standardized displacement computations performed.

and

- Spga = the global peak ground acceleration used for normalizing all the horizontal acceleration time-history sets of data.

- SpgaUnits = identifies the units of Spga.

Value for SpgaUnits	Units Acceleration
32.174	ft/sec ²
386.086	in./sec ²
9.80665	m/sec ²
980.665	cm/sec ²
9806.65	mm/sec ²
1.0	g's
980.665	gal's

- Spgv = the global peak ground velocity used for normalizing the peak ground velocity.

- SpgvUnits = identifies the units of the Spgv global velocity value.

Value for SpgvUnits	Units Velocity
32.174	ft/sec
386.086	in./sec
9.80665	m/sec
980.665	cm/sec
9806.65	mm/sec

Note: Second Row of Part 1 data will not be read when no standardized displacement computations are to be performed. (Key_GlobalAccVel = 0)

Part 2: TH_State, Nset, H1set, H2set

with

TH_State	= 1, time-history for horizontal component 1.
	= 2, time-history for horizontal component 2.
	= 3, both time-histories for horizontal components 1 & 2.
	Always used for multiple time-history analyses.
Nset	= the overall number of sets of horizontal components
H1set	= the number of sets available for horizontal component 1
H2set	= the number of sets available for horizontal component 2

Depending on the value of TH_State, the following input will either have one or two filenames.

A.4 Group 3 –Time-history information with input listed in two parts

Part 1: Acceleration time-history parameters and data for horizontal component 1

Note: For TH_State=2, the time-history information will be specified for horizontal component 2 and Part 2 will be omitted.

The data given in the following two sections list the acceleration time-history file[s] and summarize the parameters used to characterize each

acceleration time-history. The horizontal component[s] evaluated will be dependent on the values of TH_State and Nset of information.

Section 1: SetId, DT, GACC, Xscale, NheaderLines, NvalsPerLine, DataFmt

H1_TimehistoryFile

with

- SetId = the index of Nset (i.e., 1, 2, ... to Nset, sequentially).
- DT = the time step in seconds.
- GACC = the constant of acceleration due to gravity. The value for GACC identifies the units of acceleration, velocity and intrinsic displacement according to following tabulation.

Value for GACC	Units of Acceleration	Units of Velocity	Units of Intrinsic Displacement
32.174	ft/sec ²	ft/sec	feet
386.086	in./sec ²	in./sec	inches
9.80665	m/sec ²	m/sec	meters
980.665	cm/sec ²	cm/sec	centimeters
9806.65	mm/sec ²	mm/sec	millimeters
32.174	ft/sec ²	ft/sec	feet

- Xscale = the scale factor applied to the horizontal acceleration time history (negative value when time-history is inverted).

- NheaderLines = number of header lines within the H1_TimehistoryFile.

- NvalsPerLine = number of horizontal acceleration time-history values per line within the H1_TimehistoryFile.
- DataFmt = 0, free format, the horizontal acceleration time history values are delimited by either a comma or space[s].
- = 1, fixed format, the horizontal acceleration time history values are expressed as 8 characters per value (F8.).
- = 2, fixed format, the horizontal acceleration time history values are expressed as 9 characters per value (F9.).

and

- H1_TimehistoryFile = name of file containing the horizontal acceleration time-history data.
(Complete path to file is required.)

Contents of H1_TimehistoryFile

Section 2: ACCX (I = 1 to NOACC)

with

- ACCX = Horizontal acceleration time-history data at every DT. Data is located within the H1_TimehistoryFile.

Part 2: Acceleration time-history parameters and data for horizontal component 2 (Not included for single time-history analysis)

The data given in the following two sections list the acceleration time-history file[s] and summarize the parameters used to characterize each acceleration time-history. The horizontal component[s] evaluated will be dependent on the value of TH_State and Nset of information.

Section 1: SetId, DT, GACC, Xscale, NheaderLines, NvalsPerLine, DataFmt

H2_TimehistoryFile

with

- SetId = the index of Nset. (i.e., 1, 2, ... to Nset, sequentially).
- DT = the time step in seconds.
- GACC = the constant of acceleration due to gravity. The value for GACC identifies the units of acceleration, velocity and intrinsic displacement according to the following tabulation.

Value for GACC	Units of Acceleration	Units of Velocity	Units of Intrinsic Displacement
32.174	ft/sec ²	ft/sec	feet
386.086	in./sec ²	in./sec	inches
9.80665	m/sec ²	m/sec	meters
980.665	cm/sec ²	cm/sec	centimeters
9806.65	mm/sec ²	mm/sec	millimeters
32.174	ft/sec ²	ft/sec	feet

- Xscale = the scale factor applied to the horizontal acceleration time history

(negative value when time-history is inverted).

- NheaderLines = number of header lines within the H2_TimehistoryFile.
- NvalsPerLine = number of horizontal acceleration values per line within the H2_TimehistoryFile.
- DataFmt = 0, free format, the horizontal acceleration time-history values are delimited by either a comma or space[s].
- = 1, fixed format, the horizontal acceleration time-history values are expressed as 8 characters per value (F8.).
- = 2, fixed format, the horizontal acceleration time-history values are expressed as 9 characters per value (F9.).

and

- H2_TimehistoryFile = name of file containing the horizontal acceleration time-history data.
(Complete path to file is required.)

Contents of H2_TimehistoryFile

Section 2: ACCX (I = 1 to NOACC)

with

- ACCX = Horizontal acceleration time-history data at every DT. Data is located within the H2_TimehistoryFile.

Note: Values for the horizontal accelerations used in NEWMARK are equal to ACCX(I) times XSCALE times GACC.

A.5 Group 4 – Regression Analysis for multiple acceleration time histories with input listed in two parts

Note: For a single Newmark analysis (KEY_NEWMARK_Analysis = 1) there will be no regression analysis: Group 4 will be skipped.

Part 1: KEY_REGRESSION

with

- | | |
|----------------|--|
| KEY_REGRESSION | = 0, No Regression Analyses performed.
(Default) |
| | = 1, Common Log transformation for
estimation of two parameters (β_4, β_5) |
| | = 2, Natural Log transformation for
estimation of two parameters (β_1, β_2) |
| | = 3, Natural Log transformation for
estimation of three parameters ($\beta_1, \beta_2,$
β_3) |
| | = 4, combination of KEY_REGRESSION
1 & 2 |
| | = 5, combination of KEY_REGRESSION
1 & 3 |
| | = 6, combination of KEY_REGRESSION
2 & 3 |
| | = 7, combination of KEY_REGRESSION
1 & 2 & 3 |

Part 2: SetId, KeyH1p, KeyH1n, KeyH2p, KeyH2n (lines of input from SetId = 1 to Nset)

with

SetId	= the index of Nset. (i.e., 1, 2, ... to Nset, sequentially).
KeyH1p	= 0, No regression required. = 1, Regression analysis of horizontal component 1 on the positive side for SetId.
KeyH1n	= 0, No regression required = 1, Regression analysis of horizontal component 1 on the negative side for SetId.
KeyH2p	= 0, No regression required = 1, Regression analysis of horizontal component 2 on the positive side for SetId.
KeyH2n	= 0, No regression required = 1, Regression analysis of horizontal component 2 on the negative side for SetId.

*Note: Part 2 data will not be read when there is no regression analysis.
(KEY_REGRESSION=0)*

A.6 Group 5 – The classification and value[s] of the Maximum Transmissible Acceleration provide input in two parts, with part 2 only valid for Crit_Acc_State = 2.

Part 1: Crit_Acc_State, Crit_Acc_Units, Crit_Acc_Value

with

Crit_Acc_State = 1, value of ($k_c g$), the maximum transmissible acceleration

with

Crit_Acc_Units = identifies the units of the maximum transmissible acceleration ($k_c g$) or input variable Crit_Acc_Value.

Value for Crit_Acc_Units	Units Acceleration
32.174	ft/sec ²
386.086	in./sec ²
9.80665	m/sec ²
980.665	cm/sec ²
9806.65	mm/sec ²
1.0	g's
980.665	gal's

and

Crit_Acc_Value = $k_c g$, the maximum transmissible acceleration.

or

Crit_Acc_State = 2, value[s] of $\left(\frac{k_c}{k_m}\right)$, the ratio of the maximum transmissible acceleration value for the retaining wall ($k_c g$) and the peak ground acceleration ($k_m g$).

with

$$\text{Crit_Acc_Units} = 1.0, \text{ (Not Used)}$$

and

$$\text{Crit_Acc_Value} = 1.0, \text{ One } \frac{k_c}{k_m} \text{ value, for single Newmark analysis.}$$

$$> 1.0, \text{ Number of } \frac{k_c}{k_m} \text{ values}$$

Experience by the authors suggests a minimum of 15 well spaced values (as judged by natural logarithm plotting requirements) are needed to conduct meaningful regression analyses as well as producing useful graphs of permanent earthquake displacements.

Part 2: Crit_Acc_Ratio (I = 1 to Crit_Acc_Value)

with

$$\text{Crit_Acc_Ratio} = \text{value[s] of } \frac{k_c}{k_m}$$

For valid values between $0 < \frac{k_c}{k_m} < 1$, and in ascending order, the authors recommend the following,

Values for Crit_Acc_Ratio
0.02
0.04
0.06
0.08
0.1
0.15
0.2

0.25
0.3
0.35
0.4
0.5
0.6
0.7
0.8
0.9

A.7 Group 6 – Designate the output units for computed displacements.

DISPACC

with

DISPACC = identifies the units of the scaled acceleration, computed velocity and computed displacements according to the following tabulation in a Complete Time-History Analysis.

Value for DISPACC	Units of Acceleration	Units of Velocity	Units of Displacement
32.174	ft/sec ²	ft/sec	feet
386.086	in./sec ²	in./sec	inches
9.80665	m/sec ²	m/sec	meters
980.665	cm/sec ²	cm/sec	centimeters
9806.65	mm/sec ²	mm/sec	millimeters

Appendix B: Listing of Newmark ASCII Data Output Files

This appendix lists the Newmark ASCII Output Data Files. Table B.1 lists the output box labels and corresponding files for the visual modeler analysis tabs and briefly describes the contents.

Table B.1. Output data files used by output buttons in the visual modeler analysis tab.

Visual Modeler View Output Label	Name of File	Description
Show Log of Newmark Execution	Newmark.run	Displays a listing of the runtime execution process.
Show Input Echo of Newmark Execution	Newmark.out	Displays a listing of the input as read from Newmark.in
Plot Time Histories AccX – H1	PLOTaccX1[xxxx].TMP[1/2]	Scaled acceleration time-history for horizontal component 1.
	StandardizedPlotaccX1[xxxx].TMP[1/2]	For a standardized displacement computation, a corresponding file for horizontal component 1 with the standardized computations will be provided.
Plot Time Histories AccX – H2	PLOTaccX2[xxxx].TMP[1/2]	Scaled acceleration time-history for horizontal component 2.
	StandardizedPlotaccX2[xxxx].TMP[1/2]	For a standardized displacement computation, a corresponding file for horizontal component 2 with the standardized computations will be provided.
Plot Sliding Time-History – H1	PLOTslideTH1[xxxx].TMP[1/2]	Time-history of sliding block analysis for horizontal component 1.
	StandardizedPLOTslideTH1[xxxx].TMP[1/2]	For a standardized displacement computation, a corresponding file for horizontal component 1 with the standardized computations will be provided.
	SinglePLOTslideTH11.TMP[1/2]	For a single analysis, and with the critical acceleration as a fractional g.

Visual Modeler View Output Label	Name of File	Description
Plot Sliding Time-History - H2	PLOTslideTH2[xxxx].TMP[1/2] StandardizedPLOTslideTH2[xxxx].TMP[1/2]	Time-history of sliding block analysis for horizontal component 2. For a standardized displacement computation, a corresponding file for horizontal component 2 with the standardized computations will be created.
Plot Non-Dimensionalized Displacement	Non-Dimensionalized_disp[xxxx].tmp	Resultant non-dimensionalized displacement is provided for each set of horizontal time histories.
Plot Standardized Maximum Displacement	Standardized Maximum_disp[xxxx].tmp	For a standardized displacement computation, the resultant standardized maximum displacement is provided for each set of horizontal time histories.
Plot Permanent Displacement	Permanent_disp[xxxx].tmp	For a standardized displacement computation, the resultant permanent displacement is provided for each set of horizontal time histories.
Plot Standardized Maximum Displacement	Reg_standardized_disp.tmp and StandardizedMaximum_sets.tmp	For a regression analysis with a standardized displacement computation, the resultant standardized displacements and their representative mean and both upper and lower 68 percent prediction intervals are presented for the defined regression analysis type. This output data is provided from two files.
Plot Mean, 68 percent Prediction Intervals and 95 percent Probability of non-exceedance for Non-dimensionalized Displacement	Reg_Non-Dimensionalized_disp.tmp and Non_Dimensionalized_disp_sets.tmp	For a regression analysis, the resultant non-dimensionalized displacements and their representative mean, 95 percent probability of non-exceedance and both upper and lower 68 percent prediction intervals are presented for the defined regression analysis type from output data within two files.

Note: Part of the file names with [xxxx] as listed in Table B.1 represent the number id of the output file. This establishes the maximum number of time-history sets for an analysis to be 9999 files.

REPORT DOCUMENTATION PAGE

Form Approved
OMB No. 0704-0188

Public reporting burden for this collection of information is estimated to average 1 hour per response, including the time for reviewing instructions, searching existing data sources, gathering and maintaining the data needed, and completing and reviewing this collection of information. Send comments regarding this burden estimate or any other aspect of this collection of information, including suggestions for reducing this burden to Department of Defense, Washington Headquarters Services, Directorate for Information Operations and Reports (0704-0188), 1215 Jefferson Davis Highway, Suite 1204, Arlington, VA 22202-4302. Respondents should be aware that notwithstanding any other provision of law, no person shall be subject to any penalty for failing to comply with a collection of information if it does not display a currently valid OMB control number. **PLEASE DO NOT RETURN YOUR FORM TO THE ABOVE ADDRESS.**

1. REPORT DATE (DD-MM-YYYY) February 2009		2. REPORT TYPE Final report		3. DATES COVERED (From - To)	
4. TITLE AND SUBTITLE Permanent Seismically Induced Displacement of Rock-Founded Structures Computed by the Newmark Program				5a. CONTRACT NUMBER	
				5b. GRANT NUMBER	
				5c. PROGRAM ELEMENT NUMBER	
6. AUTHOR(S) Robert M. Ebeling, Moira T. Fong, Donald E. Yule, Amos Chase, Sr., and Raju V. Kala				5d. PROJECT NUMBER	
				5e. TASK NUMBER	
				5f. WORK UNIT NUMBER 142082	
7. PERFORMING ORGANIZATION NAME(S) AND ADDRESS(ES) U.S. Army Engineer Research and Development Center Information Technology Laboratory and Geotechnical and Structures Laboratory 3909 Halls Ferry Road, Vicksburg, MS 39180-6199; Science Applications International Corporation 3532 Manor Drive, Suite 4, Vicksburg, MS 39180				8. PERFORMING ORGANIZATION REPORT NUMBER ERDC TR-09-2	
9. SPONSORING / MONITORING AGENCY NAME(S) AND ADDRESS(ES) Headquarters, U.S. Army Corps of Engineers Washington, DC 20314-1000				10. SPONSOR/MONITOR'S ACRONYM(S)	
				11. SPONSOR/MONITOR'S REPORT NUMBER(S)	
12. DISTRIBUTION / AVAILABILITY STATEMENT Approved for public release; distribution is unlimited.					
13. SUPPLEMENTARY NOTES					
14. ABSTRACT This research report describes the engineering formulation and corresponding software developed for the translational response of rock-founded structural systems to earthquake ground motions. The PC software Newmark (and Newmark _{VM}) is developed to perform an analysis of the permanent sliding displacement response for a structural system founded on rock for a user specified earthquake acceleration time history via a Complete Time History Analysis, also know as the Newmark sliding block method of analysis. The PC-based program Newmark performs a permanent sliding block displacement analysis given a baseline corrected rock site-specific acceleration time history. Newmark can also conduct regression analyses for sets of rock founded acceleration time histories in order to develop up to three user selected forms of generalized equations of simplified permanent displacement relationships. The rock-founded structural system can be a variety of structural feature types; a concrete gravity dam, a concrete monolith, a retaining wall, etc. <div style="text-align: right;">(Continued)</div>					
15. SUBJECT TERMS Baseline corrected Maximum transmissible acceleration					
Newmark sliding block analysis		Permanent displacement		Rock earthquake ground motions	
Rock		Seismic		Yield Acceleration	
Translation					
16. SECURITY CLASSIFICATION OF:			17. LIMITATION OF ABSTRACT	18. NUMBER OF PAGES	19a. NAME OF RESPONSIBLE PERSON
a. REPORT	b. ABSTRACT	c. THIS PAGE			19b. TELEPHONE NUMBER (include area code)
UNCLASSIFIED	UNCLASSIFIED	UNCLASSIFIED		203	

14. ABSTRACT (Concluded).

The results of the regression analyses discussed in this report resulted in Simplified permanent displacement relationships that were developed using data generated by Newmark for an extensive data base of 122 sets of baseline corrected rock acceleration time histories in the moment magnitude 5 to 7 range. The resulting simplified permanent displacement relationships allow the engineer to rapidly determine the earthquake-induced permanent displacement for a given rock-founded structural system. This alternative procedure requires only rudimentary design/analysis ground motion characterization and use of a simplified permanent seismic displacement relationship for a sliding block (structural) system model. The resulting simplified permanent displacement relationships discussed in this report are being implemented in other Corps permanent (seismically-induced) displacement software such as $C_{\text{orps}}W_{\text{allSlip}}$, and $C_{\text{orps}}D_{\text{amSlip}}$.